THE UNIVERSITY *of* EDINBURGH

This thesis has been submitted in fulfilment of the requirements for a postgraduate degree (e. g. PhD, MPhil, DClinPsychol) at the University of Edinburgh. Please note the following terms and conditions of use:

- This work is protected by copyright and other intellectual property rights, which are retained by the thesis author, unless otherwise stated.
- A copy can be downloaded for personal non-commercial research or study, without prior permission or charge.
- This thesis cannot be reproduced or quoted extensively from without first obtaining permission in writing from the author.
- The content must not be changed in any way or sold commercially in any format or medium without the formal permission of the author.
- When referring to this work, full bibliographic details including the author, title, awarding institution and date of the thesis must be given.

Investigating the role of EnvZ-OmpR, BaeSR and RamA in the resistance of *Klebsiella pneumoniae* to Cefiderocol

Laura Elizabeth Leigh Founde S1930611

THE UNIVERSITY *of* EDINBURGH

Submitted for the degree of Infectious Diseases (Masters by Research)

The University of Edinburgh

2024

Declaration

I declare that this thesis has been comprised solely by myself and that it has not been submitted, in whole or in part, to any previous application for a degree or professional qualification. Except where stated otherwise by reference or acknowledgment, the work presented is entirely my own.

Signed:

Date: **07.09.2024**

Acknowledgements

I would like to firstly extent my gratitude to my supervisor Dr. Thamarai Schneiders for her support and enouragement over the last 12 months, for building my confidence as an aspiring scientist and for pushing me to achieve to the best of my ability. I would also like to thank the MScR Infectious Diseases course co-ordinator Kim Picozzi for her assistance in organising my assignment to this project. I extend my deepest thanks to Kyriakos Vidalis (PhD Student, TS Lab) for his unwavering patience as I navigated this degree, for always being around to answer my incessant questions and hone my practical skills, and for being not only a brilliant secondary mentor, but a valued friend. Special thanks go to Nur Afifah Izzati Saiful Bahari for her additional support throughout this thesis' duration, and for making long, tiring days in the lab that much brighter. Further gratitude goes to previous and current TS Lab members Dr. Martin Vandeputte, Jaiyu Wang and Oliver Coombs O'brien, for their assistance with both bioinformatic and practical aspects of this project and for being lovely company over the year. Lastly, I can't thank my partner, family and friends enough for their continual patience and support during the process of this thesis' completion – without whom I would not be where I am today.

Contents Page

Figure List **7**

Table List **12**

Abstract **13**

Lay Summary **15**

1. Introduction and Literature Review **16**

1.1. The Threat of Antimicrobial Resistance **16**

1.2. Klebsiella pneumoniae **16**

1.2.1. AMR Mechanisms of *Kp* 17

1.3. The Introduction of Cefiderocol **18**

1.4. Fe^{3+} Acquisition in *Kp* **19**

1.4.1. The Influx of Trojan Horse CFDC 19

1.5. Master Regulator FUR **20**

1.6. Two-Component Systems **21**

1.6.1. The TCS EnvZ-OmpR and its Regulon 23

1.6.1.1. CirA *25*

1.6.1.2. Fiu *26*

1.6.1.3. FepA *26*

1.6.1.4. FecA *27*

1.6.2. The TCS BaeSR and its Regulon 27

1.6.2.1. MdtABC-TolC and AcrA-AcrD-TolC *28*

1.7. The AraC-type Regulator RamA **29**

1.8. The Exopolysaccharide Capsule **30**

1.8. Significance, Summary and Rationale **30**

1.9. Hypothesis and Aims **33**

1.9.1. Overarching Hypothesis 33

1.9.2. Main Aims 33

2. Materials and Methods 34

2.1. Bacterial Strains and Stock Preparation 34

2.2. Media Preparation 35

2.3. Overnight Culture Preparation 36

2.4. Polymerase Chain Reaction (PCR) Techniques 36

2.5. Cloning Techniques (Making of Mutants) 37

2.5.1. Non-Conjugative Homologous Recombination using pTOF 37

2.5.1.1. Plasmid DNA Extraction 37

2.5.1.2. Restriction Digest 37

2.5.1.3. Exchange 38

2.5.2. Conjugative Homologous Recombination using pKNGS 39

2.5.2.1. Construction of Gene Flank Fragments for pKNGS Insertion 39

2.5.2.2. NoCo Construct Cloning into pKNGS Plasmid Vector (Assembly Ligation) 40

2.5.2.3. Exchange 40

2.6. Capsule Quantification: Glucuronic Acid Assay 41

2.7. RNA Extraction for RT-(q)PCR 42

2.8. Real-Time Quantitative PCR (RT-[q]PCR) and Delta-Delta CT (ΔΔCT) Fold Change Analysis 42

2.8.1. Primer Efficiency 42

2.8.2. RT-(q)PCR for Gene Expression Quantification 43

2.9. Chrome Azurol S (CAS) Agar Assaying 43

2.10. Antibiotic Susceptibility Testing 44

2.10.1. Disk Diffusion 45

2.10.2. Broth Microdilution 45

2.11. Bioinformatics 46

2.12. Statistical Analysis 47

3. Results 48

3.1. CHAPTER ONE: Bioinformatics: Analysing the Integrity of IROMPs Prior to CFDC Exposure ... 48

3.1.1. CirA ... 49

3.1.2. Fiu ... 52

3.2. CHAPTER TWO: Investigating the Influx of CFDC Through IROMPs ... 54

3.2.1. Transcriptomic Analyses – How Does Iron Limitation Drive RNA Transcript Expression of IROMP encoding genes *cirA, fiu*, *fepA* and *fecA*? ... 54

3.2.2. Generation of IROMP Deletion Mutants in Ecl8 and *Kp* 52145 Backgrounds ... 58

3.2.3. Susceptibility Testing of IROMP Deleted Strains ... 73

3.2.3.1. CFDC Susceptibility ... 74

3.2.3.2. CAZ Susceptibility ... 74

3.2.5. Transcriptomic Analyses – How Does *cirA* Deletion Impact RNA Transcript Expression of IROMP Genes *fiu, fepA* and *fecA* Under Iron Limitation? ... 74

3.3. CHAPTER THREE: Investigating the Efflux of CFDC Through MdtABC-TolC, AcrA-AcrD-TolC and AcrAB-TolC ... 77

3.3.1. Transcriptomic Analyses - How does Iron Limitation Drive Expression of RND Efflux Pump Encoding Genes *mdtB*, *acrD* and *acrB*? ... 77

3.3.2. Generation of RND Efflux Pump Deletion Mutants in Ecl8 and Kp 52145 Backgrounds ... 80

3.3.3. Measuring the Impact of Iron Limitation on Capsule Production in *Kp* 52145*mdtABC*<km> ... 90

3.3.4. Semi-Quantitative Analysis of Siderophore Export Under Efflux Component Deletion: Chrome Azurol S (CAS) Agar Assaying ... 92

3.3.5. Susceptibility Testing of Efflux Component Deleted Strains ... 94

3.3.5.1. CFDC Susceptibility ... 95

3.3.5.2. CAZ Susceptibility ... 96

3.4. CHAPTER FOUR: Confirming the Impact of TCS EnvZ-OmpR, TCS BaeSR and AraC/XylS Transcription Factor RamA on the Permeability of the OM to CFDC ... 97

3.4.1. Transcriptomic Analyses - How does Iron Limitation Drive RNA Transcript Expression of Regulatory Factor Encoding Genes *ompR, baeR* and *ramA*? ... 98

3.4.2. Measuring the Impact of Iron Limitation on Capsule Production in *Kp* 52145*ramR*<km>. 101

3.4.3. Semi-Quantitative Analysis of Siderophore Export Under Regulatory Factor Deletion and Overexpression: Chrome Azurol S (CAS) Agar Assaying ... 103

3.4.4. Susceptibility Testing of EnvZ-OmpR, BaeSR and RamA Deleted and Overexpressed Strains 105

3.4.4.1. CFDC Susceptibility 107

3.4.4.2. CAZ Susceptibility 108

3.4.5. Transcriptomic Analyses - How does RamA Drive RNA Transcript Expression of Efflux Pump Encoding Genes *mdtB* and *acrD* Under Iron Limitation? 108

3.4.6. Transcriptomic Analyses - How does RamA Drive RNA Transcript Expression of IROMP Encoding Genes *cirA, fiu, fepA* and *fecA* Under Iron Limitation? 110

3.4.6.1. The Impact of ramA Overexpression on RNA Transcript Expression of cirA, fiu, fepA and fecA Under Iron Limitation 110

3.4.6.2. The Impact of ramA Deletion on RNA Transcript Expression of cirA, fiu, fepA and fecA Under Iron Limitation 112

4. Discussion 115

4.1. Limitations 120

4.2. Concluding Remarks 121

5. Directions for Future Research 122

APPENDIX I. PRIMERS EMPLOYED IN THE PRESENT STUDY 124

APPENDIX II. RT-(q)PCR PRIMER EFFICIENCY VALUES 127

APPENDIX III. DISK DIFFUSION TRIAL 128

APPENDIX IV. PRELIMINARY CHROME AZUROL S (CAS) AGAR ASSAY TRIAL 133

APPENDIX V. COLLATED CAS AGAR ASSAY PLATE IMAGES FOR ALL TESTED STRAINS 136

APPENDIX VI. VALIDATION OF IROMP DEREPRESSION UNDER FUR DELETION 137

APPENDIX VII. RT-(q)PCR VALIDATION OF IDM1 and IDM7 140

APPENDIX VIII. RT(q)-PCR ANALYSIS OF Ecl8*omrA*<km> 144

References 147

Figure List

Figure 1. Molecular schematic of the structure of CFDC. 16

Figure 2. Schematic representation of siderophore, IROMP and FeoB regulation by FUR. 19

Figure 3. Schematic representation of TCS activation and subsequent control of genetic transcription. 20

Figure 4. Schematic representation showing control of activated response regulator OmpR over IROMP-encoding genes *cirA, fiu, fepA* and *fecA*, including the involvement of Hfq-dependent OmrA and OmrB, *feoB* and FUR. 23

Figure 5. Regulatory pathways of constitutively active EnvZ-OmpR, constitutively active BaeSR and constitutively active RamA under iron limitation and their proposed involvement in the resistance of *Kp* to CFDC. 30

Figure 6. Blank-corrected standard curve for glucuronic acid concentration extrapolation. 40

Figure 7. The iTOL distance tree of aligned CirA amino acid sequences from *Kp* ST11. 48

Figure 8. The results of PolyPHen-2 predictive profiling of amino acid substitutions found in Kp ST11 CirA amino acid sequences of Asian origin (Y183W) (A) and European origin (T172A) (B). 49

Figure 9. The iTOL distance tree of aligned Fiu amino acid sequences from *Kp* ST258. 50

Figure 10. The result of PolyPHen-2 predictive profiling of an amino acid substitution (A463T) found in Kp ST258 Fiu amino acid sequences of North American origin.. ..... 51 **Figure 11. Log_2 fold change expression of *cirA, fiu, fepA, fecA* in iron deplete media (ID-CAMHB) relative to iron replete media (ID-CAMHB+$FeCl_3$) under Ecl8.** ..... 53 **Figure 12. Log_2 fold change expression of *cirA, fiu, fepA, fecA* under *Kp* 52145 relative to Ecl8 in iron deplete media (ID-CAMHB).** 55

Figure 13. Gel electrophoresis image showing *fepA* CoCi and NoNi fragment Phusion PCR products. 57

Figure 14. Gel electrophoresis image showing extracted and purified *fepA* CoCi and NoNi fragment DNA band size checks.. 58

Figure 15. Gel electrophoresis image showing *fiu* CoCi and NoNi fragment Phusion PCR products.. 59
Figure 16. Gel electrophoresis image showing extracted and purified *fiu* CoCi and NoNi fragment DNA band size checks.. 60
Figure 17. Gel electrophoresis image showing NoCo*fepA* and NoCo*fiu* construct Phusion PCR products, with the *fiu* constructs made using the combinations of NoNi 1, CoCi 1 and CoCi 2 as shown in Figure 16. 61
Figure 18. Gel electrophoresis image showing extracted and purified NoCo*fepA* and NoCo*fiu* construct DNA band size checks. 62
Figure 19. Gel electrophoresis image of One*Taq* PCR products showing successful pKNGSNoCo*fepA* construct cloning in *E. coli* DH5α *pir* from the 60ng:10ng insert:vector ligation after addition of DMSO to the PCR mixture. 63
Figure 20. Gel electrophoresis image of One*Taq* PCR products showing successful pKNGSNoco*fepA* and pKNGSNoCo*fiu* construct cloning in *E. coli* DH5α *pir* from the 90ng:15ng insert:vector ligations after addition of DMSO to the PCR mixture. 64
Figure 21. Gel electrophoresis image of One*Taq* PCR products showing successful pKNGSNoCo*fepA* and pKNGSNoCo*fiu* construct cloning in *E. coli* DH5α *pir* from the 60ng:10ng insert:vector ligations after re-electroporation with 15µl clean ligation product and addition of DMSO to the PCR mixture. 64
Figure 22. Gel electrophoresis image showing all successful and DH5α pirpKNGSNoCo*fepA* and DH5α pirpKNGSNoCo*fiu* construct clone DNA, confirming correct banding sizes...... 65
Figure 23. Images of LB+Km 100mg/ml (denoted Km) plates of each respective *fepA* and *fiu* (denoted Fe and Fi, respectively) DH5α pirpKNGSNoCo clone transformed into *E. coli* MFD S17 λ*pir* after attempts for recipient conjugation and plasmid excision. 66
Figure 24. Gel electrophoresis image showing SmaI & SalI restriction digest validation of 2x DH10βpTOFNoCo*cirA*<km> constructs of Schneiders Lab - labelled here as DH10βpTOFNoCo*cirA*<km> 1 and DH10βpTOFNoCo*cirA*<km> 2 (1 and 2, respectively). 67
Figure 25. Gel electrophoresis image showing NotI and NotI & SmaI restriction digest validation of 2x DH10βpTOFNoCo*cirA*<km> constructs of Schneiders Lab - labelled here as DH10βpTOFNoCo*cirA*<km> 1 and DH10βpTOFNoCo*cirA*<km> 2 (1 and 2, respectively). 68
Figure 26. Gel electrophoresis image showing validation of DH10βpTOFNoCo*cirA*<km> PCR products following PCR using RT-(q)PCR primers. 69
Figure 27. Gel electrophoresis image showing failed insertion of DH10βpTOFNoCo*cirA*<km> in the

Kp 52145 background. 70
Figure 28. Log_2 fold change expression of *fiu, fepA, fecA* under Ecl8*cirA*<km> relative to Ecl8 in iron deplete media (ID-CAMHB). 73
Figure 29. Log_2 fold change expression of mdtB, acrD and acrB in iron deplete media (ID-CAMHB) relative to iron replete media (ID-CAMHB+$FeCl_3$) under Ecl8. 76
Figure 30. Log_2 fold change expression of *mdtB, acrD, acrB* in Kp 52145 relative to Ecl8 under iron deplete media (ID-CAMHB). 78
Figure 31. Gel electrophoresis image showing the successful insertion of DH10βpTOFNoCo*mdtABC*<km> knockout constructs in both Ecl8 and *Kp* 52145 backgrounds. 79
Figure 32. Gel electrophoresis image showing *acrD* CoCi and NoNi fragment Phusion PCR products. 81
Figure 33. Gel electrophoresis image showing extracted and purified *acrD* CoCi and NoNi fragment band size checks. 82
Figure 34. Gel electrophoresis image showing NoCo*acrD* fragment Phusion PCR products made using the combinations of NoNi 1, CoCi 1 and CoCi 2 as shown in Figure 33. 83
Figure 35. Gel electrophoresis image showing extracted and purified NoCo*acrD* construct DNA band size checks. 84
Figure 36. Gel electrophoresis image of One*Taq* PCR products showing successful pKNGSNoCo*acrD* construct cloning in *E. coli* DH5α *pir* from the 5µl:50µl 60ng:10ng insert:vector ligation after the optimized addition of DMSO to the PCR mixture. 85
Figure 37. Gel electrophoresis image of One*Taq* PCR products showing successful pKNGSNoCo*acrD* construct cloning in *E. coli* DH5α *pir* from the 90ng:15ng insert:vector ligation after the optimized addition of DMSO to the PCR mixture. 86
Figure 38. Gel electrophoresis image of OneTaq PCR products showing successful pKNGSNoCo*acrD* construct cloning in *E. coli* DH5α *pir* for AcrD from the 60ng:10ng insert:vector ligation after addition of DMSO and 15µl clean ligation product for electroporation. 86
Figure 39. Gel electrophoresis image showing all successful DH5αpirpKNGSNoCo*acrD* construct clone DNA, confirming correct banding sizes. 87
Figure 40. Images of LB+Km 100mg/ml (denoted Km) plates of DH5α pirpKNGSNoCo*acrD* (denoted A) clones transformed into *E. coli* MFD S17 λ*pir* after attempts for recipient conjugation and plasmid excision. 88
Figure 41. Glucuronic acid concentration (ng/OD_{520}) of *Kp* 52145 and *Kp* 52145*mdtABC*<km>

averaged across biological and technical replicates equalling n=3. 89

Figure 42. Average orange halo diameters (mm) on CAS agar plates after inoculation with Ecl8, Ecl8*mdtABC*<km>, Ecl8*acrAB*<km>, *Kp* 52145 and *Kp* 52145*mdtABC*<km> grown overnight in iron deplete media (ID-CAMHB)...... 91

Figure 43. Log_2 fold change expression of *ompR, baeR* and *ramA* in iron deplete media (ID-CAMHB) relative to iron replete media (ID-CAMHB+$FeCl_3$)...... 97

Figure 44. Log_2 fold change expression of *ompR, baeR* and *ramA* in *Kp* 52145 relative to Ecl8 under iron deplete media (ID-CAMHB)...... 99

Figure 45. Glucuronic acid concentration (ng/OD_{520}) of *Kp* 52145 and *Kp* 52145*ramR*<km> averaged across biological and technical replicates equalling n=3. 100

Figure 46. Average orange halo diameters (mm) on CAS agar plates after inoculation with Ecl8, Ecl8*baeSR*<km>, Ecl8Δ*ramR, Kp* 52145 and *Kp* 52145*ramR*<km> grown overnight in iron deplete media (ID-CAMHB). 102

Figure 47. Log_2 fold change expression of *mdtB* and *acrD* in Ecl8Δ*ramR* relative to Ecl8 under iron deplete media (ID-CAMHB). 107

Figure 48. Log_2 fold change expression of *cirA, fiu, fepA, fecA* under Ecl8Δ*ramR* relative to Ecl8 in iron deplete media (ID-CAMHB)...... 109

Figure 49. Log_2 fold change expression of *cirA, fiu, fepA, fecA* under Ecl8Δ*ramA* relative to Ecl8 in iron deplete media (ID-CAMHB)...... 111

Figure 50. Average inhibition zone diameters (mm) after inoculation of strains incubated overnight in iron deplete media (ID-CAMHB) or iron replete media (ID-CAMHB+$FeCl_3$) onto respective iron deplete ID-CAMH agar or iron replete ID-CAMH+$FeCl_3$ agar with CFDC (A) or CAZ (B).. 126

Figure 51. Example disk diffusion plates swabbed with Ecl8 (denoted 62) (A and B) and Ecl8Δ*envZompR*<km> (denoted 62Δ*envZompR*) (C and D) on iron depleted agar (ID-CAMH agar) (denoted 'D') and iron replete agar (ID-CAMH+$FeCl_3$ agar) (denoted 'R'). 128

Figure 52. Image of CAS trial plate inoculated with strains Ecl8 (denoted '62') and Ecl8Δ*fur* (denoted 'F') following strain growth in iron limited media (ID-CAMHB) (denoted D for deplete).

..... 131

Figure 53. Average orange halo diameters (mm) on CAS plates after inoculation with Ecl8 and Ecl8Δfur grown in iron deplete media (ID-CAMHB).. 131

Figure 54. Collated images of CAS plates inoculated with all tested strains following strain growth in iron limited media (ID-CAMHB) (denoted D for deplete). 133

Figure 55. Log_2 fold change expression of *cirA, fiu, fepA, fecA* in iron deplete media (ID-CAMHB) (A) and iron replete media (ID-CAMHB+$FeCl_3$) (B) under Ecl8Δ*fur* relative to Ecl8. 135

Figure 56. Log_2 fold change expression of *ompR, baeR, cirA, fiu* in iron deplete media (ID-CAMHB) (A) and iron replete media (ID-CAMHB+$FeCl_3$) (B) under IDM1 relative to Ecl8...... 137

Figure 57. Log_2 fold change expression of *ompR, baeR, cirA, fiu* in iron deplete media (ID-CAMHB) (A) and iron replete media (ID-CAMHB+$FeCl_3$) (B) under IDM7 relative to Ecl8...... 138

Figure 58. Log_2 fold change expression of *cirA, fiu, fepA, fecA* and *ompR* under Ecl8omrA<km> relative to Ecl8 in iron deplete media (ID-CAMHB).. 141

Table List

Table 1. List of strains used in the present study. 32

Table 2. Standard three-step protocol PCR conditions using Phusion. 34

Table 3. Standard 30 cycle PCR conditions using OneTaq. 35

Table 4. Zone of Inhibition Breakpoints of antibiotic resistance applicable to both CFDC and CAZ. . 43

Table 5. Layout of initial media volume added to pipette reservoir during broth microdilution. ... 43

Table 6. Concentration of each vertical well row of the round-bottomed 96 well plate after media and antibiotic mixture pipetted during broth microdilution. 44

Table 7. Minimum Inhibitory Concentration breakpoints of antibiotic resistance applicable to CFDC and CAZ. 44

Table 8. Modal CFDC and CAZ MIC values (mg/L) of Ecl8*cirA*<km> and Ecl8. ID-CAMHB represents iron deplete media and ID-CAMHB+$FeCl_3$ represents iron replete media. 71

Table 9. Modal CFDC and CAZ MIC values (mg/L) of RND efflux pump deleted strains and respective wild types. 93

Table 10. Modal CFDC and CAZ MIC values (mg/L) of TCS and AraC/XylS regulator deleted and overexpressed strains and relative wild types. 104

Table 11. List of primers used in the present work. 123

Table 12. RT-(q)PCR primer set efficiencies allowing use in a 1:1 ratio 124

Abstract

Antimicrobial resistance (AMR) is one of the most serious global public health threats of this century. The modified Cephalosporin Cefiderocol (CFDC) was clinically approved in the EU as of 2020 to attempt to combat multi-drug resistant (MDR) bacteria, including Gram-negative ESKAPES pathogen *Klebsiella pneumoniae* (*Kp*). Like all bacteria, *Kp* requires ferric iron (Fe^{3+}) for viability, due to its involvement in many essential cellular processes. Limited iron stores in an infected host impose a significant challenge for bacterial iron uptake. Hence, *Kp* must compete with the host for this nutrient. This is achieved by the release and re-uptake of high affinity Fe^{3+} chelating molecules called siderophores, including the catecholate-type siderophore enterobactin. Enterobactin efflux from the cell has been shown to occur synergistically through resistance-nodulation-division (RND) family efflux pumps MdtABC-TolC, AcrAAcrD-TolC and AcrAB-TolC. The re-uptake of enterobactin into *Kp* in complex with Fe^{3+} has been shown to occur through iron regulated outer membrane (OM) proteins (IROMPs) CirA, Fiu, FepA and FecA.

CFDC can mimic enterobactin's action of Fe^{3+} binding due to its conjugation with a catechol moiety. This allows CFDC to hijack the IROMPs to gain cellular entry. However, with the catechol moiety conferring an element of structural similarity between CFDC and enterobactin, it has been speculated that CFDC could also be effluxed from the cell by MdtABC-TolC, AcrA-AcrD-TolC and AcrAB-TolC. It is known that the two-component system (TCS) EnvZ-OmpR negatively regulates the IROMPs, the TCS BaeSR positively regulates MdtABC-TolC and AcrA-AcrD-TolC, and the AraC-XylS family regulator RamA positively regulates AcrAB-TolC. Thus, EnvZ-OmpR, BaeSR and RamA have been implicated in reducing *Kp* susceptibility to CFDC. Therefore, this study's primary objective was to establish how *Kp* resists CFDC under iron limitation through EnvZ-OmpR, BaeSR and RamA. Broth microdilution susceptibility testing confirmed *cirA* deletion to confer a biologically insignificant 2-fold increase to CFDC MIC, with RT-(q)PCR evidencing this to be the consequence of upregulated RNA transcript expression of *fiu, fepA* and *fecA*. Deletion of *envZompR* reduced CFDC MIC by 8-fold. A gain-of-function substitution in histidine kinase EnvZ (L230Q), which rendered EnvZ-OmpR constitutively active, increased CFDC MIC by 4 to 8-fold. Thus, EnvZ-OmpR was confirmed to inhibit CFDC influx into *Kp via* its repression of *cirA, fiu, fepA* and *fecA* transcription. The Chrome Azurol S (CAS) agar assay revealed *mdtABC* and *baeSR* deletions to significantly reduce siderophore export from *Kp*, which was positively correlated with both deletions conferring a 4 to 8-fold decrease in CFDC MIC. Thus, BaeSR was confirmed to induce CFDC efflux from *Kp via* its activation of *mdtABC* transcription. The CAS assay revealed no impact on siderophore export due to *acrAB* deletion or *ramA* overexpression. Further, *acrAB* deletion conferred no impact to CFDC susceptibility. However, *ramA* overexpression increased CFDC MIC by 4-fold. Results from subsequent RT-(q)PCR analysis suggest the overexpression of *ramA* to indirectly induce the repression of *cirA, fiu, fepA* and *fecA* through an unspecified intermediary regulator, exposing an

avenue for further research. Thus, the present work has highlighted fundamental implications of EnvZOmpR, BaeSR and RamA in *Kp* Fe^{3+} homeostasis, virulence and pathogenicity, which are imperative to investigate further as the global usage of CFDC increases.

Lay Summary

The silent pandemic of antimicrobial resistance (AMR) is one of the most serious threats to global public health of the 21st century. By 2050, AMR is predicted to cause 10 million annual deaths worldwide (O'Neill, 2016). As of 2024, the multi-drug resistant (MDR) bacterium *Klebsiella pneumoniae (Kp)* has been labelled the primary critical priority for the development of new treatments by the World Health Organization. The antibiotic Cefiderocol (CFDC) was released to the market in 2020 in attempts to combat MDR bacteria, including *Kp*. In an infected host, iron stores are limited. Like all bacteria, *Kp* needs iron to survive, as it is an essential nutrient for many processes. Hence, *Kp* must compete with the infected host for this nutrient. To do so, *Kp* releases small molecules which act as iron magnets, that bind and transport the nutrient into the cell. CFDC displays an element of structural similarity to these iron magnets, which allows the antibiotic to also bind to iron. Due to this, CFDC can hijack the bacteria's iron uptake transportation system to gain cellular entry, acting as a trojan horse. Several specific proteins have been shown across research to control different aspects of this iron transportation pathway in *Kp*. Therefore, these proteins have been suggested to impact the uptake and effectiveness of CFDC, and thereby contribute to the progressive onset of CFDC resistance in *Kp*. However, to date, studies investigating the relationship of these proteins to CFDC resistance remain scarce, and the mechanisms by which they may act to impact CFDC effectiveness under iron limitation are not well defined. Hence, the primary objective of this work was to establish how *Kp* resists CFDC under iron limitation through these proteins.

1. Introduction and Literature Review

1.1. The Threat of Antimicrobial Resistance

The silent pandemic of antimicrobial resistance (AMR) is one of the most serious threats to global public health of this century (Salam *et al.*, 2023). By 2050, AMR is predicted to cause 10 million annual deaths, and concomitantly cost a cumulative 100 trillion USD in global economic ouput (O'Neill, 2016). ESKAPES pathogens (*Enterococcus faecium, Staphylococcus aureus, Klebsiella pneumoniae, Acinteobacter baumannii, Pseudomonas aeruginosa, Enterobacter* species and *Stenotrophomonas maltophilia*) are a group of bacteria designated as the leading causative agents of nosocomial infections worldwide. They are a major source of clinical concern due to their increasing presentation of challenge to currently available antibiotics, resulting in the increasing emergence of multi-drug resistant (MDR) strains of these species (Martin and Bachman, 2018; Rajput *et al.*, 2018). The pace at which the ESKAPES bacteria are acquiring MDR status has been significantly expedited due to selection pressures conferred by clinical antibiotic over-consumption (OECD, 2018). The drought in new antibiotic discoveries since the 'Golden Age' of 1940 to 1970, combined with the rampant increase in MDR bacterial dissemination, poses the imminent risk of entrance into an era of untreatable infections (O'Neill, 2016; Hutchings, Truman and Wilkinson, 2019). Therefore, it is of critical importance to establish the physiological mechanisms by which ESKAPES evade currently available antimicrobials. This would facilitate moving toward the development of adjunctive therapy strategies which may re-sensitise bacteria to widespread use of antibiotics.

1.2. Klebsiella pneumoniae

The Gram-negative bacillus *Klebsiella pneumoniae* (*Kp*) of the *Enterobacteriaceae* family is an established non-motile pathogen belonging to one of two distinct pathotypes: classical (c*Kp*) or hypervirulent (hv*Kp*). The classical pathotype most frequently causes opportunistic infection, limited to hospital-based acquisition in immunocompromised individuals. This pathotype usually colonises the urinary and respiratory tracts, but can also cause septicaemia (Martin and Bachman, 2018). The hypervirulent pathotype is more recently emerged, and is continuously evolving to be of increasing concern in otherwise healthy individuals in the community setting. This pathotype is most commonly responsible for serious incidences of meningitis, non-hepatic abscesses and endophthalmitis (Choby,

Howard-Anderson and Weiss, 2020). As of 2024, the World Health Organisation (WHO) Bacterial Priority Pathogens List categorised Carbapenem-resistant *Kp* as being of primary critical priority for the development of new treatments. This was closely followed in position six by *Kp* with third-generation Cephalosporin resistance (WHO Bacterial Priority Pathogens List, 2024). In the UK alone, *Kp* third-generation Cephalosporin resistance rates were shown to have reached 17.4% as of 2022, compared to the rate of 13.5% recorded as of 2018 (UK Health Security Agency, 2023). Moreover, secondary infection with

Kp has been recently reported in patients with COVID-19, which heightens the current relevance of *Kp* as a major clinical threat (Chang, Sharma, Dela Cruz and Zhang, 2021).

1.2.1. AMR Mechanisms of *Kp*

Gram-negative bacteria such as *Kp* may either intrinsically resist or acquire resistance to antibiotics. Intrinsic resistance is the result of an inherent characteristic of the bacteria associated with its structure or function. A major example of this is the Gram-negative outer membrane (OM): an asymmetric bilayer consisting of a lipopolysaccharide (LPS) outer leaflet, and phospholipid inner leaflet, which acts as a selective permeability barrier between the extracellular and intracellular spaces (Alteri and Mobley, 2007; Reygaert, 2018). Intrinsic resistance determinants may also be encoded on the chromosome, including, for example, antibiotic efflux pumps. The acquisition of antibiotic resistance, on the other hand, may occur as a result of spontaneous or selected chromosomal mutations. These may arise in genes which, for example, encode proteins that facilitate an antibiotic's penetration of the cell, such as hydrophilic OM porins. Such mutations may also occur in genes encoding the intracellular targets of the antibiotic, such as penicillin binding proteins (PBPs). These mutations frequently confer a survival advantage to the bacteria under exposure to the antibiotic, driving adaptive evolution. Resistance is also acquired through the between-organism transmission of antimicrobial resistance determinants, such as β-lactamase enzymes OXA-48, NDM and KPC (Tooke *et al.*, 2019). This is achieved *via* the natural phenomenon of horizontal gene transfer, where resistance genes are carried on and exchanged between chromosomes, plasmids or mobile genetic elements such as transposons (Burmeister, 2015).

1.3. The Introduction of Cefiderocol

One example of a novel antibiotic introduced with intention to tackle MDR *Kp* is modified Cephalosporin Cefiderocol (CFDC), formerly known as S-649266 or Fetcroja®. CFDC was approved for EU clinical use as of 2020 (Karakonstantis, Rousaki and Kritsotakis, 2022). As a modified β-lactam, CFDC maintains the bactericidal mode of action of inhibiting the synthesis and cross-linking of the cell wall macromolecule peptidoglycan, resulting in bacteriolysis (Sato and Yamawaki, 2019). This is achieved *via* the binding of CFDC to PBPs, with a particular affinity for PBP2 and PBP3 in *Kp* (Ito *et al.,* 2018; Syed, 2021). The structure of CFDC is modelled from third and fourth-generation Cephalosporins Ceftazidime (hereafter CAZ) and Cefepime (Isler *et al.,* 2023). Notably, CFDC maintains the C-7 side chain carboxypropanoxyimino moiety and C-3 side chain pyrrolidinium group of each antibiotic, respectively (Saisho *et al.*, 2018). This confers enhanced penetration of the OM, and has been suggested to increase the hydrolytic stability of the antibiotic's β-lactam ring against degradation by most β-lactamases (Sato and Yamawaki 2019; El-Lababidi and Rizk, 2020; Karakonstantis, Rousaki and Kritsotakis, 2022). CFDC also possesses a chlorocatechol moiety, being 2-chloro-3,4-dihydroxybenzoic acid, which is conjugated to the compound's C-3 side chain (Wu, Srinivas and Pogue, 2020; Liu *et al.*, 2023) (Figure 1). This enables CFDC to exploit the essential pathway of ferric iron (Fe^{3+}) uptake in *Kp*, which it uses to gain entry into the cell.

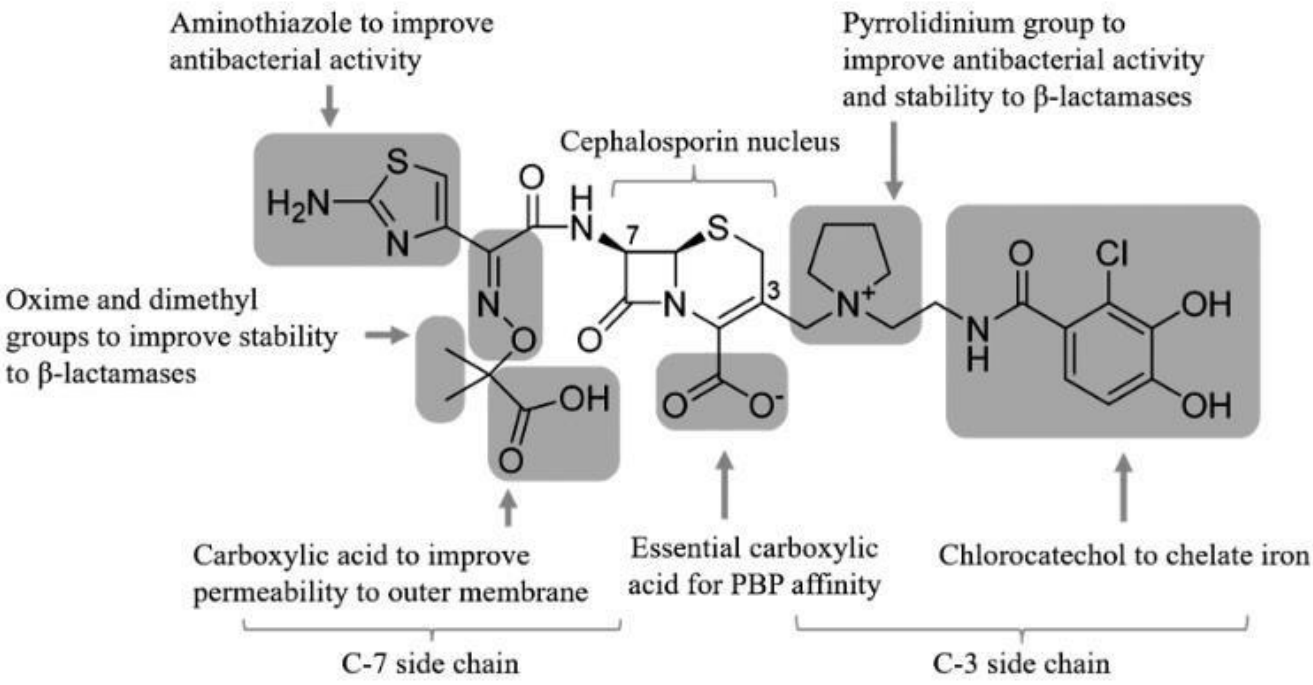

Figure 1. Molecular schematic of the structure of CFDC. Figure obtained from Sato and Yamawaki (2019).

1.4. Fe^{3+} Acquisition in *Kp*

For viability during *in vivo* infection, a Gram-negative bacterial cell must acquire Fe^{3+}. This is due to its essential requirement in a range of cellular processes, such as DNA replication and metabolism (Litwin and Calderwood, 1993; Caza and Kronstad, 2013). In a human body, as little as 10^{-18}M of Fe^{3+} is bioavailable within serum – approximately 7 times less than is required for the optimal proliferation of *Kp* (Nairz, Schroll, Sonnweber and Weiss, 2010). The rest is sequestered by host proteins including lactoferrin, transferrin, ferritin and haemoglobin (Cissé *et al.*, 2014; Folsom, Parker and Carlson, 2014). Therefore, *Kp* needs to compete for the iron, as Fe^{3+} depletion affects the cell envelope in ways which decrease pathogenesis and virulence. *Kp* does this by exporting high affinity Fe^{3+} acquisition proteins called siderophores out of the cell. An example of such is the catecholate type siderophore enterobactin (Raymond, 2003). The entrance of these siderophores back into the cell, together with chelated Fe^{3+}, is achieved *via* TonB-ExbB-ExbD-dependent signal transduction through catecholate receptor transporters called iron regulated outer membrane proteins (IROMPs). The binding of the Fe^{3+} ligand to a 22-stranded antiparallel β-barrel domain of these IROMPs induces a conformational change to the IROMP secondary structure, which essentially 'unplugs' the otherwise occluded permeability channel lumen (Noinaj, Guillier, Barnard and Buchanan, 2010; Braun, Ratliff, Celia and Buchanan, 2023). This initiates the hydrolysis of adenosine triphosphate (ATP) by the cross-linked tripartite protein complex TonB-ExbB-ExbD, which creates an electrochemical gradient (Kocer *et al.*, 2023). The resultant proton motive force generated drives the active transport of the siderophore-Fe^{3+} complex across the Gram-negative OM from the extracellular to intracellular space (Braun, 1995; Noinaj, Guillier, Barnard and Buchanan, 2010; Grinter and Lithgow 2019).

1.4.1. The Influx of Trojan Horse CFDC

The chlorocatechol moiety of CFDC confers an element of structural similarity between the antibiotic and the catecholate-type siderophore enterobactin (Zhanel *et al.,* 2019; Lan *et al.*, 2022). This allows CFDC to mimic the siderophore's action of Fe^{3+} binding (Yamano, Nakamura, Takemura and Echols, 2020). Consequentially, CFDC can itself act as a siderophore. Thus, the antibiotic is able to be taken

up into the bacterial cell in complex with sequestered Fe^{3+}, through hijacking the usual pathway of siderophore re-uptake: TonB-ExbB-ExbD-dependent IROMPs (Wu, Srinivas and Pogue, 2020; Daoud *et al.*, 2022; Rodríguez and González-Bello, 2023). Due to this trojan horse mode of entry, CFDC can bypass the selective permeability barrier of the OM. Therefore, CFDC has been shown to be able to overcome common AMR mechanisms of *Kp*, including mutations in OM porins (Karakonstantis, Rousaki and Kritsotakis, 2022). Despite this, CFDC resistance is increasing rapidly (Cruz-López *et al.*, 2022). To establish how *Kp* might resist the catechol-conjugated antibiotic, it is important to evaluate the core regulatory systems of *Kp* shown to possess a role in the Fe^{3+} iron uptake pathway.

1.5. Master Regulator FUR

Dynamic Fe^{3+} sensing, sequestration, storage and hence homeostasis in Gram-negative bacteria is primarily governed by the Ferric Uptake Regulator (FUR). FUR is universally recognised as the 'master controller' of Fe^{3+} cycling. When Fe^{3+} is sufficient, FUR in its holo- form binds to its divalent cation cofactor: ferrous iron (Fe^{2+}). This increases the affinity of holo-FUR to the DNA of transcription repressive 'FUR boxes', located on the promoter regions of a collection of iron uptake-associated genes (Yuan *et al.,* 2020). In this way, FUR limits toxic effects of excess Fe^{3+} accumulation, such as oxidative damage and mutagenesis (Escolar, Pérez-Martín and de Lorenzo, 1999; Santos, Batista and da Silva Neto, 2020). When Fe^{3+} is scarce, holo-FUR dimerizes to the apo-FUR state and releases Fe^{2+}. This gradually shifts the FUR box binding equilibrium and derepresses the transcription of the iron uptake-associated genes (Choi and Ryu, 2019; Hou *et al.*, 2023) (Figure 2). The known regulon under FUR control in Enterbacterales has been evidenced to include: the enterobactin biosynthetic gene cluster *entABCDFE* and *fes,* IROMP-associated genes *fhuABCDE*, *cirA, fiu, fepABCDEG, fecABCDE, tonB,* and *exbBD*, and Fe^{2+} acquisition gene, *feoB* (Lin *et al.*, 2011; Vajrala, Sayavedra-Soto, Bottomley and Arp, 2011; Seo *et al.*, 2014; Ho and Ellermeier, 2015).

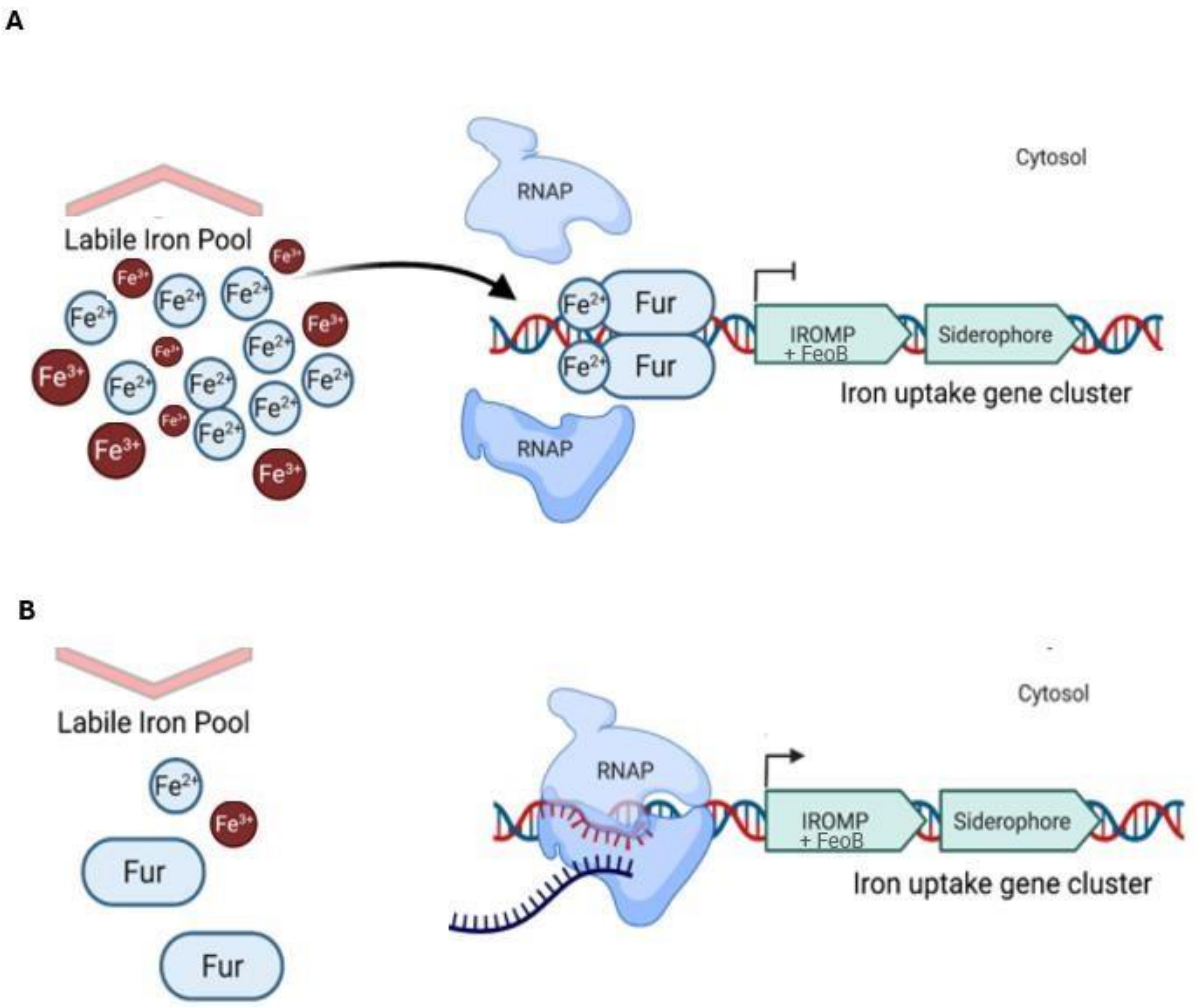

Figure 2. Schematic representation of siderophore, IROMP and FeoB regulation by FUR. A represents repression of iron uptake-associated gene transcription under iron repletion (high labile iron pool). **B** represents derepression of iron uptake-associated gene transcription under stress induced by iron limitation (low labile iron pool). Figure adapted and modified from Stanton (2022).

1.6. Two-Component Systems

Two-component systems (TCS) are a major regulatory protein class by which Gram-negative bacteria sense and respond to environmental stimuli (Tierney and Rather, 2019). TCS canonically consist of a histidine kinase sensor protein and a cognate response regulator effector protein. These systems are one of the most established mechanisms of Gram-negative bacterial signalling. When an external stressor, such as Fe^{3+} limitation, is sensed by the histidine kinase, the histidine kinase catalyzes the transfer of a phosphate group from ATP to its own histidine residue. This is known as autophosphorylation (Rajput *et al.*, 2021). This phoshate is then transferred to the aspartate residue

of the response regulator. Following this, the response regulator enters a state of activation. This allows its binding to promoter regions of select genes, resulting in differential expression of a specific regulon (Groban *et al.*, 2009; Li *et al.*, 2023) (Figure 3). Two specific TCS implicated in contributing to CFDC resistance in *Kp* are EnvZ-OmpR and BaeSR.

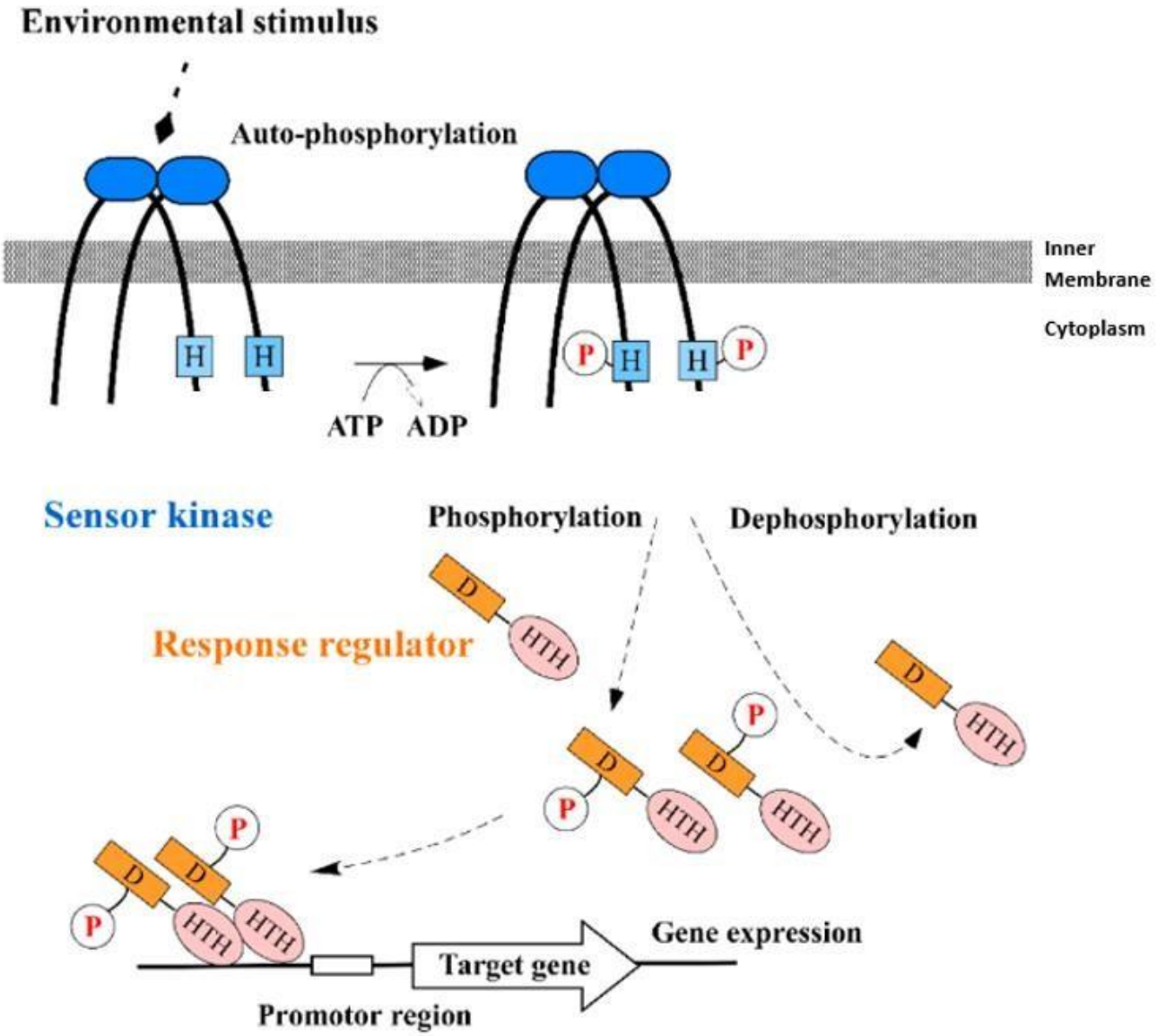

Figure 3. Schematic representation of TCS activation and subsequent control of genetic transcription. The schematic shows the initial autophosphorylation of the sensor kinase's histidine residue (denoted H) in an ATP hydrolysis-dependent manner. The kinase then transfers its phosphate group to the cognate response regulator's conserved receiver domain, being the aspartate residue (denoted D). This causes response regulator activation, and the regulator is then able to bind to the promotor regions of genes *via* its helix-turnhelix domain (denoted HTH) to influence target gene expression. Figure obtained from Hirakawa, Kurushima, Hashimoto and Tomita (2020).

1.6.1. The TCS EnvZ-OmpR and its Regulon

Clinical isolates of *Kp* exhibiting CFDC resistance are being increasingly reported to harbour overexpression mutations in the histidine kinase gene *envZ* (Coppi *et al.,* 2022; Simner *et al.,* 2022; Ko and Choi 2022; Stanton, 2022; Padovani *et al.*, 2023). This results in constitutive *envZ* autophosphorylation, leading to constitutive *ompR* phosphorylation, and hence constitutive EnvZOmpR activity. The specifics of how the constitutive activation of this TCS contributes to progressive CFDC resistance, however, are not well defined. EnvZ-OmpR is most frequently discussed across the literature in the context of its negative regulation of non-specific OM porin OmpK35, homologous to
OmpF of *Escherichia coli* (*E. coli*) (Mizuno and Mizushima, 1987; Zhang *et al.*, 2022; Zhou *et al.,* 2023). The loss of OmpK35 is well evidenced to confer β-lactam resistance in *Kp*, specifically to Cephalosporins, for which it is the primary entry channel (Sugawara, Kojima and Nikaido, 2016; Shen *et al.*, 2017). However, this porin has also been repeatedly evidenced not to be involved in facilitating CFDC influx into the cell: studies record any change to CFDC minimum inhibitory concentration (MIC) following OmpK35 loss-of-function to be insignificant (Ito *et al.*, 2018; Poirel, Sadek, Kusaksizoglu and Nordmann, 2022; Kaye, Naas, Pogue and Rossolini, 2023; Schaufler *et al.*, 2023). Thus, these data strongly suggest that constitutively active EnvZ-OmpR does not contribute to CFDC resistance through its regulation of this porin.

As mentioned above, CFDC is known to enter the bacterial cell *via* IROMPs (Daoud *et al.,* 2022). The specific IROMPs suggested to be most relevant to CFDC influx are CirA, Fiu, FepA and FecA (Sato and Yamawaki, 2019; Stanton, 2022; Domingues, Lima, Saavedra and Da Silva, 2023; Padovani *et al.,* 2023). These IROMPs are not only under negative regulation by FUR, but are also known to be under negative regulation by EnvZ-OmpR (Lundrigan and Earhart, 1981; Leaden *et al.*, 2018; Zhang *et al.*, 2022; Stanton, 2022).

CirA, FepA and FecA have been shown to be indirectly regulated by EnvZ-OmpR through a negative feedback loop orchestrated by the small RNAs (sRNAs) OmrA and OmrB (Noinaj, Guillier, Barnard and Buchanan, 2010). Under iron limitation in wild type Enterobacterales, *ompR* expression initially increases (Ramos *et al.*, 2016; Gerken, Vuong, Soparkar and Misra, 2020; Avican *et al.* 2021). This triggers the increased expression of *omrAB* (Brosse, Korobeinikova, Gottesman and Guillier, 2016). OmrA and OmrB then associate with the RNA binding chaperone protein Hfq. This promotes base

pairing of the sRNAs with cognate mRNA of target genes *cirA, fepA* and *fecA*, which results in the transcriptional repression of these genes (Lodge, Williams and Brown, 1986; Møller *et al*., 2002; Stanton, 2022). When both *omrA* and *omrB* expression is increased past a certain threshold, the sRNAs eventually limit expression of their positive regulator, *ompR* (Guillier and Gottesman, 2006). This auto-regulatory feedback then results in the limitation of the expression of the sRNAs, hence derepressing the transcription of the three IROMP genes (Salvail, Caron, Bélanger and Massé, 2013; Brosse, Korobeinikova, Gottesman and Guillier, 2016). Interestingly, recent study by Stanton (2022), on the basis of study by Guillier and Gottesman (2006) and Guillier and Gottesman (2008), also evidenced this feedback loop to include transcriptional regulation of *fiu*.

EnvZ-OmpR is also known to be a positive regulator of Fe^{2+} acquisition protein FeoB (Salgado *et al.,* 2023). Activation of FeoB, by increasing the intracellular availability of holo-FUR divalent cofactor Fe^{2+}, induces IROMP repression, as well as repression of itself (Hou *et al.*, 2023) (**1.5.**; Figure 2).
Therefore, this introduces another simultaneous pathway by which EnvZ-OmpR can indirectly repress CirA, Fiu, FepA and FecA. This pathway is currently the most evidenced route by which EnvZ-OmpR represses *fiu* (Gerken, Vuong, Sparkar and Misra, 2020; Cunrath and Palmer, 2021).

Hence, the ability of EnvZ-OmpR to indirectly repress catecholate receptor transporters exposes a plausible mechanism through which the constitutive activity of this TCS may contribute to clinical CFDC resistance. This requires investigation. Both networks of wild type IROMP regulation by EnvZ-OmpR are outlined in Figure 4.

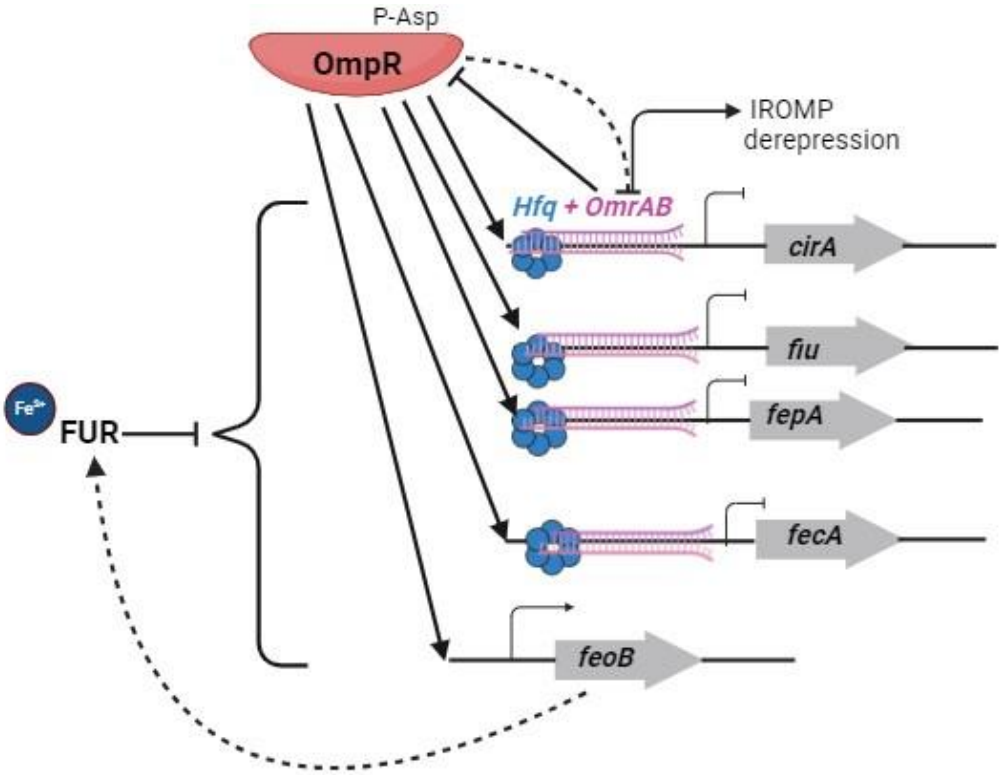

Figure 4. Schematic representation showing control of activated response regulator OmpR over IROMPencoding genes *cirA, fiu, fepA and fecA,* including the involvement of Hfq-dependent OmrA and OmrB, *feoB* and FUR. Figure created using https://biorender.com/ based on findings of Brosse, Korobeinikova, Gottesman and Guillier (2016), Gerken, Vuong, Soparkar and Misra (2020) and Stanton (2022).

1.6.1.1. CirA

CirA is the most broadly studied IROMP of CirA, Fiu, FepA and FecA (Klein *et al.*, 2022). The gene *cirA* is transcribed as monocistronic mRNA and is translated into a 663 amino acid length polypeptide chain, with its active β-barrel domain spanning amino acid 220 to 636 (Noinaj, Guillier, Barnard and Buchanan, 2010). The most common *cirA* alleles in *Kp* are *cirA1* and *cirA198* (Lan *et al.*, 2022). Of all the IROMPs, CFDC resistant clinical isolates of *Kp* are most frequently reported to exhibit a functional loss of CirA (McElheny *et al.*, 2021; Wang *et al.*, 2022; Arcari *et al.*, 2023, Freiberg *et al.*, 2024). However, surrounding *in vitro* studies have evidenced that CirA loss confers just a 2-fold decrease to CFDC susceptibility (Ito *et al.*, 2018; Kaye, Naas, Pogue and Rossolini, 2023; Schaufler *et al.*, 2023). Thus, these reports suggest that CirA may not be the primary IROMP responsible for CFDC influx, and hence, for the onset of clinical CFDC resistance.

1.6.1.2. Fiu

The gene *fiu* is transcribed as monocistronic mRNA and is translated into a 760 amino acid length polypeptide, with it's β-barrel domain spanning amino acid 180 to 760 (Grinter and Lithgow, 2019). Similarly to CirA, a large number of studies report CFDC resistant clinical isolates of *Kp* to demonstrate the functional loss of Fiu (Deroche *et al.*, 2023; Padovani *et al.*, 2023; Freiberg *et al.*, 2024). Interestingly, a multitude of *in vitro* studies have evidenced that deletion of both *fiu* and *cirA* confers synergistic 8 to 16-fold decreases in CFDC susceptibility (McCreary, Heil and Tamma, 2021; Yao, Wang, Chen and Cai, 2021; Nordmann *et al.*, 2022; Deroche *et al.*, 2023). Furthermore, investigations into monosulfactam and monocarbam catechol-conjugated antibiotics which failed to reach market, namely BAL30072 and MC-1, offer similar evidence for loss of efficacy to have been conferred by premature truncations of both Fiu and CirA concomitantly (Landman *et al.*, 2014; Tillotson, 2016; Page, 2019). Together, these studies concluded a possible combined lead role of the two IROMPs in the Gram-negative internalization of catechol-conjugated antibiotics, including CFDC. However, studies which investigate the relative CFDC susceptibility contribution of Fiu without CirA are lacking.

1.6.1.3. FepA

The IROMP-encoding gene *fepA* is transcribed as polycistronic mRNA with *fepBCDEG*, and is translated into a 746 amino acid length peptide. The active β-barrel domain of FepA spans amino acid 174 to 746 of the polypeptide chain – similar to the primary structure of Fiu (Moynié *et al.*, 2019; Nemati Zargaran *et al.*, 2021). Compared to CirA and Fiu, there is a significantly fewer number of studies which have investigated the association of FepA with CFDC resistance. Yet, CFDC susceptibility has been shown to be positively correlated with *fepA* expression (Daoud *et al.*, 2022). Further, two recent studies have evidenced a functional loss of FepA in a total of four CFDC resistant clinical isolates of Enterobacterales, two of which being from *Kp* (Zhang *et al.,* 2022; Padovani *et al.*, 2023). Together, this strongly implies FepA to possess a similar extent of importance in facilitating CFDC uptake as that suggested for the combination of Fiu and CirA. Again, however, a major gap to note across the literature is the lack of investigation into the independent relative contribution of FepA to catechol-conjugated antibiotic susceptibility. This is a limitation which also applies to the final IROMP of interest, FecA.

1.6.1.4. FecA

FecA is translated as a 744 amino acid length polypeptide following the transcription of *fecA* as a polycistronic mRNA with *fecBCDE*. The active β-barrel domain of FecA is situated at amino acid 255 to 774 (Krewulak and Vogel, 2008). Single study in *E. coli* evidenced FecA to be a lower affinity enterobactin receptor than FepA (Zhou, van der Helm and Venkatramani, 1995). Subsequently, single study has shown that under iron limitation in *E. coli,* the expression of *fecA* was of a lower level comparatively to both *fepA* and *cirA* (Daoud *et al.*, 2022). Together, both studies suggest FecA may have a less significant role in facilitating the influx of CFDC into *E. coli* relative to CirA, Fiu or FepA. However, thus far, no studies have investigated the impact of individual *fecA* deletion on CFDC susceptibility in *Kp*. Furthermore, recent study reported two clinical isolates of CFDC resistant *Kp* to possess non-functional FecA proteins (Padovani *et al.*, 2023). Therefore, the independent relative contribution of FecA in facilitating CFDC influx in *Kp* should not be overlooked.

1.6.2. The TCS BaeSR and its Regulon

Much like EnvZ-OmpR, clinical isolates of *Kp* displaying resistance to CFDC are also being increasingly reported to possess overexpression mutations in the histidine kinase gene *baeS* (Coppi *et al.,* 2022; Padovani *et al.,* 2023). This results in constitutive *baeS* autophosphorylation, constitutive *baeR* phosphorylation, and hence constitutive BaeSR activity. Thus, BaeSR has also been implicated to contribute to progressive CFDC resistance. Yet, again much like EnvZ-OmpR, the specifics of how it does so remain poorly understood (Yamano, Nakamura, Takemura and Echols, 2020; Simner *et al.*, 2021; Klein *et al.,* 2022). BaeSR is a known regulator of over 60 genes, associated with a range of functions including chemotaxis, flagellum biosynthesis and the transport of maltose (Nagakubo, Nishino, Hirata and Yamaguchi, 2002; Li, Plésiat and Nikaido, 2015). However, genes of the BaeSR regulon which are of specific relevance to this thesis are the positively regulated multicistronic operon *mdtABCD* and the gene *acrD*. Respectively, these encode components of the resistancenodulation-division (RND) family efflux pumps MdtABC-TolC and AcrA-AcrD-TolC (Nishino, Honda and Yamaguchi, 2005).

1.6.2.1. MdtABC-TolC and AcrA-AcrD-TolC

MdtABC-TolC and AcrA-AcrD-TolC are tripartite efflux pumps anchored to the OM which facilitate the export of substrates, including antibiotics, out of the cell (Zgurskaya, Krishnamoorthy, Ntreh and Lu, 2011). Both are therefore well known intrinsic resistance determinants, evidenced to confer an MDR phenotype of *Kp* against a range of antimicrobials including Fosfomycin, Oxacillin, Norfloxacin and Novobiocin (Baranova and Nikaido, 2002; Nishino *et al.*, 2003; Leblanc, Oates and Raivio, 2011; De Gaetano *et al.*, 2023). Yet, their role in the Gram-negative resistance of catechol-conjugated antibiotics has been significantly less studied.

MdtABC-TolC and AcrA-AcrD-TolC have previously been shown to efflux enterobactin. Studies by Bleuel *et al.* (2005) and Horiyama and Nishino (2014) found the combined deletion of both *mdtABC* and *acrD* to confer the synergistic effect of significantly decreasing enterobactin export from *E. coli* under iron limitation. Importantly, the conjugation of CFDC with a chlorocatechol moiety means the antibiotic possesses an element of structural similarity to enterobactin, as prior mentioned (Zhanel *et al.*, 2019; Lan *et al.*, 2022). Thus, since the publishing of these studies, there has been speculation that these efflux pumps may also be able to efflux CFDC under iron limitation (Rebizant, 2022; Liu *et al.*, 2023; Kriz *et al.,* 2024). Thus, this exposes a potential pathway through which BaeSR may contribute to clinical CFDC resistance when constitutively active, which is important to investigate. However, only single study thus far has tested the impact of the loss of either MdtABC-TolC or AcrAAcrD-TolC on CFDC susceptibility. Ikawa, Yamasaki, Morita and Nishino (2022), in deleting *mdtABC* in *E. coli*, evidenced only a 2-fold decrease in CFDC MIC under conditions of iron repletion. No studies have performed CFDC susceptibility testing on MdtABC-TolC or AcrA-AcrD-TolC deleted strains in *Kp* under iron limitation. Importantly, from these studies combined, any isolated relative contribution of MdtABC-TolC or AcrA-AcrD-TolC to enterobactin efflux and associated possible CFDC efflux from *Kp* under iron limitation remains ambiguous.

1.7. The AraC-type Regulator RamA

RamA is a member of the family of AraC/XylS transcription factor proteins in *Kp*, and is homologous to the global regulator MarA of *E. coli* (Cramer and Eikmanns, 2007). In wild type *Kp*, the expression of *ramA* is negatively regulated by TetR-type family regulator RamR (De Majumdar *et al.*, 2015). Thus, basal expression levels of *ramA* are usually low. However, the functional loss of RamR, and therefore the overexpression of *ramA*, which renders RamA constitutively active, has been reported in numerous clinical isolates of MDR *Kp* (Molitor *et al.*, 2018). Thus, RamA is an attractive target for AMR research. RamA is a known regulator of several genes involved in the biosynthesis of Gram-negative OM lipopolysaccharide (LPS) component, lipid A. Further, RamA is known to negatively regulate OM porin OmpK35 (sharing regulatory control with EnvZ-OmpR), and positively regulate RND family tripartite efflux pump AcrAB-TolC (Bailey *et al.*, 2010; Jiménez-Castellanos *et al.*, 2016; Jiménez-Castellanos *et al.*, 2018; Cheng *et al.,* 2020; Xu *et al.*, 2021). Collectively, therefore, RamA reduces LPS negative charge, increases OM stability, and reduces OM permeability of *Kp*. This, in turn, leads to increased bacterial virulence, perturbed OM diffusion of antibiotics and lowered affinity of membrane active antimicrobial peptides to the OM (De Majumdar *et al.*, 2015). The overexpression of *ramA* in *Kp* has most commonly been reported to contribute to resistance against β-lactam antibiotics Ceftazidime, Tigecycline, and Chloramphenicol, as well as the Polymyxin class of antibiotic, Colistin (Li, Plésiat and
Nikaido, 2015; Jiménez-Castellanos *et al.*, 2016; Jiménez-Castellanos *et al*., 2018; Stanton, 2022).

The expression of *ramA* has been evidenced to increase under iron limitation (Avican *et al.*, 2021). Moreover, the prior mentioned studies by Bleuel *et al.* (2005) and Horiyama and Nishino (2014) also reported the deletion of *acrAB* in combination with *mdtABC* and *acrD* to confer a synergistic reduction in enterobactin export from *E. coli* under iron limitation. Therefore, AcrAB-TolC has also been speculated to be able to efflux CFDC from Enterobacterales (Liu *et al.*, 2023; Kriz *et al.,* 2024). Hence, it has been suggested that the constitutive activity of RamA may be a contributing factor in clinical CFDC resistance (Stanton, 2022). This is an important avenue to investigate. Additionally, despite its known regulation of a range of OM permeability factors, it remains unknown whether RamA may regulate the IROMPs, MdtABC-TolC or AcrA-AcrD-TolC. Thus, it remains unknown whether RamA could act to reduce *Kp* susceptibility to CFDC under iron limitation through the same pathways by which EnvZ-OmpR and BaeSR have been speculated to do so.

1.8. The Exopolysaccharide Capsule

In discussing core *Kp* regulatory systems and the associated OM permeability factors speculated to impact CFDC susceptibility, it is important to also discuss the exopolysaccharide capsule. The exopolysaccharide capsule is a glycosidic bond-linked mucoid layer which is covalently anchored to the external surface of the Gram-negative OM (Rendueles, 2020). Approximately 79 different chemical structures of capsule have been identified in *Kp* (Hsu *et al.,* 2016). To note, not all strains of *Kp* are capsular, however one example is *Kp* 52145, which possesses major capsular serotype K2 (Wang *et al.*, 2019). The presence of a K2 capsule is a significant pathogenic virulence determinant for pyogenic liver abscess formation. This is partly due to the capsule's role in increasing adherence of *Kp* to the host's intestinal wall, facilitating sustained infection (Rice, 2012; Zapun, Contreras-Martel and Vernet, 2008). The K2 capsule has been previously reported to contribute to resistance of βlactam Carbapenems, by acting as a physical barrier inhibiting antibiotic entry into the cell (Lin *et al.*, 2014; Opoku-Temeng, Kobayashi and DeLeo, 2019). At present, there is no evidence to suggest that the extracellular export or uptake of catecholate-type siderophore enterobactin is affected by the K2 capsule (Buffet, Rocha and Rendueles, 2021). However, the effect of the K2 capsule on *Kp* susceptibility to catechol-conjugated antibiotic CFDC has yet to be investigated.

1.8. Significance, Summary and Rationale

Severe antibiotic-resistant infections have increased mortalities from 2,110 to 2,202 per annum from 2021 to 2022 in the UK alone (Chen *et al.*, 2022). Therefore, understanding the physiological mechanisms by which clinically threatening Gram-negative pathogens such as *Kp* resist last-line agent CFDC is paramount to help circumvent the spread of AMR and save lives.

To summarize, the re-modelling of the Gram-negative bacterial OM in response to iron limitation is vital to maintain pathogenic viability *in vivo*. To obtain sufficient Fe^{3+} to perform essential cellular processes, Gram-negative bacteria release high affinity Fe^{3+} chelators called siderophores, an example of which being the catecholate-type siderophore enterobactin. The efflux of enterobactin has been shown to occur synergistically through RND family of efflux pumps MdtABC-TolC, AcrA-AcrDTolC and AcrAB-TolC (Bleuel *et al.,* 2005; Horiyama and Nishino, 2014). The re-uptake of enterobactin in complex with Fe^{3+} has been shown to occur through IROMPs CirA, Fiu, FepA and FecA (Leaden *et al.,* 2018; Sato and Yamawaki 2019). The modified Cephalosporin CFDC, introduced in attempts to tackle MDR Gram-negative bacteria including *Kp*, is able to mimic enterobactin's Fe^{3+}

binding due to its conjugation with a chlorocatechol moiety on its C-3 side chain (Ito *et al.*, 2016; Ito *et al.*, 2018). Hence, CFDC can hijack the Fe^{3+} transportation system, acting as a trojan horse to gain cellular entry through the IROMPs. However, the chlorocatechol moiety of CFDC confers an element of structural similarity between this antibiotic and enterobactin. Therefore, studies have speculated that the RND family of efflux pumps MdtABC-TolC, AcrA-AcrD-TolC and AcrAB-TolC may also be able to efflux CFDC (Rebizant, 2022; Liu *et al.,* 2023; Kriz *et al.,* 2023). The TCS EnvZ-OmpR is known to negatively regulate the transcriptional expression of *cirA, fiu, fepA* and *fecA* (Guillier and Gottesman 2008; Stanton 2022). The TCS BaeSR is known to positively regulate the transcriptional expression of *mdtABC* and *acrD* (Nishino, Honda and Yamaguchi, 2005). The AraC-type regulator RamA is known to positively regulate the transcriptional expression of *acrAB* (De Majumdar *et al.*, 2015). Therefore, all three regulators have been individually implicated in reducing the susceptibility of *Kp* to CFDC (Daoud *et al.,* 2022; Simner *et al.,* 2022; Stanton, 2022). However, available studies which address the topic of CFDC resistance in *Kp* present the frequent limitations of: proportionally neglecting investigation into the CFDC susceptibility impact of FepA and FecA relative to CirA and Fiu, failing to investigate the independent relative contribution of each IROMP and the RND family of efflux pumps on

CFDC susceptibility, and ultimately failing to establish the cumulative contribution of EnvZ-OmpR, BaeSR and RamA to CFDC inefficacy. Therefore, the rationale of the present study is to close these gaps in understanding and elucidate a clarified mechanism by which *Kp* withstands catecholconjugated antibiotic challenge. To this end, the primary, overarching objective of this work is to establish how *Kp* resists CFDC under iron limitation through EnvZ-OmpR, BaeSR and RamA (Figure 5).

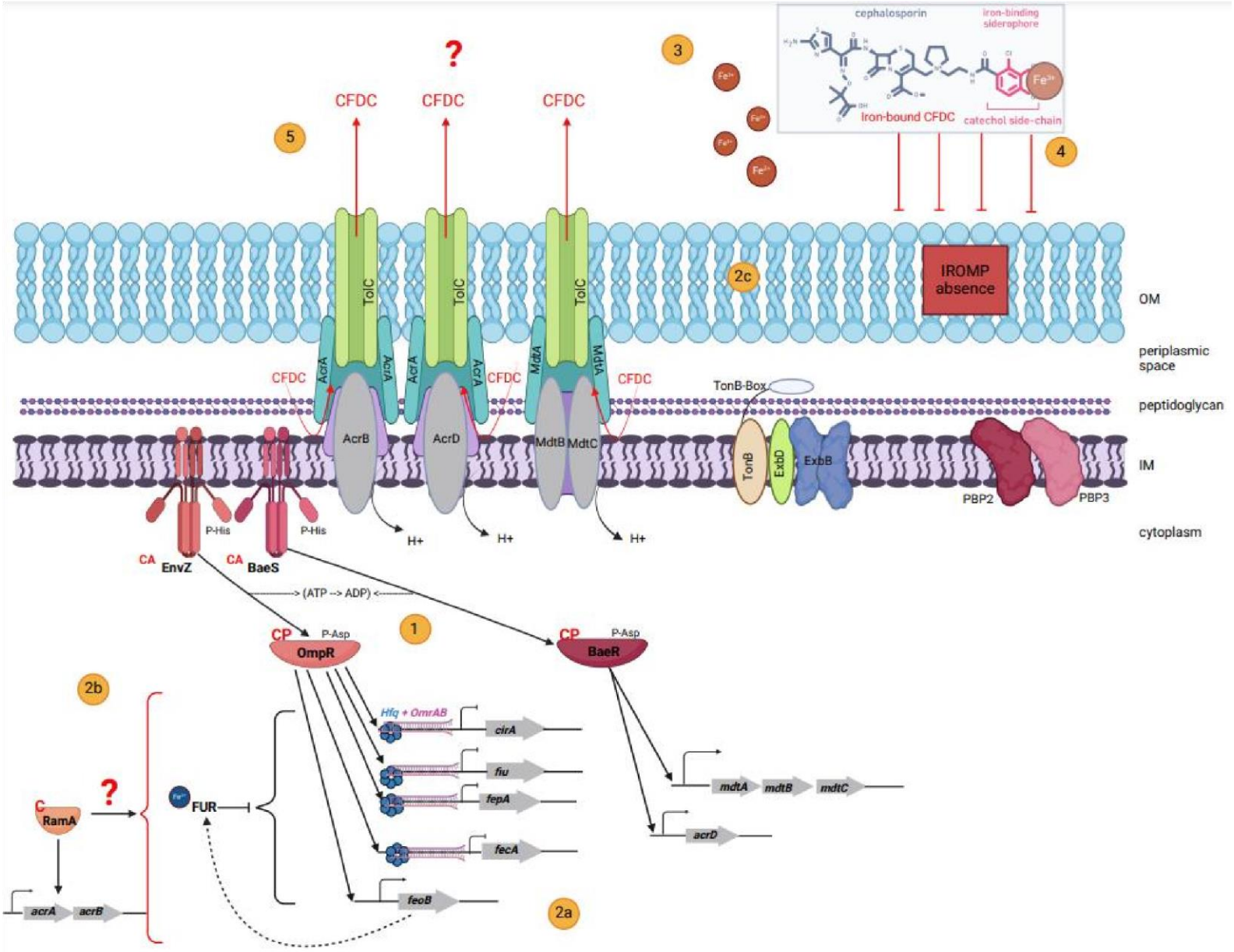

Figure 5. Regulatory pathways of constitutively active EnvZ-OmpR, constitutively active BaeSR and constitutively active RamA under iron limitation and their proposed involvement in the resistance of *Kp* to CFDC. The figure shows **1)** Constitutively autophosphorylated (CA) TCS histidine kinases EnvZ and BaeS, resulting in constitutive phosphorylation (CP) of TCS response regulators OmpR and BaeR. **2a)** Subsequent transcriptional repression of IROMP genes due to lack of *omrAB* negative feedback under constitutive activity of EnvZ-OmpR, and transcriptional activation of RND efflux pump genes *mdtABC* and *acrD* under constitutive activity of BaeSR. **2b)** The constitutive activation (C) of RamA and subsequent activation of *acrAB*, with a possible regulatory role of RamA on IROMP, *mdtABC* and *acrD* expression postulated. **2c)** Post-transcriptional and post-translational activity of the key RND efflux pumps MdtABC-TolC, AcrA-AcrD-TolC and AcrAB-TolC, and the absence of the IROMPs CirA, Fiu, FepA and FecA from the OM. **3)** Binding of siderophore antibiotic CFDC with available Fe^{3+} in the extracellular mileu. **4)** Inhibited influx of the CFDC-Fe^{3+} complex into *Kp* due to IROMP absence at the OM. **5)** Possible export of CFDC from the cell through RND efflux pumps MdtABC-TolC, AcrAAcrD-TolC and AcrAB-TolC. Figure created using https://biorender.com/ based on findings of Horiyama and Nishino (2014), Ito *et al.* (2018), Simner *et al.* (2021), Ikawa, Yamasaki, Morita and Nishino (2022), Lan *et al.* (2022), Poirel, Sadek, Kusaksizoglu and Nordmann (2022), Stanton (2022), Liu *et al.* (2023) and Schaufler *et al.* (2023).

1.9. Hypothesis and Aims

1.9.1. Overarching Hypothesis

Through cumulatively reducing OM permeability, the TCS EnvZ-OmpR, the TCS BaeSR and the AraC/XylS transcription factor RamA will decrease the susceptibility of *Kp* to CFDC under iron limitation.

1.9.2. Main Aims

- Investigate the effect of iron limitation on the RNA transcript expression of IROMP genes *cirA, fiu, fepA* and *fecA*, RND family of efflux pump genes *mdtB*, *acrD* and *acrB*, TCS response regulators *ompR* and *baeR* and AraC/XylS transcription factor *ramA* in wild type *Kp.*
- Elucidate how MdtABC-TolC, AcrA-AcrD-TolC, AcrAB-TolC, BaeSR and RamA, when absent or overexpressed, impact siderophore export from *Kp* under iron limitation.
- Assess how the IROMPs, MdtABC-TolC, AcrA-AcrD-TolC, AcrAB-TolC, EnvZ-OmpR, BaeSR and RamA, when absent or overexpressed, impact the susceptibility of *Kp* to CFDC under iron limitation.
- Determine whether RamA may impact the CFDC susceptibility of *Kp* in an iron limitation dependent manner through the same regulatory pathways as EnvZ-OmpR and BaeSR, by ascertaining the impact of *ramA* overexpression on the RNA transcript expression of the RND family of efflux pump genes *mdtB* or *acrD*, and IROMP genes *cirA, fiu, fepA and fecA*.

2. Materials and Methods

2.1. Bacterial Strains and Stock Preparation

See below for the list of strains employed in the present work (Table 1).

Strain Name	Source
Ecl8 (Schneiders Lab strain name TS62)	Fookes *et al.* (2013)
***Kp* 52145 (Schneiders Lab strain name TS440)**	Lery *et al.* (2014)
Ecl8*cirA*<km>	Schneiders Lab
Ecl8*acrAB*<km>	Schneiders Lab
Ecl8*mdtABC*<km>	This study
Kp 52145*mdtABC*<km>	This study
Ecl8*envZompR*<km>	Schneiders Lab
Ecl8*envZ*$_{L230Q}$	Schneiders Lab
Ecl8*omrA*<km>	Schneiders Lab
Ecl8Δ*fur*	Schneiders Lab
Ecl8*baeSR*<km>	Schneiders Lab
IDM1	Schneiders Lab
IDM7	Schneiders Lab
Ecl8Δ*ramR* (Schneiders Lab strain name TS68)	De Majumdar *et al.* (2015)
***Kp* 52145*ramR*<km>**	Schneiders Lab
Ecl8Δ*ramA*	De Majumdar *et al.* (2015)

Table 1. List of strains used in the present study.

For the preparation of strain stocks, cultures were frozen down in 1ml aliquots with 10% glycerol diluted from ≥99% absolute glycerol (Invitrogen, Thermo Fisher) and 90% LB and stored at -80°C.

2.2. Media Preparation

Luria bertani (LB) media was prepared as per manufacturer's instruction. LB agar was made using 7.5g of bacteriological grade granulated agar (Formedium), 5g NaCl (Sigma-Aldrich), 5g tryptone (Formedium) and 3.5g yeast extract (Oxoid) in 500ml sterile distilled water (SDW). All were autoclaved to sterilize, with agar stored at 60°C and media stored at room temperature.

For preparation of iron deplete and iron replete media, protocols were optimized from Ito *et al.* (2016) and Hackel *et al*. (2019), in concordance with the Clinical Laboratory Standards Institute (CLSI) recommendations currently used by Shionogi and colleagues and IHMA. One litre of autoclaved Cation Adjusted Mueller Hinton Broth (CAMHB) (22g BBL™ Mueller Hinton II Broth [Cation-Adjusted] [Becton, Dickinson and Company] in 1L of SDW) was stirred for 2h with 100g of Chelex 100 Resin (Bio-Rad) to chelate cations including Fe^{3+}. This was then filtered under vacuum using a 1L 0.2µm filter to remove the resin-cation complex. The pH was normalised to 7.2-7.4 using 6M HCl and supplemented with 561µl of 1M $CaCl_2$, 463µl of 1M $MgCl_2$ and 1ml 0.1M $ZnSO_4$ (final concentrations 22.5mg/L, 11.25mg/L and 0.56mg/L). The pH was re-normalised and the media filtered through 2x 500ml 0.2 µm filters. Iron concentration was confirmed as ≤0.03mg/L with the Visocolor HE Iron High Sensitivity Kit as per manufacturer's instruction (https://www.mn-net.com/StartpageWaterAnalysisTesting/VISOCOLOR/VISOCOLORHE/VISOCOLORHEIron/tabid/5044/language/en-US/Default.aspx.16). A 500µl volume of 0.1M Iron (III) Chloride ($FeCl_3$) (Sigma-Aldrich) solution was then added to 1x 500ml to achieve a 100µM final concentration. Iron repletion was considered successful at Visocolor concentration >0.15mg/L. Media were stored at 4°C with IDCAMHB+$FeCl_3$ wrapped in aluminium foil to account for $FeCl_3$ light sensitivity.

For preparation of respective agars, 5g of bacteriological grade granulated agar was added to 250ml of each media (Kolesnik-Goldmann *et al.*, 2023), autoclaved to sterilize and stored at 60°C.

2.3. Overnight Culture Preparation

Stationary phase culture was added to 5ml media to achieve a 1:1000 dilution. Cultures were incubated overnight at 37°C with 200 revolutions per minute (RPM) shaking to encourage sufficient growth and aeration after propagation and subculture. From plating, cultures were obtained from single colony.

2.4. Polymerase Chain Reaction (PCR) Techniques

Standard, colony and cloning PCRs were set up in Greiner Bio-one Sapphire PCR Consumables tubes and ran using the Techne® Prime Thermal Cycler with either the Thermo Cycler Phusion™ Plus DNA Polymerase Buffer Kit (Thermo-Fisher), or One*Taq* Quick-Load 2X Master Mix with Standard Buffer kit (New England Biolabs [NEB]) as per manufacturer's instructions (Table 2; Table 3). For each, 5-100ng of genomic deoxyribonucleic acid (gDNA) was extracted using the Wizard® Genomic DNA Purification Kit (Promega) for use as template with 10µM appropriate primers (Appendix I). Gel electrophoresis of PCR products was ran on 1% agarose (CSL-AG500 LE Multi-purpose agarose [Cleaver Scientific]) using GelRed Nucleic Acid Gel Stain (Biotium, UK) at 110v for ~35 minutes.

PCR Step	Temperature °C	Duration
Initial Denaturation	98°C	30s
Denature Template	98 °C	5s - 10s
Anneal Primers	60°C	10s
Extension	72°C	15s - 30s / kb (7.5kb approx. for pTOF *mdtABC* WT) (2kb approx. for all pKNGS mutants)
Final Extension	72°C	5 minutes
Hold	4°C	

Table 2. Standard three-step protocol PCR conditions using Phusion. PCR was ran for a standard 30 (25-35) cycles. Phusion DNA polymerase was used due to universal annealing temperature and duration irrespective of primer set.

PCR Step	Temperature °C	Duration
Initial Denaturation	94°C	30s
Denature Template	94°C	15-30s (optimized to 25s)
Anneal Primers	45°C - 68°C	15s – 60s (optimized to 45s)
Extension	68°C	1 minute / kb (7.5kb approx. for pTOF *mdtABC* WT) (2kb approx. for all pKNGS mutants)
Final Extension	68°C	5 minutes
Hold	4°C	

Table 3. Standard 30 cycle PCR conditions using One*Taq*. Annealing temperature with appropriate ramping was calculated for individual primer sets using Tm Calculator (NEB) (https://tmcalculator.neb.com/#!/main).

2.5. Cloning Techniques (Making of Mutants)

2.5.1. Non-Conjugative Homologous Recombination using pTOF

The protocol for homologous recombination exchange of chromosomal genes with a Kanamycin cassette in the pTOF plasmid was adapted from Merlin, McAteer and Masters (2002).

Plasmid constructs of DH10βpTOFNoCo*mdtABC*<km>, DH10βpTOFNoCo*cirA*<km> and DH10βpTOFNoCo*envZompR*<km> were provided by Schneiders Lab for use in the exchange protocol.

2.5.1.1. Plasmid DNA Extraction

Plasmid constructs were prepared for electroporation *via* DNA extraction using E.Z.N.A® Plasmid DNA Mini Kit I (Omega Bio-tek), as per manufacturer's instructions.

2.5.1.2. Restriction Digest

A 1µl volume of 10X FastDigest Green Buffer (Thermo Fisher Scientific) was added to a PCR tube. To this, 7µl of extracted plasmid DNA was added, with either 1µl of restriction endonuclease enzyme FastDigest SmaI (200µl) (Thermo Fisher Scientific) and 1µl SalI (1500U, 10U/µl) (Thermo Fisher Scientific), 2µl of restriction enzyme NotI (500U, 10U/µl) (Thermo Fisher Scientific) or 1µl of each of NotI and SmaI. The reaction mixture was incubated statically at 37°C for 20 minutes before banding visualization *via* 1% agarose gel electrophoresis at 110v for ~35 minutes.

2.5.1.3. Exchange

A 5µl volume of plasmid construct DNA was added to 100µl of Ecl8 or *Kp* 52145 electrocompetent cells. Content was transferred to an ice-cold 1mm brown cap electro cuvette for electroporation (Bio-Rad Gene Pulser Xcell™, Interface Version 3.15) using the pre-set bacterial protocol of '*E. coli* – 1mm, 1.8kV' to insert the plasmid construct into the bacteria. Electro cuvette contents was then immediately recovered by addition of 1ml LB before 1h shaking at 30°C, 450RPM. After centrifugation (13,200xg, 1 minute, 4°C), the pellet was resuspended with 100µl LB broth and plated on 2x LB+Km 50-100mg/ml antibiotic selection plates preceeding incubation overnight at 30°C.

Single transformant colony was isolated and incubated overnight with Chloramphenicol (Cm) 50mg/ml at 30°C with 200RPM shaking before diluting in phosphate buffered saline (PBS) to 10^{-6}, 10^{-8} and 10^{-10}. A 200µl volume of each was spread on duplicate LB+Cm 50mg/ml plates, with one incubated statically at 30°C and the other at 42°C overnight to initiate chromosomal exchange. Six colonies were selected from 42°C incubated plates, streaked onto fresh LB+Cm 50mg/ml and incubated at 42°C overnight to purify chromosomally integrated plasmids. From each streaking, 1 colony was pooled in LB+Kanamycin (Km) 50mg/ml and incubated at 30°C with 200RPM shaking to encourage plasmid resolution from the chromosome and loss from population. Cultures were re-inoculated 1:1000 into fresh LB+Km 50mg/ml before 30°C incubation with 200RPM shaking. Ten-fold serial dilutions were made as above and 100µl of each spread onto LB+Km 50mg/ml before 30°C overnight incubation. Up to 75 colonies were patched onto LB+Km 50mg/ml and LB+Cm 50mg/ml, and incubated overnight at 30°C.
Exchange was deemed successful if growth was observed only with Km.

If no Cm susceptible colonies were recovered, 5-10 colonies were streaked onto fresh LB and incubated at 42°C overnight in attempts to induce I-SceI endonuclease plasmid excision before

repeating patching. If this also produced no Cm susceptibility, from the six colony streak plates, 1 colony was re-pooled in LB, re-grown, re-inoculated 1:1000 into fresh LB with 10-fold dilutions made, but then plated on LB-NaCl+Km 50mg/ml + fresh 5% w/v ≥99.5% sucrose (Sigma-Aldrich) before patching.

Plates were then stored at 4°C preceeding PCR validation using the One*Taq* method as per **2.4.** with relevant Next, Cext and Kan-2 primers (see Appendix I).

2.5.2. Conjugative Homologous Recombination using pKNGS

Plasmid DNA of the amplified pKNGS suicide vector backbone was provided by Olaya Renduelas. Protocol for exchange, bacterial mating and positive selection for recombinants using pKNGS was adapted from (Nucci, Rocha and Rendueles, 2022).

2.5.2.1. Construction of Gene Flank Fragments for pKNGS Insertion

Phusion PCR was set up as per the method of **2.4.** utilizing 10µM Co and Ci or No and Ni primers (Appendix I) for the amplification of N- and C-terminus flanking regions of the gene of interest for deletion.

Following 1% agarose gel electrophoresis, bands were excised, and DNA extracted and purified using the GenElute Gel Extraction Kit (Sigma-Aldrich). Concentration was confirmed *via* nanodrop analyses (NanoDrop ND-100 spectrophotometer [LabTech, UK]) and gel electrophoresis repeated with 3µl of the CoCi and NoNi fragment DNA to re-confirm banding sizes. Eluted NoNi and CoCi fragment DNA was then carried forward for a secondary Phusion PCR requiring an isomolar volume of both overlap fragments alongside only No and Co primers (Appendix I).
Resultant NoCo construct banding sizes were again confirmed through gel electrophoresis preceding DNA band excision and purification. Concentration was confirmed *via* nanodrop analyses, and gel electrophoresis repeated with 3µl of the NoCo construct DNA to re-confirm banding sizes.

2.5.2.2. NoCo Construct Cloning into pKNGS Plasmid Vector (Assembly Ligation)

A 5µl volume of NEBuilder® HiFi DNA Assembly Master Mix was combined with the NoCo insert and linearized pKNGS plasmid vector DNA in the molar ratio of 6:1 in a PCR tube. NoCo fragment and pKNGS vector concentrations were adjusted to both 60ng:10ng and 90ng:15ng. Tubes were inputted into the Applied Biosystems Veriti™ 96 Well Thermal Cycler and ligation incubation set to 50°C for 15 minutes. The 60ng:10ng ligation product was cleaned up for electroporation using the MicroElute® Cycle-Pure Gel Extraction Kit (Omega Bio-tek), from which product was eluted with 20µl nuclease free water (Monarch NEB). The 90ng:15ng ligation product was not cleaned up as insert concentration was deemed sufficiently pure.

2.5.2.3. Exchange

A 5µl volume of ligation product was electroporated into 50µl of *E. coli* DH5α *pir* electrocompetent cells. After 48h, visible colonies were patched onto LB+Km 100mg/ml selection plates and incubated overnight at 30°C. NoCo-pKNGS DH5α *pir* construct clone patches were then validated for pKNGS backbone insertion *via* One*Taq* PCR with appropriate pKNGS verification primers (Appendix I). If banding was present, overnight culture was made from the corresponding patch and DNA extracted before PCR repeated to confirm banding size.

If there were no visible transformant colony successes from the One*Taq* PCR validation, PCR was repeated using the same colonies but with each reaction mixture containing 0.6µl (3%) Dimethylsulfoxide (DMSO) (Sigma-Aldrich) to aid in denaturing GC-rich template DNA. Electroporation was also repeated using the remaining 15µl of each FepA and Fiu 60ng:10ng clean ligation product, before repeating the PCR again with DMSO addition.

The NoCo-pKNGS *E. coli* DH5α *pir* construct clones were then transformed *via* electroporation into a conjugative donor strain: *E. coli* S17 MFD *pir* electrocompetent cells grown in LB and supplemented with 0.3mM diaminopimelic acid (DAP) (Sigma-Aldrich).

Single colony was streaked on LB+Km 100mg/ml+ 0.3mM diaminopimelic acid (DAP) with overnight culture made alongside. Recipient strains for mutation (Ecl8 and *Kp* 52145) were streaked on LB agar with overnight culture made and incubated overnight at 30°C and 37°C with 200RPM shaking, respectively. To set up the solid conjugation assay, 100µl of donor and recipient cultures were overlaid

on LB+0.3mM DAP plates before 30°C overnight incubation. Plates were flushed with 5ml PBS and 100µl plated on fresh LB+Km 100mg/ml, again incubated at 30°C overnight. If colony formation was too dense, 10^{-4} and 10^{-6} dilutions were made from cell suspensions and plating repeated. Six Km resistant transconjugants were streaked onto LB+Km 100mg/ml with single colonies from each then pooled in LB culture before re-incubation at 30°C 200RPM. A 100µl volume was then plated onto LB-NaCl+10% w/v sucrose, with control dilutions of 10^{-5} and 10^{-6} plated on LB-NaCl, and incubated again overnight at 30°C. Plasmid excision was validated by observing ~3 log difference in colony numbers between agar plates with and without sucrose. Approximately 20-30 colonies from LB-NaCl+sucrose plates were patched on LB+/-Km 100mg/ml. Km susceptibility indicated plasmid loss.

If all clones were Km resistant, more colonies from the LB-NaCl+sucrose plates were tested. If unsuccessful, patched colonies were pooled in LB and incubated 42°C 200RPM for I-SceI endonuclease induction, prior to 100µl plating of 10^{-4} and 10^{-6} dilutions on LB, before repeating patching. Lack of Km susceptible colonies at this stage meant plasmid excision had failed, and there could be no validation of recipient mutation conferral using Next and Cext primer One*Taq* PCR.

2.6. Capsule Quantification: Glucuronic Acid Assay

This protocol was adapted from Favre-Bonte, Joly and Forestier (1999). Overnight culture was centrifuged (13,200xg, 10 minutes, 4°C) and pellet resuspended with 1.5ml PBS before further 10 minute centrifugation. This was repeated before final resuspension in 1.5ml PBS and transfer of 500µl to a fresh 1.5ml eppendorf. A 100µl volume from a 50ml stock of capsule extraction buffer (0.5M anhydrous citric acid [Sigma] + 1% w/v Zwittergent® 3-10 [Merck Millipore] normalised to pH 2) was added, samples were diluted 4-fold, OD_{600} was measured and multiplied by 4 to normalise glucuronic acid concentration per 1 OD, avoiding spectrophotometric saturation. Eppendorfs were incubated at 50°C for 20 minutes before 5 minute centrifugation. A 300µl volume of supernatant was then transferred to fresh 1.5ml eppendorfs with 1.2ml ≥99.8% absolute ethanol (Formedium), followed by 30 minute 4°C incubation. Centrifugation was repeated for 20 minutes, with the supernatant carefully removed from the transparent pellet and the eppendorf airdried of solvent for 5 minutes at 42°C. The pellet was resuspended in 100µl SDW, 600µl capsule quantification buffer from a 10ml stock (12.5mM $Na_2[B_4O_5(OH)_4]$ [Sigma-Aldrich] in concentrated ≥99% H_2SO_4 [SigmaAldrich]) was added and the eppendorf stored on ice for 10 minutes, then incubated at 95°C for 5 minutes,

then on ice for a final 10 minutes. Absorbances were measured at OD_{520} and glucuronic acid concentration extrapolated from standard curve (Figure 6).

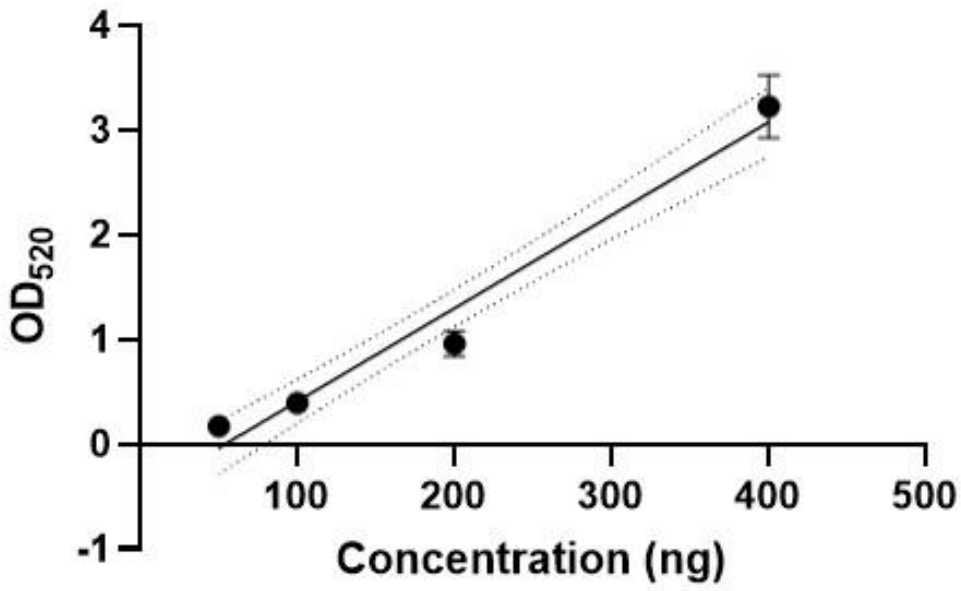

Figure 6. Blank-corrected standard curve for glucuronic acid concentration extrapolation. Standard curve was provided by Dr. Martin Vandeputte (PhD Student, TS Lab).

2.7. RNA Extraction for RT-(q)PCR

RNA was extracted from overnight culture at exponential phase OD_{600} using NEB Monarch Total RNA Minprep Kit (with lysozyme [Thermo-Fisher]). Concentration (ng/ml) and purity (A260/280 and A260/230) were measured by nanodrop analyses before immediate -80°C storage.

2.8. Real-Time Quantitative PCR (RT-[q]PCR) and Delta-Delta CT (ΔΔCT) Fold Change Analysis

2.8.1. Primer Efficiency

RT-(q)PCR primer efficiency was tested *via* standard curve measurement protocol optimized from https://www.thermofisher.com/uk/en/home/life-science/pcr/real-time-pcr/real-time-pcr-learningcenter/real-time-pcr-basics/real-time-pcr-troubleshooting-tool/gene-expression-

quantitationtroubleshooting/poor-pcr-efficiency.html. Ecl8 gDNA was diluted in 1:10 to concentrations of 50 ng/µl, 5ng/µl, 0.5ng/µl and 0.05ng/µl. A 2µl volume of each was added into 2x wells of a 96-well qPCR microplate (Lightcycler Type, White) (Starlab Group) in a vertical row. GoTaq® qPCR Master Mix (Promega) components excluding reverse transcriptase were combined with forward and reverse qPCR hexamer primers (Appendix I) as per manufacturer's instructions and added to each well.

Primer efficiency linearity was measured and optimal ratio of forward to reverse primer calculated. An efficiency of 90-110% allowed for use in a 1:1 (0.5µl:0.5µl) ratio. Primer efficiency values are shown in Appendix II.

2.8.2. RT-(q)PCR for Gene Expression Quantification

Protocol was followed as previously published (Rocha, Castro, Aguiar and Pacheco, 2020).

Briefly, RNA was diluted in nuclease free water to 12.5µg/µl and added to the 96-well RT-(q)PCR microplate at 25µg/well. GoTaq® RT-(q)PCR Master Mix components and hexamer primers of the gene of interest for amplification (Appendix I) were combined and added to each well according to manufacturer's instructions. The number of amplification cycles employed was optimized to 40, with housekeeping *16s* employed as reference standard gene. At the end of each PCR cycle, dissociation curves were generated to confirm amplification of genes. After RT-(q)PCR completion, RNA transcript expression ratios of the target gene under the test condition (e.g. from Ecl8 RNA extracted after growth in iron limited media [ID-CAMHB]) relative to that of the target gene under the control condition (e.g. from Ecl8 RNA extracted after growth in iron replete media [ID-CAMHB+$FeCl_3$]) was calculated according to the ΔΔCT method of Livak and Schmittgen (2001). From this, $\log_2$ fold change was calculated.

2.9. Chrome Azurol S (CAS) Agar Assaying

This protocol was adapted and optimized from Schwyn and Neilands (1987) and Himpsl and Mobley (2019).

Casamino acids (Formedium) were extracted *via* adding 10g to 10g of chelex in 90ml SDW and stirring for 2h before overnight separation and filtration through a 10ml Millipore syringe (BD Emerald) fitted with a 0.22µM filter. A 250ml stock of iron(III) solution was prepared (1mM $FeCl_3 \cdot 6H_2O$ [Sigma-Aldrich], 10mM HCl [Formedium]). This was followed by preparation of 10× MM9 Salts. Per 1L SDW, 3g of KH_2PO_4 (22mM), 0.5 g of NaCl (8.5mM), and 10 g of NH_4Cl (0.186M) were added, and the solution autoclaved to sterilize. For fume cupboard preparation of Fe^{3+}-CAS-HDTMA solution: in a 1L glass bottle, 605mg Chrome Azurol S (CAS) (Acros Organics) was dissolved in 500ml of SDW to 2mM concentration. A 100ml volume of the iron(III) solution and 400ml SDW containing 729mg of HDTMA (Sigma-Aldrich) (5mM concentration) solution were added, autoclaved and incubated at 60°C.

A 6g measure of NaOH (Sigma-Aldrich) was dissolved in 750ml SDW to a 0.2M concentration. A 30.24g measure of 1,4-piperazinediethanesulfonic acid (PIPES) (free acid) (Sigma-Aldrich) was stirred into solution to a 13mM concentration. To this, 100ml 10x MM9 salts and 15g Bacteriological grade granulated agar (Formedium) were added before autoclaving and 60°C incubation. A 30ml volume of 10% casamino acids, 10ml of 20% glucose (Sigma-Aldrich), 1ml of 1M $MgCl_2$ (Sigma-Aldrich), 1ml of 0.1M anhydrous $CaCl_2$ (Melford), 1ml of 1% nicotinic acid (Sigma-Aldrich) and 1ml of 1M $MgSO_4 \cdot 7H_2O$ (Merck Millipore) were then added with 100ml of the Fe^{3+}-CAS-HDTMA. Agar was stored at 60°C until use within 3 weeks. Poured plates were allowed to solidify overnight at room temperature before immediate use.

From overnight cultures standardized to OD_{600} 1.5, 5µl droplets were evenly inoculated to plates before incubation at 30 °C overnight (minimum 18h) before measuring mm diameters of orange halos surrounding the deposited culture droplets.

2.10. Antibiotic Susceptibility Testing

Susceptibility testing was performed in compliance with Clinial and Laboratory Standards Institute (CLSI) guidelines and clinical breakpoint values version M100 ED34:2024. (https://clsi.org/standards/products/microbiology/documents/m100/). The below protocols were adapted and optimized from Ito *et al.* (2016), Ito *et al.* (2018) and Kolesnik-Goldmann *et al*. (2023).

2.10.1. Disk Diffusion

Overnight cultures were diluted to OD_{600} 0.42 - matching 0.5 McFarland Standard cellular density as per CLSI recommendation. Plate agar surface was evenly swabbed with inoculum in three different directions, ensuring no gaps. CFDC and CAZ 30µg disks (Fisher) stored at 4°C were added to the plates with even spacing before incubation at 37°C overnight. Results were examined *via* measuring the diameter (mm) of the zone of inhibition. Strains were classified as sensitive or resistant depending on the diameter measurement according to clinical breakpoints (Table 4).

Organism	**Antibiotic**	**Disk Content (µg)**	**Zone Diameter Breakpoint (mm)**	
			S ≥	**R<**
Enterobacterales	CFDC	30	22	22
Enterobacterales	CAZ	30	23	23

Table 4. Zone of Inhibition Breakpoints of antibiotic resistance applicable to both CFDC and CAZ. Table adapted from CLSI Clinical Breakpoints v. M100 ED34:2024, Yang *et al.* (2019) and Borde *et al.* (2023).

2.10.2. Broth Microdilution

Firstly, iron limited media (ID-CAMHB) was added into each well of a Scienceware® 12 well pipette reservoir (Millipore Sigma) in the volumes shown in Table 5. This was then repeated in a fresh 12 well pipette reservoir for iron replete media (ID-CAMHB+$FeCl_3$).

Broth Volume Added (µl)	2000	1000	3500	1500	1000	3500	1500	1000	3500	1500	1000	0
Reservoir Well	1	2	3	4	5	6	7	8	9	10	11	12

Table 5. Layout of initial media volume added to pipette reservoir during broth microdilution.

Next, CFDC powder (Shionogi) stored at 4°C was made up to 100mg/L stock concentration in 10ml saline and stored with opaque covering in 500µl aliquots at -20°C, with 4°C-stored CAZ powder (Sigma-

Aldrich) made up to 80mg/L stock concentration in 1ml SDW. From a 0.008mg/L dilution of antibiotic stock in ID-CAMHB or ID-CAMHB+$FeCl_3$, 2000µl, 1000µl, 500µl and 500µl was transferred to wells 12,11,10 and 9 respectively and mixed thoroughly. From well 9, 1000µl, 500µl and 500µl was transferred to wells 8,7, and 6. Then, 1000µl, 500µl and 500µl was transferred from well 6 to well 5,4 and 3. A final volume of 1000µl was added from well 3 to 2. 50µl from each well was then transferred to each of 12 vertical well rows of a round-bottomed 96 well plate (Corning® 96 Well Clear Polystyrene Round-Bottomed Microplate [Sigma-Aldrich]). Resultant antibiotic concentrations were as follows in Table 6.

Vertical Plate Row	1	2	3	4	5	6	7	8	9	10	11	12
Conc. (mg/L)	0	0.004	0.008	0.016	0.031	0.063	0.125	0.250	0.1	1	2	4

Table 6. Concentration of each vertical well row of the round-bottomed 96 well plate after media and antibiotic mixture pipetted during broth microdilution.

Overnight cultures were diluted with PBS to OD_{600} 0.01. A 50µl volume was transferred to each horizontal well of a 12 well row. Plates were incubated overnight at 37°C before observing for presence of a button-like pellet in each well. The first well in a horizontal row which was absent of a pellet was the MIC, interpreted according to CLSI clinical breakpoints (Table 7).

Organism	**Antibiotic**	**MIC Breakpoint (mg/L)**	
		S≤	**R>**
Enterobacterales	CFDC	4	16
Enterobacterales	CAZ	8	8

Table 7. Minimum Inhibitory Concentration breakpoints of antibiotic resistance applicable to CFDC and CAZ. Table adapted from CLSI Clinical Breakpoints v. M100 ED34:2024, Borde et al. (2023) and Yang et al. (2019).

2.11. Bioinformatics

Bioinformatic analyses was undertaken using pre-aligned nucleotide sequences of *cirA* and *fiu* in *Kp* lineage populations of sequence type (ST) 11, ST15 and ST258. Nucleotide sequences were provided by Jiayu Wang (PhD Student, TS Lab). The number of collated sequences used for each of the alignments of *cirA* and *fiu* totalled 1157, 848 and 1193 for each of ST11, ST15 and ST258, respectively. Nucelotide sequence alignments were then ran through ExPASy (Gasteiger *et al.*, 2003) to translate

nucleotide to amino acid. The amino acid sequences of both CirA and Fiu were then ran through MobaXterm Version 23.6 MAFFT (Katoh and Standley, 2013) followed by Mview (Brown, Leroy and Sander, 1998) to re-align and visualize. Distance trees were created on Interactive Tree of Life phylogenetic annotation tool (iTOL) (Letunic and Bork, 2021) to observe amino acid sequence clustering by geographical location (continent) of origin. From these clusters, population representative sequences were selected. Using Mview, sites of amino acid sequence substitutions were mapped and visualised relative to the CirA and Fiu amino acid sequences of reference strain *Klebsiella pneumoniae* KCTC 2242, sourced from NCBI (https://www.ncbi.nlm.nih.gov/). Substitution locations were then inputted into PolyPHen-2 (Polymorphism Phenotyping v2) (Flanagan, Patch and Ellard, 2010). This produced a predicted result of whether amino acid substitutions were deleterious (affecting protein structure and function) or tolerated (otherwise referred to as non-damaging: protein structure and function remain intact).

2.12. Statistical Analysis

Statistical analysis for RT-(q)PCR $\log_2$ fold change data relative to the baseline (0), disk diffusion zone of inhibition diameter data, CAS plate orange halo diameter data and OD_{520}-extrapolated glucuronic acid concentration data was performed using the student's two-tailed unpaired *t*-test on Excel due to equal between-group variance. The statistical significance threshold was set at $p<0.05$. Figures were made using GraphPad Prism version 10.2.2. (397). Statistical analysis was not performed for MIC values of broth microdilution susceptibility testing due to the data being geometric. A 4-fold or higher change in MIC was denoted biologically significant. A 2-fold change was considered to have fell within the range of experimental variability, so was hence labelled biologically insignificant margin of error threshold.

3. Results

3.1. CHAPTER ONE: Bioinformatics: Analysing the Integrity of IROMPs Prior to CFDC Exposure

Iron limitation results in the synthesis and export of catecholate-type siderophore enterobactin, and the derepression of its influx channels: the TonB-ExbB-ExbD-dependent IROMPs CirA, Fiu, FepA and FecA (Gerken, Vuong, Soparkar and Misra, 2020). The chlorocatechol moiety conjugated to the C-3 side chain of modified Cephalosporin CFDC allows this antibiotic to bind to Fe^{3+}, and thereby hijack enterobactin's IROMP transportation pathway to gain cellular entry (Ito *et al.*, 2018). Previous studies have reported that clinical isolates of CFDC resistant *Kp* exhibit functional losses of CirA, Fiu, FepA and FecA (Arcari *et al.*, 2023; Simner *et al.*, 2023; Freiberg *et al.*, 2024). However, of all four IROMPs, these losses are most frequently reported for CirA and Fiu (Deroche *et al.*, 2023; Padovani *et al.*, 2023). The functional loss of proteins is a result of nonsynonymous single nucleotide polymorphisms (SNPs) in the DNA nucleotide sequence, which cause changes in the amino acid sequence, known as substitutions. The amino acid substitutions then impact the structure and stability of the encoded protein, which results in dysfunction or non-function, for example through misfolding. These loss-offunction substitutions are referred to as being deleterious. In the context of the IROMPs CirA and Fiu, deleterious substitutions therefore confer reduced entry of CFDC into *Kp*. However, substitutions may not always impact the protein's structure and function. Substitutions can also be categorised as tolerated. An amino acid substitution being tolerated means that the usual function of the encoded protein remains intact despite the amino acid change – the substitution is hence non-damaging (Garofalo *et al.*, 2019). Thus, the purpose of this chapter was to investigate whether deleterious substitutions within the amino acid sequences of both CirA and Fiu proteins are already embedded within *Kp* populations prior to CFDC selection.

To ascertain whether damaging substitutions that could impact CFDC influx were present in the amino acid sequences of the proteins of interest: CirA and Fiu, bioinformatic analyses was undertaken. For these analyses, strains from Carbapenem-resistant *Kp* sequence types ST11, ST15 and ST258 were employed. These were chosen for analyses as they are diverse MDR *Kp* lineages of increasing public health concern due to their rapid dissemination - particularly across Eastern China, Europe and, more recently, the Americas (Xie *et al.*, 2021). Aligned amino acid sequences of each of CirA and Fiu were isolated from 1157, 848 and 1193 strains of each sequence type. There were no premature truncations found across the aligned sequences of each protein from each lineage, thus, all

sequences were imported into iTOL for creation of phylogenetic distance trees as per the method outlined in **2.11.**. CirA and Fiu amino acid sequences were clustered on the distance trees according to the continent from which the strain they were isolated from originated. One sequence was chosen from each cluster originating from the same continent to ensure a population representative sample was taken for analysis. These sequences were then inputted into Mview to observe substitutions relative to the respective CirA and Fiu amino acid sequences of a reference strain: being *Kp* KCTC 2242. To predict whether these substitutions would confer a deleterious or tolerated effect to protein function, the substitution and its position in the sequence was inputted into phenotyping tool PolyPHen-2 along with the *Kp* KCTC 2242 reference sequence. The PolyPHen-2 output scored the substitution on a scale of 0 to 1 to indicate the probability of the substitution being deleterious. A score of 0 indicated the substitution to confer a tolerant effect – displayed on a PolyPHen-2 output as being 'benign'. A score of 0.4 to 0.7 was indicative of a 'possibly' deleterious effect, with a score of 0.7 to 1 meaning a deleterious effect would highly likely be conferred (Flanagan, Patch and Ellard, 2010). The iTOL phylogenetic trees of *Kp* lineage sequence alignments for which amino acid substitutions were not found were not included in this text.

3.1.1. CirA

Of the CirA amino acid sequence alignments from the *Kp* lineages ST11, ST15 and ST258, substitutions were found only in ST11. The substitutions found were predicted by PolyPHen-2 to confer a tolerated impact. The iTOL distance tree of ST11 CirA amino acid sequences, showing continental clustering of sequences, the sequences chosen for Mview analysis from these clusters, and the substitutions recorded, are shown in Figure 7.

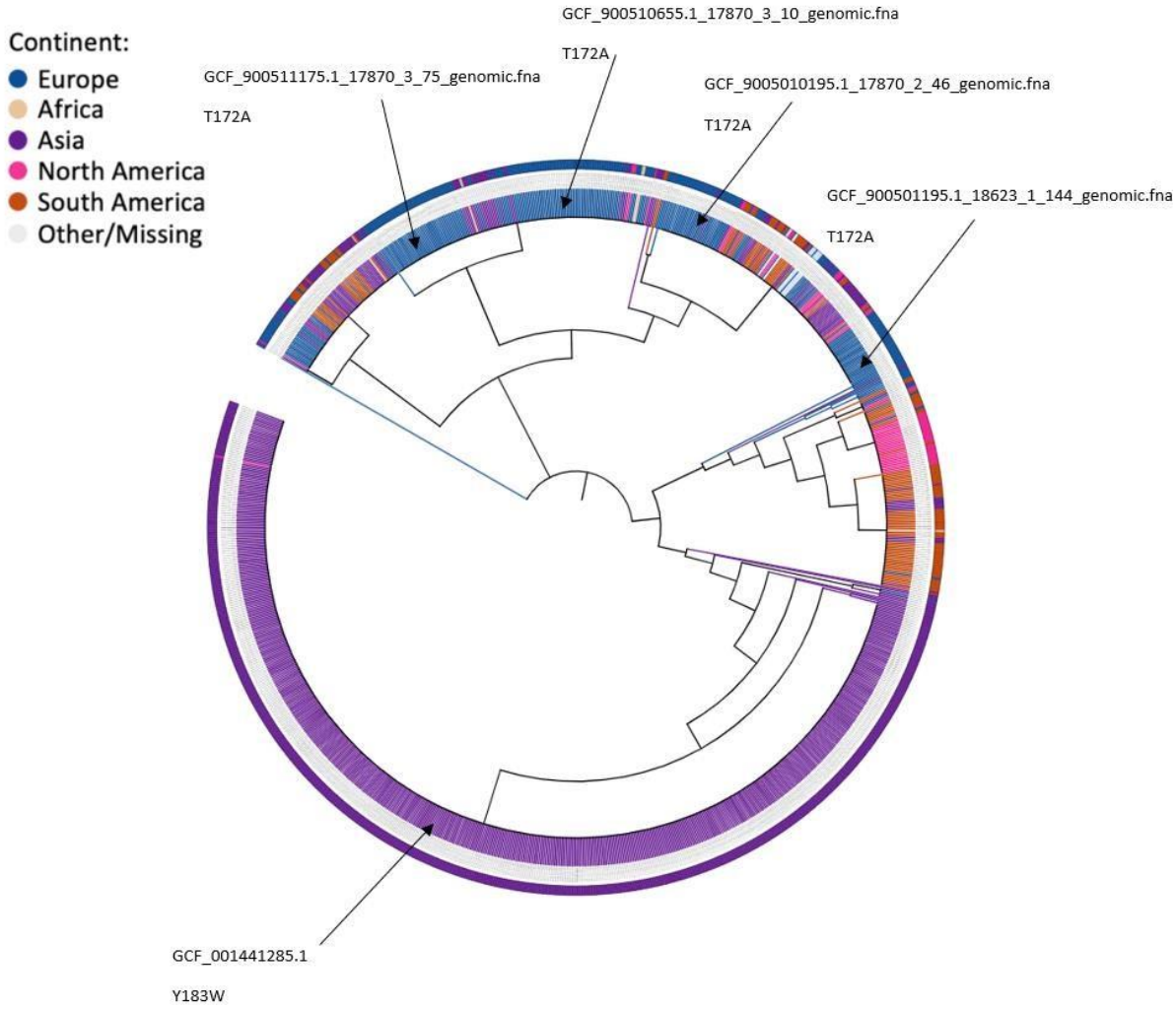

Figure 7. The iTOL distance tree of aligned CirA amino acid sequences from *Kp* ST11. The outermost ring of the tree shows a geographic colour strip map, which is reflected in the innermost ring of the tree for easier observation. The respective continent origin of each sequence cluster can be identified by colour coding using the attached Continent key. As shown for the single Asian cluster (in purple), the selected strain sequence (see name), after Mview input, was shown to harbour the substitution Y183W. As shown for each of the 4 European clusters (in blue), the selected strain sequences (see names) inputted into Mview with a reference sequence from strain *Kp* KCTC 2242 were shown to harbour the substitution T172A.

Figure 7 shows the iTOL distance tree output for CirA ST11 sequences to exhibit predominant clustering in the continents of Asia and Europe. Following Mview analysis of the chosen sequences from each continent, it was found that there was only 1 substitution in the sequences from Asia, and only 1 substitution in sequences from Europe. The recorded substitution in aligned sequences of Asian origin was the replacement of tyrosine with tryptophan at position 183 of the 633 amino acid length protein (Y183W). The substitution in aligned sequences of European origin was the replacement of threonine with alanine at position 172 (T172A). The substitutions from both Asian and European sequences, when inputted into PolyPHen-2, produced a 'benign' output with scores of 0.004 and

0.244, respectively. This meant both substitutions would confer a non-damaging effect to the structure, stability and function of CirA. The PolyPHen-2 outputs of both substitutions are shown in Figure 8.

A

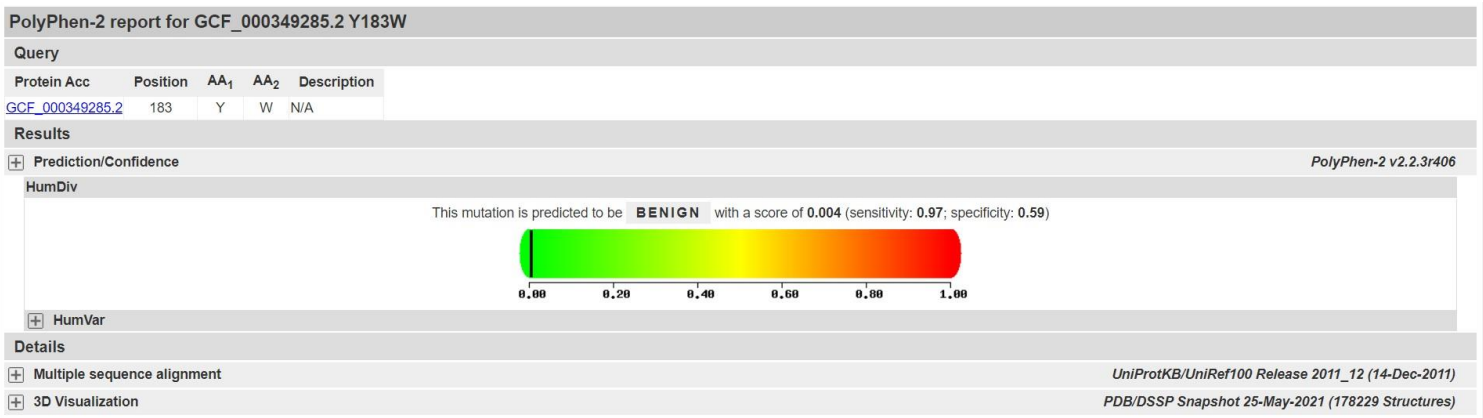

B

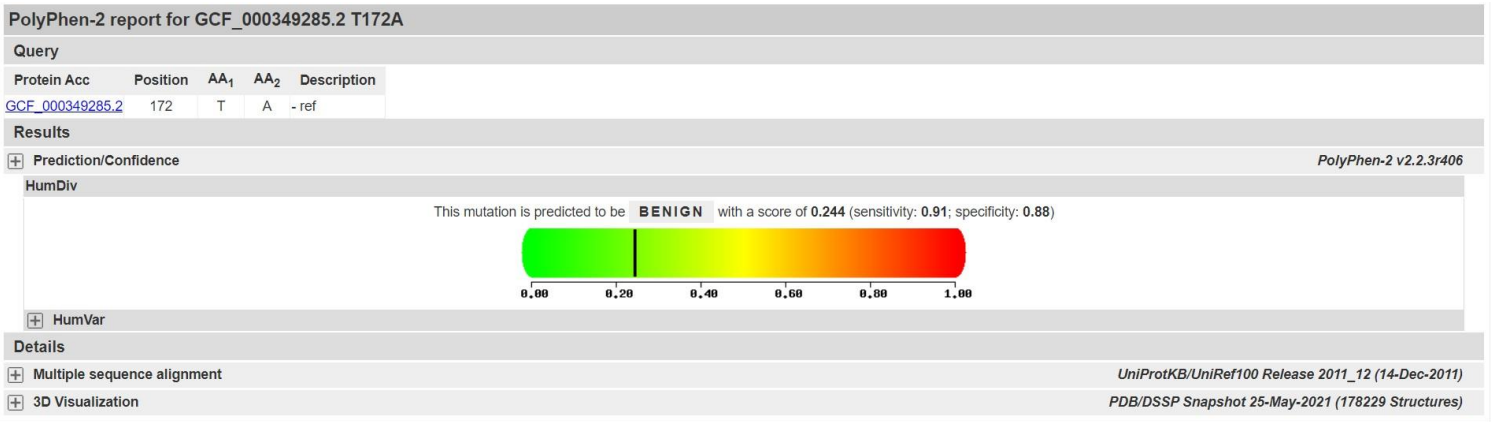

Figure 8. The results of PolyPHen-2 predictive profiling of amino acid substitutions found in *Kp* ST11 CirA amino acid sequences of Asian origin (Y183W) (A) and European origin (T172A) (B). Reports were generated under the name of the reference strain used (GCF_000349285.2). Scores were 0.004 **(A)** and 0.244 **(B).** The outputs also show sensitivity and specificity scores of 0.97 and 0.59 **(A)**, and 0.91 and 0.88 **(B)**, respectively. The sensitivity value corresponds to the true positive rate (the proportion of deleterious substitutions correctly predicted, represented as a value 0 to 1 correlating to 0% to 100%). The specificity value corresponds to the true negative rate (the proportion of tolerated substitutions correctly predicted, again represented as 0 to 1 correlating to 0% to 100%). Here, the sensitivity and specificity scores respectively indicate there was a low probability of the predictions being false negatives, and a moderate to high likelihood the substitutions had been correctly categorised.

3.1.2. Fiu

Of the Fiu amino acid sequence alignments from the *Kp* lineages ST11, ST15 and ST258, a substitution was found only in ST258. The substitution found was predicted by PolyPHen-2 to confer a tolerated impact. The iTOL distance tree of ST258 Fiu amino acid sequences, showing continental clustering of sequences, the sequences chosen for Mview analysis from these clusters, and the substitution recorded, are shown in Figure 9.

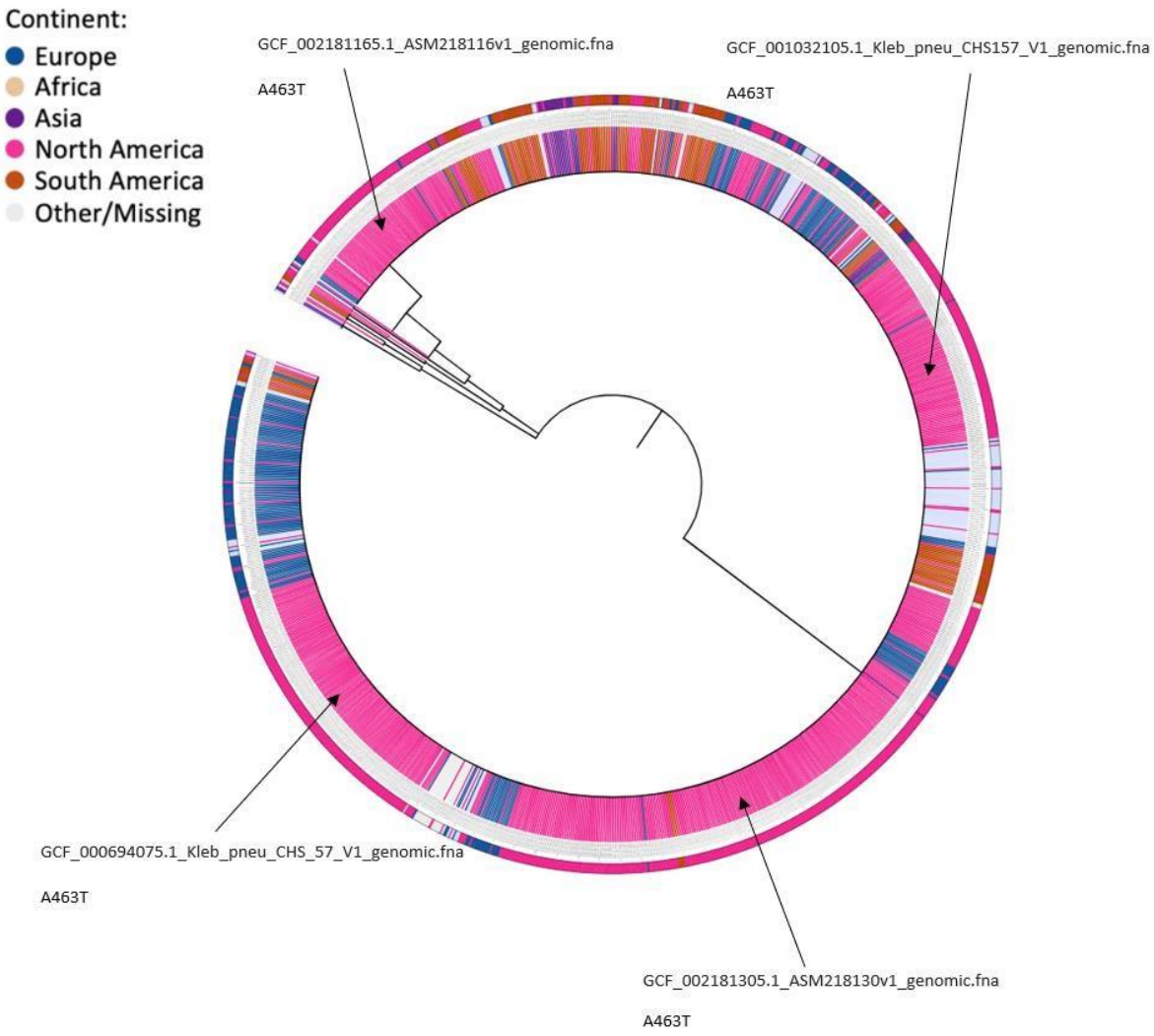

Figure 9. The iTOL distance tree of aligned Fiu amino acid sequences from *Kp* ST258. The outermost ring of the tree shows a geographic colour strip map, which is reflected in the innermost ring of the tree for easier observation. The respective continent origin of each sequence cluster can be identified by colour coding using the attached Continent key. As shown for each of the 3 North American clusters (in pink), the selected strain sequences (see names) inputted into Mview with a reference sequence from strain *Kp* KCTC 2242 were shown to harbour the substitution A463T.

The iTOL distance tree output for Fiu ST258 sequences showed clustering to be dominant in North America. Following Mview analysis of chosen sequences from the North American clusters, again only 1 substitution was recorded. This was a replacement of alanine with threonine at position 463 of the 760 amino acid length protein (A463T). The PolyPHen-2 output of this substitution again predicted a 'benign', non-damaging impact to Fiu structure and function with a score of 0.016, as shown in Figure 10.

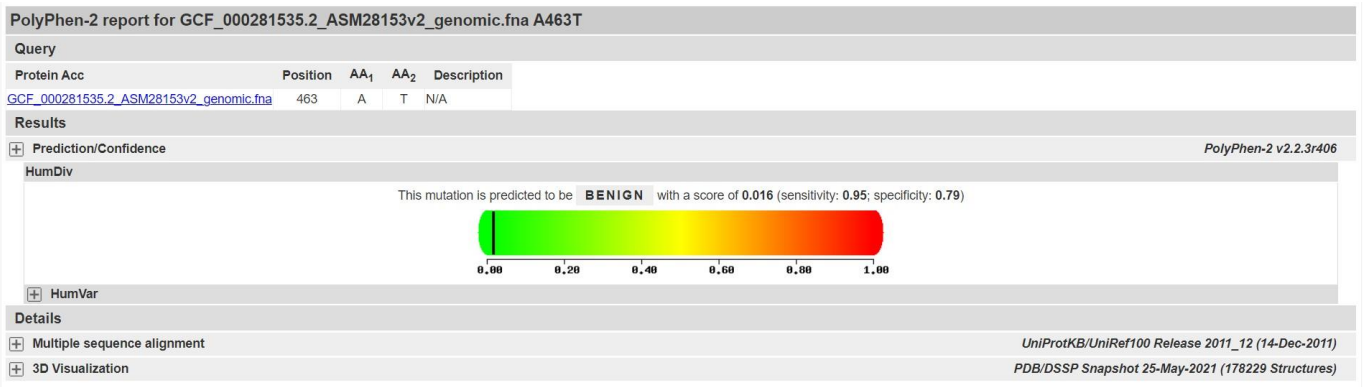

Figure 10. The result of PolyPHen-2 predictive profiling of an amino acid substitution (A463T) found in *Kp* ST258 Fiu amino acid sequences of North American origin. The report was generated under the name of the reference strain used (GCF_000281535.2_ASM28153v2_genomic.fna). The score was 0.016. The output also shows a sensitivity and specificity value of 0.95 and 0.79, respectively. The sensitivity value corresponds to the true positive rate (the proportion of deleterious substitutions correctly predicted, represented as a value 0 to 1 correlating to 0% to 100%). The specificity value corresponds to the true negative rate (the proportion of tolerated substitutions correctly predicted, again represented as 0 to 1 correlating to 0% to 100%). Here, the sensitivity and specificity scores respectively indicate there was a low probability of the prediction being a false negative, and a high likelihood the substitution had been correctly categorised.

Thus, to close, the bioinformatic analyses conducted on CirA and Fiu amino acid sequences isolated from clinically relevant MDR *Kp* lineages ST11, ST15 and ST258 evidenced no pre-exisiting deleterious substitutions embedded in the populations that could confer functional loss of either IROMP. These results therefore confirm the functional loss of IROMPs to be the consequence of selective pressure exerted by CFDC in the clinical setting. With functional losses of not only CirA and Fiu, but FepA and FecA, all being associated with the resistance of *Kp* to CFDC, this chapter thus prompted investigations to confirm the role of the IROMPs in facilitating the cellular uptake of CFDC into *Kp*. This was to be achieved through investigating the effect of IROMP loss on the susceptibility of *Kp* to CFDC.

3.2. CHAPTER TWO: Investigating the Influx of CFDC Through IROMPs

As introduced in Chapter One, IROMPs are the TonB-ExbB-ExbD-dependent siderophore receptors through which CFDC gains entry into *Kp* (Ito *et al.,* 2018). The IROMPs currently suggested to be of the most relevance to CFDC uptake are CirA, Fiu, FepA and FecA (Sato and Yamawaki, 2019; Domingues, Lima, Saavedra and Da Silva, 2023). Previous studies have reported that clinical isolates of CFDC resistant *Kp* exhibit the functional loss of these IROMPs (Arcari *et al.*, 2023; Simner *et al.*, 2023; Padovani *et al.,* 2023; Freiberg *et al.*, 2024). The analysis conducted in Chapter One confirmed that deleterious amino acid substitutions conferring these functional losses are not embedded in *Kp* populations prior to selection by CFDC. Therefore, this chapter sought to confirm the role and independent relative contribution of CirA, Fiu, FepA and FecA in facilitating CFDC uptake into *Kp* under the physiologically relevant condition of iron limitation. To do this, it will firstly be confirmed that the expression of *cirA, fiu, fepA* and *fecA* is upregulated under iron limitation in wild type *Kp*. From this, it will be identified which IROMP encoding genes were most upregulated, and these genes will then be selected for further investigation through genetic deletion. As of yet, there has been no evidence to suggest the presence of a K2 serotype capsule impedes the influx of enterobactin into *Kp* (Buffet, Rocha and Rendueles, 2021). However, the effect of the K2 serotype capsule on CFDC susceptibility is yet to be investigated. Thus, this chapter intends to generate IROMP genetic deletion mutants in both non-capsulated and capsulated backgrounds. The susceptibility of these isogenic mutants to CFDC will then be tested.

3.2.1. Transcriptomic Analyses – How Does Iron Limitation Drive RNA Transcript Expression of IROMP encoding genes *cirA, fiu, fepA* and *fecA*?

This chapter first intended to confirm the derepression of the IROMPs under iron limitation. To ascertain the impact of iron limitation on the expression of IROMP RNA transcripts, Fe^{3+} was depleted in the growth media of Ecl8, RNA was extracted after overnight incubation, and the RNA transcript expression levels of *cirA, fiu, fepA* and *fecA* were analysed *via* RT-(q)PCR. RNA transcript expression levels of *cirA, fiu, fepA* and *fecA* obtained by RT-(q)PCR after overnight incubation of Ecl8 in Fe^{3+} replete growth media were used as the baseline controls. Respective iron limited and iron replete medias employed were ID-CAMHB, and the same media supplemented with 100µM of $FeCl_3$ solution: ID-CAMHB+$FeCl_3$.

It was found that there was a consistent upregulation in RNA transcript expression for *cirA, fiu, fepA* and *fecA* under iron limitation (ID-CAMHB) relative to iron repletion (ID-CAMHB+$FeCl_3$). Results are shown in Figure 11.

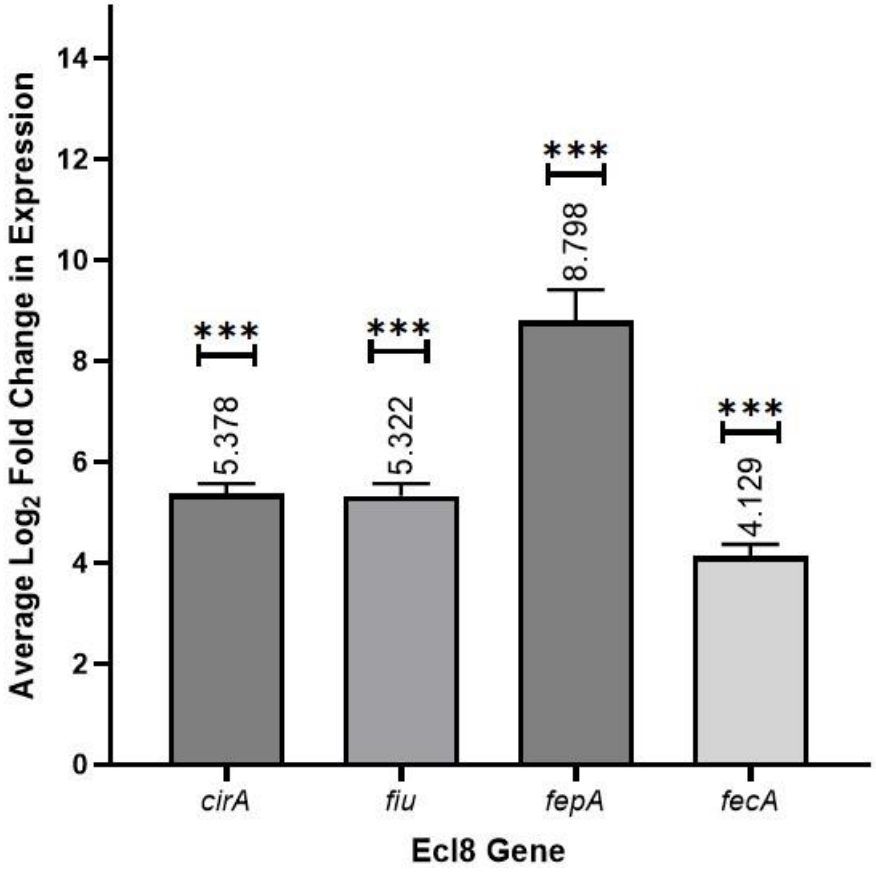

Figure 11. Log_2 fold change expression of *cirA, fiu, fepA, fecA* in iron deplete media (ID-CAMHB) relative to iron replete media (ID-CAMHB+$FeCl_3$) under Ecl8. Average log_2 fold-change ± SEM is plotted, showing the log_2 fold change in gene expression as a ratio of Ecl8 ID-CAMHB: Ecl8 ID-CAMHB+$FeCl_3$ – test:control. The label *** indicates statistically significant at p<0.001 as identified by *t*-test. Log_2 fold change was averaged after conducting investigation under biological and technical replicates both equalling n=3.

Figure 11 illustrates that the RNA transcript expressions of *cirA, fiu, fepA* and *fecA* were all statistically significantly upregulated under iron limitation (ID-CAMHB) relative to iron repletion (IDCAMHB+$FeCl_3$) in Ecl8, at p<0.001 as identified by *t*-test. Log_2 fold increases were 5.378, 5.322, 8.798 and 4.129 for *cirA, fiu, fepA* and *fecA*, respectively. The log_2 fold increase in RNA transcript expression of *fepA* was found to be 3.42, 3.476 and 4.669 log_2 fold higher than the log_2 fold increases of *cirA, fiu* and *fecA,* respectively. This was shown to be statistically significant at $p<0.05$, $p<0.05$ and $p<0.01$, as identified by *t*-test.

Thus, these data confirm the derepression of the IROMPs under iron limitation.

It was next of importance to determine whether capsulation had any impact on the RNA transcript expression of *cirA, fiu, fepA* and *fecA* in response to iron limitation. This was necessary to ensure that any CFDC susceptibility impact conferred by capsulated strains under iron limitation would not be the result of the confounding variable of differential IROMP expression relative to non-capsulated strains. To assess this, *Kp* 52145 was incubated overnight in iron limited media (ID-CAMHB), RNA was extracted and RT-(q)PCR analyses of *cirA, fiu, fepA* and *fecA* RNA transcript expression was performed. RNA transcript expression levels of *cirA, fiu, fepA* and *fecA* obtained by RT-(q)PCR after overnight incubation of Ecl8 in ID-CAMHB acting as the baseline controls.

It was found that there was no statistically significant $\log_2$ fold change difference in the RNA transcript expression of *cirA, fiu, fepA* and *fecA* in *Kp* 52145 relative to Ecl8 under ID-CAMHB. Results are shown in Figure 12.

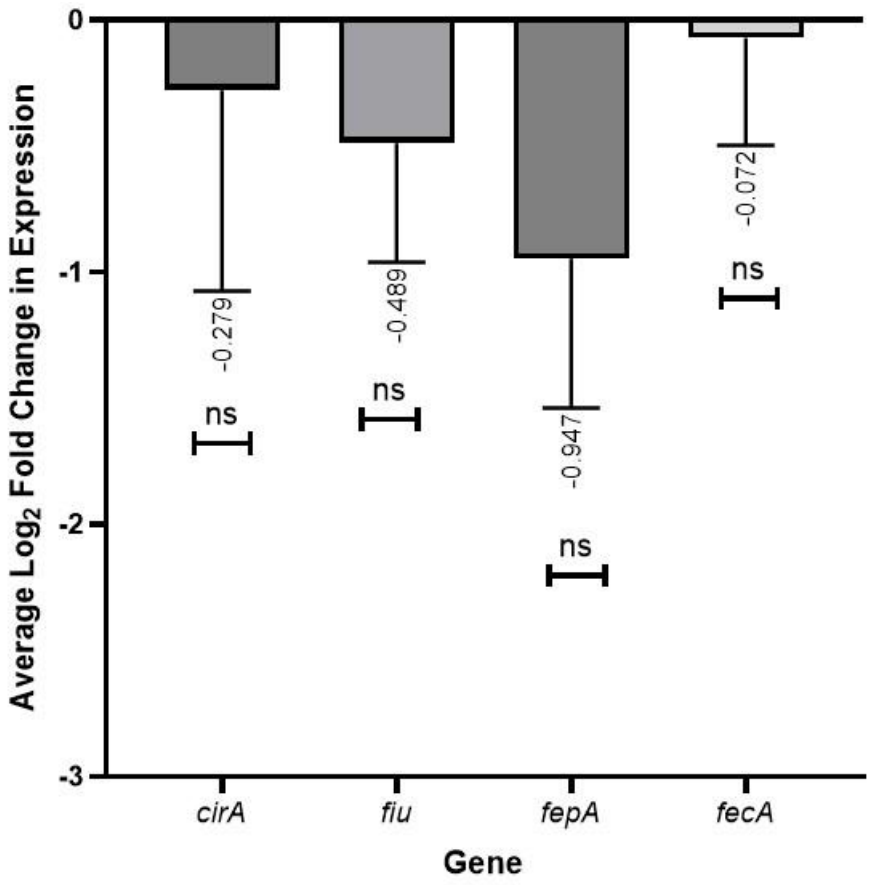

Figure 12. Log_2 fold change expression of *cirA, fiu, fepA, fecA* under *Kp* 52145 relative to Ecl8 in iron deplete media (IDCAMHB). Average log_2 fold-change ± SEM is plotted showing the log_2 fold change in gene expression as a ratio of *Kp* 52145 ID-CAMHB:Ecl8 ID-CAMHB – test:control. The label ns indicates not statistically significant as identified by *t*-test. Log_2 fold change was averaged after conducting investigation under biological and technical replicates both equalling n=3.

IROMP expression in response to iron limitation was therefore shown to be capsulation independent.

To summarise, the data confirms the consistent derepression of the IROMPs when iron is depleted from growth media. Thus, this confirms the role of the IROMPs in the Fe^{3+} acquisition pathway of *Kp,* which CFDC uptake is known to exploit. It was shown that *fepA, cirA* and *fiu* respectively exhibited the greatest log_2 fold upregulation in expression of *cirA, fiu, fepA* and *fecA* under iron limitation. Log_2 fold increases were 8.798, 5.378 and 5.322, respectively. Thus, *fepA, cirA* and *fiu* were selected for further analysis through genetic deletion in non-capsulated (Ecl8) and capsulated (*Kp* 52145) backgrounds.

3.2.2. Generation of IROMP Deletion Mutants in Ecl8 and *Kp* 52145 Backgrounds

To attempt to generate individual deletions of both *fepA* and *fiu* in Ecl8 and *Kp* 52145 backgrounds, the conjugative homologous recombination protocol was performed as outlined in 2.5.2.. The pKNGS plasmid was employed as the suicide vector as per the outlined protocol for attempts to introduce individual *fepA* and *fiu* knockout constructs into the chromosomes of both the capsulated and noncapsulated wild type strains.

To ensure specific target site knockout, the N- and C- termini of the genes of interest for deletion (*fepA* and *fiu*) were firstly amplified with NoNi and CoCi primers *via* Phusion PCR as per the method of *2.5.2.1.*. For each gene, NoCo fragment constructs which included the regions flanking the gene of interest for deletion were then made, again using Phusion PCR as per the method of *2.5.2.1.*. Gel electrophoresis results validating each CoCi fragment, NoNi fragment and NoCo construct Phusion PCR product are shown in Figures 13 - 18.

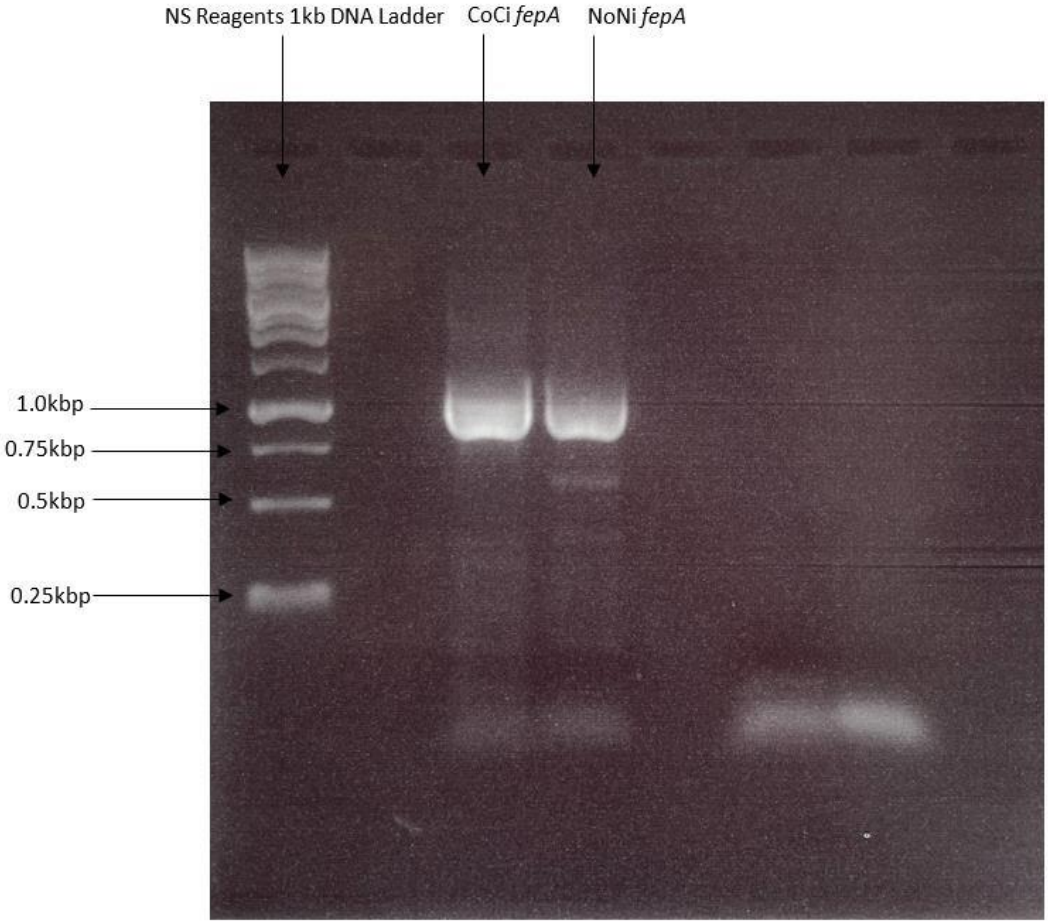

Figure 13. Gel electrophoresis image showing *fepA* CoCi and NoNi fragment Phusion PCR products. The image clearly shows the respective bands both at approximately 1kbp – representing the CoCi band at length 1096kbp, and the NoNi band at length 1100kbp. These bands were then taken forward for gel extraction and purification to a reasonable concentration for NoCo making. See Appendix I for primers used.

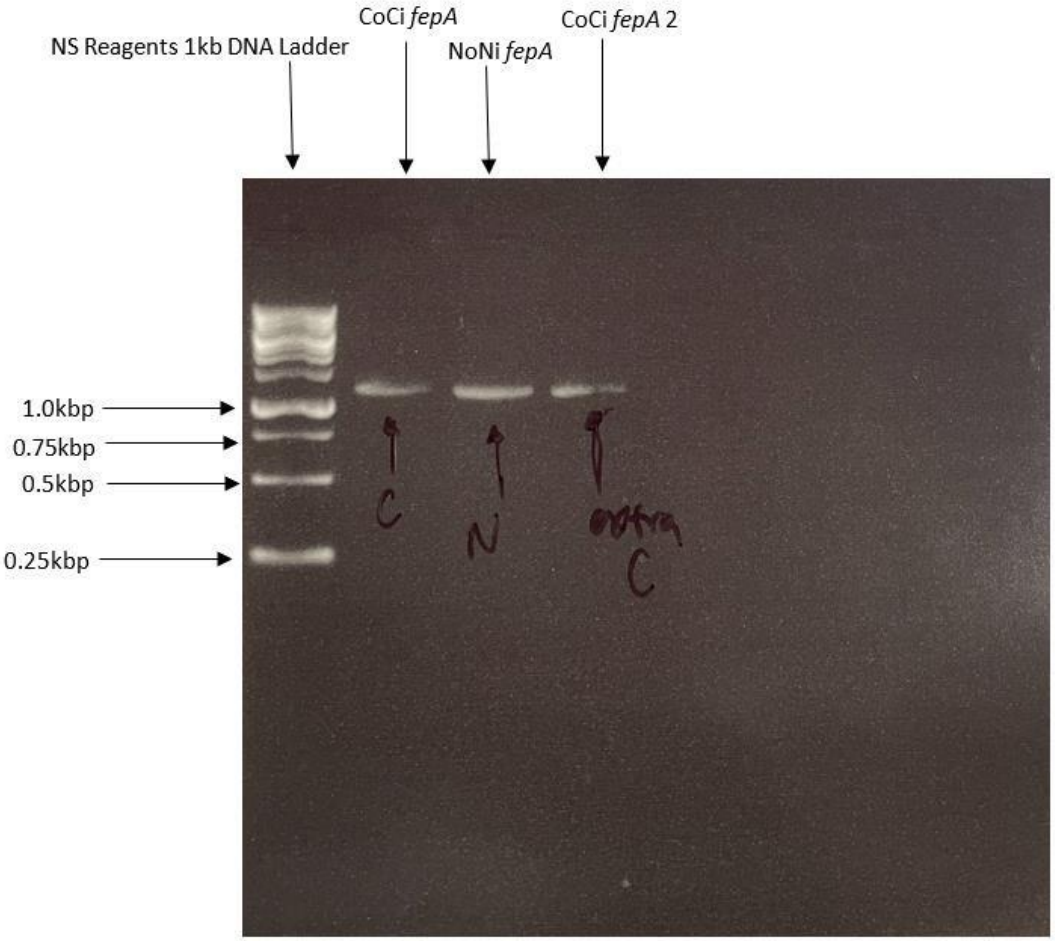

Figure 14. Gel electrophoresis image showing extracted and purified *fepA* CoCi and NoNi fragment DNA band size checks. Here, there are clear bands at approximately 1kbp, representative of the *fepA* CoCi and NoNi fragment respective band lengths of 1096kbp and 1100kbp. As written on the image, an extra gel well run of CoCi PCR product was included as a back-up due to the first gel well sample not settling sufficiently to the bottom of the well when loading. See Appendix I for primers used.

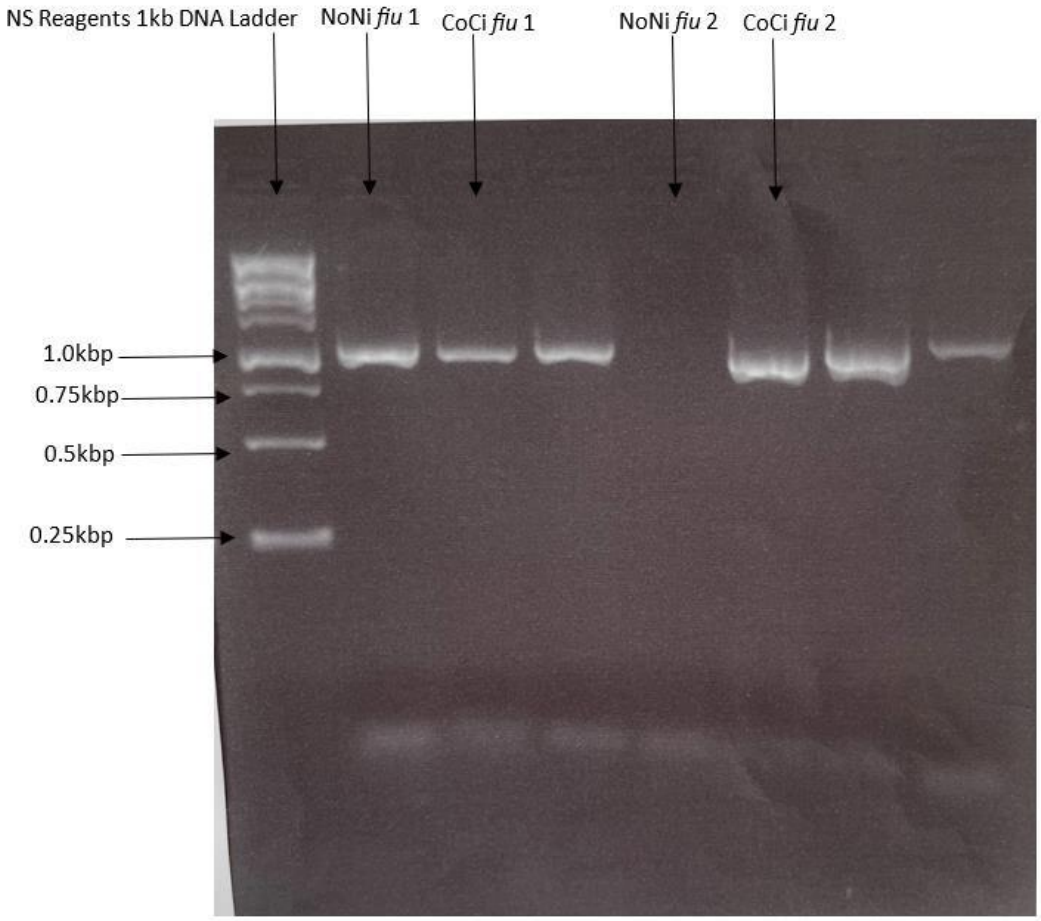

Figure 15. Gel electrophoresis image showing *fiu* CoCi and NoNi fragment Phusion PCR products. The image clearly shows two respective bands at approximately 1kbp – representing the CoCi band at 1025kbp, and the NoNi band at 964kbp. Note, for each CoCi and NoNi there were two separate wells representing two separate PCR products, this was due to one PCR containing a low concentration of 62 gDNA template, so duplicate PCR was performed to ensure strong banding and reasonable fragment concentration. As shown, one of the NoNi bands did not appear due to the gDNA concentration having been too low. Bands were then taken forward for gel extraction and purification to a reasonable concentration for NoCo making. Bands without labels were representative of other fragments. See Appendix I for primers used.

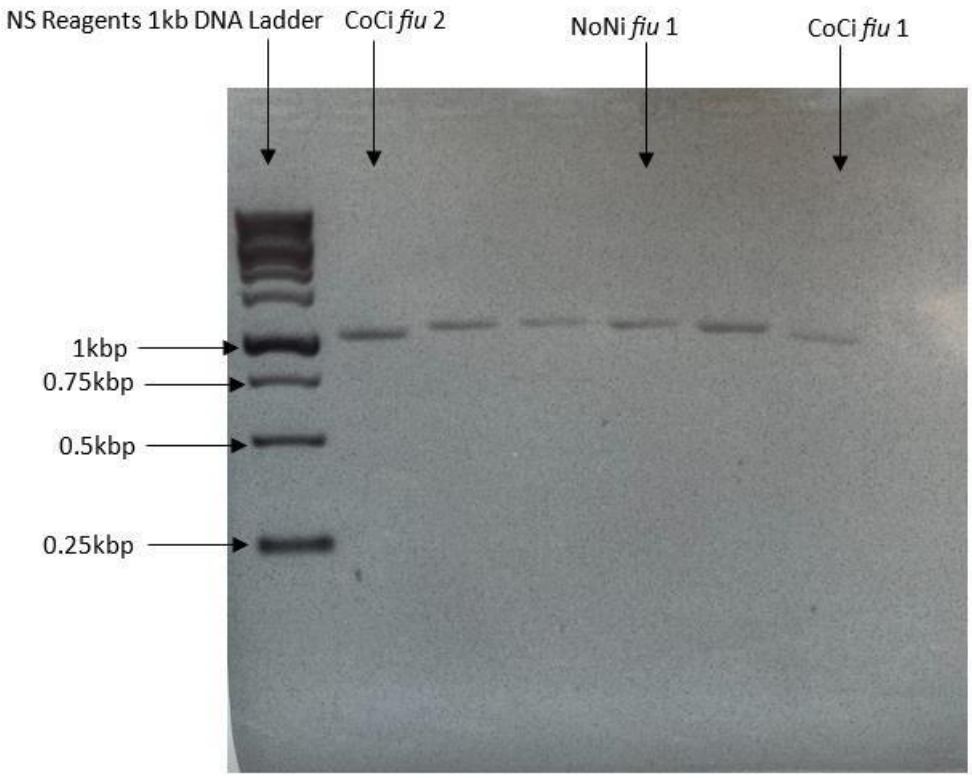

Figure 16. Gel electrophoresis image showing extracted and purified *fiu* CoCi and NoNi fragment DNA band size checks. Here, there are clear bands at approximately 1kbp, representative of the *fiu* CoCi and NoNi respective bands lengths of 1025kbp and 964kbp. Bands not labelled were representative of other fragments. See Appendix I for primers used.

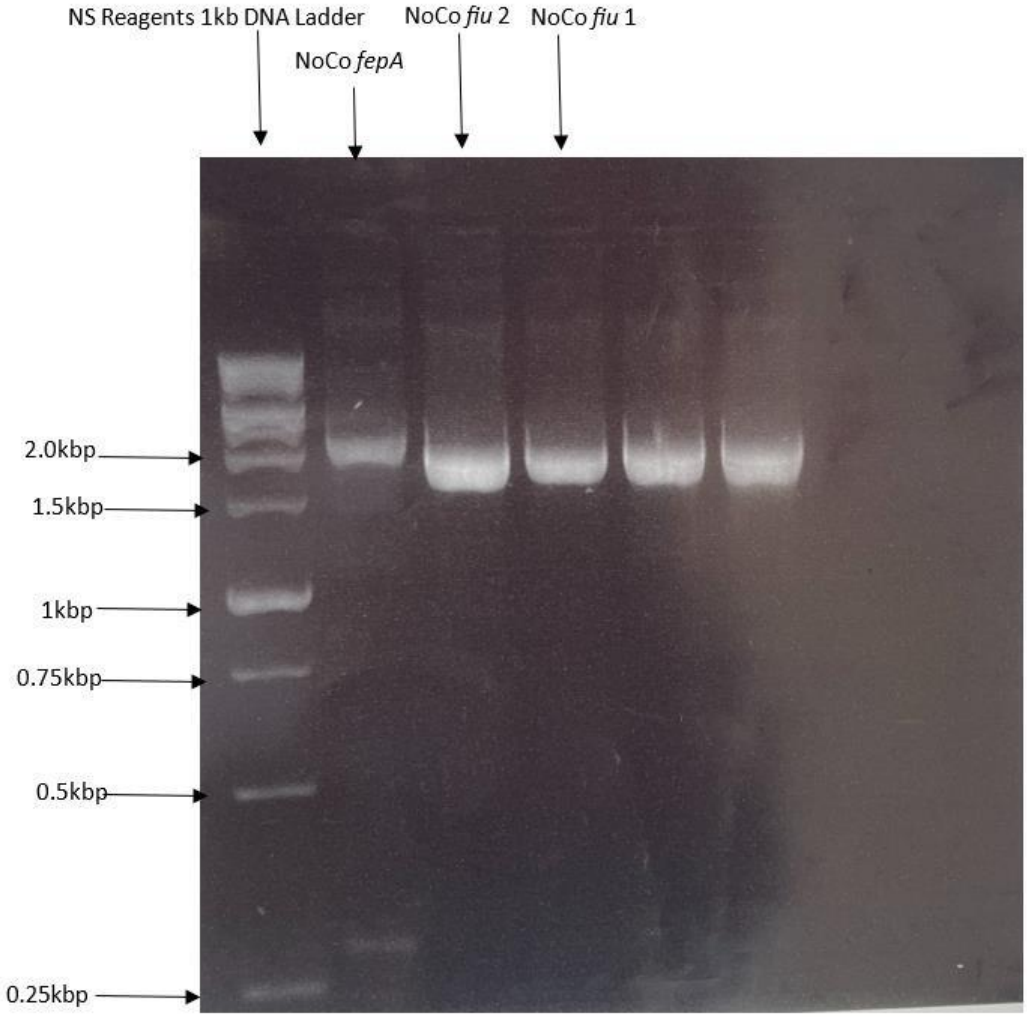

Figure 17. Gel electrophoresis image showing NoCo*fepA* and NoCo*fiu* construct Phusion PCR products, with the *fiu* constructs made using the combinations of NoNi 1, CoCi 1 and CoCi 2 as shown in Figure 16. The *fepA* NoCo is shown at band size of 2196kbp, with banding just below 2kbp representing the *fiu* NoCo fragment size 1989kbp. Bands not labelled on this image represent other fragments. See Appendix I for primers used.

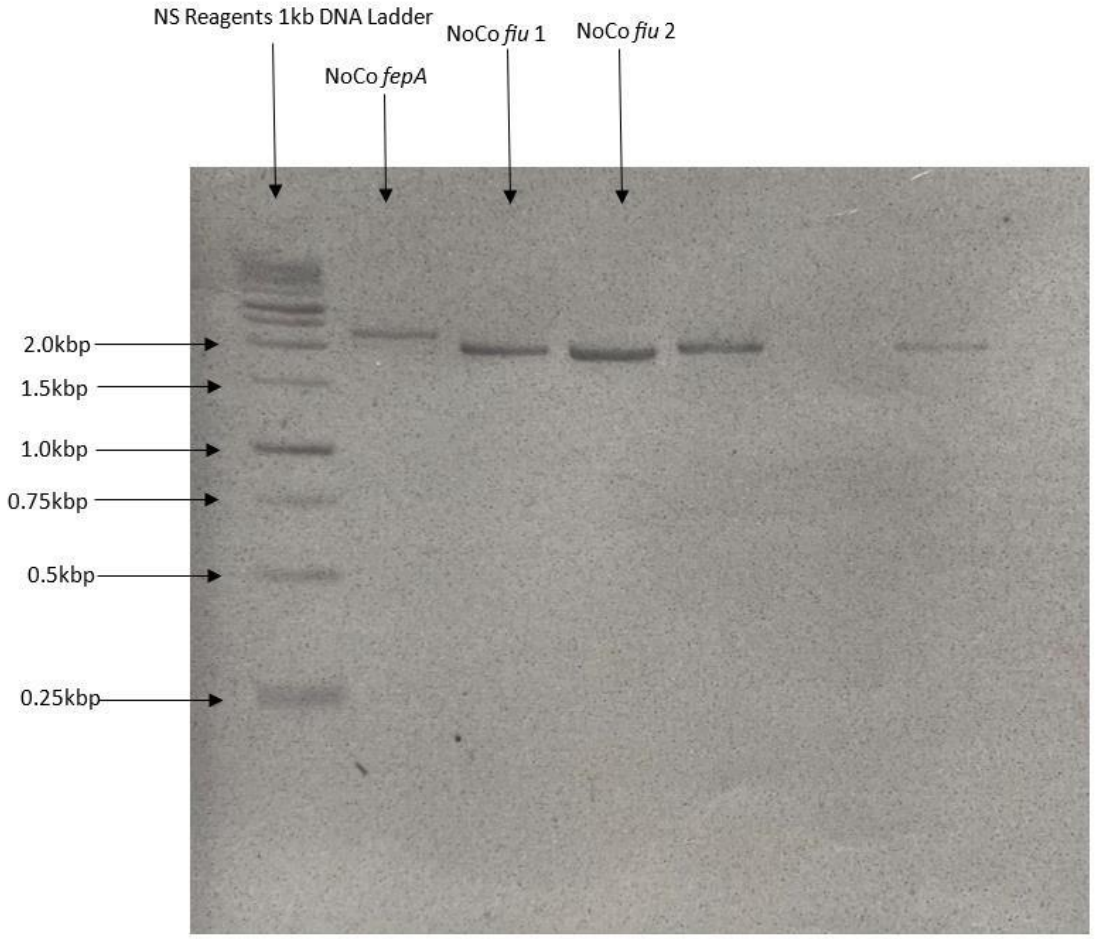

Figure 18. Gel electrophoresis image showing extracted and purified NoCo*fepA* and NoCo*fiu* construct DNA band size checks. The bands shown clearly represent *fepA* at 2196kbp and *fiu* at 1989kbp. The *fiu* NoCo with the highest concentration after nanodrop analyses was taken forward for ligation and electroporation. The bands not labelled represent different fragments. See Appendix I for primers used.

Concentrations of the selected purified NoCos were 11.8ng/µl for NoCo*fepA* and 20.7ng/µl for NoCo*fiu*. NoCos were then ligated with the pKNGS vector in a molar ratio of 6:1 as per the method of *2.5.2.2.*. To maintain plasmid stability and ensure high efficiency plasmid replication during exchange, the pKNGSNoCo*fepA* and pKNGSNoCo*fiu* constructs were then cloned into *E. coli* DH5α *pir* as per the method of *2.5.2.3.*. To confirm the pKNGSNoCo constructs had been cloned into *E. coli* DH5α *pir*, One*Taq* colony PCR was performed to validate pKNGS backbone insertion, using the appropriate pKNGS verification primer set (see Appendix I) as per the methods of *2.5.2.3.* and **2.4.**. Gel electrophoresis results of successful cloning into the bacteria are shown in Figure 19 - 21. Figure 22 shows the result of a repeat PCR following DH5α*pir*pKNGSNoCo construct DNA extraction to confirm banding sizes for transformation into the conjugative donor strain: *E. coli* S17 MFD λpir.

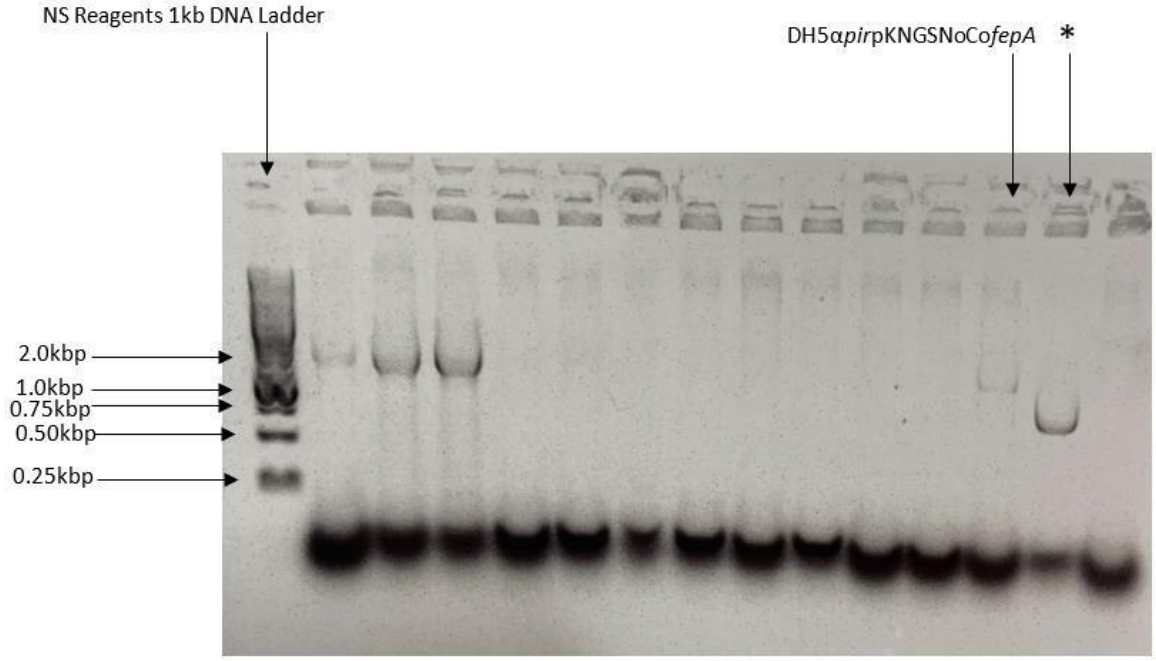

Figure 19. Gel electrophoresis image of One*Taq* PCR products showing successful pKNGSNoCo*fepA* construct cloning in *E. coli* DH5α *pir* from the 60ng:10ng insert:vector ligation after addition of DMSO to the PCR mixture. Bands not labelled represent other fragments. The band labelled * represents an anomalous fragment size below the correct NoCo*fepA* size of 2196kbp, which was therefore deemed as an unsuccessful cloning attempt. See Appendix I for primers used.

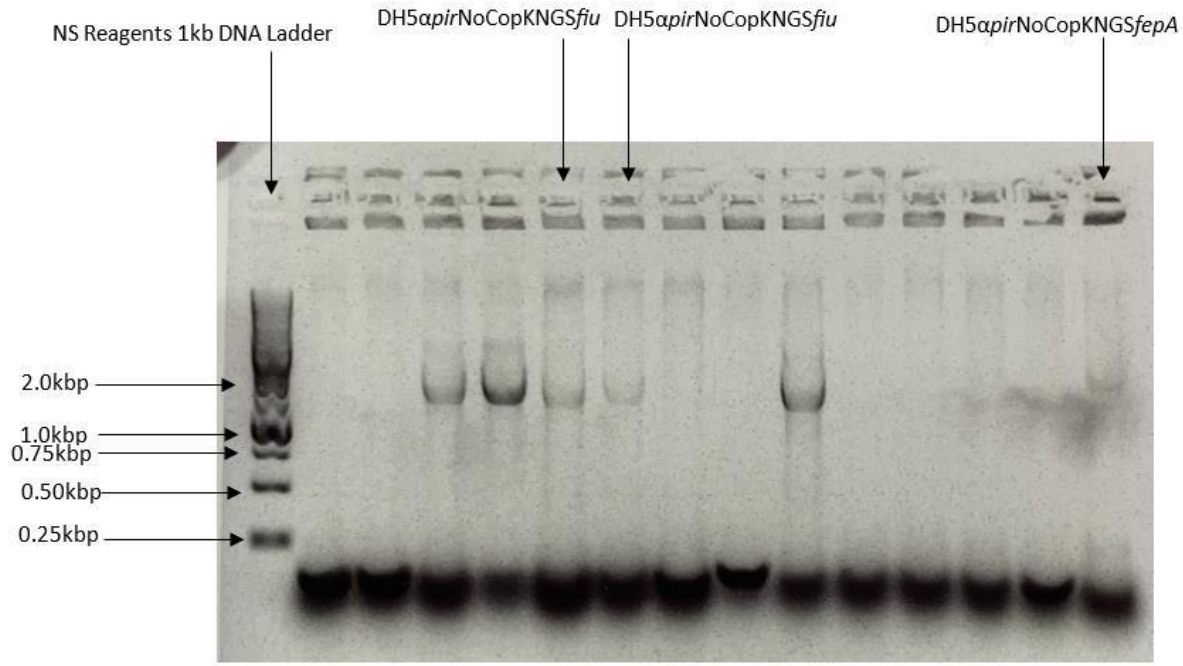

Figure 20. Gel electrophoresis image of One*Taq* PCR products showing successful pKNGSNoco*fepA* and pKNGSNoCo*fiu* construct cloning in *E. coli* DH5α *pir* from the 90ng:15ng insert:vector ligations after addition of DMSO to the PCR mixture. Bands not labelled represent other fragments. See Appendix I for primers used.

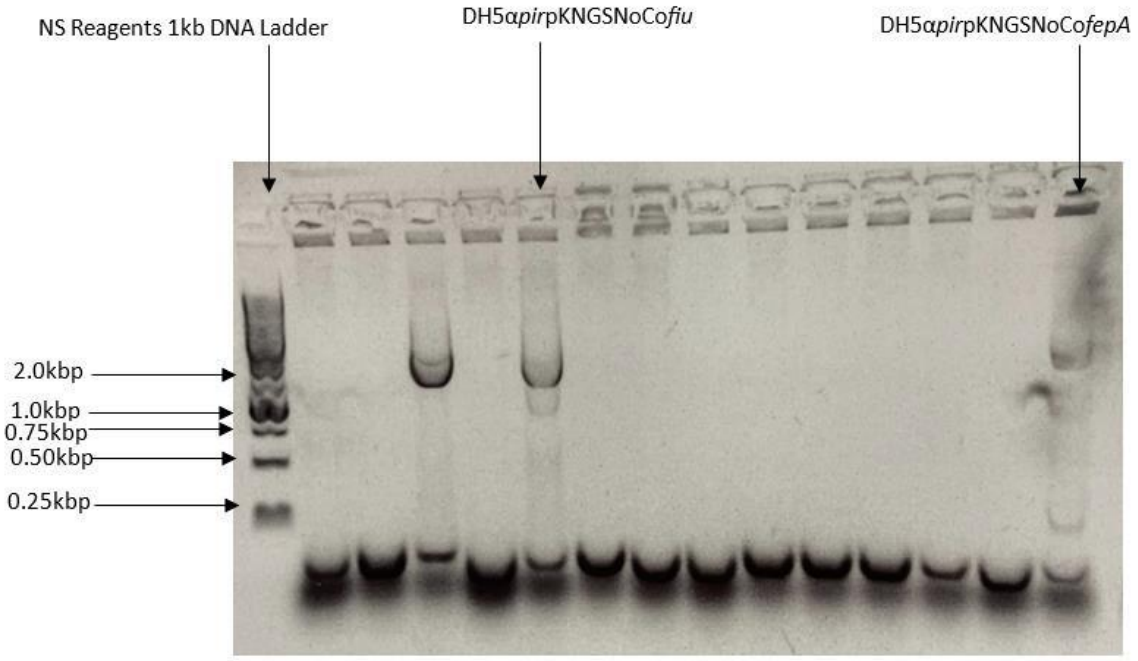

Figure 21. Gel electrophoresis image of One*Taq* PCR products showing successful pKNGSNoCo*fepA* and pKNGSNoCo*fiu* construct cloning in *E. coli* DH5α *pir* from the 60ng:10ng insert:vector ligations after reelectroporation with 15µl clean ligation product and addition of DMSO to the PCR mixture. Bands not labelled represent other fragments. See Appendix I for primers used.

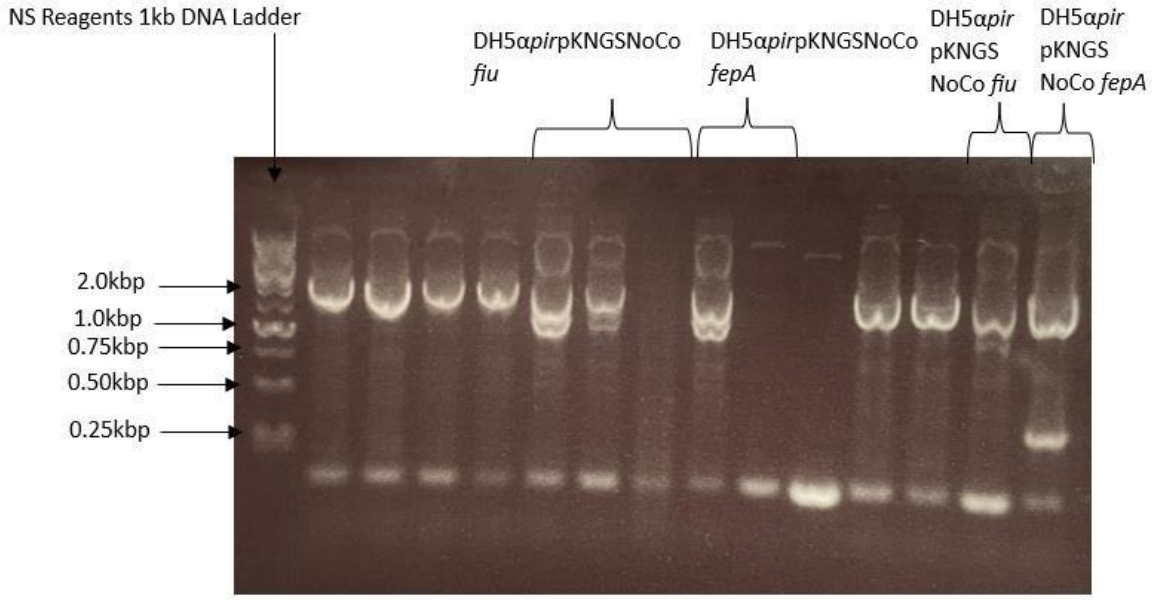

Figure 22. Gel electrophoresis image showing all successful and DH5α *pir*pKNGSNoCo*fepA* and DH5α *pir*pKNGSNoCo*fiu* construct clone DNA, confirming correct banding sizes. Bands not labelled represent other fragments. Wells within the DH5α *pir*pKNGSNoCo*fepA and* DH5α *pir*pKNGSNoCo*fiu* labelled brackets which show no banding represent plasmid loss, and the respective constructs were not used for transformation. See Appendix I for primers used.

To allow for plasmid transfer into Gram-negative recipient strains Ecl8 and Kp 52145, the nonconjugative DH5α *pir*pKNGSNoCo clones had to first be transformed into conjugative strain *E. coli* S17 MFDλ*pir*. Only a single successful DH5α *pir*pKNGSNoCo clone for each of *fepA* and *fiu* was selected for this transformation, performed as per the method outlined in *2.5.2.3.*. After conjugation into Ecl8 and *Kp* 52145, no Km susceptibility was observed. After troubleshooting as per the repeated colony patching and 42°C pooled colony incubation of *2.5.2.3.*, this outcome was unchanged. Therefore, plasmid excision from the conjugated recipient strain had been unsuccessful. Thus, these mutants could not be employed for the analysis of impact to CFDC susceptibility. For images of Km resistant transconjugants, see Figure 23.

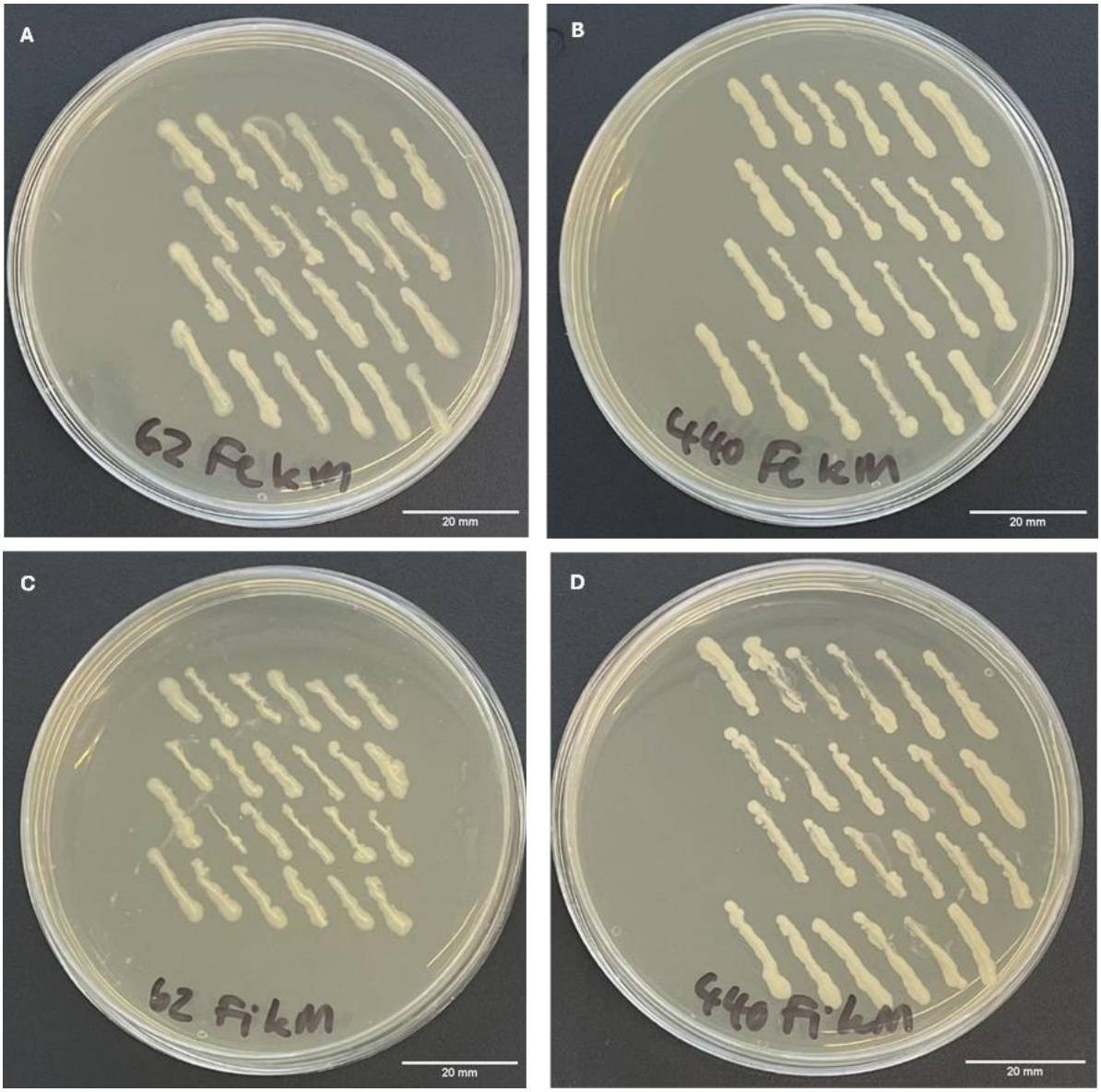

Figure 23. Images of LB+Km 100mg/ml (denoted Km) plates of each respective *fepA* and *fiu* (denoted Fe and Fi, respectively) DH5α *pir*pKNGSNoCo clone transformed into *E. coli* MFD S17 λ*pir* after attempts for recipient conjugation and plasmid excision. Recipients were Ecl8 (denoted 62) (**A,C**) and *Kp* 52145 (denoted 440) (**B,D**). Images show no Km susceptibility. Images were fitted with a pixel-mm representative scale bar of 20mm using ImageJ software (Schneider, Rasband and Eliceiri, 2012).

To next attempt to delete *cirA* in the *Kp* 52145 background, the non-conjugative homologous recombination protocol was performed as outlined in 2.5.1.. The pTOF plasmid was employed as the suicide vector as per the outlined protocol for attempts to introduce a DH10βpTOFNoCo*cirA*<km> knockout construct into the chromosome of the capsulated wild type strain. To validate DH10βpTOFNoCo*cirA*<km> knockout constructs preceeding insertion into *Kp* 52145, restriction digest was conducted on plasmid DNA with combinations of SmaI & SalI, NotI and NotI & SmaI enzymes as per the method outlined in *2.5.1.2.*. Results of the SmaI & SalI digest are shown in Figure

24. Results of the NotI and NotI & SmaI digests are shown in Figure 25.

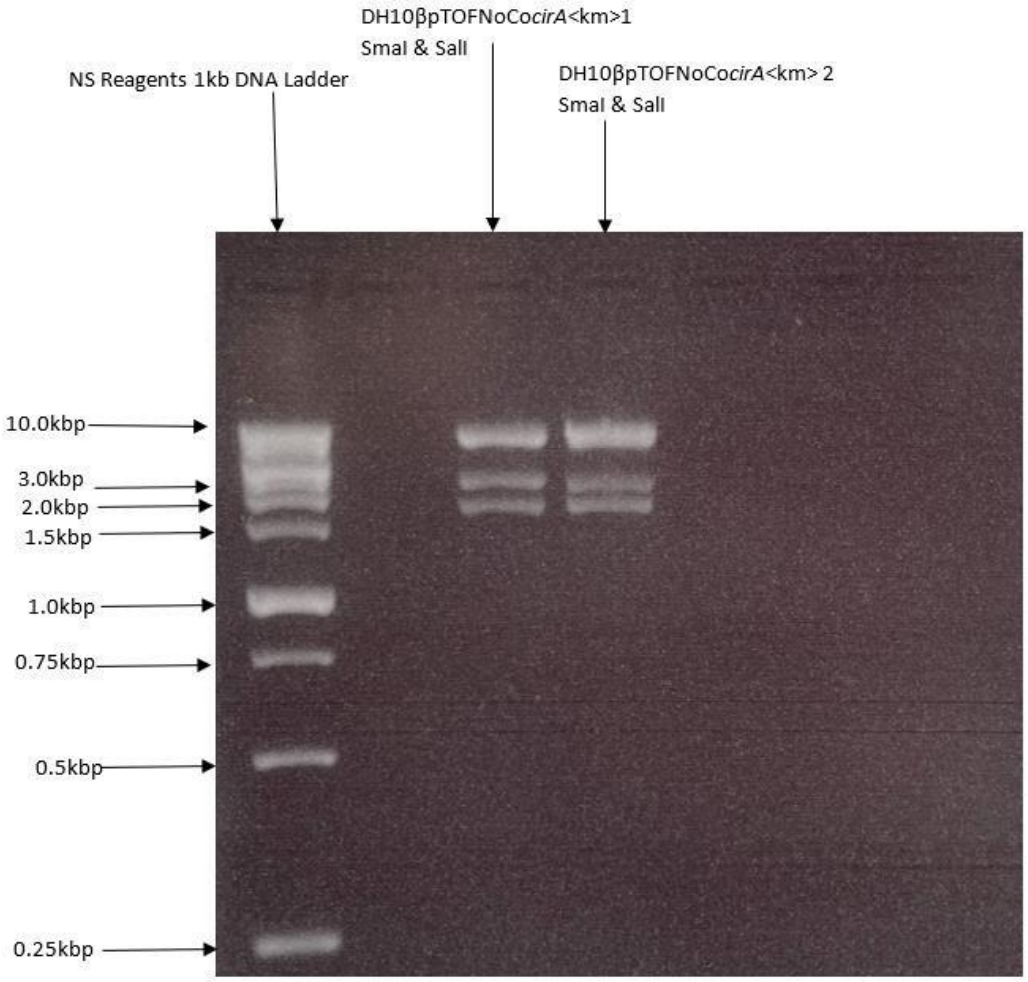

Figure 24. Gel electrophoresis image showing SmaI & SalI restriction digest validation of 2x DH10βpTOFNoCo*cirA*<km> constructs of Schneiders Lab - labelled here as DH10βpTOFNoCo*cirA*<km> 1 and DH10βpTOFNoCocirA<km> 2 (1 and 2, respectively). The banding just above 3kb indicates separation of the NoCo fragment with central Km cassette inserted (approximately 3.7kbp combined), and the banding at approximately 2kbp indicates further separation of the 1.7kbp length Km cassette, leaving behind the NoCo*cirA* construct only (approximately 1974kbp for *cirA* [Salgado *et al.,* 2023]). See Appendix I for primers used.

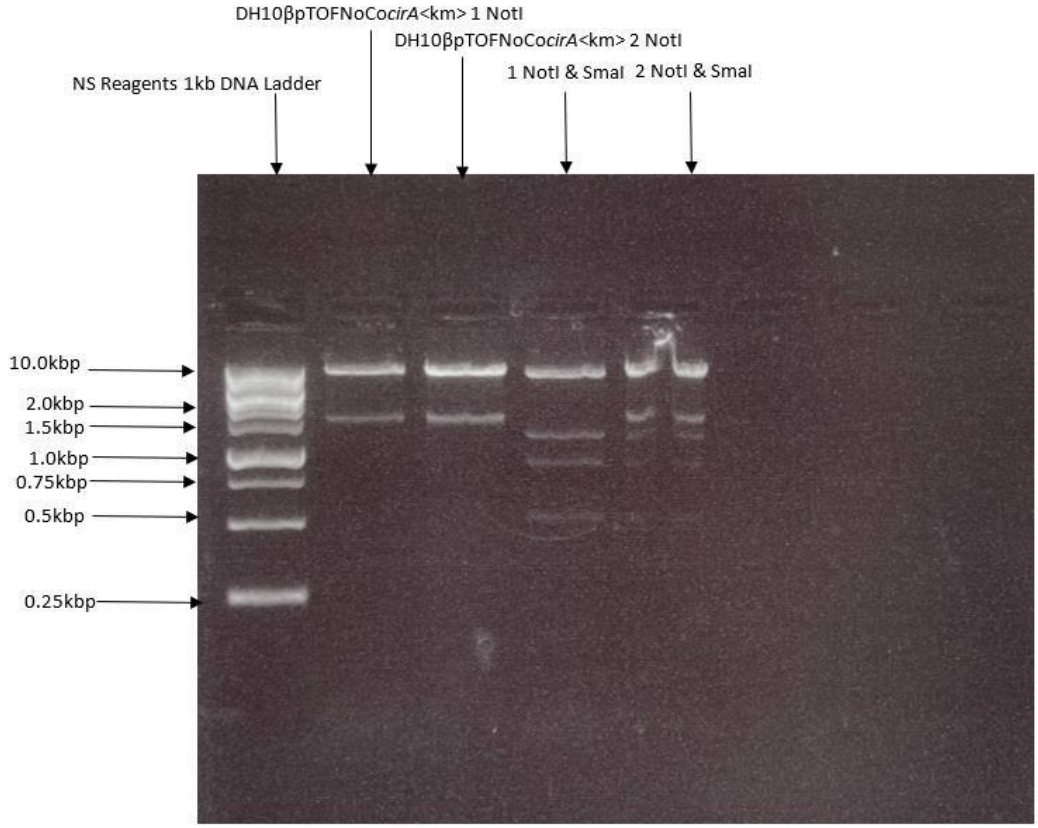

Figure 25. Gel electrophoresis image showing NotI and NotI & SmaI restriction digest validation of 2x DH10βpTOFNoCo*cirA*<km> constructs of Schneiders Lab - labelled here as DH10βpTOFNoCo*cirA*<km> 1 and DH10βpTOFNoCo*cirA*<km> 2 (1 and 2, respectively). 1.5kbp - 2kbp banding for NotI only indicates separation of the 1.7kbp Km cassette, with the lower bandings of NotI & SmaI indicating separation of the combined 1974kbp CoCi and NoNi *cirA* fragments. See Appendix I for primers used.

Due to the successful digests of both DH10βpTOFNoCo*cirA*<km> constructs of Schneiders Lab, only one was taken forward for insertion into *Kp* 52145, for which DH10βpTOFNoCo*cirA*<km> 1 was chosen. To further validate the DH10βpTOFNoCo*cirA*<km> 1 plasmid prior to insertion attempts, it was ensured that *cirA* was absent from the construct *via* performing standard PCR with the plasmid DNA as per the One*Taq* protocol outlined in **2.4.**. Results of the PCR are shown in Figure 26.

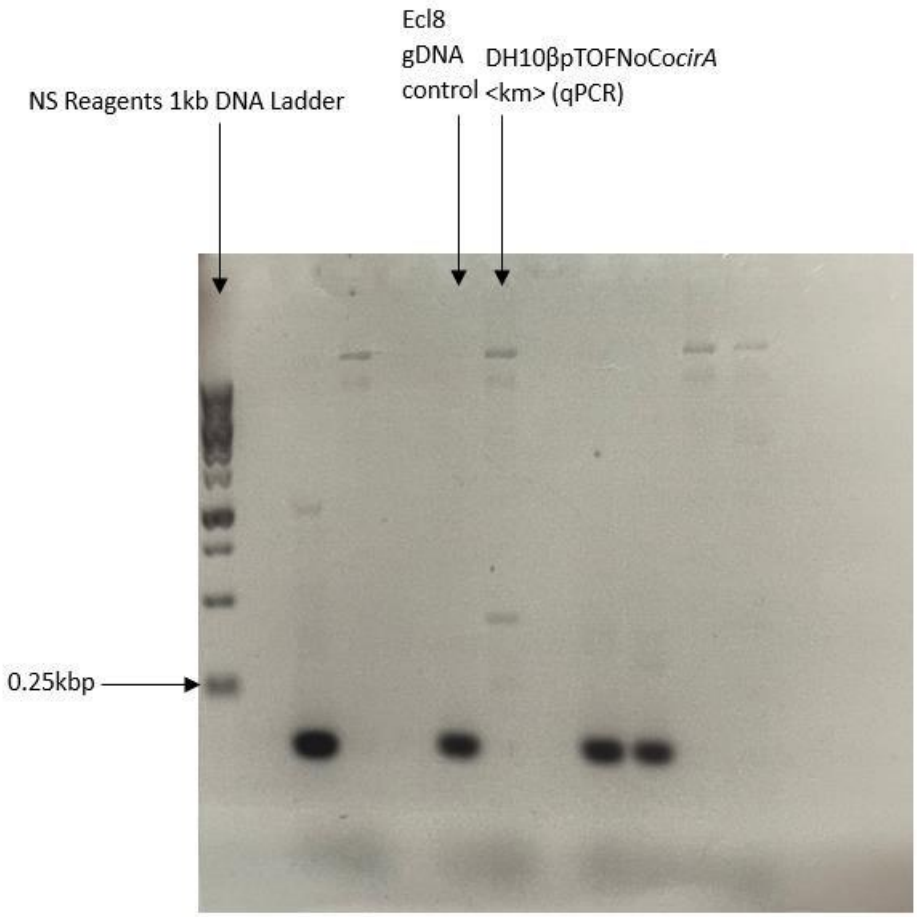

Figure 26. Gel electrophoresis image showing validation of DH10βpTOFNoCo*cirA*<km> PCR products following PCR using RT-(q)PCR primers. Relevant RT-(q)PCR primers were used in this instance instead of Next, Cext and Kan-2 primers (Appendix I) as this allowed more definitive confirmation of gene of interest absence in DH10βpTOFNoCo*cirA*<km> relative to the control. Banding between approximately 0.15kbp to 0.25kbp indicates binding of relevant RT-(q)PCR primers to the gene of interest (*cirA*) in the respective Ecl8 controls. Absence of banding indicates absence of the gene in the plasmid constructs tested. Bands not labelled represent other fragments.

Having confirmed the absence of *cirA* from the construct, it was next attempted to introduce DH10βpTOFNoCo*cirA*<km> into the *Kp* 52145 chromosome. To do this, the non-conjugative homologous recombination exchange protocol was performed as per the method outlined in 2.5.1.. To assess whether the DH10βpTOFNoCo*cirA*<km> construct had been successfully inserted into *Kp* 52145, One*Taq* PCR was performed using appropriate Next and Cext primers (see Appendix I) as per the methods of *2.5.1.3.* and **2.4.**. For the PCR result showing the unsuccessful attempt to delete *cirA* in the *Kp* 52145 background, see Figure 26.

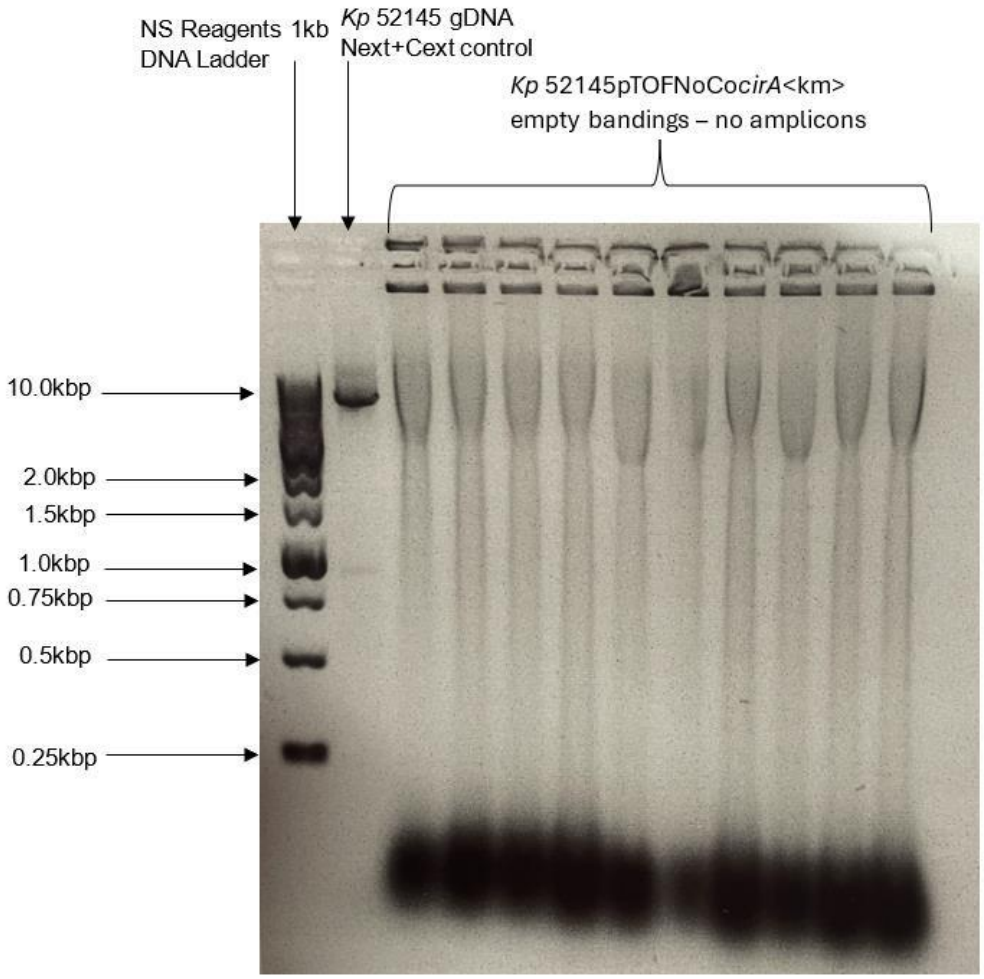

Figure 27. Gel electrophoresis image showing failed insertion of DH10βpTOFNoCo*cirA*<km> in the *Kp* 52145 background. The image clearly shows absence of any banding approximately 2kb lower than the control banding, which would otherwise represent the amplicons for which deletion of *cirA* (of known, conserved 1974kbp fragment length in Enterobacterales as per Regulon DB v12.0 [Salgado et al., 2023]) would have been successful. See Appendix I for primers used.

As a result of unsuccessful generation of *fepA, fiu* and *cirA* deletion mutants in the *Kp* 52145 background, this chapter therefore did not employ capsulated wild type strain *Kp* 52145 in CFDC susceptibility testing.

3.2.3. Susceptibility Testing of IROMP Deleted Strains

To establish the impact of IROMP deletion on the permeability of the OM to CFDC under iron limitation, CFDC susceptibility testing was next performed on an isogenic strain of Ecl8 deleted of *cirA* (Ecl8*cirA*<km>). Susceptibility testing was conducted *via* broth microdilution in iron deplete (IDCAMHB) and iron replete (ID-CAMHB+$FeCl_3$) medias as per the method outlined in 2.10.2.. This method was employed according to recommendations of the CLSI (Ito *et al.*, 2016; Ito *et al.,* 2018), and as a result of inconsistencies recorded using disk diffusion (see Appendix III).

During this testing, CAZ was used as a baseline control. This was because this antibiotic, unlike CFDC, does not exploit the Fe^{3+} transportation system for its influx or efficacy. Hence, its mode of action is not dependent on iron availability, and it could be anticipated that CAZ susceptibility would not be affected by iron limitation (Ito *et al.*, 2016), or by IROMP deletion.

The *in vitro* activity of CFDC against *Kp* wild type strain Ecl8 was enhanced under iron limitation, whereas the activity of CAZ against Ecl8 was unaffected. There was no biologically significant impact of *cirA* deletion to CFDC susceptibility relative to Ecl8, irrespective of conditions of iron limitation or iron repletion. The susceptibility of Ecl8*cirA*<km> to CAZ also showed no biologically significant change irrespective of iron limitation or iron repletion. Results are shown in Table 8.

Strain	**CFDC ID-CAMHB**	**CAZ ID-CAMHB**	**CFDC ID-CAMHB+$FeCl_3$**	**CAZ ID-CAMHB+$FeCl_3$**
Ecl8	0.5	1	2	0.5
Ecl8*cirA*<km>	1	1	4	1

Table 8. Modal CFDC and CAZ MIC values (mg/L) of Ecl8*cirA*<km> and Ecl8. ID-CAMHB represents iron deplete media and ID-CAMHB+$FeCl_3$ represents iron replete media. This data was recorded as the modal value due to the data being geometric. Investigation was conducted under biological and technical replicates both equalling n=3.

3.2.3.1. CFDC Susceptibility

Table 8 shows CFDC susceptibility to have been increased by 4-fold under iron limitation (ID-CAMHB) relative to iron repletion (ID-CAMHB+$FeCl_3$) for Ecl8. With the present work having confirmed increased expression of Fe^{3+} transportation system IROMPs under ID-CAMHB in Ecl8 (3.2.1.), this result confirms CFDC exploits the IROMPs to gain cellular entry. The CFDC susceptibility of *Ecl8cirA*<km> was also increased by 4-fold under ID-CAMHB relative to ID-CAMHB+$FeCl_3$. However, this strain demonstrated the biologically insignificant change to CFDC MIC of only a 2-fold increase under both iron concentrations relative to Ecl8. This result confirms that CFDC influx under iron limitation is not solely dependent on CirA.

3.2.3.2. CAZ Susceptibility

Table 8 shows the CAZ susceptibility of Ecl8 to have been increased by 2-fold under ID-CAMHB+$FeCl_3$ relative to ID-CAMHB. This is a biologically insignificant difference, therefore it can be concluded that there was no impact of iron concentration to CAZ susceptibility, as anticipated. These results thus confirm the mode of entry of CAZ not to be IROMP exploitative. Similarly, Ecl8*cirA*<km> demonstrated the same CAZ MIC across both iron concentrations, showing no biologically significant difference to Ecl8. This result adds further confirmation that CAZ does not enter the cell through CirA.

To summarise, Ecl8*cirA*<km> conferred a biologically insignificant impact to CFDC susceptibility relative to Ecl8 irrespective of iron concentration. From this, it was postulated that the RNA transcript expressions of other IROMP genes *fiu, fepA* and *fecA* may increase to compensate for *cirA* loss. To assess this, RT-(q)PCR was performed on Ecl8*cirA*<km>.

3.2.5. Transcriptomic Analyses – How Does *cirA* Deletion Impact RNA Transcript Expression of IROMP Genes *fiu, fepA* and *fecA* Under Iron Limitation?

To determine whether the biologically insignificant impact of Ecl8*cirA*<km> to CFDC susceptibility under iron limitation was a result of the expression of other known CFDC entry portal IROMPs increasing to compensate for *cirA* loss, further RT-(q)PCR was performed. Ecl8*cirA*<km> was

incubated overnight in iron limited media (ID-CAMHB), RNA was extracted and RNA transcript expression levels of *fiu, fepA* and *fecA* were analysed. RNA transcript expression levels of *fiu, fepA* and *fecA* obtained by RT-(q)PCR after overnight incubation of Ecl8 in ID-CAMHB were used as the baseline controls.

All of *fiu, fepA* and *fecA* RNA transcript levels showed consistent upregulation in Ecl8*cirA*<km> relative to Ecl8 under iron limitation (ID-CAMHB). Results are shown in Figure 28.

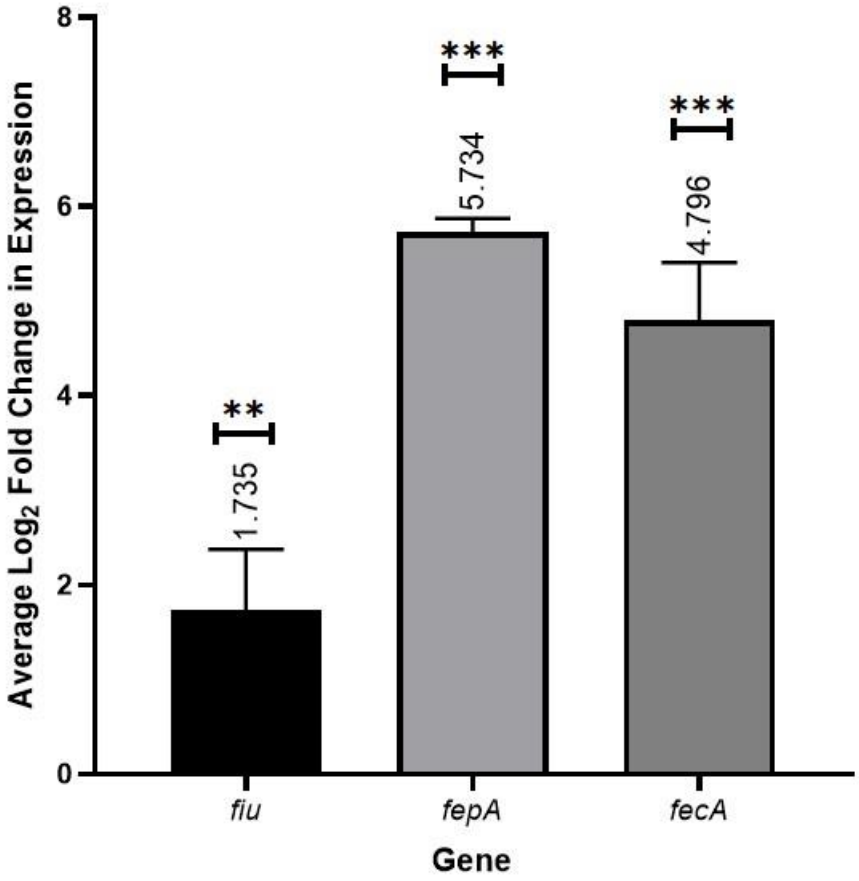

Figure 28. Log_2 fold change expression of *fiu, fepA, fecA* under Ecl8*cirA*<km> relative to Ecl8 in iron deplete media (ID-CAMHB). Average log_2 fold-change ± SEM is plotted showing the log_2 fold change in gene expression as a ratio of Ecl8*cirA*<km> ID-CAMHB: Ecl8 ID-CAMHB – test:control. The label ** indicates statistically significant at $p<0.01$, with *** indicating statistically significant at $p<0.001$ as identified by *t*-test. Log_2 fold change was averaged after conducting investigation under biological and technical replicates both equalling n=3.

Figure 28 shows that respectively, RNA transcripts of *fiu, fepA* and *fecA* showed statistically significant upregulated expression under Ecl8*cirA*<km> relative to Ecl8 under iron deplete media (ID-

CAMHB). Log_2 fold increases were 1.735, 5.734 and 4.796 for *fiu, fepA* and *fecA* at $p<0.01$ to $p<0.001$, as identified by *t*-test. Thus, this confirms that the RNA transcript expression of *fiu, fepA* and *fecA*, and thus the production of Fiu, FepA and FecA, can increase to compensate for the loss of CirA.

To close, the present chapter has shown the optimal uptake of CFDC into *Kp* under iron limitation requires at least three of the four IROMPs CirA, Fiu, FepA and FecA. Next, it was to be investigated whether efflux permeability factors MdtABC-TolC, AcrA-AcrD-TolC and AcrAB-TolC could be responsible for the cellular export of CFDC from *Kp* under iron limitation.

3.3. CHAPTER THREE: Investigating the Efflux of CFDC Through MdtABC-TolC, AcrA-AcrD-TolC and AcrAB-TolC

As previously mentioned, CFDC is conjugated with a chlorocatechol moiety at its C-3 side chain. This allows CFDC to mimic the Fe^{3+} binding action of catecholate-type siderophore enterobactin, and thereby gain entry into the cell through hijacking enterobactin uptake channel IROMPs. Importantly, this chlorocatechol moiety also confers an element of structural similarity between CFDC and enterobactin (Zhanel *et al.*, 2019; Lan *et al.*, 2022). Previous studies have evidenced a synergistic role of RND efflux pumps MdtABC-TolC, AcrA-AcrD-TolC and AcrAB-TolC in the export of enterobactin from *E. coli* under iron limitation (Bleuel *et al.*, 2005; Horiyama and Nishino, 2014). Hence, subsequent studies have postulated that these RND efflux pumps may also be able to export CFDC from the cell under iron limitation (Rebizant, 2022; Liu *et al.*, 2023; Kriz *et al.,* 2024). Thus far, no studies have isolated each pump's relative contribution to enterobactin efflux in *Kp*. Moreover, there have been no studies in *Kp* which investigate the impact of MdtABC-TolC, AcrA-AcrD-TolC and AcrABTolC deletion to CFDC susceptibility under iron limitation. Therefore, this chapter sought to establish the independent relative contributions of MdtABC-TolC, AcrA-AcrD-TolC and AcrAB-TolC to siderophore efflux, and similarly, CFDC efflux, from *Kp*. To do this, it will first be confirmed that the expression of genes encoding MdtABC-TolC, AcrA-AcrD-TolC and AcrAB-TolC efflux pumps increases under iron limitation. This will be subsequented by the further investigation of these genes through genetic deletion. Currently, there is no evidence to suggest the K2 capsule impedes siderophore export out of the cell (Buffet, Rocha and Rendueles, 2021). Yet, no studies have investigated the impact of the K2 capsule on CFDC susceptibility thus far. Hence, this chapter intends to generate RND efflux pump deletion mutants in both non-capsulated and capsulated backgrounds, in alignment with the prior described intentions of Chapter Two. The ability of these RND efflux pump deleted mutants to export siderophore under iron limitation will then be assessed, with the outcome used to predict their ability to efflux CFDC. This prediction will then be tested by investigating the susceptibility of the capsulated and non-capsulated isogenic mutants to CFDC.

3.3.1. Transcriptomic Analyses - How does Iron Limitation Drive Expression of RND Efflux Pump Encoding Genes *mdtB*, *acrD* and *acrB*?

To establish the impact of iron limitation on RNA transcript expression of RND efflux pump encoding genes *mdtB, acrD* and *acrB*, Ecl8 was incubated overnight in iron limited media (ID-CAMHB), RNA was extracted, and the RNA transcript expression levels of *mdtB, acrD* and *acrB* were analysed *via* RT(q)PCR. RNA transcript expression levels of *mdtB, acrD* and *acrB* after overnight incubation of Ecl8 in iron replete media (ID-CAMHB+$FeCl_3$*)* were used as the baseline controls.

It was found that there was a consistent upregulation in *mdtB, acrD* and *acrB* RNA transcript expression levels under iron limitation (ID-CAMHB) relative to iron repletion (ID-CAMHB+$FeCl_3$). Results are shown in Figure 29.

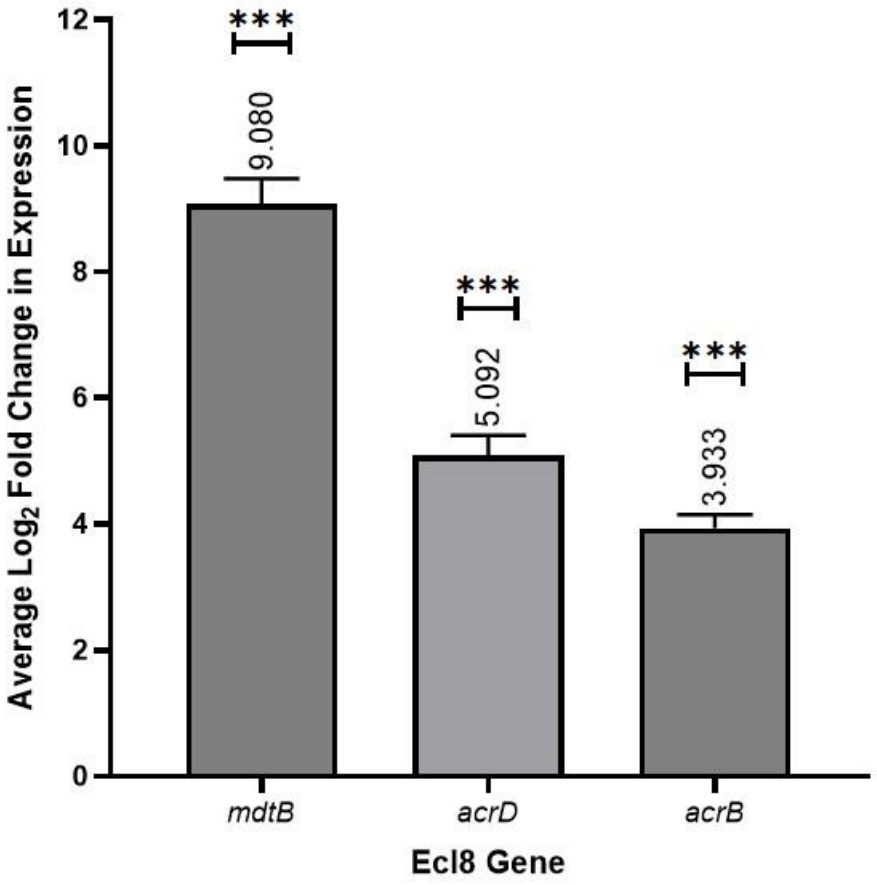

Figure 29. Log_2 fold change expression of *mdtB, acrD* and *acrB* in iron deplete media (ID-CAMHB) relative to iron replete media (ID-CAMHB+$FeCl_3$) under Ecl8. Average log_2 fold-change ± SEM is plotted showing the log_2 fold change in gene expression as a ratio of Ecl8 ID-CAMHB:ID-CAMHB+$FeCl_3$ – test:control. The label *** indicates statistically significant at $p<0.001$ as identified by *t*-test. Log_2 fold change was averaged after conducting investigation under biological and technical replicates both equalling n=3.

Figure 29 shows the statistically significantly upregulated expression of *mdtB, acrD* and *acrB* under ID-CAMHB relative to ID-CAMHB+$FeCl_3$ at log_2 fold increases of 9.08, 5.092 and 3.933, respectively, as identified by *t*-test ($p<0.001$). The log_2 fold upregulation observed for *mdtB* was significantly higher than that of both *acrD* and *acrB* at log_2 fold increases of 3.988 and 5.147, respectively, shown to be significant at $p<0.05$ for both.

In alignment with the prior description of 3.2.1., it was next necessary to determine whether capsulation impacted the RNA transcript expression of *mdtB, acrD* and *acrB* under iron limitation. This was to ensure that any siderophore export or CFDC susceptibility impact conferred by capsulated strains under iron limitation would not be the result of the confounding variable of differential RND efflux pump expression relative to non-capsulated strains. To do this, *Kp* 52145 was incubated overnight in iron limited media (ID-CAMHB), RNA was extracted and the expression of *mdtB, acrD* and *acrB* analysed *via* RT-(q)PCR. Ecl8 expression levels of *mdtB*, *acrD* and *acrB* obtained by RT-(q)PCR after overnight incubation in ID-CAMHB were employed as baseline controls.

There was no statistically significant log_2 fold change difference in the RNA transcript expression of *mdtB, acrD* and *acrB* in *Kp* 52145 relative to Ecl8 under ID-CAMHB. Results are shown in Figure 30.

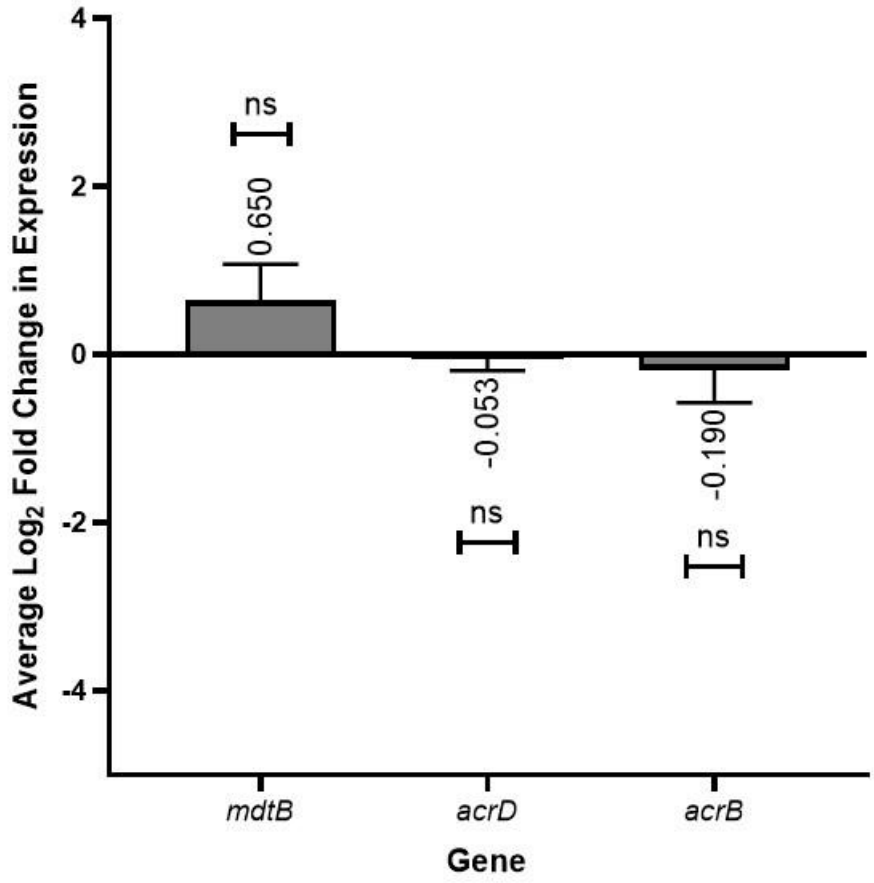

Figure 30. Log_2 fold change expression of *mdtB, acrD, acrB* in *Kp* 52145 relative to Ecl8 under iron deplete media (ID-CAMHB). Average log_2 fold-change ± SEM is plotted showing the log_2 fold change in gene expression as a ratio of *Kp* 52145 ID-CAMHB:Ecl8 ID-CAMHB – test:control. The label ns indicates not statistically significant as identified by *t*-test. Log_2 fold change was averaged after conducting investigation under biological and technical replicates both equalling n=3.

RND efflux pump component expression in response to iron limitation was therefore shown to be capsulation independent.

To summarise, the above data confirms the consistently increased RNA transcript expression of RND efflux pumps MdtABC-TolC, AcrA-AcrD-TolC and AcrAB-TolC under iron limitation in *Kp*. Thus, this supports the hypothesis that these pumps may be involved in the export of enterobactin from *Kp* under conditions of low iron. Therefore, *mdtB, acrD* and *acrB* were selected for further analysis through genetic deletion in both Ecl8 and *Kp* 52145.

3.3.2. Generation of RND Efflux Pump Deletion Mutants in Ecl8 and Kp 52145 Backgrounds

To introduce DH10βpTOFNoCo*mdtABC*<km> into the Ecl8 and *Kp* 52145 chromosomes, the nonconjugative homologous recombination exchange protocol was performed as per the method

outlined in *2.5.1.3.*. To assess whether the DH10βpTOFNoCo*mdtABC*<km> construct had been successfully inserted into Ecl8 and *Kp* 52145, One*Taq* PCR was performed using appropriate Next and Cext primers (see Appendix I) as per the methods of *2.5.1.3.* and **2.4.**. For the PCR result showing the successful deletion of *mdtABC* in the Ecl8 and *Kp* 52145 backgrounds, see Figure 31.

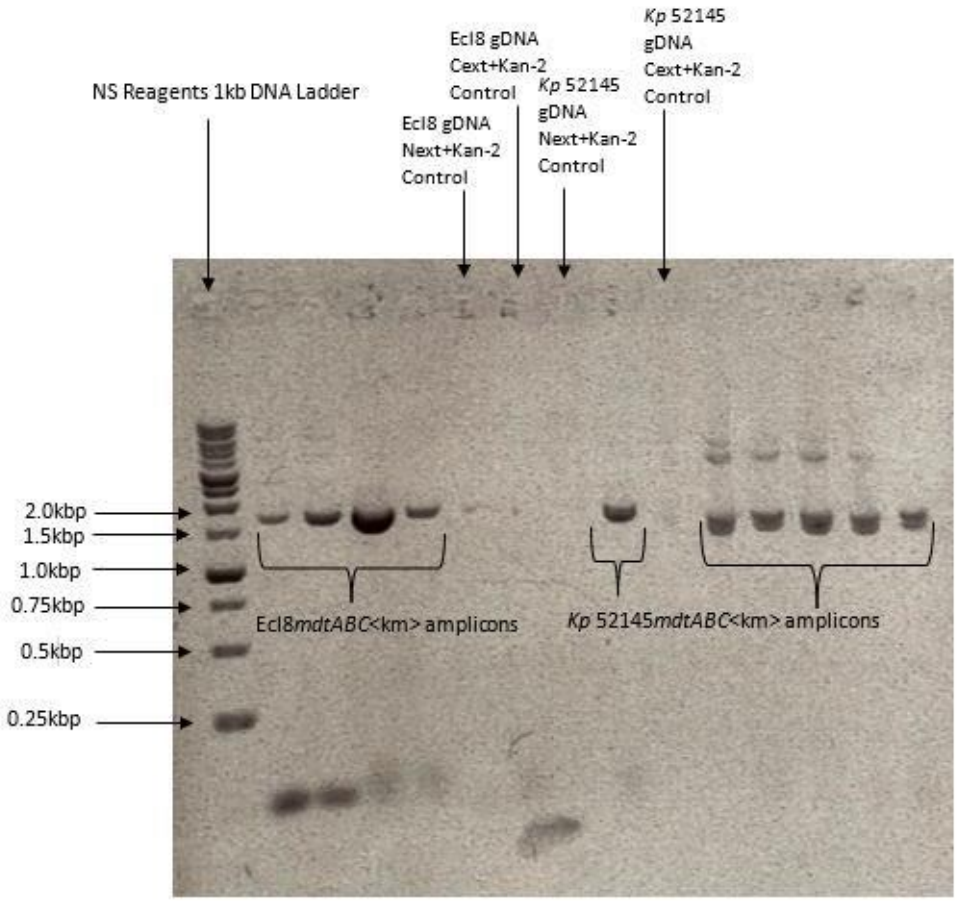

Figure 31. Gel electrophoresis image showing the successful insertion of DH10βpTOFNoCo*mdtABC*<km> knockout constructs in both Ecl8 and *Kp* 52145 backgrounds. Banding at approximately 1.5kbp to 2kbp represents Kan-2 amplification of the successfully inserted 1.7kbp Km cassette of the knockout construct, adjacent to the forward and reverse flanking regions of the gene of interest to be deleted (*mdtABC*) (where Next or Cext binds respectively). This therefore confirms *mdtABC* replacement with the Km cassette knockout construct, and hence *mdtABC* deletion, in both backgrounds. Absence of control banding shows expected absence of Km cassette knockout construct presence. Of the successful mutants for each strain background, one of each was selected for use in subsequent experiments. See Appendix I for primers used.

To next attempt to induce the deletion of *acrD* in the Ecl8 and *Kp* 52145 backgrounds, the conjugative homologous recombination protocol was performed as outlined in 2.5.2.. The pKNGS plasmid was

employed as the suicide vector as per the outlined protocol for attempts to introduce an *acrD* knockout construct into the chromosomes of both non-capsulated and capsulated strains.

Firstly, to ensure specific target site knockout, the N- and C- termini of the gene of interest for deletion (*acrD*) was amplified with NoNi and CoCi primers *via* Phusion PCR as per the method of *2.5.2.1.*. NoCo fragment constructs including the regions flanking the gene of interest for deletion were then made using Phusion PCR as per the method of *2.5.2.1.*. Gel electrophoresis results validating each CoCi fragment, NoNi fragment and resultant NoCo construct Phusion PCR products are shown in Figures 32 - 37.

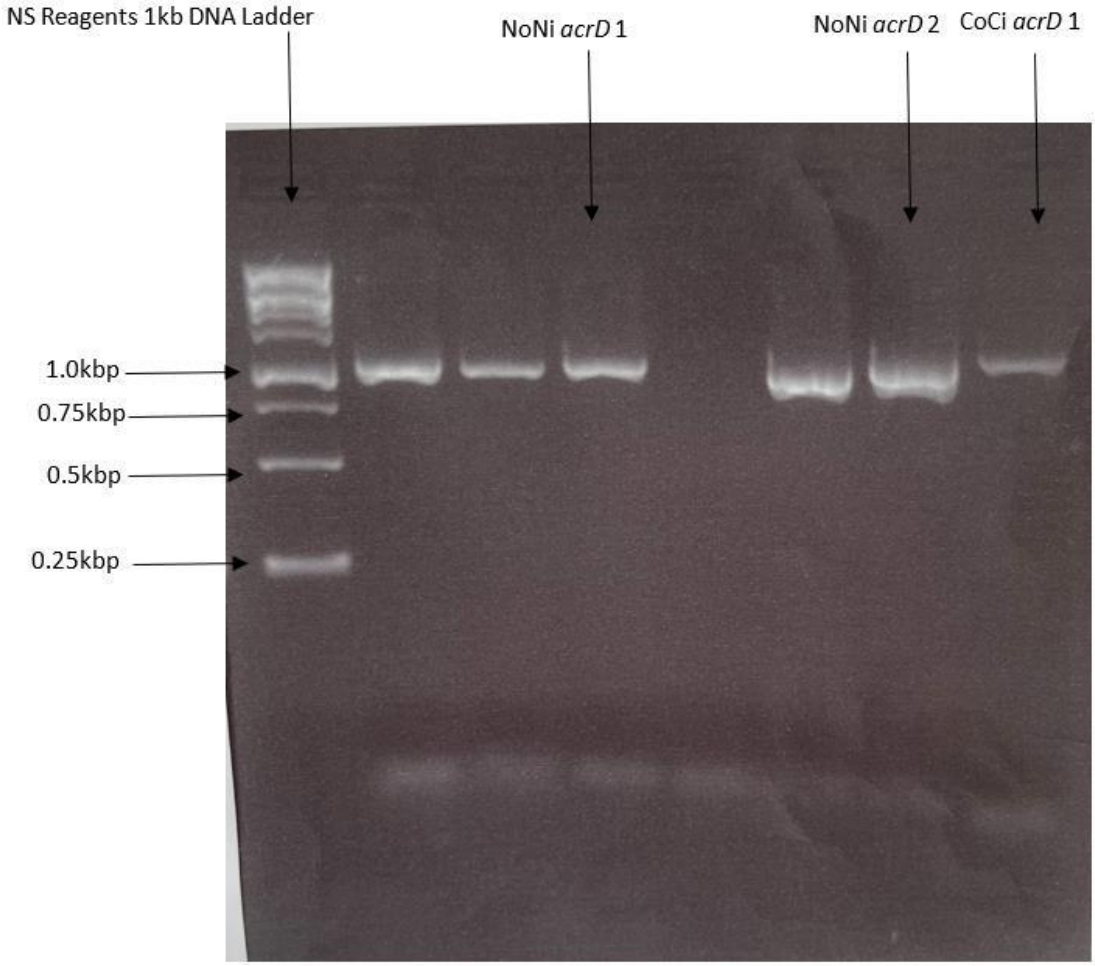

Figure 32. Gel electrophoresis image showing *acrD* CoCi and NoNi fragment Phusion PCR products. The image clearly shows two respective bands at approximately 1kbp – representing the CoCi band at 1025kbp, and the NoNi band at 1036kbp. Note, for each CoCi and NoNi there were two separate wells representing two separate PCRs, this was due to one reaction containing a low concentration of Ecl8 gDNA template, so duplicate reaction was performed to ensure strong banding and reasonable fragment concentration. These bands were then taken forward for gel extraction and purification to a reasonable concentration for NoCo making. The bands without labels here were representative of other fragments. See Appendix I for primers used.

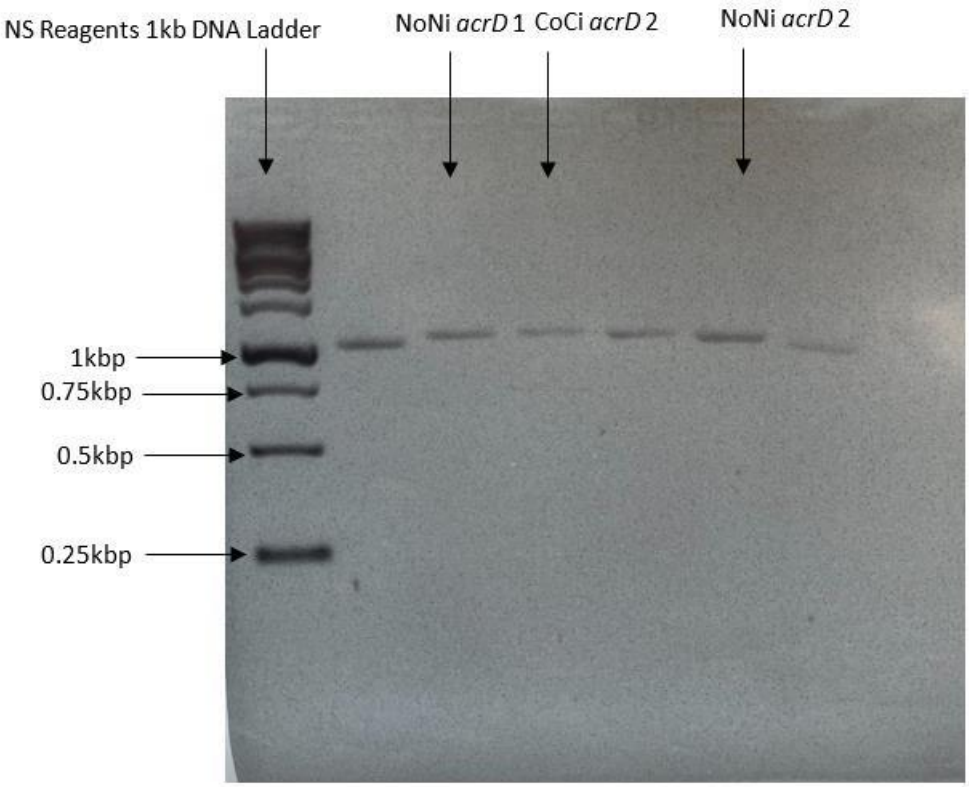

Figure 33. Gel electrophoresis image showing extracted and purified *acrD* CoCi and NoNi fragment band size checks. Here, there are clear bands at approximately 1kbp, representative of the *acrD* CoCi and NoNI respective bands lengths of 1036kbp and 1025kbp. The bands not labelled here were representative of other fragments. See Appendix I for primers used.

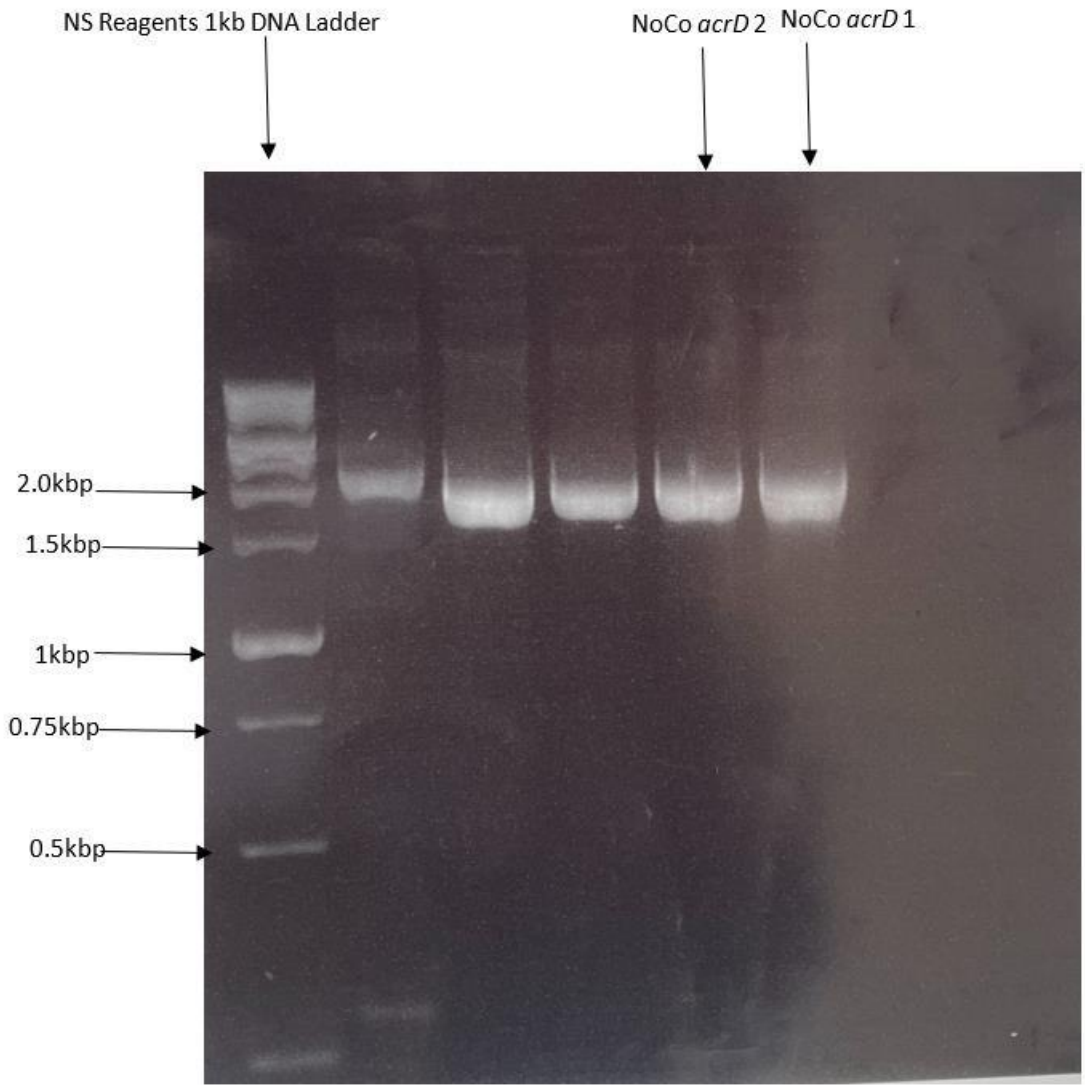

Figure 34. Gel electrophoresis image showing NoCo*acrD* fragment Phusion PCR products made using the combinations of NoNi 1, CoCi 1 and CoCi 2 as shown in Figure 33. The banding at approximately 2kbp represents the *acrD* NoCo fragment size of 2061kbp. The bands not labelled on this image represent other NoCo fragments. See Appendix I for primers used.

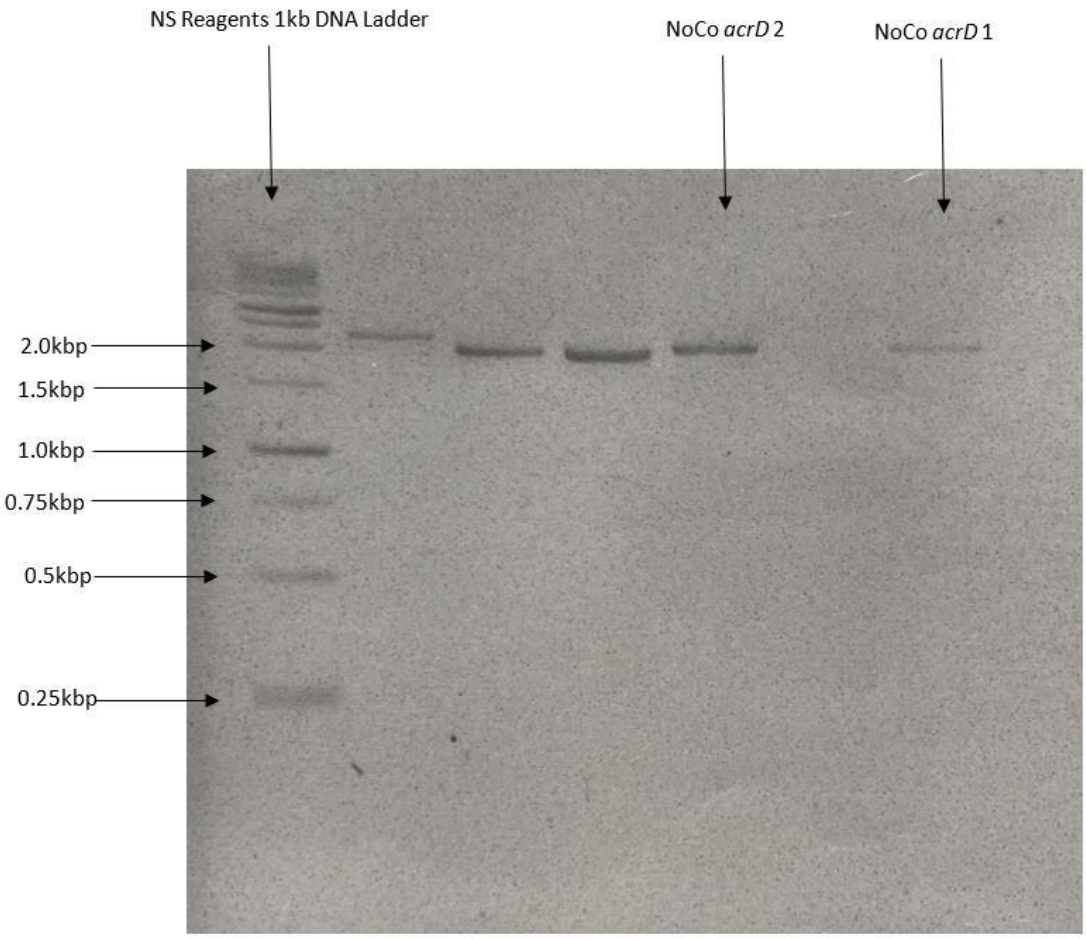

Figure 35. Gel electrophoresis image showing extracted and purified NoCo*acrD* construct DNA band size checks. The bands shown represent *acrD* clearly at 2061kbp. The NoCo with the highest concentration after nanodrop analyses was selected for ligation and electroporation. The bands not labelled represent different fragments. See Appendix I for primers used.

The concentration of the selected purified NoCo*acrD* was 16.7ng/µl. The NoCo was then ligated with the pKNGS vector in a molar ratio of 6:1 as per the method of *2.5.2.2.*. To maintain plasmid stability and ensure high efficiency plasmid replication during exchange, the NoCo-pKNGS constructs were then cloned into *E. coli* DH5α *pir* as per the method of *2.5.2.3.*. To confirm the pKNGSNoCo constructs had been cloned into *E. coli* DH5α *pir*, One*Taq* colony PCR was performed to validate pKNGS backbone insertion, using the appropriate pKNGS verification primer set (see Appendix I) as per the methods of *2.5.2.3.* and **2.4.**. Gel electrophoresis results of successful cloning are shown in Figure 36 - 38. Figure 39 shows the result of a repeat PCR following NoCo-pKNGS *E. coli* DH5α *pir* construct DNA extraction to confirm banding sizes for transformation into the conjugative donor strain: *E. coli* S17 MFD λpir.

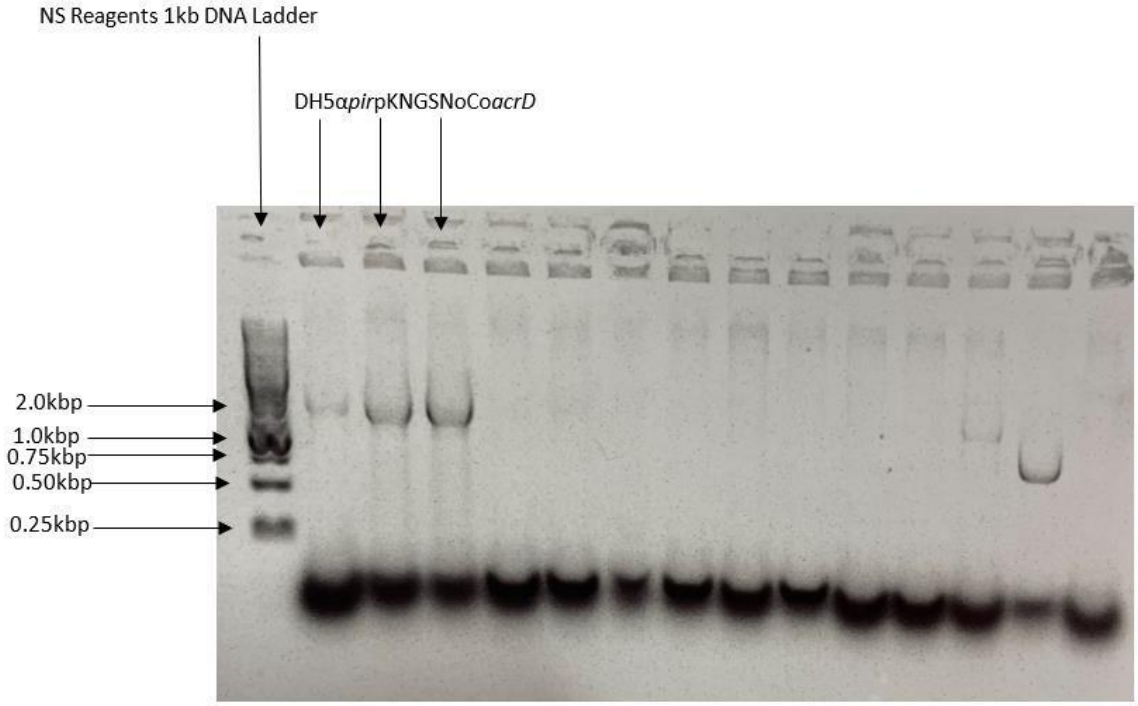

Figure 36. Gel electrophoresis image of One*Taq* PCR products showing successful pKNGSNoCo*acrD* construct cloning in *E. coli* DH5α *pir* from the 5µl:50µl 60ng:10ng insert:vector ligation after the optimized addition of DMSO to the PCR mixture. Bands not labelled here represent other fragments. See Appendix I for primers used.

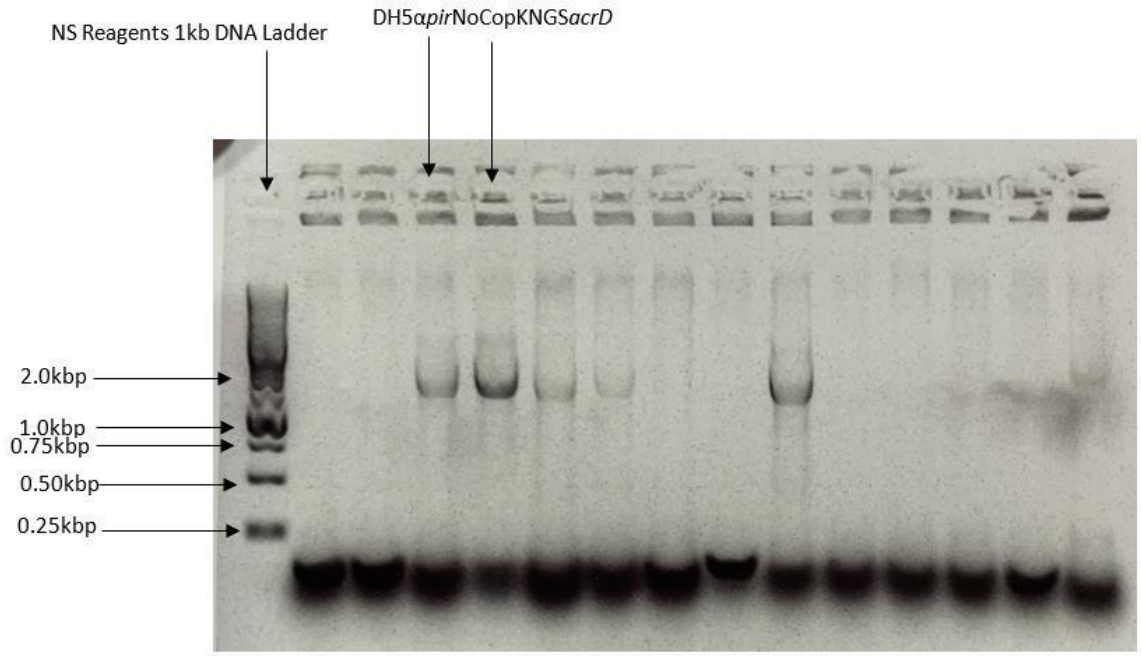

Figure 37. Gel electrophoresis image of One*Taq* PCR products showing successful pKNGSNoCo*acrD* construct cloning in *E. coli* DH5α *pir* from the 90ng:15ng insert:vector ligation after the optimized addition of DMSO to the PCR mixture. Bands not labelled here represent other fragments. See Appendix I for primers used.

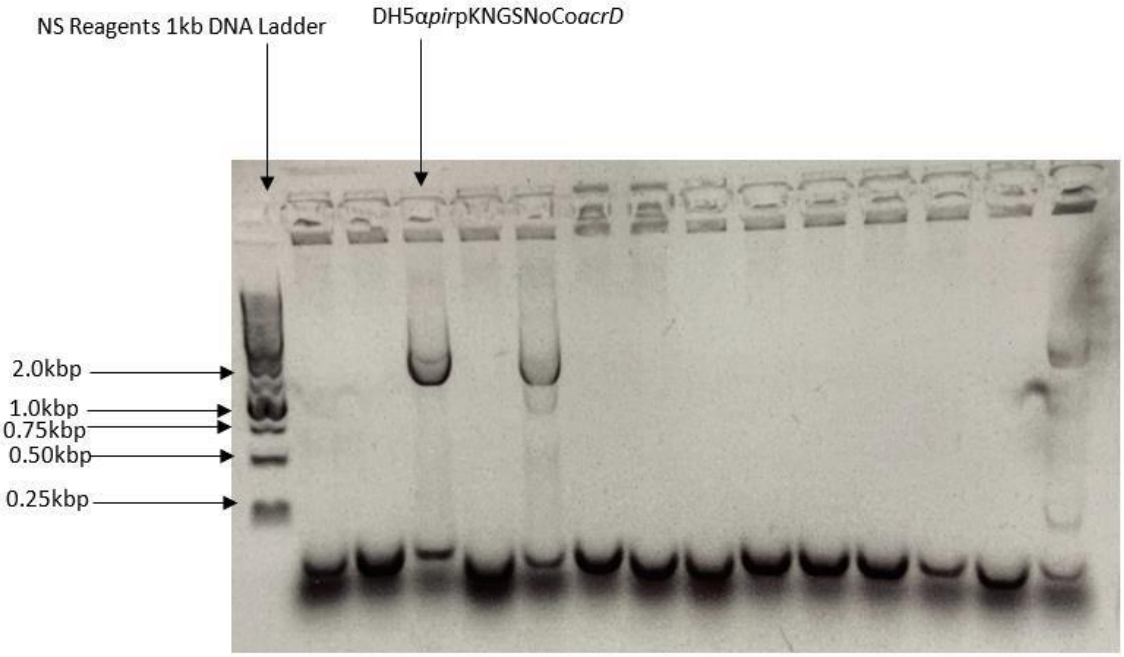

Figure 38. Gel electrophoresis image of One*Taq* PCR products showing successful pKNGSNoCo*acrD* construct cloning in *E. coli* DH5α *pir* for AcrD from the 60ng:10ng insert:vector ligation after addition of DMSO and 15µl clean ligation product for electroporation. Bands not labelled here represent other fragments. See Appendix I for primers used.

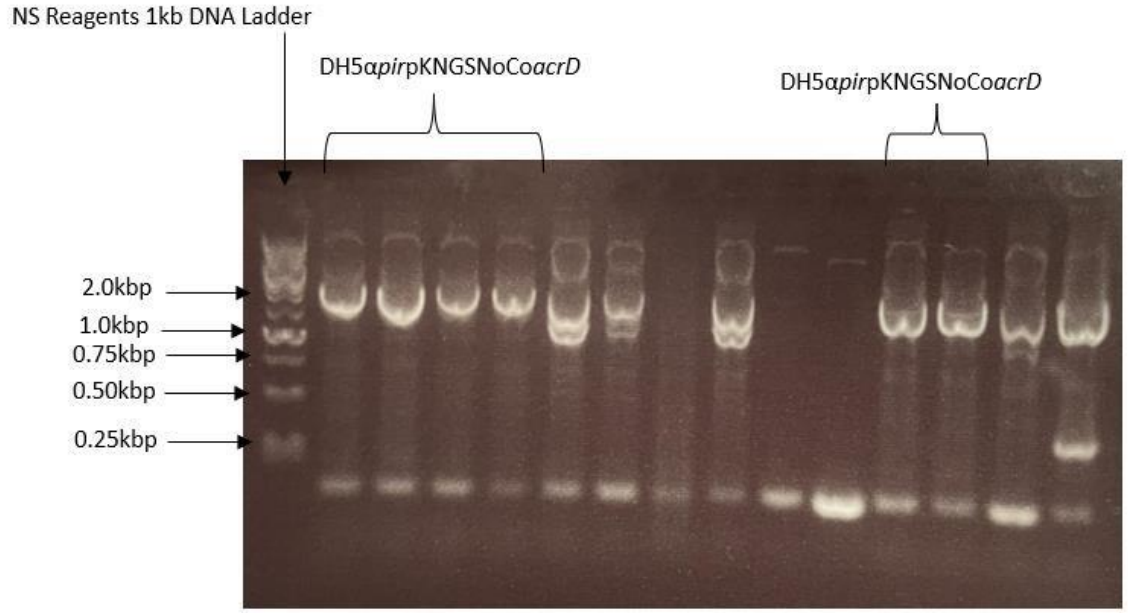

Figure 39. Gel electrophoresis image showing all successful DH5α*pir*pKNGSNoCo*acrD* construct clone DNA, confirming correct banding sizes. Bands not labelled represent other fragments. See Appendix I for primers used.

To allow for plasmid transfer into Gram-negative recipient strains Ecl8 and Kp 52145, the nonconjugative DH5a *pir*pKNGSNoCo*acrD* clones were next transformed into conjugative strain *E. coli* S17 MFDλ*pir*. Only a single successful DH5α *pir*pKNGSNoCo clone was selected for this transformation, performed as per the method outlined in *2.5.2.3.*. After conjugation into Ecl8 and *Kp* 52145, no Km susceptibility was observed. After troubleshooting as per the repeated colony patching and 42°C pooled colony incubation of *2.5.2.3.*, this outcome was unchanged. Therefore, plasmid excision from the conjugated recipient strain had been unsuccessful. Thus, these mutants could not be employed for the analysis of impact to siderophore export and CFDC susceptibility. For images of Km resistant transconjugants, see Figure 40.

Figure 40. Images of LB+Km 100mg/ml (denoted Km) plates of DH5α *pir*pKNGSNoCo*acrD* (denoted A) clones transformed into *E. coli* MFD S17 λ*pir* after attempts for recipient conjugation and plasmid excision. Recipients were Ecl8 (denoted 62) (**A**) and *Kp* 52145 (denoted 440) (**B**). Images show no Km susceptibility. Images were fitted with a pixel-mm representative scale bar of 20mm using ImageJ software (Schneider, Rasband and Eliceiri, 2012).

3.3.3. Measuring the Impact of Iron Limitation on Capsule Production in *Kp* 52145*mdtABC*<km>

Before the *Kp* 52145*mdtABC*<km> mutant and its respective *Kp* 52145 wild type could be employed in further analysis, it was firstly necessary to rule out any impact of iron limitation on both strain's ability to produce the K2 serotype exopolysaccharide capsule. This was necessary to ensure that any impact to siderophore export or CFDC susceptibility conferred by *Kp* 52145*mdtABC*<km> and *Kp* 52145 under iron limitation would not be the result of the confounding variable of iron limitation effecting capsule density.

Glucuronic acid is a major capsular component. Therefore, measuring the concentration of 4-O(I-1Carboxyethyl)-d-glucuronic acid allows for the indirect quantification of total exopolysaccharide density (Clements *et al.*, 2008). Hence, to measure the effect of iron limitation on K2 capsule production, MdtABC-TolC deletion mutant *Kp* 52145*mdtABC*<km> and wild type strain *Kp* 52145 were incubated overnight in iron limited media (ID-CAMHB), and the concentration of 4-O(I-1Carboxyethyl)-d-glucuronic acid was quantified as per the method outlined in **2.6.**. The concentration of 4-O(I-1-Carboxyethyl)-d-glucuronic acid was also measured following overnight

incubation of *Kp* 52145*mdtABC*<km> and *Kp* 52145 in iron replete media (ID-CAMHB+$FeCl_3$), with these resultant values acting as the baseline controls.

It was found that there was no difference in the average 4-O(I-1-Carboxyethyl)-d-glucuronic acid concentration of either *Kp* 52145*mdtABC*<km> or *Kp* 52145 under iron limitation relative to iron repletion. Results are shown in Figure 32.

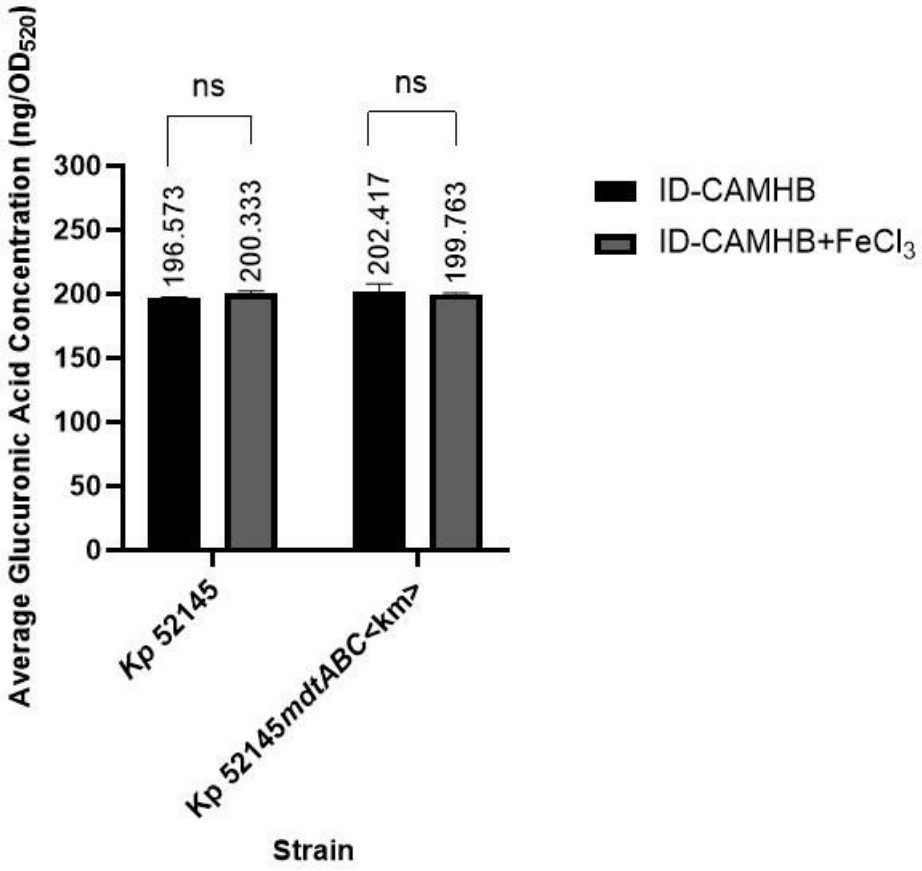

Figure 41. Glucuronic acid concentration (ng/OD_{520}) of *Kp* 52145 and *Kp* 52145*mdtABC*<km> averaged across biological and technical replicates equalling n=3. ID-CAMHB represents iron deplete media, with IDCAMHB+$FeCl_3$ representing iron replete media. The label ns indicates not statistically significant as identified by *t*-test.

Figure 32 shows that the glucuronic acid concentration of *Kp* 52145 after overnight incubation in iron depleted media (ID-CAMHB) was of no statistically significant difference relative to the glucuronic acid concentration after overnight incubation in iron replete media (ID-CAMHB+$FeCl_3$), as identified by *t*-test. Concentrations were 196.573 ng/OD_{520} in ID-CAMHB, and 200.333 ng/OD_{520} in IDCAMHB+$FeCl_3$, respectively. Similarly, the glucuronic acid concentration of *Kp* 52145*mdtABC*<km> after incubation in

ID-CAMHB showed no statistically significant difference relative to the glucuronic acid concentration after incubation ID-CAMHB+$FeCl_3$. Concentrations were 202.417 ng/OD_{520} in IDCAMHB, and 199.763 ng/OD_{520} in ID-CAMHB+$FeCl_3$, respectively. Further, there was no statistically significant difference in the glucuronic acid concentration of *Kp* 52145*mdtABC*<km> relative to *Kp* 52145 after incubation in both ID-CAMHB and ID-CAMHB+$FeCl_3$, as identified by *t*-test. Therefore, these data confirm that any impact to siderophore export and CFDC susceptibility conferred by *Kp* 52145*mdtABC*<km> and *Kp* 52145 under iron limitation would not be the result of iron limitation having impacted capsule density. Hence, both strains could be taken forward for the subsequent investigation of their ability to export siderophore under iron limitation.

3.3.4. Semi-Quantitative Analysis of Siderophore Export Under Efflux Component Deletion: Chrome Azurol S (CAS) Agar Assaying

To establish the impact of RND efflux pump deletion on the ability of *Kp* to export enterobactin under iron limitation, extracellular siderophore production from isogenic strains of Ecl8 and *Kp* 52145 deleted of *mdtABC*, and an isogenic strain of Ecl8 deleted of *acrAB*, was quantified. This was achieved using the semi-quantitative method of the Chrome Azurol S (CAS) agar assay. The CAS assay works on the basis of exploiting the capacity of siderophores to bind Fe^{3+}. Within the agar media, blue CAS dye is complexed with Fe^{3+} and the surfactant hexadecyltrimethylammonium (HDTMA). Following inoculation of bacterial strains onto the plate, the release of siderophores from the bacteria results in the chelation of the Fe^{3+} from the CASFe^{3+}-HDTMA complex. This results in a distinctive colour change of the agar from blue to orange in a 'halo' around the inoculum droplet. The diameter of this halo can then be measured, and can be used to correlate the amount of siderophore effluxed from the bacteria. For example, a larger orange halo diameter around the inoculum droplet is directly proportional to there being a larger amount of siderophore effluxed from the bacteria (Schwyn and Neilands, 1987; Himpsl and Mobley, 2019). To the best of our knowledge, this method has not been previously utilised to measure siderophore efflux from MdtABC-TolC or AcrAB-TolC deleted strains of *Kp*. For the preliminary trial of the CAS agar media which validated it's use for this thesis' duration, see Appendix IV.

Following overnight incubation of Ecl8*mdtABC*<km>, Kp 52145*mdtABC*<km> and Ecl8*acrAB*<km> alongside wild type controls Ecl8 and *Kp* 52145 in iron limited media (ID-CAMHB), cultures were

standardized to OD_{600} 1.5 and 5µl droplets of each were inoculated onto CAS agar plates. Plates were then incubated for 18h at 30°C as per the protocol outlined in **2.9.**.

It was recorded that the deletion of *mdtABC* resulted in decreased siderophore export from *Kp* under iron limited media (ID-CAMHB) relative to wild type controls Ecl8 and *Kp* 52145. The deletion of *acrAB* conferred no difference in siderophore export relative to wild type control Ecl8. Results are shown in Figure 42.

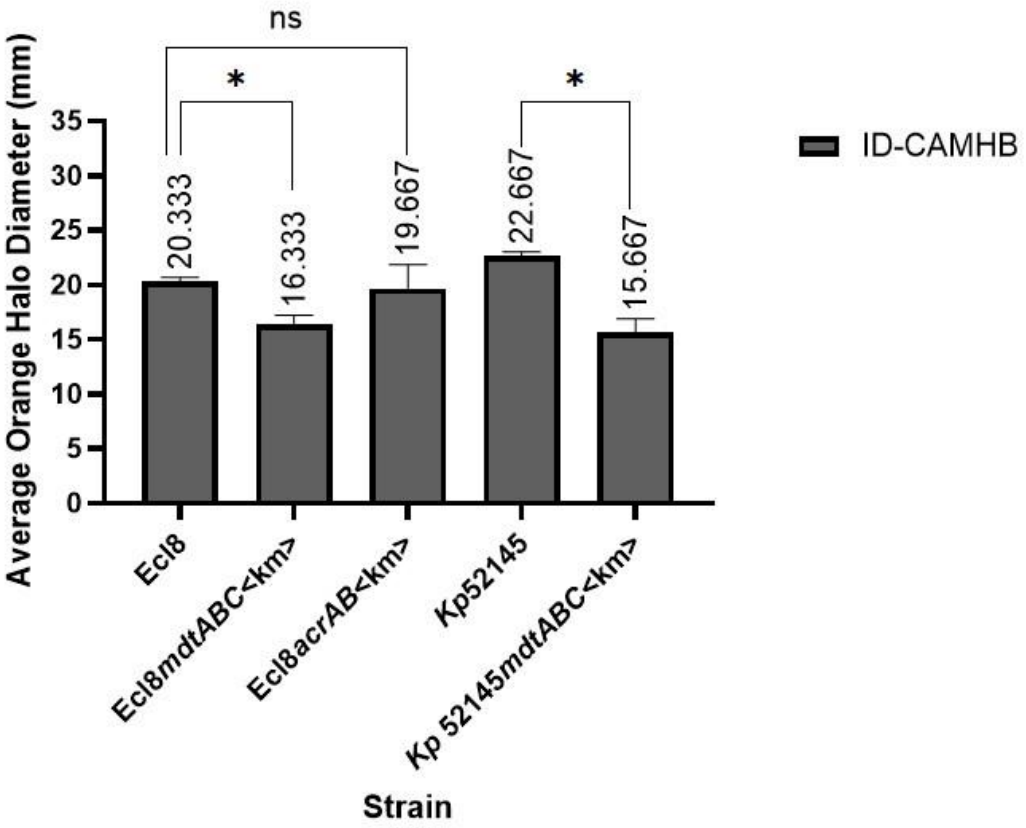

Figure 42. Average orange halo diameters (mm) on CAS agar plates after inoculation with Ecl8, Ecl8*mdtABC*<km>, Ecl8*acrAB*<km>, *Kp* 52145 and *Kp* 52145*mdtABC*<km> grown overnight in iron deplete media (ID-CAMHB). The label ns indicates not statistically significant as identified by *t*-test. The label * indicates statistically significant at $p<0.05$ as identified by *t*-test. Halo diameter was averaged after conducting investigation under biological replicates equalling n=3.

Figure 42 shows both Ecl8*mdtABC*<km> and *Kp* 52145*mdtABC*<km> to have conferred a statistically significant decrease to siderophore export under ID-CAMHB relative to Ecl8 and *Kp* 52145, respectively, at $p<0.05$ as identified by *t*-test. Average orange halo diameters of Ecl8*mdtABC*<km> and *Kp* 52145*mdtABC*<km> were 16.333mm and 15.666mm, respectively. These were 4mm (approximately 20%) lower and 7mm (approximately 31%) lower than respective wild type average

orange halo diameters. No statistically significant difference was recorded between average halo diameters of Ecl8 and *Kp* 52145 after incubation in ID-CAMHB (20.3mm and 22.667mm, respectively). Much like the wild type controls, there was no statistically significant difference recorded between the orange halo diameters of Ecl8*mdtABC*<km> and *Kp* 52145*mdtABC*<km>. Thus, the ability of *Kp* to export siderophore in both wild type and *mdtABC* deleted backgrounds was found to be capsule independent. Deletion of *acrAB* conferred no statistically significant impact to siderophore export relative to Ecl8 under ID-CAMHB, producing an orange halo of diameter 19.667mm. For collated images of all CAS agar plates showing orange halo production, see Appendix V.

The results presented therefore show a significant role of MdtABC-TolC in the efflux of siderophore from *Kp* under iron limitation. The results also show that AcrAB-TolC has no independent effect on siderophore efflux from *Kp*.

To subsequently ascertain the impact of both MdtABC-TolC and AcrAB-TolC on the efflux of CFDC from *Kp*, susceptibility testing was performed on Ecl8*mdtABC*<km>, *Kp* 52145*mdtABC*<km> and Ecl8*acrAB*<km>.

3.3.5. Susceptibility Testing of Efflux Component Deleted Strains

To determine the impact of RND efflux pump deletion on the permeability of the OM to CFDC, broth microdilution susceptibility testing was performed on isogenic strains of Ecl8 and *Kp* 52145 deleted of *mdtABC*, and an isogenic strain of Ecl8 deleted of *acrAB*. This was conducted in iron deplete (IDCAMHB) and iron replete (ID-CAMHB+$FeCl_3$) medias as per the method outlined in 2.10.2..
Susceptibility of all strains to CAZ was also tested, with this antibiotic acting as a baseline control, under the anticipation that its susceptibility would not be affected by iron limitation (Ito *et al.*, 2016) - in alignment with the prior description of 3.2.3..

The deletion of *mdtABC* resulted in a decrease in CFDC MIC under iron limitation. Deletion of *acrAB* conferred no difference to CFDC MIC, but was shown to decrease CAZ MIC irrespective of iron concentration. Capsulation had no impact on the MIC of either CFDC or CAZ. Results are shown in Table 9.

Strain	CFDC ID-CAMHB	CAZ ID-CAMHB	CFDC ID-CAMHB+$FeCl_3$	CAZ ID-CAMHB+$FeCl_3$
Ecl8	0.5	1	2	0.5
***Kp* 52145**	0.5	1	2	0.5
Ecl8*mdtABC*<km>	0.125	1	1	1
***Kp* 52145*mdtABC*<km>**	0.125	1	1	1
Ecl8*acrAB*<km>	1	0.25	1	0.125

Table 9. Modal CFDC and CAZ MIC values (mg/L) of RND efflux pump deleted strains and respective wild types. ID-CAMHB represents iron deplete media and ID-CAMHB+$FeCl_3$ represents iron replete media. This data was recorded as the modal value due to the data being geometric. Investigation was conducted under biological and technical replicates both equalling n=3.

3.3.5.1. CFDC Susceptibility

Table 9 shows there being no difference in the MIC of either CFDC or CAZ between Ecl8 and *Kp* 52145 under both iron limitation (ID-CAMHB) and iron repletion (ID-CAMHB+$FeCl_3$). Thus, the susceptibility of *Kp* to these antibiotics was shown to be capsule independent. The same capsule independency was observed for MIC values demonstrated by Ecl8*mdtABC*<km> and *Kp* 52145*mdtABC*<km>. However, it was recorded that the deletion of *mdtABC* conferred a 4-fold increase in CFDC susceptibility under ID-CAMHB relative to respective wild types. Thus, these data show MdtABC-TolC to be able to efflux CFDC from *Kp* under iron limitation, thereby decreasing the susceptibility of *Kp* to the antibiotic.

There was no biologically significant impact of Ecl8*acrAB*<km> on CFDC MIC irrespective of iron concentration, showing only a 2-fold change relative to Ecl8 in both ID-CAMHB and ID-CAMHB+$FeCl_3$. Thus, AcrAB-TolC was found to have no effect on the efflux of CFDC from *Kp* and therefore on the susceptibility of *Kp* to CFDC.

Together with the results of the CAS agar assay (3.3.4.), these results demonstrate that the ability of Ecl8*mdtABC*<km>, *Kp* 52145*mdtABC*<km> and Ecl8*acrAB*<km> to efflux siderophore is positively

correlated with the ability of Ecl8*mdtABC*<km>, *Kp* 52145*mdtABC*<km> and Ecl8*acrAB*<km> to efflux CFDC.

3.3.5.2. CAZ Susceptibility

Table 9 shows deletion of *mdtABC* had no impact on CAZ MIC irrespective of iron concentration. However, the deletion of *acrAB* conferred a 4-fold increase to CAZ susceptibility in both ID-CAMHB and ID-CAMHB+$FeCl_3$. There was no biologically significant difference between the MIC values of Ecl8*acrAB*<km> irrespective of iron concentration. Thus, these data show AcrAB-TolC to be able to efflux CAZ from *Kp* in an iron independent manner.

To close, this chapter has evidenced the independent relative contribution of both MdtABC-TolC and AcrAB-TolC to the efflux of siderophore from *Kp* under iron limitation. Further, this chapter has shown RND family efflux pump MdtABC-TolC to be able to efflux CFDC from *Kp* under iron limitation. To recap, Chapter Two evidenced a combination of at least three of the IROMPs CirA, Fiu, FepA and FecA to be required for the optimal influx of CFDC into *Kp* under iron limitation. Thus, it was of final necessity to confirm that the cumulative reduced OM permeability of *Kp* to CFDC cccurs through the respective transcriptional activation and transcriptional repression of these efflux and influx components by the TCS BaeSR and EnvZ-OmpR. Moreover, with this chapter having also ruled out any role of AcrAB-TolC in CFDC susceptibility, it was to be investigated whether the overexpression of AraC/XylS transcription factor *ramA* may still confer an impact, and whether this may be the result of RamA regulating the same RND efflux pump and IROMP encoding genes as the TCS regulators.

3.4. CHAPTER FOUR: Confirming the Impact of TCS EnvZ-OmpR, TCS BaeSR and AraC/XylS Transcription Factor RamA on the Permeability of the OM to CFDC

It is known that the TCS EnvZ-OmpR indirectly represses the transcription of IROMP encoding genes *cirA, fiu, fepA* and *fecA* through assocations with the sRNAs OmrA and OmrB and master Fe^{3+} regulator FUR (Guillier and Gottesman, 2006; Brosse, Korobeinikova, Gottesman and Guillier, 2016; Gerken, Vuong, Soparkar and Misra, 2020) (**1.5.**; Figure 2, 1.6.1.; Figure 4). It is also known that TCS BaeSR activates the transcription of RND efflux pump encoding genes *mdtB* and *acrD* (Nagakubo, Nishino, Hirata and Yamaguchi, 2002; Nishino, Honda and Yamaguchi, 2005). A growing number of studies are reporting CFDC resistant clinical isolates of *Kp* to overexpress TCS histidine kinases *envZ* and *baeS*, which render EnvZ-OmpR and BaeSR constitutively active (Coppi *et al.*, 2022; Simner *et al.*, 2022; Padovani *et al.,* 2023). Thus far, the present study has evidenced that under iron limitation, at least three of the four IROMPs CirA, Fiu, FepA and FecA are required for optimal CFDC influx. It has also been evidenced that RND efflux pump MdtABC-TolC is able to export CFDC out of the cell. Thus, these findings must now be substantiated at the regulatory level to confirm the proposed pathway by which *Kp* resists CFDC through EnvZ-OmpR and BaeSR (Figure 5). The present study also evidenced RND efflux pump AcrAB-TolC to confer no impact to *Kp* CFDC susceptibility. However, the overexpression of its known positive regulator RamA is known to induce a range of OM perturbations, and has therefore been implicated to contribute to a clinical MDR phenotype of *Kp* (De Majumdar *et al.*, 2015; Jiménez-Castellanos *et al.*, 2016; Jiménez-Castellanos *et al*., 2018). Hence, it is of equal necessity to investigate whether RamA may impact the susceptibility of *Kp* to CFDC, and, from this, investigate whether this impact may be mediated through any shared regulation of MdtABC-TolC, AcrA-AcrD-TolC or the IROMPs with BaeSR and EnvZ-OmpR. Therefore, this chapter sought to establish the impact of the loss and clinically relevant overexpression of EnvZOmpR, BaeSR and RamA on *Kp* susceptibility to CFDC under iron limitation. To achieve this, it will firstly be assessed what the impact of iron limitation is to the expression of each response regulator gene. Subsequently, these genes will be taken forward for further investigation through their genetic deletion and overexpression. Next, it will be assessed how the respective deletion and overexpression of known RND efflux pump regulators *baeSR* and *ramA* affects siderophore export under iron limitation. This will be followed by investigating the impact of *baeSR* deletion and *ramA* overexpression on CFDC susceptibility. At this stage, the effect of deletion and overexpression of EnvZ-OmpR on CFDC susceptibility will also be assessed. Finally, after determining the impact of

ramA overexpression on CFDC susceptibility, it will be investigated whether *ramA* overexpression can induce differential RNA transcript expression of *mdtB, acrD*, *cirA, fiu, fepA* and *fecA* under iron limitation.

3.4.1. Transcriptomic Analyses - How does Iron Limitation Drive RNA Transcript Expression of Regulatory Factor Encoding Genes *ompR, baeR* and *ramA*?

To ascertain the impact of iron limitation on the RNA transcript expression of TCS response regulators *ompR* and *baeR,* and AraC/XylS regulator *ramA*, Ecl8 was incubated overnight in iron limited media (ID-CAMHB), RNA was extracted, and and the expression of *ompR, baeR* and *ramA* was analysed *via* RT-(q)PCR. RNA transcript expression levels of the same genes obtained by RT-(q)PCR after overnight incubation of Ecl8 in iron replete media (ID-CAMHB+$FeCl_3$) were used as the baseline controls.

It was found that there was a consistent upregulation in *ompR, baeR* and *ramA* RNA transcript expression levels after incubation of Ecl8 in iron limited media (ID-CAMHB) relative to iron replete media (ID-CAMHB+$FeCl_3$). Results are shown in Figure 43.

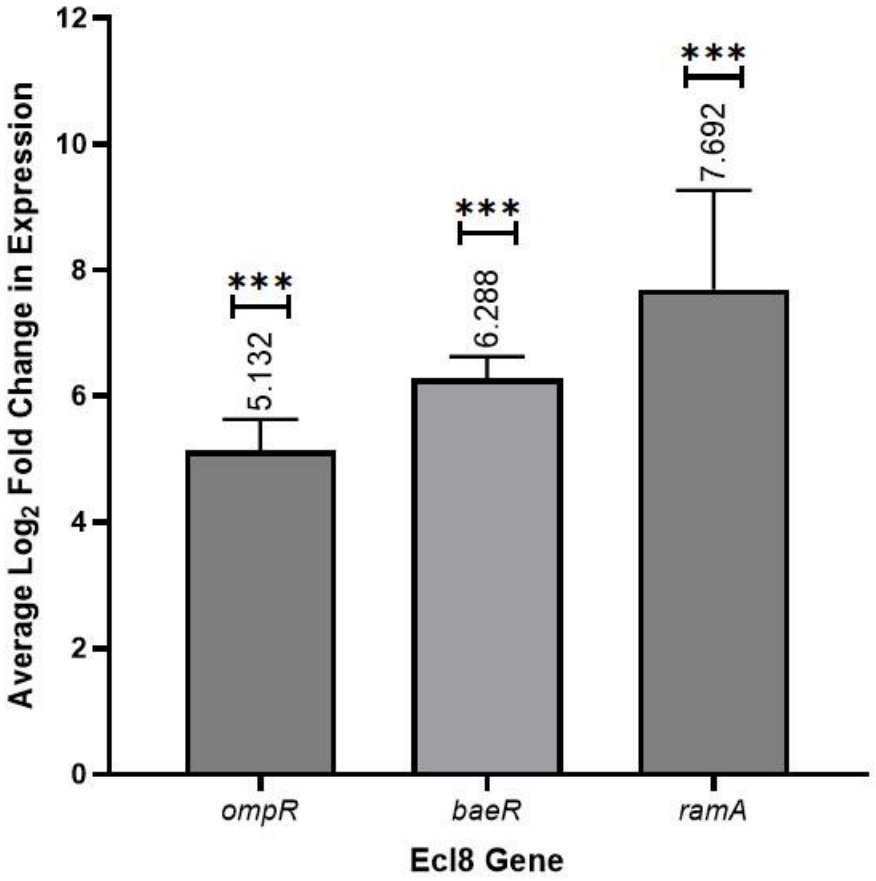

Figure 43. Log_2 fold change expression of *ompR, baeR* and *ramA* in iron deplete media (ID-CAMHB) relative to iron replete media (ID-CAMHB+$FeCl_3$). Average log_2 fold-change ± SEM is plotted showing the log_2 fold change in gene expression as a ratio of Ecl8 ID-CAMHB:ID-CAMHB+$FeCl_3$ – test:control. The label *** indicates statistically significant at $p<0.001$ as identified by *t*-test. Log_2 fold change was averaged after conducting investigation under biological and technical replicates both equalling n=3.

Figure 43 shows a statistically significant upregulation in expression of *ompR, baeR* and *ramA* at log_2 fold increases of 5.132, 6.288 and 7.692, respectively, under iron depleted media (ID-CAMHB) relative to iron replete media (ID-CAMHB+$FeCl_3$). Results were significant at $p<0.001$ as identified by *t*-test.

The log_2 fold upregulation of *ompR* was the lowest upregulation observed of all regulators by 1.156 to 2.56 log_2 fold. It was evidenced in Chapter One that the RNA transcript expression of *cirA, fiu, fepA* and *fecA* was upregulated under ID-CAMHB in Ecl8 in (3.2.1.; Figure 11). Thus, the relatively lower log_2 fold upregulation of *ompR* suggests that the negative feedback loop of *omrAB* activation, *ompR* repression and subsequent *omrAB* self-limitation had been initiated, and was occurring simultaneously to the derepression of *cirA, fiu, fepA* and *fecA* induced by apo-FUR (**1.5.**; Figure 2, 1.6.1.; Figure 4).

The upregulated RNA transcript expression for *baeR* and *ramA* under ID-CAMHB aligns directly with the upregulated RNA transcript expression of *mdtB, acrD* and *acrB* under ID-CAMHB evidenced in 3.3.1.. This confirms the respective positive regulation of MdtABC-TolC, AcrA-AcrD-TolC and AcrABTolC by BaeSR and RamA.

Chapters Two and Three confirmed no impact of capsulation on IROMP or RND efflux pump gene expression (3.2.1., 3.3.1.), siderophore export (3.3.4.) or CFDC susceptibility (3.3.5.) under iron limitation. Thus, it was of final necessity to validate and confirm that capsulation did not impact RNA transcript expression of *ompR, baeR* and *ramA* under iron limitation. To do this, *Kp* 52145 was incubated overnight in iron limited media (ID-CAMHB), RNA was extracted and the expression of *ompR, baeR* and *ramA* analysed *via* RT-(q)PCR. Ecl8 expression levels of *ompR, baeR* and *ramA* obtained by RT-(q)PCR after overnight incubation in ID-CAMHB were employed as baseline controls.

There was no statistically significant $\log_2$ fold change difference in the RNA transcript expression of *ompR, baeR* and *ramA* in *Kp* 52145 relative to Ecl8 under ID-CAMHB. Results are shown in Figure 44.

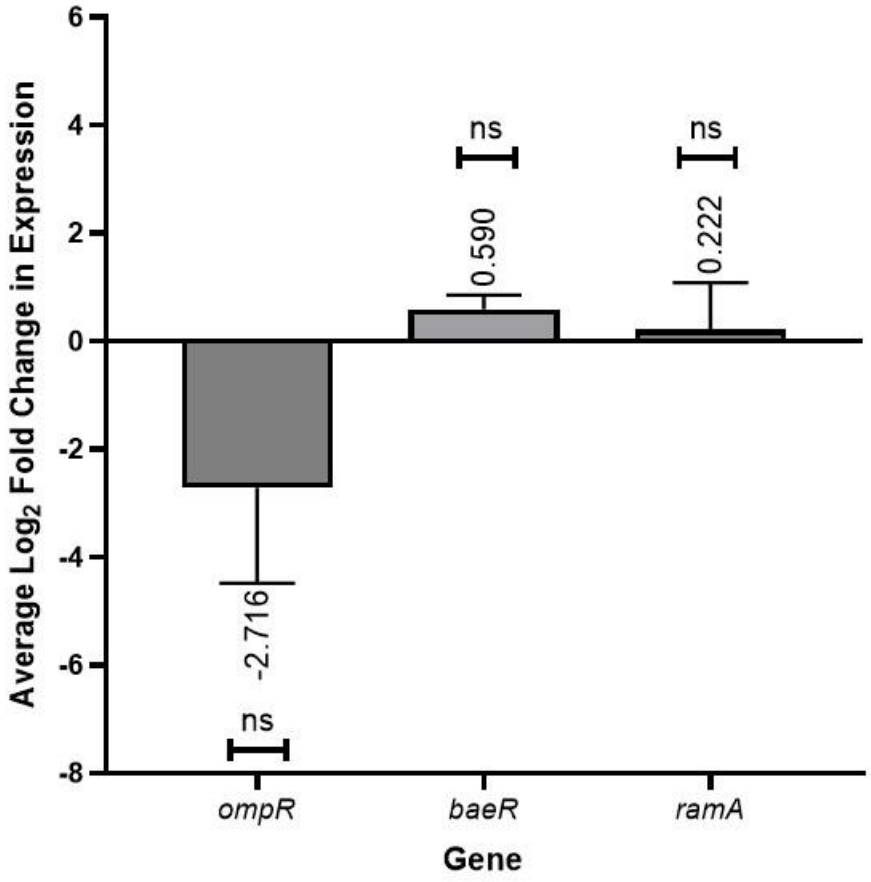

Figure 44. Log_2 fold change expression of *ompR, baeR* and *ramA* in *Kp* 52145 relative to Ecl8 under iron deplete media (ID-CAMHB). Average log_2 fold-change ± SEM is plotted showing the log_2 fold change in gene expression as a ratio of *Kp* 52145 ID-CAMHB: Ecl8 ID-CAMHB – test:control. The label ns indicates not statistically significant as identified by *t*-test. Log_2 fold change was averaged after conducting investigation under biological and technical replicates both equalling n=3.

These results confirm the capsule independent activation of *ompR, baeR* and *ramA* under iron limitation. Thus, EnvZ-OmpR, BaeSR and RamA were to be investigated further through their genetic deletion and overexpression in non-capsulated (Ecl8) and capsulated (*Kp* 52145) wild type backgrounds.

3.4.2. Measuring the Impact of Iron Limitation on Capsule Production in *Kp* 52145*ramR*<km>

In alignment with the previous explanation of 3.3.3., prior to conducting any investigation using *ramA* overexpressed strain *Kp* 52145*ramR*<km>, it was firstly of necessity to confirm that iron limitation did not affect the ability of this strain to produce exopolysaccharide capsule. This was to ensure that any

siderophore export or CFDC susceptibility impact conferred by *Kp* 52145*ramR*<km> under iron limitation would not be the result of the confounding variable of iron limitation impacting capsule density. To assess this, *Kp* 52145*ramR*<km> was incubated overnight in iron limited media (IDCAMHB) and the concentration of 4-O(I-1-Carboxyethyl)-d-glucuronic acid was measured to allow for the quantification of total exopolysaccharide density, as per the protocol of **2.6.**. The concentration of 4-O(I-1-Carboxyethyl)-d-glucuronic acid measured following the overnight incubation of *Kp* 52145*ramR*<km> in iron replete media (ID-CAMHB+$FeCl_3$) was used as the baseline control.

It was found that there was no difference in the average glucuronic acid concentration of *Kp* 52145*ramR*<km> under iron limitation relative to iron repletion. Results are shown in Figure 45.

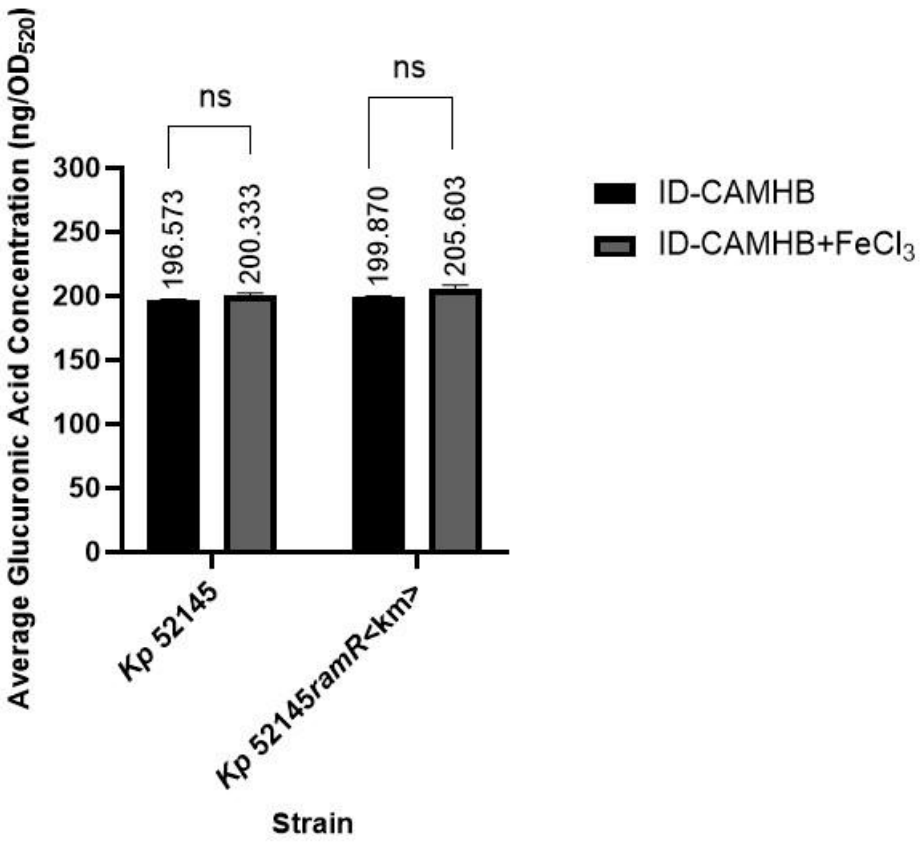

Figure 45. Glucuronic acid concentration (ng/OD_{520}) of *Kp* 52145 and *Kp* 52145*ramR*<km> averaged across biological and technical replicates equalling n=3. ID-CAMHB represents iron deplete media and ID-CAMHB+$FeCl_3$ represents iron replete media. The label ns indicates not statistically significant as identified by *t*test.

Figure 45 shows the glucuronic acid concentration of *Kp* 52145*ramR*<km> after overnight incubation in iron limited media (ID-CAMHB) to be of no statistically significant difference to the concentration of glucuronic acid after overnight incubation in iron replete media (ID-CAMHB+$FeCl_3$). Concentrations were respectively 199.87ng/OD_{520} under ID-CAMHB and 205.603ng/OD_{520} under ID-CAMHB+$FeCl_3$.

Further, there was no statistically significant difference in the glucuronic acid concentrations of *Kp* 52145*ramR*<km> relative to *Kp* 52145 after incubation in both ID-CAMHB and ID-CAMHB+$FeCl_3$, as identified by *t*-test. It was also found that there was no statistically significant difference in the glucuronic acid concentration of *Kp* 52145*ramR*<km> relative to *Kp* 52145*mdtABC*<km> (Figure 32; 3.3.3.) under both iron limitation and iron repletion, as identified by *t*-test. Therefore, these data confirm that any impact of *Kp* 52145*ramR*<km> on siderophore export or CFDC susceptibility under iron limitation would not be a result of iron limitation having affected the capsule density of this strain. Thus, *Kp* 52145*ramR*<km> was approved for employment in subsequent investigation of its ability to export siderophore under low iron.

3.4.3. Semi-Quantitative Analysis of Siderophore Export Under Regulatory Factor Deletion and Overexpression: Chrome Azurol S (CAS) Agar Assaying

To investigate the impact of respective deletion and overexpression of RND efflux pump activators *baeSR* and *ramA* on the ability of *Kp* to export enterobactin under iron limitation, CAS agar assaying was performed. This assessment was conducted on isogenic strains of Ecl8 deleted for *baeSR* and *ramR*, and on an isogenic strain of *Kp* 52145 deleted for TetR-type family regulator *ramR*. In alignment with the previous explanation of 3.3.4. and the method of **2.9.**, Ecl8*baeSR*<km>, Ecl8Δ*ramR* and *Kp* 52145*ramR*<km> were incubated overnight in iron limited media (ID-CAMHB), cultures were standardized to OD_{600} 1.5 and 5µl of each was inoculated onto CAS agar plates. Plates were then incubated at 30°C for 18h.

It was found that the deletion of *baeSR* resulted in the reduced capacity of *Kp* to export siderophore from the cell. The overexpression of *ramA* did not confer any impact to the ability of Ecl8 or *Kp* 52145 to export siderophore. Results are shown in Figure 46.

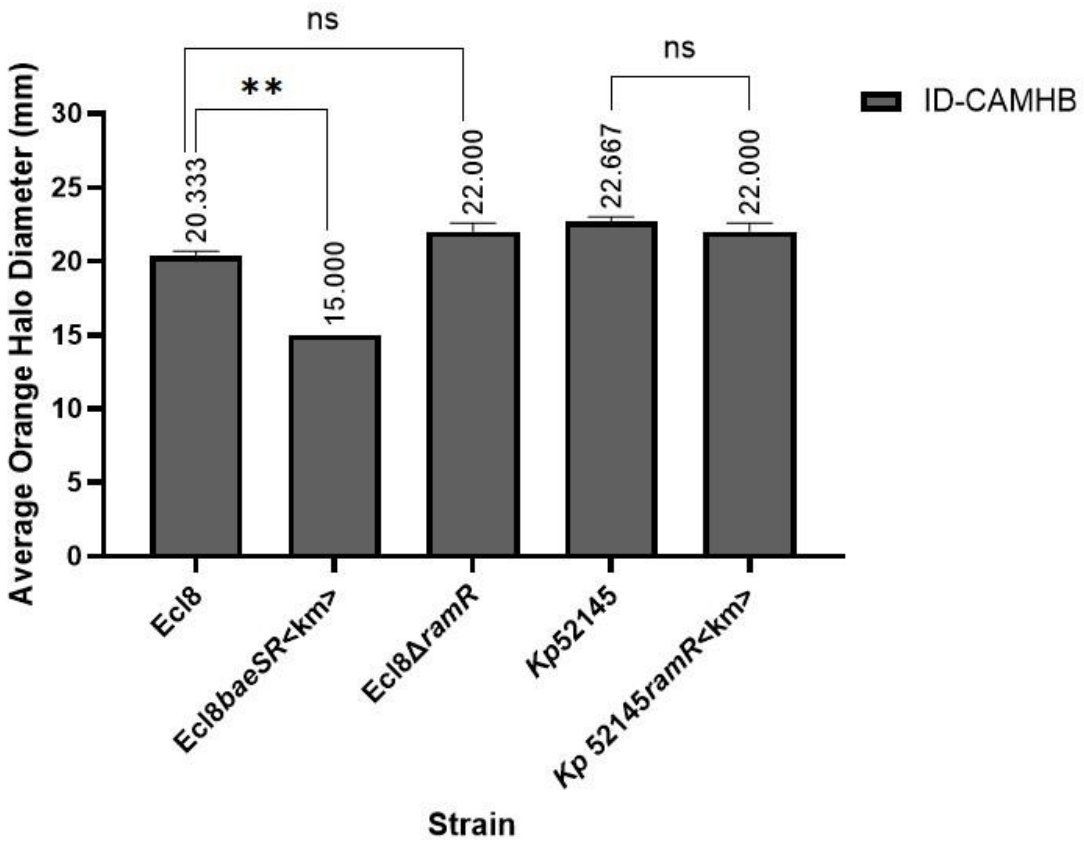

Figure 46. Average orange halo diameters (mm) on CAS agar plates after inoculation with Ecl8, Ecl8*baeSR*<km>, Ecl8Δ*ramR*, *Kp* 52145 and *Kp* 52145*ramR*<km> grown overnight in iron deplete media (IDCAMHB). The label ns indicates not statistically significant as identified by *t*-test. The label ** indicates statistically significant at $p<0.01$ as identified by *t*-test. Halo diameter was averaged after conducting investigation under biological replicates equalling n=3.

Figure 46 shows a statistically significant decrease in siderophore production under Ecl8*baeSR*<km> relative to Ecl8 after incubation in ID-CAMHB as identified by *t*-test ($p<0.01$). The average orange halo diameter of Ecl8*baeSR*<km> (15mm) was reduced by 5.333mm (approximately 25%) relative to Ecl8 (20.333mm). There was no statistically significant difference between average orange halo diameter for Ecl8*mdtABC*<km> (16.333mm, see Figure 33, 3.3.4.) and Ecl8*baeSR*<km> (15mm), as identified by *t*-test. Both Ecl8Δ*ramR* and *Kp* 52145*ramR*<km> showed no statistically significant difference in siderophore production relative to respective wild types, with average orange halo diameters for both being 22mm. For collated images of all CAS agar plates showing orange halo production, see Appendix V.

Thus, these results support those presented in 3.3.4., in firstly confirming that the loss of *baeSR* inhibits the transcriptional activation of *mdtABC*, which decreases the ability of *Kp* to efflux enterobactin. Secondly, these results confirm that AcrAB-TolC does not efflux siderophore from *Kp*,

even when constitutively activated as a result of *ramA* overexpression. Further, these results suggest that RamA may not regulate MdtABC-TolC, with *ramA* overexpression conferring no change to siderophore export, yet with the repression/deletion of *mdtABC* evidenced here and in the previous chapter (3.3.4.) to significantly reduce siderophore export.

Chapter Three evidenced that the ability of MdtABC-TolC and AcrAB-TolC to export siderophore from *Kp* is positively correlated with the ability of MdtABC-TolC and AcrAB-TolC to export CFDC from *Kp* under iron limitation. Thus, it was next of necessity to investigate the impact of MdtABC-TolC deleted strain Ecl8*baeSR*<km> and AcrAB-TolC overproducing strains Ecl8Δ*ramR* and *Kp* 52145*ramR*<km> on CFDC susceptibility. At this stage, these strains were to be investigated in conjunction with strains which were overexpressed for BaeSR, and deleted and overexpressed for EnvZ-OmpR. Together, their use was intended to confirm that the loss of IROMPs with combined RND efflux pump activation can reduce the permeability of the *Kp* OM to CFDC, thereby reducing CFDC susceptibility of *Kp*.

3.4.4. Susceptibility Testing of EnvZ-OmpR, BaeSR and RamA Deleted and Overexpressed Strains

To determine the impact of TCS regulator deletion on the permeability of the OM to CFDC, broth microdilution susceptibility testing was performed using isogenic strains of Ecl8 individually deleted of *envZompR* and *baeSR*. An isogenic strain of Ecl8 deleted of *fur* was employed as a negative control for the *envZompR* deleted strain. This was due to the *fur* deletion phenotype conferring constitutive expression of CFDC entry portal IROMP encoding genes *cirA, fiu, fepA* and *fecA*. For validation of the Ecl8Δ*fur* mutant, see Appendix VI. Further, an isogenic strain of Ecl8 deleted of sRNA *omrA* was employed with intention of its action as a second negative control for the *envZompR* deleted strain, based on its anticipated effect of constitutive IROMP expression.

To determine the impact of TCS regulator overexpression on the permeability of the OM to CFDC, this susceptibility testing employed an isogenic strain of Ecl8 which harbours a gain-of-function amino acid substitution in EnvZ (L230Q) as a consequence of CFDC selection. This mutant, Ecl8EnvZ$_{L230Q}$, thus displays the phenotype of constitutive EnvZ-OmpR activity (Stanton, 2022). Two further CFDC selection mutants which each harboured identical dual gain-of-function amino acid substitutions in both EnvZ (L230Q) and BaeS (V295G), refered to as 'Iron-Depleted Mutants' or IDMs, were also employed. These were IDM1 and IDM7. These mutants display the phenotype of constitutive activity of both EnvZ-OmpR and BaeSR (Stanton, 2022). For validation of IDM mutants, see Appendix VII.

To determine the impact of *ramA* overexpression on the OM permeability to CFDC, susceptibility testing was performed on isogenic strains of Ecl8 and *Kp* 52145 deleted of *ramR*.

The susceptibility of all strains to CFDC was assessed *via* broth microdilution in iron deplete (IDCAMHB) and iron replete (ID-CAMHB+$FeCl_3$) medias, as per the method outlined in 2.10.2.. Susceptibility of all strains to baseline control CAZ was also assessed in alignment with the prior descriptions of 3.2.3. and 3.3.5..

It was found that deletion and overexpression of the TCS regulators conferred respective hypersusceptibility and decreased susceptibility of *Kp* to CFDC. Deletion of *ramR* conferred decreased susceptibility to CFDC. CAZ susceptibility was decreased as a result of both EnvZ gain-offunction and *ramA* overexpression, irrespective of iron limitation. Results are shown in Table 10.

Strain	CFDC ID-CAMHB	CAZ ID-CAMHB	CFDC ID-CAMHB+$FeCl_3$	CAZ ID-CAMHB+$FeCl_3$
Ecl8	0.5	1	2	0.5
***Kp* 52145**	0.5	1	2	0.5
Ecl8*envZompR*<km>	0.063	0.5	0.5	0.5
Ecl8Δ*fur*	0.125	1	0.25	1
Ecl8*omrA*<km>	2	1	2	1
Ecl8EnvZ$_{L230Q}$	2	2	4	2
Ecl8*baeSR*<km>	0.063	1	0.5	1
IDM1	4	2	4	2
IDM7	4	2	4	2
Ecl8Δ*ramR*	2	4	4	4
***Kp* 52145*ramR*<km>**	2	4	4	4

Table 10. Modal CFDC and CAZ MIC values (mg/L) of TCS and AraC/XylS regulator deleted and overexpressed strains and relative wild types. ID-CAMHB represents iron deplete media and ID-CAMHB+$FeCl_3$ represents iron replete media. This data was recorded as the modal value due to the data being geometric. Investigation was conducted under biological and technical replicates both equalling n=3.

3.4.4.1. CFDC Susceptibility

Table 10 shows the deletion of *envZompR* from Ecl8 to have conferred an 8-fold increase in CFDC susceptibility relative to Ecl8 under iron limitation (ID-CAMHB) and a 4-fold increase in susceptibility relative to Ecl8 under iron repletion (ID-CAMHB+$FeCl_3$). The MIC values under Ecl8*envZompR*<km> were of a biologically insignificant 2-fold difference relative to those of Ecl8Δ*fur*, irrespective of iron concentration. This result confirms the loss of EnvZ-OmpR to confer the constitutive transcriptional expression of *cirA, fiu, fepA* and *fecA*. In corroboration of this, Ecl8$EnvZ_{L230Q}$ was shown to decrease CFDC susceptibility by 4-fold relative to Ecl8 under ID-CAMHB. Interestingly, however, Ecl8*omrA*<km> was also shown to confer a 4-fold decrease in CFDC susceptibility under ID-CAMHB relative to Ecl8. Thus, it is implied that IROMP repression was still conferred by unperturbed activity of OmrB, and that the activity of OmrB, alone, was insufficient to initiate the negative feedback loop of *ompR* repression and hence its own self-limitation. This was confirmed to have been the case *via* RT-(q)PCR of Ecl8*omrA*<km>, as shown in Appendix VIII. As a result of this lack of anticipated outcome, the designation of Ecl8*omrA*<km> as a negative control for this assessment was subsequently withdrawn.

Ecl8*baeSR*<km> exhibited the same CFDC hypersusceptible phenotype as Ecl8*envZompR*<km>, showing an 8-fold and 4-fold increased CFDC susceptibility relative to Ecl8 under ID-CAMHB and IDCAMHB+$FeCl_3$, respectively. It is again of interest to note that the MIC of this strain under ID-CAMHB (0.063mg/L) was of no biologically significant difference to the MIC of Ecl8*mdtABC*<km> under IDCAMHB (2-fold higher at 0.125mg/L - see 3.3.5., Table 9).

There was an 8-fold decrease in CFDC susceptibility exhibited by both IDMs (IDM1 and IDM7) relative to Ecl8 in ID-CAMHB. However, the MIC values for both IDMs were only a biologically insignificant 2fold higher than that of Ecl8$EnvZ_{L230Q}$. Thus, whilst futher corroborating the results of Ecl8*envZompR*<km> and Ecl8$EnvZ_{L230Q}$, the IDMs did not allow for confirmation of the isolated impact of BaeS (V295G) to CFDC susceptibility.

Overexpression of *ramA* resulted in a 4-fold decrease in CFDC susceptibility under ID-CAMHB in a capsule independent manner. It was found that there was a biologically insignificant (2-fold) impact of *ramA* overexpression on CFDC MIC under ID-CAMHB+$FeCl_3$. Thus far, the present study has found that Ecl8*acrAB*<km> does not effect CFDC susceptibility relative to Ecl8 (3.3.5.; Table 9), and that overexpression of *ramA* does not impact the ability of *Kp* to export siderophores under iron limitation (Figure 45; 3.4.3.). Thus, taken together, these data suggest RamA to have decreased *Kp*

susceptibility to CFDC under low iron in a manner independent of CFDC being effluxed through AcrAB-TolC or MdtABC-TolC.

3.4.4.2. CAZ Susceptibility

Table 10 shows Ecl8EnvZ$_{L230Q}$, IDM1 and IDM7 to have all conferred 4-fold decreases in CAZ susceptibility relative to Ecl8 under the iron replete baseline control media (ID-CAMHB+$FeCl_3$). Strains overexpressing *ramA* (Ecl8Δ*ramR* and *Kp* 52145*ramR*<km>) conferred 4 to 8-fold decreases in CAZ susceptibility relative to Ecl8 and *Kp* 52145 irrespective of iron concentration and capsulation. Importantly, each strain produced the same MIC value irrespective of iron limitation or iron repletion, thereby upholding the fact that CAZ does not exploit the iron transportation pathway.

To summarise, these data show that a loss of multiple IROMPs conferred by the constitutive activity of EnvZ-OmpR combined with the activation of RND efflux pump MdtABC-TolC by BaeSR reduces the permeability of the *Kp* OM to CFDC. Thus, these data implicate both TCS to work cumulatively to contribute to the CFDC resistance of *Kp*. However, whilst these data also show that *ramA* overexpression can reduce *Kp* CFDC susceptibility under iron limitation, the mechanism by which this occurs, having been shown to be independent of AcrAB-TolC, remains unknown. With the CAS assay result of 3.4.3. suggesting that *ramA* overexpression may not reduce CFDC susceptibility through regulatory control of MdtABC-TolC, it was next of necessity to confirm this. This was achieved by assessing the impact of *ramA* overexpression on both *mdtB* and *acrD* RNA transcript expression under iron limitation.

3.4.5. Transcriptomic Analyses - How does RamA Drive RNA Transcript Expression of Efflux Pump Encoding Genes *mdtB* and *acrD* Under Iron Limitation?

To determine the impact of *ramA* overexpression on the RNA transcript expression levels of *mdtB* and *acrD* under iron limitation*, Ecl8ΔramR* was incubated overnight in ID-CAMHB, RNA was extracted and RT-(q)PCR analyses was performed. RNA transcript expression levels of *mdtB* and *acrD* obtained by RT-(q)PCR after overnight growth of Ecl8 in iron deplete (ID-CAMHB) media were used as baseline controls.

It was found that there was no difference in the RNA transcript expression of *mdtB* and *acrD* relative to Ecl8 after incubation of Ecl8Δ*ramR* in either iron limited media. Results are shown in Figure 47.

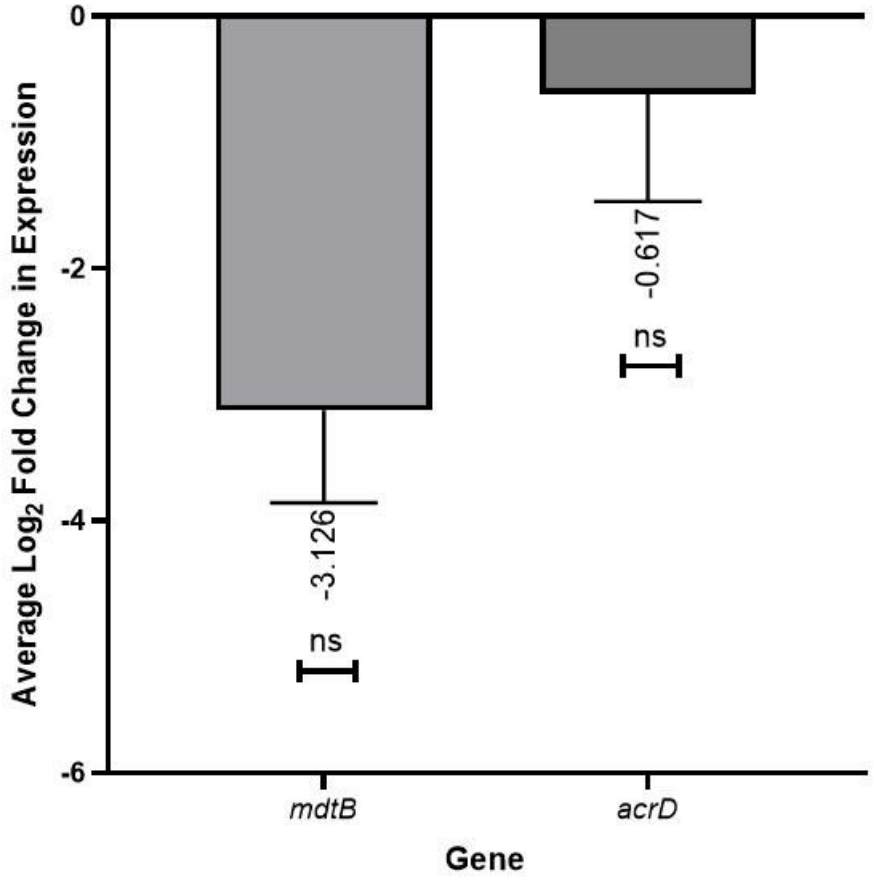

Figure 47. Log_2 fold change expression of *mdtB* and *acrD* in Ecl8Δ*ramR* relative to Ecl8 under iron deplete media (ID-CAMHB). Average log_2 fold-change ± SEM is plotted showing the log_2 fold change in gene expression as a ratio of Ecl8Δ*ramR* ID-CAMHB:Ecl8 ID-CAMHB – test:control. The label ns indicates no statistically significant difference as identified by *t*-test. Log_2 fold change was averaged after conducting investigation under biological and technical replicates both equalling n=3.

Figure 47 shows that there was no statistically significant log_2 fold difference in the RNA transcript expression levels of *mdtB* or *acrD* in Ecl8Δ*ramR* relative to Ecl8 under iron limitation, as identified by *t*-test. Log_2 fold change values were -3.126 for *mdtB* and -0.617 for *acrD,* respectively.

Thus, these results confirm, in agreement with the hypotheses posed in 3.4.3. and 3.4.4., that RamA does not regulate MdtABC-TolC, or AcrA-AcrD-TolC, under iron limitaton. This supports the CAS agar assay results of Ecl8Δ*ramR* and *Kp* 52145*ramR*<km> not conferring an impact to siderophore efflux relative to respective wild types under iron limitation (3.4.3.). Further, this result confirms that *ramA* overexpression does not contribute to CFDC resistance through inducing efflux of the antibiotic from the cell through RND efflux pump MdtABC-TolC. Therefore, it was next of necessity to investigate

whether the decrease in CFDC susceptibility recorded for Ecl8Δ*ramR* in 3.4.4. was instead a result of RamA regulating known CFDC entry portal IROMPs. To do this, it was assessed whether *ramA* overexpression induced a change in RNA transcript expression of *cirA, fiu, fepA* or *fecA* under iron limitation.

3.4.6. Transcriptomic Analyses - How does RamA Drive RNA Transcript Expression of IROMP Encoding Genes *cirA, fiu, fepA* and *fecA* Under Iron Limitation?

3.4.6.1. The Impact of ramA Overexpression on RNA Transcript Expression of cirA, fiu, fepA and fecA Under Iron Limitation

To determine the impact of *ramA* overexpression on RNA transcript expression levels of *cirA, fiu, fepA* and *fecA* under iron limitation, RT-(q)PCR was performed on RNA extracted from Ecl8Δ*ramR* after overnight incubation in iron deplete media (ID-CAMHB). RNA transcript expression levels of *cirA, fiu, fepA* and *fecA* obtained by RT-(q)PCR after overnight incubation of Ecl8 in ID-CAMHB were used as baseline controls.

It was found that there was a consistent downregulation of RNA transcript expression levels of *cirA, fiu, fepA* and *fecA* in Ecl8Δ*ramR* relative to Ecl8 under iron limitation. Results are shown in Figure 48.

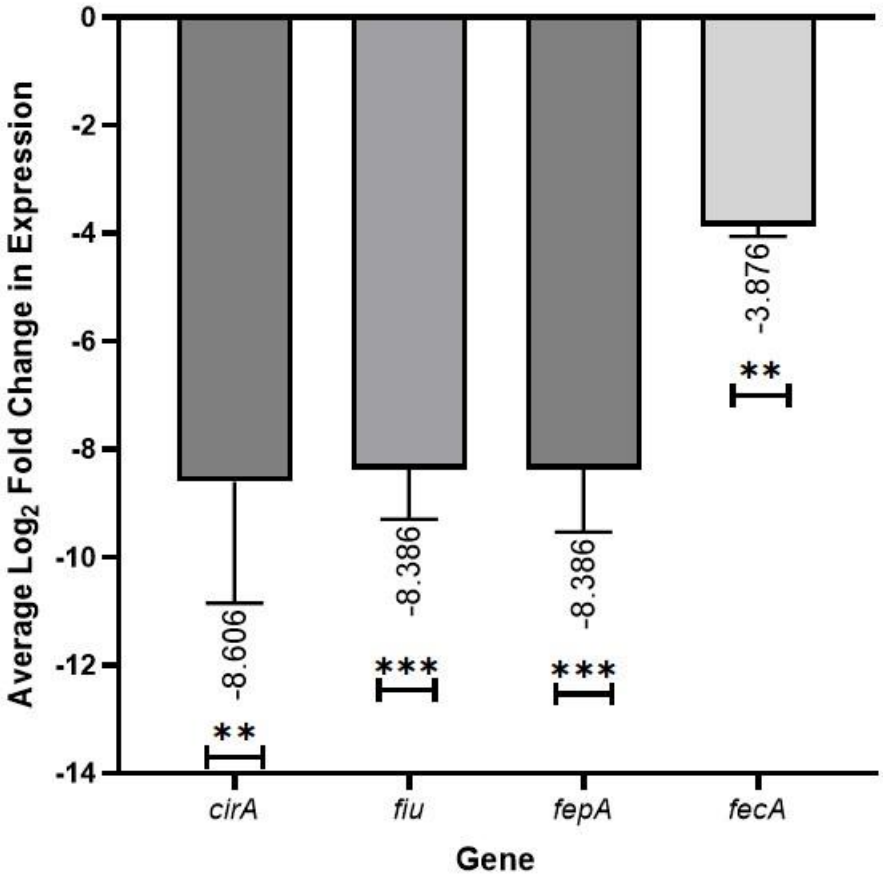

Figure 48. Log_2 fold change expression of *cirA, fiu, fepA, fecA* under Ecl8Δ*ramR* relative to Ecl8 in iron deplete media (ID-CAMHB). Average log_2 fold-change ± SEM is plotted showing the log_2 fold change in gene expression as a ratio of Ecl8Δ*ramR* ID-CAMHB:Ecl8 ID-CAMHB – test:control. The label ** indicates statistically significant at $p<0.01$, and *** indicates statistically significant at $p<0.001$, as identified by *t*-test. Log_2 fold change was averaged after conducting investigation under biological and technical replicates both equalling n=3.

Figure 48 shows a statistically significant downregulation in the expression of *cirA, fiu, fepA* and *fecA* in Ecl8Δ*ramR* under iron limitation (ID-CAMHB) relative to Ecl8. Log_2 fold decreases were -8.606, -8.385, -8.385 and -3.875, respectively, as identified by *t*-test at $p<0.01$ to $p<0.001$.

Thus, these data suggest that *ramA*, when overexpressed, may repress the IROMPs under iron limitation. Thus, this may have been the mechanism through which *ramA* overexpression conferred a 4-fold increase to CFDC MIC under ID-CAMHB. To validate this further, RT-(q)PCR investigation was performed to assess the RNA transcript levels of *cirA, fiu, fepA* and *fecA* under the deletion of *ramA*.

3.4.6.2. The Impact of ramA Deletion on RNA Transcript Expression of cirA, fiu, fepA and fecA Under Iron Limitation

To determine the impact of *ramA* deletion on RNA transcript expression levels of *cirA, fiu, fepA* and *fecA* under iron limitation, RT-(q)PCR was performed on RNA extracted from Ecl8Δ*ramA* after overnight incubation in iron deplete media (ID-CAMHB). RNA transcript expression levels of *cirA, fiu, fepA* and *fecA* obtained by RT-(q)PCR after overnight incubation of Ecl8 in ID-CAMHB were used as baseline controls.

It was found that there was, again, a consistent downregulation of RNA transcript levels of *cirA, fiu, fepA* and *fecA* under Ecl8Δ*ramA* relative to Ecl8 under iron limited media (ID-CAMHB). Results are shown in Figure 49.

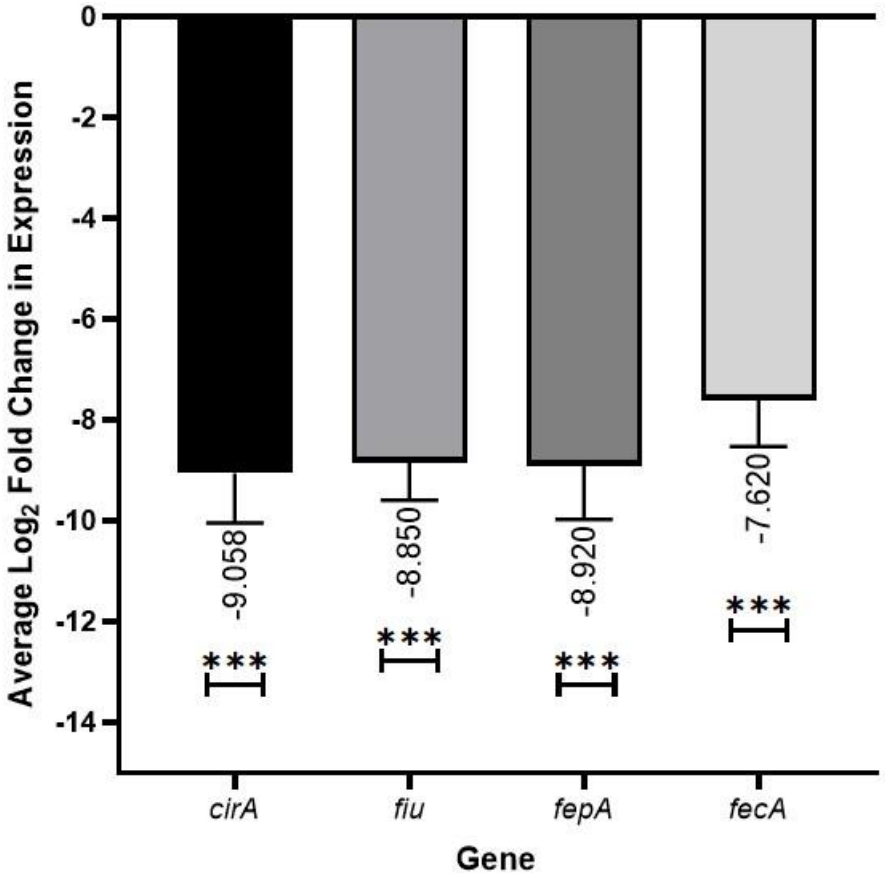

Figure 49. Log_2 fold change expression of *cirA, fiu, fepA, fecA* under Ecl8Δ*ramA* relative to Ecl8 in iron deplete media (ID-CAMHB). Average log_2 fold-change ± SEM is plotted showing the log_2 fold change in gene expression as a ratio of Ecl8Δ*ramA* ID-CAMHB:Ecl8 ID-CAMHB – test:control. The label *** indicates statistically significant at $p<0.001$ as identified by *t*-test. Log_2 fold change was averaged after conducting investigation under biological and technical replicates both equalling n=3.

Figure 49 shows a statistically significant downregulation of *cirA, fiu, fepA* and *fecA* under Ecl8Δ*ramA* relative to Ecl8 at $p<0.001$ as identified by *t*-test, with log_2 fold decreases of -9.057, -8.850, -8.92 and -7.62, respectively.

Interestingly, the opposite phenotype of *ramA* deletion conferred the same impact to *cirA, fiu, fepA* and *fecA* IROMP RNA transcript expression under iron limitation as was conferred by *ramA* overexpression. For both, there was consistently downregulated RNA transcript expression of *cirA, fiu, fepA* and *fecA* relative to Ecl8. Therefore, with the RT-(q)PCR investigations having been performed across biological and technical replicates summing n=3, this conflicting data forces the conclusion that RamA is not a direct regulator of the IROMPs under iron limitation.

Thus, the RT-(q)PCR result of IROMP downregulation in Ecl8Δ*ramR* under ID-CAMHB offers feasible explanation for the decreased CFDC susceptibility phenotype of Ecl8Δ*ramR* under ID-CAMHB. However, this data alone does not explain the mechanism by which the overexpression of *ramA* is able to indirectly induce this IROMP repression to result in this phenotype.

4. Discussion

Principally, the present work has shown that the TCS EnvZ-OmpR and the TCS BaeSR can reduce the susceptibility of *Kp* to the siderophore Cephalosporin CFDC under iron limitation, through cumulatively reducing OM permeability. The overexpression of *ramA* has been shown to also reduce *Kp* CFDC susceptibility under iron limitation, however, the precise mechanism by which it does so remains unspecified.

Modified Cephalosporin CFDC is conjugated with the chlorocatechol moiety 2-chloro-3,4dihydroxybenzoic acid at its C-3 side chain. This allows CFDC to bind to Fe^{3+} and hijack TonB-ExbBExbD-dependent IROMPs for active transport across the Gram-negative OM (Rodríguez and González-Bello, 2023). CFDC resistant clinical isolates of *Kp* are reported to exhibit functional losses of the IROMPs, with these losses reported most frequently for CirA and Fiu (McElheny *et al.*, 2021; Wang *et al.*, 2022; Arcari *et al.*, 2023, Freiberg *et al.*, 2024). These functional losses are a result of deleterious substitutions in the amino acid sequences of the proteins. The present study showed, through predictive profiling using PolyPHen-2, that there were no deleterious substitutions in the amino acid sequences of CirA and Fiu embedded in wild type populations of clinically relevant, rapidly disseminating MDR *Kp* lineages: ST11, ST15 and ST258. Thus, it was confirmed that CFDC selects for these deleterious substitutions in the clinical setting. This in turn confirmed the survival advantage exhibited by *Kp* following CirA and Fiu loss to be the direct result of both orchestrating CFDC influx into the cell under iron limitation. Alongside CirA and Fiu, the IROMPs FepA and FecA are also implicated to be of relevance in driving CFDC influx (Sato and Yamawaki, 2019; Padovani *et al.*, 2023). However, the impact of FepA and FecA on CFDC susceptibility has been less studied relative to the impact of CirA and Fiu. RT-(q)PCR analysis in non-capsulated *Kp* wild type strain Ecl8 and capsulated wild type strain *Kp* 52145 confirmed iron limitation to induce the consistent, capsule independent upregulation of *cirA*, *fiu*, *fepA* and *fecA* RNA transcript expression. Interestingly, this study demonstrated the $\log_2$ fold upregulation of *fepA* to exceed that of *cirA* and *fiu* in wild type *Kp* under iron limitation, shown to be by 3.42 and 3.476 $\log_2$ fold, respectively. This result suggests FepA to be of significant necessity for CFDC uptake under iron limitation in *Kp*. This, in turn, considerably challenges the current postulation of Fiu and CirA being the combined lead role IROMPs facilitating Gram-negative internalization of catechol-conjugated antibiotics (Wang, Chen and Cai, 2021; Nordmann *et al.*, 2022; Deroche 2023). It was then found that the deletion of *cirA* conferred a biologically insignificant 2-fold decrease to CFDC susceptibility relative to Ecl8 under iron limitation

following susceptibility testing by broth microdilution. This was consistent with findings of previous studies (Ito *et al.*, 2018; Kaye, Naas, Pogue and Rossolini, 2023; Schaufler *et al.*, 2023), which the present work then advanced on through RT-(q)PCR to evidence RNA transcript expression levels of *fiu, fepA* and *fecA* to be upregulated under *cirA* deletion relative to Ecl8. This strongly suggests that CirA is functionally redundant with Fiu, FepA and FecA in facilitating CFDC influx. This result was particularly interesting for *fecA*, as RT-(q)PCR investigation in wild type *Kp* found RNA transcript expression of *fecA* to exhibit the lowest $\log_2$ fold upregulation of the four genes tested by approximately 2 $\log_2$ fold, consistent with previous investigation in *Kp* NCTC 13439 (Daoud *et al.*, 2022). Thus, this finding furthered the 2022 study to suggest that despite the proportionally reduced induction of *fecA* expression under low iron relative to *cirA, fiu* and *fepA*, the independent relative contribution of FecA to CFDC uptake in *Kp* may be equal to that of CirA, Fiu and FepA. This further bolsters the hypothesis that Fiu and CirA may not be the most important IROMPs of CirA, Fiu, FepA and FecA facilitating CFDC entry into *Kp* under iron limitation. Taken together, these results suggest that CFDC uptake into *Kp* does not preferentially depend on any of CirA, Fiu, FepA or FecA individually, but confirm that optimal uptake requires at least three of the four in any combination.

The TCS EnvZ-OmpR is known to indirectly negatively regulate the expression of *cirA, fiu, fepA* and *fecA via* two key pathways: positive regulation of the sRNAs OmrA and OmrB, and induction of master Fe^{3+} regulator FUR through positive regulation of FeoB (**1.5.**, Figure 2; 1.6.1.; Figure 4). Clinical isolates of *Kp* exhibiting resistance to CFDC are being increasingly reported to overexpress *envZ*, which renders EnvZ-OmpR constitutively active (Simner *et al.,* 2022). A gain-of-function substitution in EnvZ (L230Q), which also renders EnvZ-OmpR constitutively active, was demonstrated by the present study to confer a 4 to 8-fold decrease in CFDC susceptibility under iron limitation. This result was consistent with the findings of Yamano, Takemura, Nakamura and Echols (2020) and Stanton (2022). This finding was supported by *envZompR* deletion conferring an 8-fold increase in CFDC susceptibility. The CFDC hypersusceptibility phenotype of the *envZompR* deleted strain mirrored the

CFDC hypersusceptibility phenotype of an isogenic strain of Ecl8 deleted of master Fe^{3+} regulator FUR, which is known to constitutively express *cirA, fiu, fepA* and *fecA* (Stanton, 2022; Appendix VI). Thus, taken together, these findings confirm that constitutively active EnvZ-OmpR induces constitutive repression of *cirA, fiu, fepA* and *fecA* transcription, which inhibits CFDC uptake into *Kp* (Figure 5).

Similarly to EnvZ-OmpR, clinical isolates of *Kp* exhibiting CFDC resistance are also being increasingly reported to overexpress *baeS*, which renders the TCS BaeSR constitutively active (Simner *et al.,*

2022). BaeSR is a positive regulator of RND efflux pump encoding genes *mdtABC* and *acrD* (Nishino, Honda and Yamaguchi, 2005). Previous studies evidenced the synergistic effect of deleting both *mdtABC* and *acrD* to reduce the efflux of catecholate type siderophore enterobactin from *E. coli* under iron limitation (Bleuel *et al.,* 2005; Horiyama and Nishino, 2014). The chlorocatechol moiety of

CFDC confers an element of structural similarity between the antibiotic and enterobactin (Lan *et al.*, 2022). Hence, studies published subsequently to the above have speculated that under iron limitation, MdtABC-TolC and ArA-AcrD-TolC may also be able to efflux CFDC (Rebizant, 2022; Liu *et al.,* 2023; Kriz *et al.*, 2024) (Figure 5). The present study has shown, for the first time, that BaeSR regulated RND family efflux pump MdtABC-TolC can efflux both the siderophore enterobactin and CFDC from *Kp* under iron limitation in a K2 capsule independent manner. RT-(q)PCR evidenced that iron limitation induced the upregulation of *mdtB, acrD* and *baeR* RNA transcript expression in wild type *Kp*, consistent with the findings of Ramos *et al.* (2016) and Avican *et al.* (2021). The upregulation of *mdtB* was shown to have been 3.988 $\log_2$ fold greater than *acrD* upregulation. The CAS agar assay then demonstrated isogenic strains of non-capsulated Ecl8 and capsulated *Kp* 52145 deleted of *mdtABC* to efflux significantly less siderophore relative to respective wild type strains under iron limitation, as measured by approximate 20% and 31% respective decreases in the average diameters of orange halos surrounding inoculation droplets. Furthermore, the average orange halo diameter, and thus the amount of siderophore effluxed, from an isogenic strain of Ecl8 deleted of *baeSR* was found to be of no significant difference to that of the isogenic strain of Ecl8 deleted of *mdtABC*. Based on this result, it can be inferred that the independent relative contribution of AcrA-AcrD-TolC to the efflux of siderophores from *Kp* is negligible. This result correlates with the above outcome of the RT-(q)PCR investigation, which suggested MdtABC-TolC to be of greater involvement in the response of *Kp* to iron limitation than AcrA-AcrD-TolC. Thus, this study is the first to evidence the isolated effect of these individual RND efflux pumps on the ability of *Kp* to export siderophores under low iron. This is a significant advancement on previous study in *E. coli* by Horiyama and Nishino (2014), who evidenced only a synergistic impact to enterobactin export as a result of combined *mdtABC* and *acrD* deletion. The present study has also provided the first evidence to address, and in part support, the above speculation posed by Rebizant (2022), Liu *et al.* (2023) and Kriz *et al.* (2024), by demonstrating that the ability of MdtABC-TolC to export siderophore under low iron is positively correlated with its ability to export CFDC under low iron. Broth microdilution susceptibility testing under iron limitation confirmed a K2 capsule independent 4-fold increase in CFDC susceptibility under *mdtABC* deletion relative to respective wild types. This result was shown to be of a biologically insignificant 2-fold

difference to the 8-fold increase in CFDC susceptibility observed under *baeSR* deletion relative to Ecl8 under iron limitation. Thus, based on these data, in positive correlation with the CAS agar assay results, it can be strongly suggested that the independent relative contribution of AcrA-AcrD-TolC to the efflux of CFDC from *Kp* under iron limitation is also negligible (Figure 5). The lack of effect of *mdtABC* deletion and *baeSR* deletion on the susceptibility of *Kp* to CAZ, from which CFDC was partly modelled, was consistent with the findings of Hirakawa *et al.* (2003). Together with the CAS agar assay and broth microdilution results, this allows for the inference that the capacity for MdtABC-TolC to efflux CFDC but not CAZ may be due to a particular affinity of the binding pockets of MdtABC-TolC for catechol functional groups. Importantly, our data contradict the recent conjecture that the impact of MdtABC-TolC to CFDC susceptibility in *Kp* would likely be redundant (Stanton, 2022), and confirm that BaeSR, by activating *mdtABC* transcription, induces CFDC efflux from *Kp* through MdtABC-TolC (Figure 5).

Numerous clinical isolates of MDR *Kp* have been reported to overexpress AraC/XylS family transcription factor *ramA* (Molitor *et al.*, 2018), making this regulator highly attractive for AMR research. RamA is well known to positively regulate key intrinsic resistance determinant RND efflux pump AcrAB-TolC (Jiménez-Castellanos *et al.*, 2018). Aforementioned studies by Bleuel *et al.* (2005) and Horiyama and Nishino (2014) also evidenced a synergistic reduction in enterobactin efflux from *E. coli* under low iron as a consequence of the deletion of *acrAB* with both *mdtABC* and *acrD*. Thus, similar speculation of the AcrAB-TolC RND efflux pump being able to export CFDC from the cell has been previously raised (Rebizant, 2022; Liu *et al.,* 2023; Kriz *et al.,* 2024), which has implicated a potential role of RamA in contributing to CFDC resistance (Figure 5). To the best of our knowledge, this study is the first to evidence the overexpression of *ramA* to reduce CFDC susceptibility under iron limitation in a K2 capsule independent manner. Interestingly, however, this phenotype was not correlated with the ability of RamA to induce siderophore efflux from the cell. RT-(q)PCR confirmed RNA transcript expression levels of *acrB* and *ramA* to both increase under iron limitation in wild type *Kp*, in alignment with the findings of Avican *et al.* (2021). Yet, it was evidenced subsequently following the CAS agar assay that an isogenic strain of Ecl8 deleted of *acrAB* displayed no statistically significant difference in orange halo diameter relative to Ecl8 under iron limitation. This result again addresses gaps remaining following both prior studies by Bleuel *et al.* (2005) and Horiyama *et al.* (2014), with this study being the first to show the isolated impact of AcrAB-TolC independently of MdtABC-TolC and AcrA-AcrD-TolC on siderophore export from *Kp*. The CAS assay outcome was then, like that of MdtABC-TolC, positively correlated to the result of the broth microdilution susceptibility test. This showed no biologically significant change to CFDC susceptibility under *acrAB* deletion

relative to Ecl8, irrespective of iron concentration. This result hence leads to the refutation of the above speculation raised by Rebizant (2022), Liu *et al.* (2023) and Kriz *et al.* (2024). In alignment with these results, *ramA* overexpression was shown by the CAS agar assay not to impact siderophore export from *Kp*. However, it was subsequently recorded that *ramA* overexpression decreased CFDC susceptibility by 4-fold under iron limitation. From this, it was proposed that RamA mediates decreased CFDC susceptibility in *Kp via* a mechanism independent of AcrAB-TolC (Figure 5). The absence of impact of *ramA* overexpression on siderophore export relative to respective wild types further suggested that its impact to CFDC susceptibility may not be mediated through its regulation of MdtABC-TolC. RT-(q)PCR analysis confirmed this, in *ramA* overexpression resulting in no statistically significant difference in RNA transcript expression of both *mdtB* or *acrD* under iron limitation relative to wild type Ecl8 (Figure 5). Hence, our data led to the inference that RamA does not impact *Kp* susceptibility to CFDC through the same pathway as BaeSR. Results of further RT(q)PCR then suggested *ramA* overexpression to cause *cirA, fiu, fepA* and *fecA* RNA transcript downregulation under iron limitation – a novel finding for *Kp*. This initially implicated possible crosstalk between the AraC/XylS transcription factor and EnvZ-OmpR. However, further investigation *via* RT-(q)PCR analysis of an isogenic strain of Ecl8 deleted of *ramA* produced the directly conflicting result of the same *cirA, fiu, fepA* and *fecA* downregulation relative to Ecl8 under iron limitation. Therefore, from this study alone, our data force the conclusion that RamA is not a direct IROMP regulator (Figure 5). The results suggest the overexpression of *ramA* to induce the upregulation or downregulation of an as of yet unspecified intermediary regulator gene. It is then suggested that the subsequent modulation of this unknown intermediary regulator's activity is what causes the repression of *cirA, fiu, fepA* and *fecA*, thus resulting in the reduced OM permeability of Ecl8Δ*ramR* to CFDC. This exposes an avenue for further research.

Notably, this study found both the overexpression of *ramA* and the gain-of-function substitution of EnvZ (L230Q) to decrease CAZ susceptibility by 4 to 8-fold in iron replete baseline control media, consistently with findings of Stanton (2022). This is suggested to likely be the result of both *ramA* overexpression and EnvZ gain-of-function phenotypes having conferred the constitutive repression of primary CAZ entry portal *ompK35* (De Majumdar *et al.*, 2015; Zhang *et al.,* 2022). It is further likely that the CAZ susceptibility result under *ramA* overexpression was a consequence of the simultaneous constitutive activation of known CAZ efflux pump, AcrAB-TolC (Jiménez-Castellanos *et al.*, 2016; Shen *et al.*, 2017; Jiménez-Castellanos *et al.*, 2018), with *acrAB* deletion shown to confer an iron independent 4-fold CAZ susceptibility increase in the present work. Importantly, these data suggest

the possibility for low-level cross-resistance to occur between CAZ and last-line agent CFDC in the clinical setting, which implicates the need for heightened surveillance and monitoring.

Despite all results, it is necessary to note that no strains tested demonstrated a CFDC or CAZ MIC which exceeded the clinically susceptible breakpoints defined by the CLSI (2.10.2.; Table 6). Thus, it must be stated that EnvZ-OmpR, BaeSR and RamA, although evidenced by the present study to contribute to the progressive resistance of *Kp* to CFDC, are not the sole factors driving its clinical onset.

4.1. Limitations

The present work demonstrated the limitation of unsuccessful generation of *fepA* and *fiu* deletion mutants in both the Ecl8 and *Kp* 52145 backgrounds. Thus, it remained unconfirmed what the independent relative contribution of each was to CFDC influx. The results of Ecl8*cirA*<km> susceptibility testing and RT-(q)PCR analysis allow for the hypothesis that individual deletions of *fepA* and *fiu* would confer a biologically insignificant impact to CFDC susceptibility, as a result of the other three remaining IROMPs compensating for their loss. However, this requires testing. Similarly, despite the results of the present study suggesting any independent effect of AcrA-AcrD-TolC on enterobactin and hence CFDC efflux to be negligible, this remained unconfirmed due to unsuccessful generation and testing of Ecl8*acrD*<km> and *Kp* 52145*acrD*<km> deletion mutants.

The employment of the semi-quantitative CAS agar assay to measure extracellular siderophore export was preferential for this study due to its advantages of accessibility, efficiency and ease of output interpretation. However, whilst this assay was used to interpret the amount of enterobactin exported, it is a general assay which does not distinguish siderophore types. Therefore, it does not specifically detect enterobactin export alone. Hence, the orange halos produced following the assay were likely representative of an emalgamation of *Kp* siderophores, inclusive of enterobactin, but also of alternative catecholate-type siderophores salmochelin and yersiniabactin, and hydroxamate type siderophore aerobactin (Kumar *et al.*, 2024). More targeted methods are thus required to support the results obtained by the present study and confirm specific impacts to enterobactin export under *mdtABC* and *baeSR* deletion.

A final notable limitation of the present work is the absence of investigation of the isolated impact of BaeS gain-of-function substitution V295G on CFDC susceptibility. Previous study evidenced *Kp* ATCC 13883 with the same BaeS gain-of-function substitution (V295G), but without a simultaneous gainof-function substitution in EnvZ, to demonstrate an 8-fold increase in CFDC MIC in iron limited media (ID-

CAMHB) relative to wild type *Kp* ATCC 13883 (Simner *et al.*, 2022). In the present study, EnvZ and BaeS overproducing mutants IDM1 and IDM7 demonstrated the same 8-fold increase in CFDC MIC under ID-CAMHB relative to Ecl8. However, this MIC result was a biologically insignificant 2-fold increase relative to the CFDC MIC of Ecl8EnvZ$_{L230Q}$ under ID-CAMHB, consistently with the finding of Stanton (2022). Hence, the IDMs did not allow for confirmation of the isolated effect of the constitutive activity of BaeSR on CFDC susceptibility.

4.2. Concluding Remarks

Studies which investigate the physiological mechanisms contributing to Gram-negative bacterial resistance of novel siderophore Cephalosporin CFDC are scarce. The primary, overarching objective of the present study was therefore to establish how *Kp* resists CFDC under iron limitation through three key regulators: the TCS EnvZ-OmpR, the TCS BaeSR and the AraC/XylS transcription factor RamA. It was hypothesised that EnvZ-OmpR, BaeSR and RamA would decrease the susceptibility of *Kp* to CFDC under iron limitation through cumulatively reducing OM permeability. The results of the present study generally supported this hypothesis; it was first confirmed that the constitutive activation of EnvZ-OmpR induces the constitutively downregulated expression of IROMP encoding genes *cirA, fiu, fepA* and *fecA,* inhibiting the influx of CFDC into *Kp* under iron limitation. It was then shown, for the first time, that RND family efflux pump MdtABC-TolC can efflux CFDC from *Kp* under iron limitation. From this, it was confirmed that BaeSR, through its transcriptional activation of *mdtABC*, induces this efflux. The overexpression of *ramA* was also evidenced for the first time to reduce *Kp* susceptibility to CFDC under iron limitation. Yet, it was suggested that this effect was the result of the overexpression of *ramA* indirectly inducing the repression of *cirA, fiu, fepA* and *fecA* through an unspecified intermediary regulator, exposing an avenue for further research. The significance of this work therefore lies in its contribution to shaping understanding of the currently undefined topic of how ESKAPES pathogens, including Gram-negative *Kp*, develop clinical CFDC resistance. This significance is evident specifically due to the present study having provided clarification of the poorly understood pathways by which the overexpression of *envZ* and *baeS*, increasingly reported in CFDC resistant *Kp* clinical isolates, may reduce CFDC susceptibility. This work therefore highlights fundamental implications of EnvZ-OmpR, BaeSR and RamA in *Kp* Fe^{3+} homeostasis, virulence and pathogenicity in an infected host. These are imperative to investigate further as the global usage of CFDC increases. Conclusively, the cumulative impact of EnvZ-OmpR,

BaeSR and RamA in contributing to reduced CFDC susceptibility positions these regulators as attractive targets to consider for development of adjunctive therapy strategies to attempt to resensitise *Kp* to CFDC. Without which, it can be predicted that mutations conferring the overexpression of *envZ, baeS* and *ramA* will be selected for and acquired at increased frequencies, will disseminate within *Kp* populations, and will ultimately contribute to increasing the likelihood of entrance into an era of untreatable Gram-negative infections.

5. Directions for Future Research

To confirm the independent relative contribution of FepA and Fiu to CFDC influx, generation of deletion mutants in Ecl8 and *Kp* 52145 backgrounds followed by their susceptibility testing *via* broth microdilution under iron limitation is necessary. To further validate the susceptibility testing results of Ecl8*cirA*<km>, generation of the *cirA* deletion mutant in the *Kp* 52145 background is necessary, which this thesis attempted but failed to achieve.

To confirm the independent relative contribution of AcrA-AcrD-TolC to siderophore and CFDC efflux as being negligible, an *acrD* deletion mutant must be generated in the Ecl8 and *Kp* 52145 backgrounds and tested by CAS agar assay and broth microdilution under iron limitation. Similarly, to confirm the impact of constitutive BaeSR activity on CFDC susceptibility, generation of an Ecl8BaeS$_{V295G}$ mutant is required for assessment *via* CAS agar assay and broth microdilution susceptibility testing under iron limitation. This would support and validate the CAS agar assay and susceptibility testing results of Ecl8*mdtABC*<km>, *Kp* 52145*mdtABC*<km> and Ecl8*baeSR*<km>.

To substantiate the results of the CAS agar assay, it can be suggested that High Performance Liquid Chromatography (HPLC) should be conducted on Ecl8*mdtABC*<km>, *Kp* 52145*mdtABC*<km> and Ecl8*baeSR*<km>, as well as on Ecl8*acrD*<km>, *Kp* 52145*acrD*<km> and Ecl8BaeS$_{V295G}$ mutants following their generation. This method can precisely and sensitively separate, characterize and quantify specific siderophore molecules, including enterobactin. Employing this targeted approach would confirm the impact of BaeSR, MdtABC-TolC and AcrA-AcrD-TolC to the export of enterobactin from *Kp*. HPLC was used in previous studies by both Bleuel *et al.* (2005) and Horiyama and Nishino (2014) for measurement of the amount of enterobactin exported from *mdtABC, acrD* and *acrAB* deleted strains of *E. coli* under iron limitation.

To address the unanswered question of how *ramA* overexpression indirectly induces IROMP repression, firstly, the proteomics approaches of either sodium dodecyl-sulfate polyacrylamide gel electrophoresis (SDS-PAGE) or Liquid Chromatography-Tandem Mass Spectrometry (LC-MS/MS)

should be employed for Ecl8Δ*ramR* and Ecl8 analysis. This would compliment the present study's RT-(q)PCR results by quantifying and confirming the reduced abundance of CirA, Fiu, FepA and FecA under Ecl8Δ*ramR* relative to Ecl8. Both methods have been used previously to similarly quantify production of the OM porin protein OmpK35 in *Kp* (Cahill, Seeley, Gutel and Ellis, 2015; Sugawara, Kojima and Nikaido, 2016). Secondly, it can be recommended that high throughput Affinity Purification-Mass Spectrometry (AP-MS) could be employed, to study the protein interactome of Ecl8Δ*ramR* at near physiological conditions – inclusive of iron limitation. This method has been used previously to isolate, characterize and map protein networks in wellcharacterized *E. coli* lab strains, for which functional pathway annotations were previously lacking (Butland *et al.,* 2005; Babu *et al.,* 2012; Wuchty and Uetz, 2014). This could therefore be a promising technique to ascertain relationships between RamA and other as of yet unspecified regulators. This would then facilitate further assessment of the identified intermediary regulators, to move toward elucidating the precise mechanism by which *ramA* overexpression indirectly induces *cirA, fiu, fepA* and *fecA* repression.

To strengthen the results of CFDC susceptibility testing, it can be suggested that investigating the intracellular accumulation of CFDC in strains employed in the present study would be beneficial. This may be achieved using radioactive monitoring of [thiazole-^{14}C]CFDC uptake *via* liquid scintillation counting. This method has been employed previously in support of CFDC susceptibility testing in *Pseudomonas aeruginosa* by Ito *et al.* (2016).

Penultimately, investigations of the present work would benefit from being conducted in *Kp* strains from a clinical isolate cohort, for example, TS1171 (ST15 lineage) and TS1172 (ST15 lineage). These strains are sourced from patient blood culture and urine, respectively, and have been previously sequenced and validated (Stanton, 2022). This would increase reliability and reproducibility of results by allowing confirmation of trends in bacteria prior acclimatised to two key iron limited niches of the human body.

Lastly, this study's experiments would then benefit from employment in an *in vivo Kp* infection model to further validate results and conclusions presented at the scale of systemic whole-organism infection. This could perhaps be initially achieved using Zebrafish (*Danio rerio*).

APPENDIX I. PRIMERS EMPLOYED IN THE PRESENT STUDY

Primer	Schneiders Lab Stock No.	Sequence (5'-3')
Ni_*Kp_fiu*_pKNGS	4674	CGCTCTTGCGGCCGCTTGGAACGGGATAAATGCAGGCTTATTTTTT
No_*Kp_fiu*_pKNGS	4675	CCGCGATCAAGCAGGTGCGACAGAGACATCATGAAATCCGATCAG
***Ci_Kp_fiu*_pKNGS**	4676	CCGTTCCAAGCGGCCGCAAGAGCGGTCTGCGCGTGGGGCCGTT
***Co_Kp_fiu*_pKNGS**	4677	CGGACGCATCGGGCCGGATCTTTATCTGATTAACCGCGACTGG
Ni_*Kp_fepA*_pKNGS	4687	CGCTCTTGCGGCCGCTTGGAACGGTGTTATTCCTGCTTTTTGTCGCC
No_*Kp_fepA*_pKNGS	4686	CCGCGATCAAGCAGGTGCGACACCGCCACCGTCCGATCCGGTC
Ci_*Kp_fepA*_pKNGS	4688	CCGTTCCAAGCGGCCGCAAGAGCGTAGCGGGTTCTCCCTCCCCCG
***Co_Kp_fepA*_pKNGS**	4689	CGGACGCATCGGGCCGGATCTGGTGGCCACCGGCTCGACGGTG
Ni_*Kp_acrD*_pKNGS	4681	CGCTCTTGCGGCCGCTTGGAACGGCAGAATAAAAACCTCATATGCAC
No_*Kp_acrD*_pKNGS	4680	CCGCGATCAAGCAGGTGCGACAGGGGTGAACGGCTGATAGATCTCC
Ci_*Kp_acrD*_pKNGS	4682	CCGTTCCAAGCGGCCGCAAGAGCGACCGACGAGCTTCGGCGGCGAGG
Co_*Kp_acrD*_pKNGS	4683	CGGACGCATCGGGCCGGATCTTCGGTTCAACGGTAAAGCCGATC
pKNGS_backbone_verif_F	4504	AAGTGACGACCTGCAGGCA
pKNGS_backbone_verif_R	4505	CGCATCGGGCCGGATCTA
Next_*Kp_mdtABC*	2062	TGTCGAGGAAATGGTCGA
Cext_*Kp_mdtABC*	2063	CATCGACAGCTGCATCACCAT
Kan-2	1752	ATCCATGTTGGAATTTAATCG
Next_*Kp_cirA*	2080	GTACTCTACCGGACTCAGGC
Cext_*Kp_cirA*	2081	GGCCGATCACCGAATCTTTC
16s_*Kp*_qPCR_F	81	GTTACCCGCAGAAGAAGCAC

16s_*Kp*_qPCR_R	82	CTACGCATTTCACCGCTACA
***fur_Kp*_qPCR_F**	4575	CCATCATGTCAGTGCGGAAG
***fur_Kp*_qPCR_R**	4576	AATTCGATCACTTTGCCGCA
***cirA_Kp*_qPCR_F**	3056	GATACCACTATTCAGGACCACC
***cirA_Kp*_qPCR_R**	3057	ATTACTGGATGACTGCGGATC
***fiu_Kp*_qPCR_F**	3054	ACAGGAGTATCTTTTGACCGC
***fiu_Kp*_qPCR_R**	3055	AGGTGATATTGGTCTGGTTGG
***fepA_Kp*_qPCR_F**	3052	AACCGACCACACCAGAATG
***fepA_Kp*_qPCR_R**	3053	AGATTACCCCAGAGATTGAAGC
***fecA_Kp*_qPCR_F**	4573	GTTAAAGAGAGCGCCGATGG
***fecA_Kp*_qPCR_R**	4574	GACCTGCGTAGATGCCTTTG
***feoB_Kp*_qPCR_F**	4292	TATCGCCGAAAAGCAACAGG
***feoB_Kp*_qPCR_R**	4293	CGGATAGTGGACCAGCTCAA
***mdtB_Kp*_qPCR_F**	4252	AGGTGGCCAGCATTATCCTT
***mdtB_Kp*_qPCR_R**	4253	CTTGAGGTTGATCTGCAGGC
***acrD_Kp*_qPCR_F**	4571	GTTACCGACGCCATCAGTTC
***acrD_Kp*_qPCR_R**	4572	CGTCACCTCTGAACCATCCT
***ompK35_Kp*_qPCR_F**	339	CCAGGTACCCACTTCGATGT
***ompK35_Kp*_qPCR_R**	340	ATCTATGCGGCCGTCATGTA
***baeR_Kp*_qPCR_F**	4606	TGATGGTGACGGCGAAAATC
***baeR_Kp*_qPCR_R**	4607	GACCTTCGTCGACAATCAGC
***ramA_Kp*_qPCR_F**	85	ATTCGAAATGGCATCTGCAACGGC

***ramA_Kp*_qPCR_R**	86	TGAAGACGCGGGTAAAGGTCTGTT

Table 11. List of primers used in the present work. All primers were randomly designed and selected *via* either NEBcutter designation of restriction enzymes and respective sites using mapped plasmid pACYC177, or Primer3web design tool (https://primer3.ut.ee/). All primers were received from Integrated DNA Technologies (IDT) and stored at -20°C.

APPENDIX II. RT-(q)PCR PRIMER EFFICIENCY VALUES

Gene Primer Set (Forward and Reverse)	Efficiency Value(%)	Slope
***fur_Kp*_qPCR**	109.0282	-3.123
***cirA_Kp*_qPCR**	107.0883	-3.163
***fiu_Kp*_qPCR**	91.55193	-3.5425
***fepA_Kp*_qPCR**	104.6415	-3.2155
***fecA_Kp*_qPCR**	100.5213	-3.3095
***feoB_Kp*_qPCR**	99.87196	-3.325
***ompR_Kp*_qPCR**	100.1014	-3.3195
***baeR_Kp*_qPCR**	93.61725	-3.485
***acrD_Kp*_qPCR**	106.9693	-3.1655
***mdtB_Kp*_qPCR**	93.70911	-3.4825

Table 12. RT-(q)PCR primer set efficiencies allowing use in a 1:1 ratio. For each primer sequence see Appendix I.

The efficiency ratio of both RamA AcrB primer sets was also 1:1, with standard curve measurement and efficiency provided by Kyriakos Vidalis (PhD Student, TS Lab).

APPENDIX III. DISK DIFFUSION TRIAL

To assess the sensitivity, accuracy, reproducibility and hence suitability of a semi-quantitative method for CFDC susceptibility testing of *Kp* under iron limitation, disk diffusion was trialled. During this trial, CAZ was used as a baseline control, as this antibiotic, unlike CFDC, does not exploit the Fe^{3+} transportation system for its influx or efficacy. Hence, it could be anticipated that CAZ susceptibility would not be affected by iron limitation (Ito *et al.*, 2016).

To determine the impact of the constitutive expression of *cirA, fiu, fepA* and *fecA*, the repression and overexpression of *ompK35*, and the overexpression of *acrAB* on OM permeability to CFDC and CAZ, an isogenic mutant of Ecl8 deleted for *envZompR*, and and an isogenic mutant of Ecl8 deleted of *ramR* (overexpressed for *ramA*) were employed in disk diffusion susceptibility testing. These strains were tested alongside wild type control Ecl8. All strains were incubated overnight in both iron limited (ID-CAMHB) and iron replete (ID-CAMHB+$FeCl_3$) medias. Cultures were then standardised to OD_{600} 0.42, and respective inoculums were swabbed onto iron limited agar (ID-CAMH agar) and iron replete agar (ID-CAMH+$FeCl_3$ agar). This was followed by the addition of 30µg disks of both CFDC and CAZ to the plates, as per the method outlined in 2.10.1.. Plates were then incubated overnight at 37°C.

No difference was found in inhibition zone diameters, and therefore antibiotic susceptibility, irrespective of iron concentration or antibiotic disc used, for each strain tested relative to Ecl8. Results for CFDC are shown in Figure 50A, with results for CAZ shown in Figure 50B.

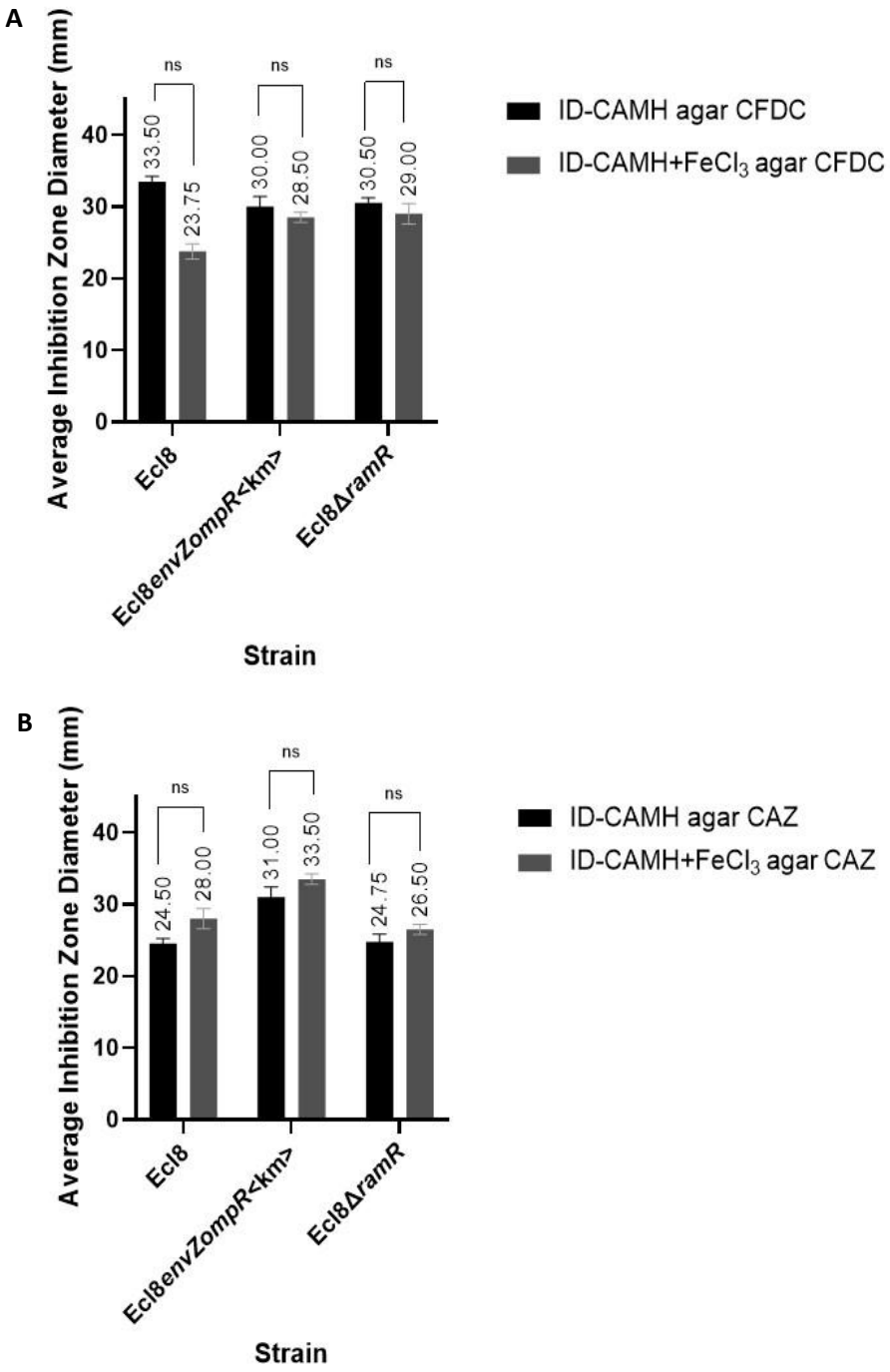

Figure 50. Average inhibition zone diameters (mm) after inoculation of strains incubated overnight in iron deplete media (ID-CAMHB) or iron replete media (ID-CAMHB+$FeCl_3$) onto respective iron deplete ID-CAMH agar or iron replete ID-CAMH+$FeCl_3$ agar with CFDC (A) or CAZ (B). Average was calculated due to this data being linear. Bars represent ± SEM. The label ns indicates not statistically significant as identified with *t*-test. Results are representative of biological repeats spanning n=2.

Figure 50A shows inhibition zone diameters after incubation with CFDC 30µg disks demonstrated no statistically significant difference between iron deplete (ID-CAMH) agar and iron replete (IDCAMH+$FeCl_3$) agar for all strains tested, as identified *via t*-test. Figure 50B shows the same lack of statistically significant difference in inhibition zone diameters between iron deplete (ID-CAMH) agar and iron replete (ID-CAMH+$FeCl_3$) agar after incubation with CAZ 30µg disks. There was no statistically significant difference in inhibition zone diameters for *envZompR* or *ramR* deleted strains relative to Ecl8 after exposure to either CFDC or CAZ under either iron concentration, as identified by *t*-test. Unexpectedly, all strains including wild type Ecl8 exceeded the inhibition zone diameter breakpoints for classification as resistant (2.10.1.; Table 4). For example plates, see Figure 51.

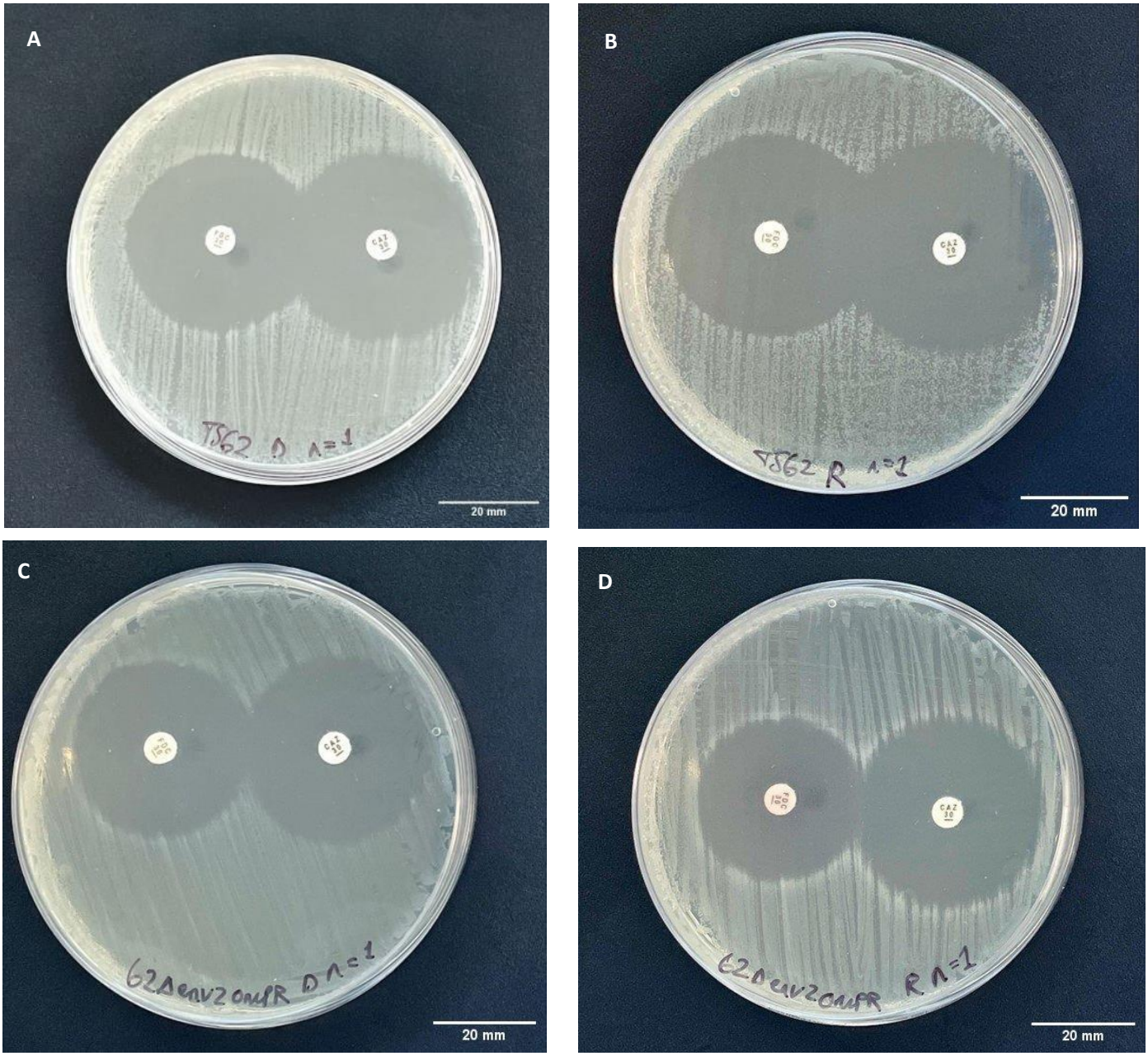

Figure 51. Example disk diffusion plates swabbed with Ecl8 (denoted 62) (A and B) and Ecl8 Δ*envZompR*<km> (denoted 62Δ*envZompR*) (C and D) on iron depleted agar (ID-CAMH agar) (denoted 'D') and iron replete agar (ID-CAMH+$FeCl_3$ agar) (denoted 'R'). Plates represent n=1 of the biological repeats spanning n=2. Images show zones of inhibition (mm) following plating and incubation with 30µg CFDC discs (left-hand disc on each plate) and 30µg CAZ discs (right-hand disc on each plate). The images show difficulty in determining any difference between inhibition zone diameters produced irrespective of strain, iron concentration or antibiotic. Images were fitted with a pixel-mm representative scale bar of 20mm using ImageJ software (Schneider, Rasband and Eliceiri, 2012).

CFDC is known to be of greater efficacy under iron limitation, due to its known exploitation of the Fe^{3+} transportation system for its cellular entry (Ito *et al.*, 2016; Ito *et al.*, 2018). Therefore, the lack of statistically significant difference in Ecl8 inhibition zone diameters after growth in ID-CAMHB and

incubation on ID-CAMH agar, relative to after growth in ID-CAMHB+$FeCl_3$ and incubation on IDCAMH+$FeCl_3$ agar, was anomalous. Furthermore, the IROMPs CirA, Fiu, FepA and FecA are known entry portals for CFDC under iron limitation, of which transcriptional expression is known to be repressed by EnvZ-OmpR (Ito *et al.*, 2018; Daoud *et al.*, 2022). Therefore, the observed absence of statistically significant impact to CFDC susceptibility due to *envZompR* deletion relative to Ecl8 on both ID-CAMH agar and ID-CAMH+$FeCl_3$ agar was anomalous.

Results aligned with the expectation that iron limitation would not impact CAZ susceptibility relative to iron repletion (Ito *et al*, 2016). However, CAZ is known to enter the cell primarily through OmpK35, and be effluxed from the cell by AcrAB-TolC (Jiménez-Castellanos *et al.*, 2016; Jiménez-Castellanos *et al*., 2018). Both EnvZ-OmpR and RamA are known to repress *ompK35*, with RamA known to positively regulate *acrAB* of the AcrAB-TolC efflux pump (De Majumdar *et al.*, 2015). Therefore, the *envZompR* deleted strain and *ramA* overexpressed strain showing no statistically significant difference in CAZ susceptibility relative to Ecl8 was also anomalous.

As a result of these inconsistencies, the quantitative method of broth microdilution became the preferred platform for susceptibility testing for this thesis' duration. This method was chosen as it demonstrates increased precision and high standardization, making it the current 'gold standard' for definitive susceptibility categorization in Gram-negative bacilli (Elias *et al.*, 2021; Bonnin *et al.*, 2022; Bianco *et al*., 2023).

APPENDIX IV. PRELIMINARY CHROME AZUROL S (CAS) AGAR ASSAY TRIAL

Before the semi-quantitative CAS agar media was employed for the investigation of siderophore export from strains of this thesis' interest, it was firstly necessary to test and validate the media's quality, consistency, detection sensitivity and strain specificity.

FUR, referred to as the 'Master Regulator' of Fe^{3+} homeostasis, is known to derepress the enterobactin biosynthetic gene cluster *entABCDFE* and *fes* under iron limitation (Lin *et al.*, 2011; Seo *et al.*, 2014; Ho and Ellermeier, 2015; Choi and Ryu 2019; Hou *et al.*, 2023). Hence, the deletion of *fur* renders enterobactin synthesis constitutive, which also results in enterobactin's constitutive cellular export (Stanton, 2022). Thus, this investigation employed an isogenic strain of Ecl8 deleted of *fur* as its positive control. This was tested alongside wild type control Ecl8, to assess the clarity of orange halo production and confirm there being a distinct difference in halo diameter between the strains which was visible with the naked eye.

Hence, to ascertain the impact of *fur* deletion on siderophore export from *Kp*, Ecl8Δ*fur* and wild type Ecl8 were incubated overnight in iron depleted media (ID-CAMHB), cultures were standardized to OD_{600} 1.5, and 5µl of each was inoculated onto CAS agar plates. Plates were then incubated for 18h at 30°C, as per the protocol outlined in **2.9.**.

It was found that the deletion of *fur* resulted in increased siderophore efflux from *Kp* under iron limitation. This was clearly observable *via* there being a distinctly larger orange halo around the Ecl8Δ*fur* inoculum droplet relative to Ecl8. Results are shown in Figure 52 and Figure 53.

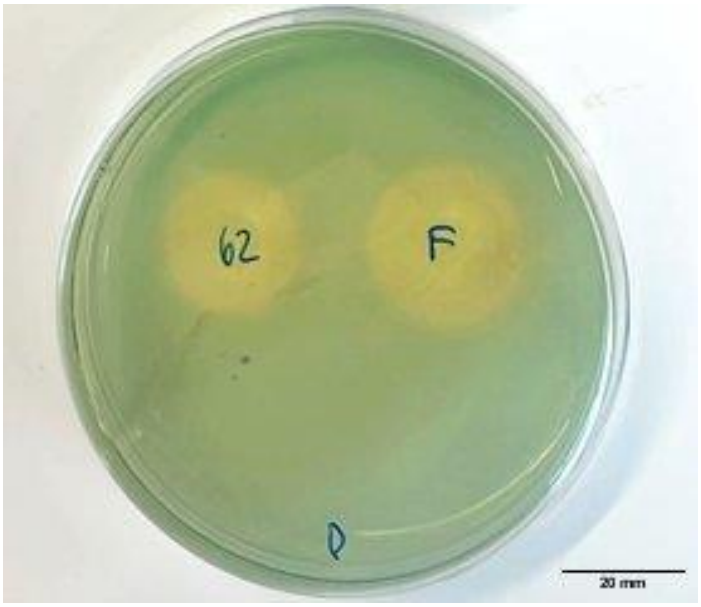

Figure 52. Image of CAS trial plate inoculated with strains Ecl8 (denoted '62') and Ecl8Δfur (denoted 'F') following strain growth in iron limited media (ID-CAMHB) (denoted D for deplete). The image shows clear colour change from blue to orange where bacteria were inoculated, clearly demonstrating extracellular siderophore export. The plate represents n=1 of the n=3 biological repeats conducted for both strains. Images were fitted with a pixel-mm representative scale bar of 20mm using ImageJ software (Schneider, Rasband and Eliceiri, 2012).

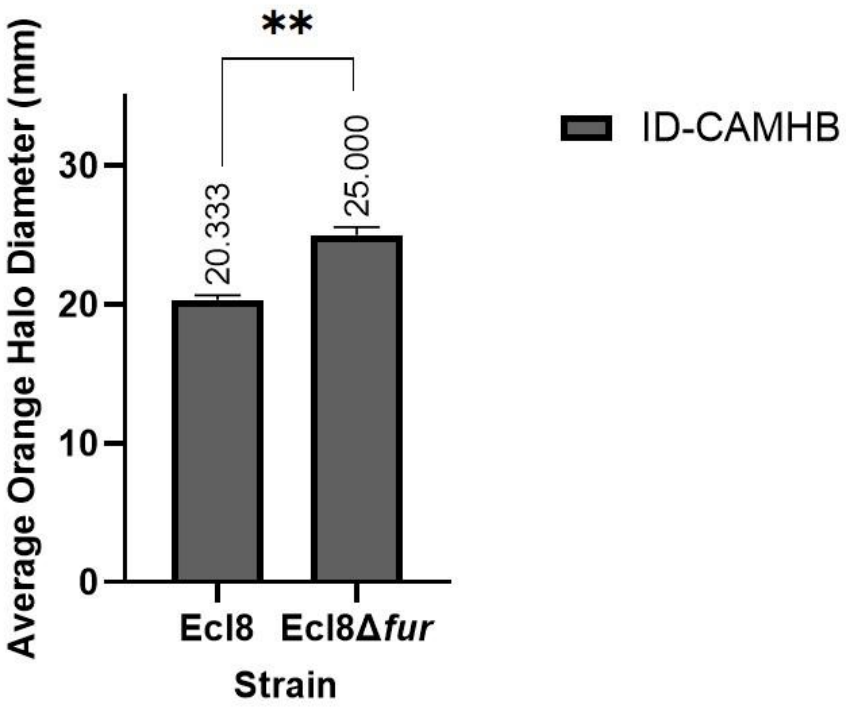

Figure 53. Average orange halo diameters (mm) on CAS plates after inoculation with Ecl8 and Ecl8Δ*fur* grown in iron deplete media (ID-CAMHB). The label ** indicates statistically significant at $p<0.01$ as identified by *t*test. Halo diameter was averaged after conducting investigation under biological replicates equalling n=3.

Figure 53 shows the average orange halo diameter of Ecl8Δ*fur* after incubation in ID-CAMHB to be statistically significantly increased by 4.667mm (approximately 23%) relative to the average orange

halo diameter of Ecl8 after incubation in ID-CAMHB, as identified by *t*-test ($p<0.01$). Average halo diameters for Ecl8Δ*fur* and Ecl8 were 25mm and 20.333mm, respectively.

Thus, this result confirms the quality, detection sensitivity, consistency and strain specificity of the CAS agar media. The agar was therefore approved for use to investigate siderophore export from strains of this thesis' interest, without requirement for further optimization.

APPENDIX V. COLLATED CAS AGAR ASSAY PLATE IMAGES FOR ALL TESTED STRAINS

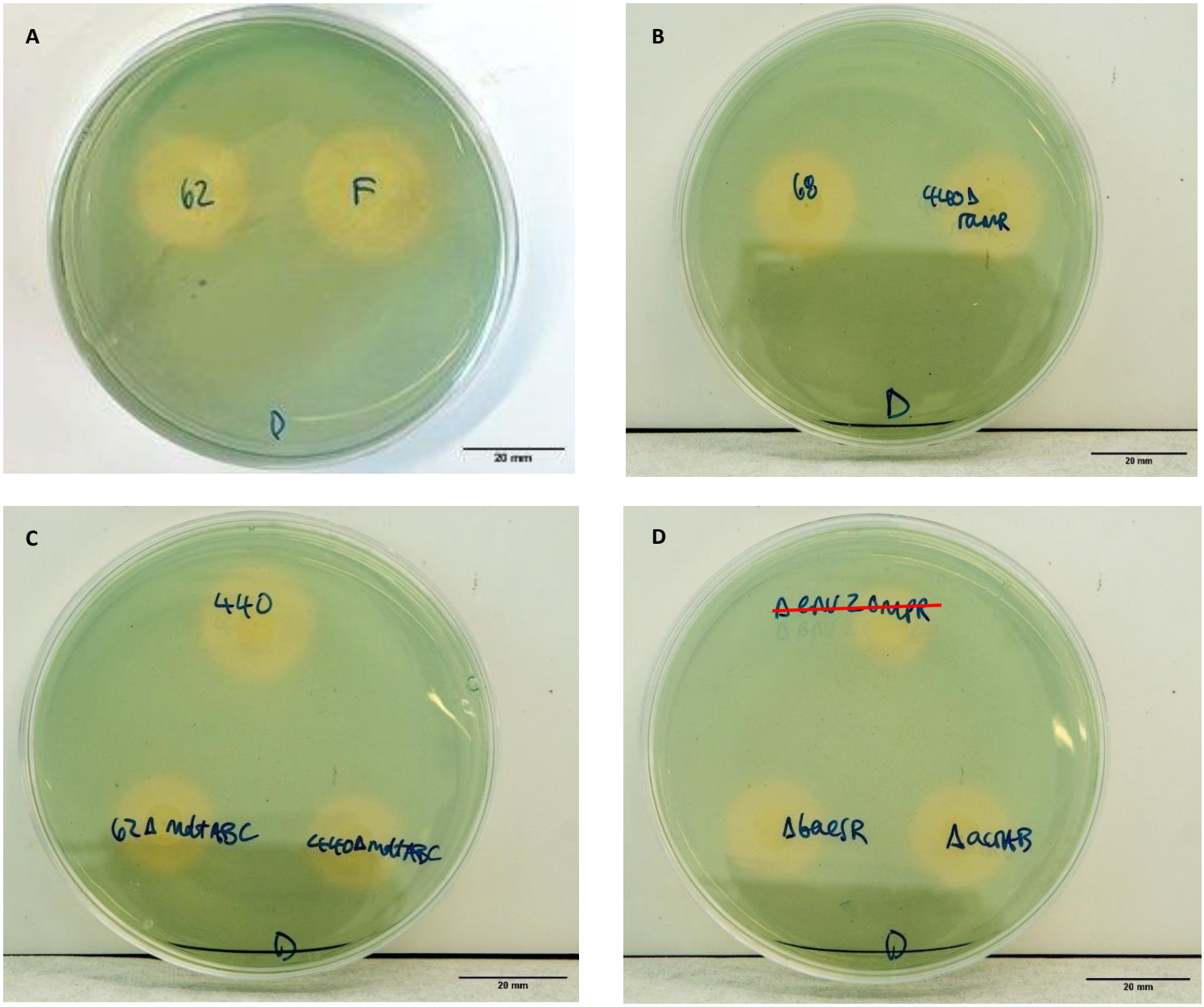

Figure 54. Collated images of CAS plates inoculated with all tested strains following strain growth in iron limited media (ID-CAMHB) (denoted D for deplete). The plates represent n=1 of the n=3 biological repeats conducted for all strains. The images show clear colour change from blue to orange where bacteria were inoculated, demonstrating extracellular siderophore export. **A** shows strains Ecl8 (denoted '62') and Ecl8Δ*fur* (denoted 'F'). **B** shows strains Ecl8Δ*ramR* (denoted '68') and Kp 52145*ramR*<km> (denoted '440Δ*ramR*'). **C** shows strains *Kp* 52145 (denoted '440'), Ecl8*mdtABC*<km> (denoted '62Δ*mdtABC*') and *Kp* 52145*mdtABC*<km> (denoted '440Δ*mdtABC*'). **D** shows strains Ecl8*baeSR*<km> (denoted 'Δ*baeSR*') and Ecl8*acrAB*<km> (denoted 'Δ*acrAB*'). The strain on plate **D** with a red line scored through it was not taken forward for further analysis or use in this thesis. Images were fitted with a pixel-mm representative scale bar of 20mm using ImageJ software (Schneider, Rasband and Eliceiri, 2012).

APPENDIX VI. VALIDATION OF IROMP DEREPRESSION UNDER FUR DELETION

FUR, being the master regulator of Fe^{3+} homeostasis in *Kp*, is known to control the RNA transcript expression of IROMP encoding genes *cirA, fiu, fepA* and *fecA*. Under iron replete conditions, holoFUR represses the expression of *cirA, fiu, fepA* and *fecA*. When iron is scarce, holo-FUR dimerizes to its apo- state, which results in the derepression of the expression of *cirA, fiu, fepA* and *fecA* (**1.5.**; Figure 2) (Seo *et al.*, 2014; Ho and Ellermeier, 2015, Choi and Ryu, 2019; Hou *et al.*, 2023). The deletion of *fur* is therefore known to render the IROMP encoding genes *cirA, fiu, fepA* and *fecA* constitutively expressed (Hou *et al.*, 2023).

Thus, to assess and validate the impact of *fur* deletion on the RNA transcript expression of *cirA, fiu, fepA* and *fecA* in *Kp*, an isogenic strain of Ecl8 deleted of *fur* was incubated overnight in iron depleted media (ID-CAMHB), RNA was extracted and the expression of *cirA, fiu, fepA* and *fecA* was analysed *via* RT-(q)PCR. RT-(q)PCR RNA transcript expression levels of *cirA, fiu, fepA* and *fecA* after overnight incubation of Ecl8 in ID-CAMHB were used as the baseline controls. The RT-(q)PCR investigation of *cirA, fiu, fepA* and *fecA* was then repeated after overnight incubation of Ecl8Δ*fur* in iron replete media (ID-CAMHB+$FeCl_3$). Here, RNA transcript expression levels of the same genes obtained from RT-(q)PCR after overnight incubation of Ecl8 in ID-CAMHB+$FeCl_3$ were used as the baseline controls.

It was found that there was consistent upregulation in RNA transcript expression levels of all of *cirA, fiu, fepA* and *fecA* under *fur* deletion relative to Ecl8, irrespective of iron concentration. Results under iron depletion (ID-CAMHB) are shown in Figure 55A, with results under iron repletion (IDCAMHB+$FeCl_3$) shown in Figure 55B.

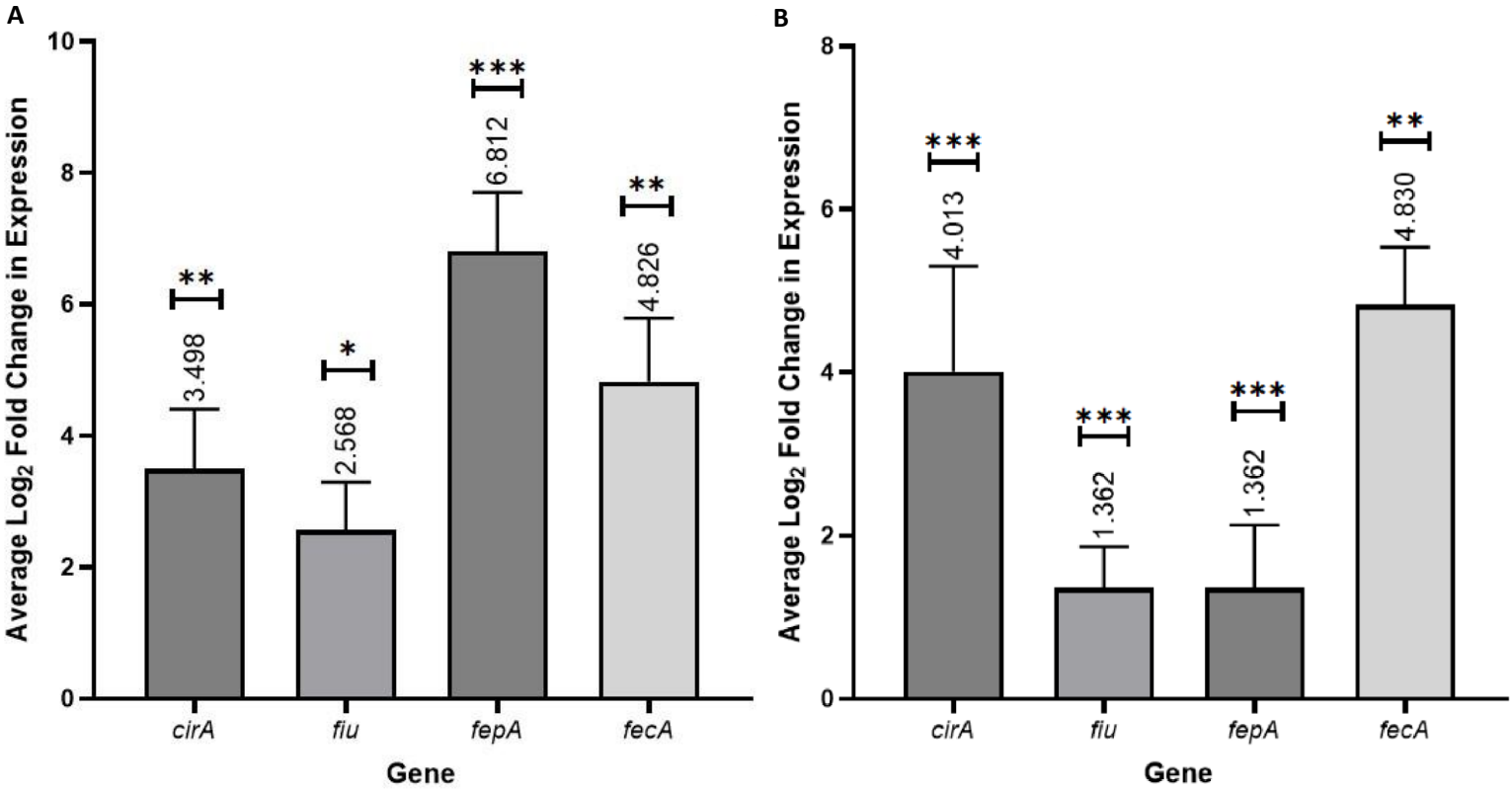

Figure 55. Log_2 fold change expression of *cirA, fiu, fepA, fecA* in iron deplete media (ID-CAMHB) (A) and iron replete media (ID-CAMHB+$FeCl_3$) (B) under Ecl8Δ*fur* relative to Ecl8. Average log_2 fold-change ± SEM is plotted showing the log_2 fold change in gene expression as a ratio of **A** Ecl8Δ*fur* ID-CAMHB:Ecl8 ID-CAMHB and **B** Ecl8Δ*fur* ID-CAMHB+$FeCl_3$:Ecl8 ID-CAMHB+$FeCl_3$ – both test:control, respectively. The label * indicates statistically significant at $p<0.05$, ** indicates statistically significant at $p<0.01$, and *** indicates statistically significant at $p<0.001$, as identified by *t*-test. Log_2 fold change was averaged after conducting investigation under biological and technical replicates both equalling n=3.

Figure 55A shows a statistically significant upregulation in RNA transcript expression of *cirA, fiu, fepA* and *fecA* under ID-CAMHB relative to Ecl8 at $p<0.05$ to $p<0.001$, as identified by *t*-test. Log_2 fold change values were 3.498, 2.568, 6.812 and 4.826, respectively. Figure 55B shows a statistically significant upregulation in RNA transcript expression of the same genes under ID-CAMHB+$FeCl_3$ relative to Ecl8 at $p<0.01$ to $p<0.001$, as identified by *t*-test. Log_2 fold change values for *cirA, fiu, fepA* and *fecA* were 4.013, 1.362, 1.362 and 4.830, respectively.

Thus, these results confirm that deletion of *fur* under Ecl8 induces a phenotype of constitutive IROMP expression in *Kp*. This approved the use of Ecl8Δ*fur* as a negative control for Ecl8*envZompR*<km> in the investigation of CFDC susceptibility.

APPENDIX VII. RT-(q)PCR VALIDATION OF IDM1 and IDM7

Iron Depleted Mutants 1 and 7 (IDM1 and IDM7) are CFDC selected mutants which both harbour identical dual gain-of-function substitutions in the histidine kinases EnvZ (L230Q) and BaeS (V295G) (Stanton, 2022). These gain-of-function substitutions render both histidine kinases constitutively autophosphorylated. This results in the constitutive phosphorylation of the aspartate residues of respective response regulator effectors *ompR* and *baeR*. This, in turn, leads to their constitutive activation, and thus to the constitutive activity of both TCS EnvZ-OmpR and BaeSR (Groban *et al.*, 2009; Rajput *et al.*, 2021; Li *et al.*, 2023). Two genes known to be under negative regulation by EnvZOmpR are the IROMPs *cirA* and *fiu*. The constitutive activation of EnvZ-OmpR is known to render these genes constitutively repressed (Guillier and Gottesman 2006; Guillier and Gottesman, 2008). Therefore, to confirm the status of constitutive EnvZ-OmpR and BaeSR activity in the IDM mutants, *ompR, baeR, cirA* and *fiu* were selected for RNA transcript expression investigation through RT(q)PCR.

To assess and validate the impact of gain-of-function substitutions in BaeS and EnvZ on the expression of *baeR, ompR*, *cirA* and *fiu,* IDM1 and IDM7 were incubated overnight in iron limited media (ID-CAMHB), RNA was extracted and the expression of *ompR, baeR, cirA* and *fiu* was analysed *via* RT-(q)PCR. RT-(q)PCR RNA transcript expression levels of *ompR, baeR*, *cirA* and *fiu* after overnight incubation of Ecl8 in ID-CAMHB were used as the baseline controls. The RT-(q)PCR investigation of *ompR, baeR*, *cirA* and *fiu* was then repeated for both IDM1 and IDM7 after incubation of the IDMs in iron replete media (ID-CAMHB+$FeCl_3$). Here, RNA transcript expression levels of *ompR, baeR, cirA* and *fiu* after incubation of Ecl8 in ID-CAMHB+$FeCl_3$ were used as the baseline controls.

There was a consistent upregulation in RNA transcript expression of *ompR* and *baeR* relative to Ecl8 irrespective of iron concentration for both IDM1 and IDM7. There was a consistent downregulation in RNA transcript expression of *cirA* and *fiu* relative to Ecl8 irrespective of iron concentration for both IDM1 and IDM7. Results for IDM1 under iron depletion and iron repletion are shown in Figure 56A and Figure 56B, respectively. Results for IDM7 under iron depletion and iron repletion are shown in Figure 57A and Figure 57B, respectively.

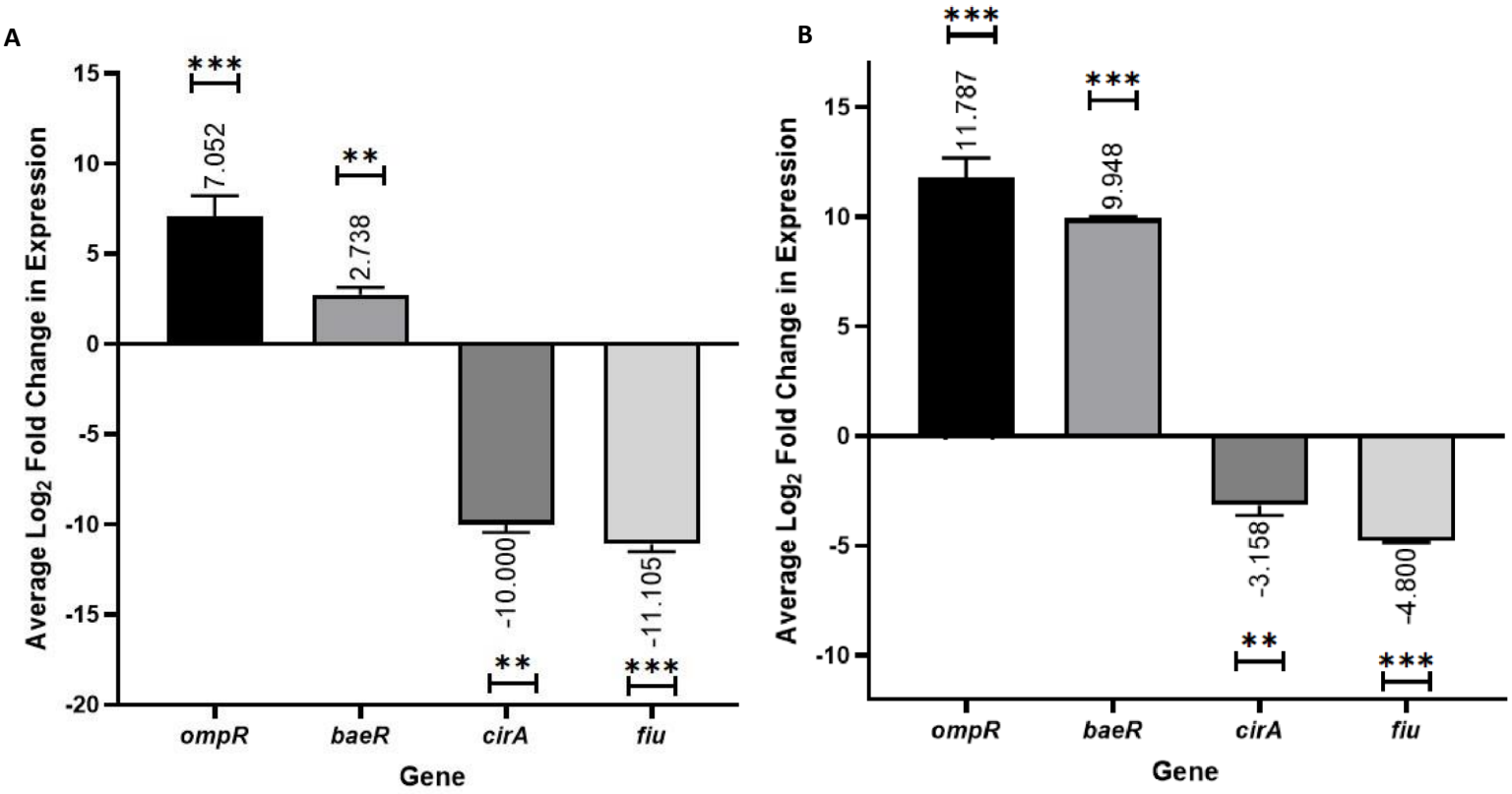

Figure 56. Log_2 fold change expression of *ompR, baeR, cirA, fiu* in iron deplete media (ID-CAMHB) (A) and iron replete media (ID-CAMHB+$FeCl_3$) (B) under IDM1 relative to Ecl8. Average log_2 fold-change ± SEM is plotted showing the log_2 fold change in gene expression as a ratio of **A** IDM1 ID-CAMHB: Ecl8 ID-CAMHB and **B** IDM1 ID-CAMHB+$FeCl_3$: Ecl8 ID-CAMHB+$FeCl_3$ – both test:control. The label ** indicates statistically significant at $p<0.01$, and *** indicates statistically significant at $p<0.001$, as identified by *t*-test. Log_2 fold change was averaged after conducting investigation under biological and technical replicates both equalling n=3.

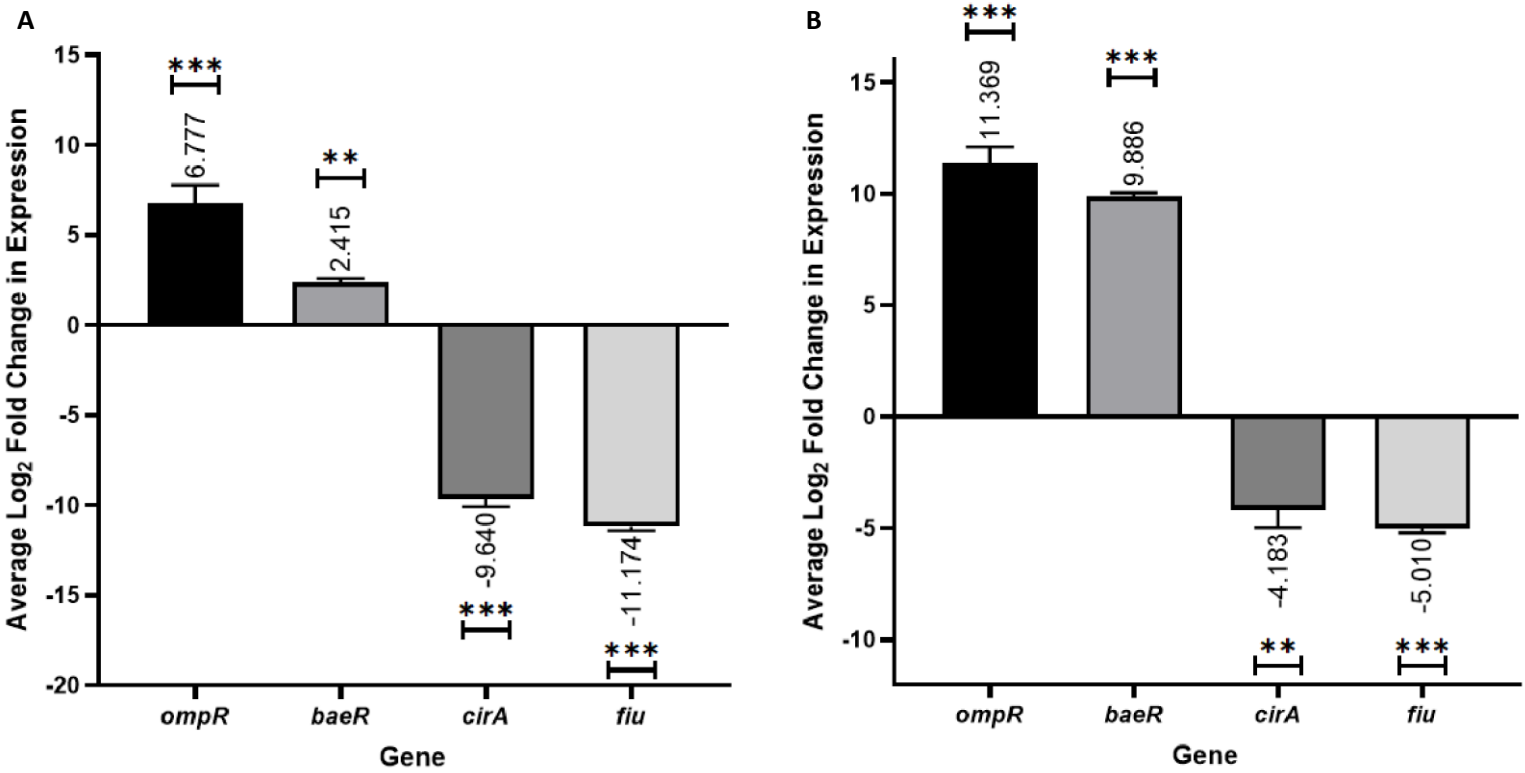

Figure 57. Log_2 fold change expression of *ompR, baeR, cirA, fiu* in iron deplete media (ID-CAMHB) (A) and iron replete media (ID-CAMHB+$FeCl_3$) (B) under IDM7 relative to Ecl8. Average log_2 fold-change ± SEM is plotted showing the log_2 fold change in gene expression as a ratio of **A** IDM7 ID-CAMHB: Ecl8 ID-CAMHB and **B** IDM7 ID-CAMHB+$FeCl_3$: Ecl8 ID-CAMHB+$FeCl_3$ – both test:control. The label ** indicates statistically significant at p<0.01 and *** indicates statistically significant at p<0.001, as identified by *t*-test. Log_2 fold change was averaged after conducting investigation under biological and technical replicates both equalling n=3.

Figure 56A shows a statistically significant upregulation of RNA transcript expression of *ompR* and *baeR* in IDM1 under iron limited media (ID-CAMHB) relative to Ecl8 at p<0.01 to p<0.001 as identified by *t*-test. Log_2 fold change values were 7.051 and 2.738, respectively. A statistically significant downregulation in RNA transcript expression was observed in *cirA* and *fiu* relative to Ecl8 at p<0.01 to p<0.001, with log_2 fold change values being -10 and -11.105, respectively. A similar trend was observed under iron replete media (ID-CAMHB+$FeCl_3$). Figure 56B shows a significant upregulation and downregulation in RNA transcript expression levels of *ompR* and *baeR* and *cirA* and *fiu*, respectively, relative to Ecl8, at p<0.01 to p<0.001 as identified by *t*-test. Log_2 fold change values were 11.786, 9.948, -3.158 and -4.8, respectively.

Similarly to the RT-(q)PCR results obtained for IDM1, Figure 57A shows a statistically significant upregulation of RNA transcript expression of *ompR* and *baeR* in IDM7 under ID-CAMHB relative to Ecl8, at p<0.01 to p<0.001. Log_2 fold change values were 6.776 and 2.415, respectively. A statistically significant downregulation in RNA transcript expression was observed in *cirA* and *fiu* relative to the

wild type control, both at $p<0.001$, with log_2 fold change values being -9.64 and -11.173, respectively. A similar trend was observed under ID-CAMHB+$FeCl_3$. Figure 57B shows a statistically significant upregulation and downregulation in RNA transcript expression levels of of *ompR* and *baeR* and *cirA* and *fiu* relative to Ecl8, at $p<0.01$ to $p<0.001$ as identified by *t*-test. Log_2 fold change values were 11.369, 9.885, -4.183 and -5.01, respectively.

Thus, these results confirm both IDMs to confer the constitutive activation of TCS EnvZ-OmpR and BaeSR. Therefore, both IDMs were approved for use in the present study for assessment of CFDC susceptibility. With it known that IROMP genes *fepA* and *fecA* are subject to the same pathway of negative regulation by EnvZ-OmpR as *cirA* and *fiu*, this data was also deemed sufficient to validate the downregulation of these genes in both IDMs relative to Ecl8.

APPENDIX VIII. RT(q)-PCR ANALYSIS OF Ecl8*omrA*<km>

To determine whether the observed impact of Ecl8*omrA*<km> to CFDC susceptibility under iron limitation was a result of unperturbed activity of sRNA OmrB, RT-(q)PCR investigation of *cirA, fiu, fepA* and *fecA* RNA transcript expression in Ecl8*omrA*<km> was conducted. To do this, Ecl8*omrA*<km> was incubated overnight in iron limited media (ID-CAMHB), RNA was extracted and the RNA transcript expression levels of *cirA, fiu, fepA* and *fecA* were analysed *via* RT-(q)PCR. The same RT(q)PCR analyses after incubation of Ecl8*omrA*<km> under ID-CAMHB was also performed to analyse RNA transcript expression levels of *ompR*. This was conducted to confirm the hypothesis that OmrB activity, in absence of OmrA activity, was also insufficiently able to induce the negative feedback repression of positive regulator *ompR*, thus rendering the IROMP repression constitutive. RNA transcript expression levels of *cirA, fiu, fepA, fecA* and *ompR* obtained *via* RT-(q)PCR after overnight incubation of Ecl8 in ID-CAMHB were used as the baseline controls.

It was found that there was a consistent downregulation of RNA transcript expression of IROMP genes *cirA, fiu, fepA* and *fecA* under *omrA* deletion relative to Ecl8 under ID-CAMHB. There was an upregulation in RNA transcript expression in TCS response regulator *ompR* under *omrA* deletion relative to Ecl8. Results are shown in Figure 58.

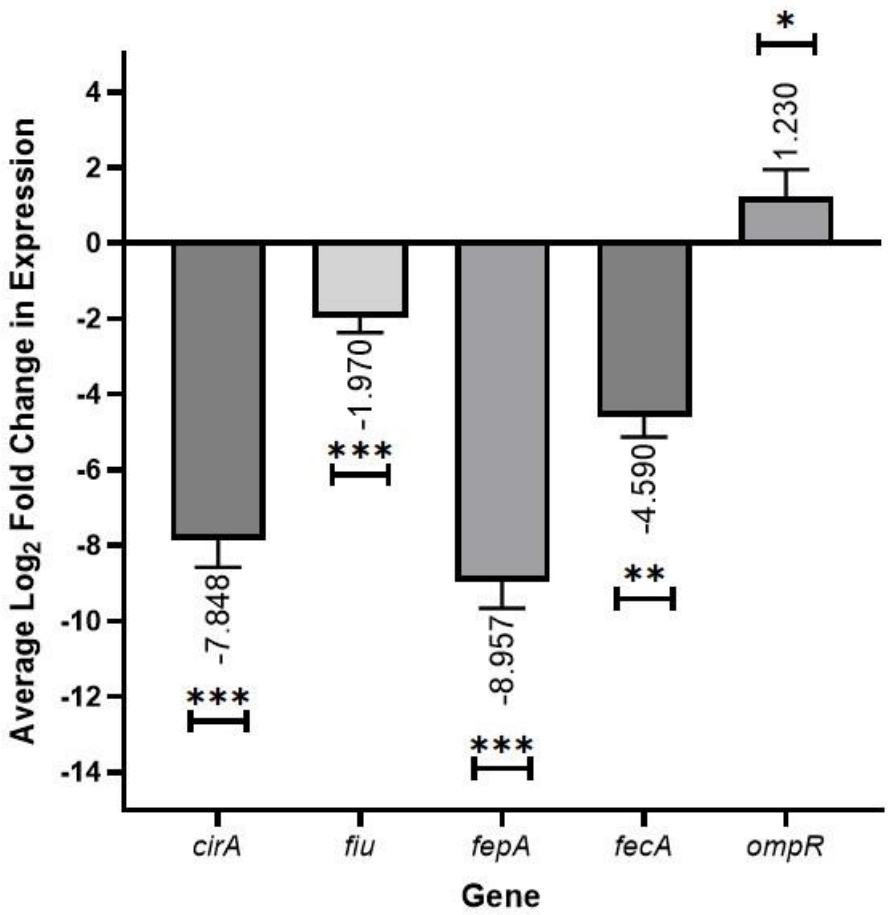

Figure 58. Log_2 fold change expression of *cirA, fiu, fepA, fecA* and *ompR* under Ecl8*omrA*<km> relative to Ecl8 in iron deplete media (ID-CAMHB). Average log_2 fold-change ± SEM is plotted showing the log_2 fold change in gene expression as a ratio of Ecl8*omrA*<km> ID-CAMHB: Ecl8 ID-CAMHB - test:control. The label * indicates statistically significant at $p<0.05$, ** indicates statistically significant at $p<0.01$, and *** indicates statistically significant at $p<0.001$, as identified by *t*-test. Log_2 fold change was averaged after conducting investigation under biological and technical replicates both equalling n=3.

Figure 58 shows that there was a statistically significant downregulation in RNA transcript expression levels of *cirA, fiu, fepA* and *fecA* relative to Ecl8 at $p<0.01$ to $p<0.001$, as identified by *t*-test. Log_2 fold change values were -7.848, -1.970, -8.957 and -4.950, respectively. There was a statistically significant upregulation in RNA transcript expression of *ompR* at $p<0.05$, as identified by *t*-test. The log_2 fold change value was 1.230.

Thus, this result shows that under deletion of only *omrA*, OmrB repressed the IROMPs unperturbed. It also shows that OmrB alone was unable to initiate the negative feedback loop of repression of its positive regulator *ompR*, and therefore unable to initiate its self-limitation. Thus, the IROMP repression under iron limitation was rendered constitutive (1.6.1.; Figure 4). These data also confirm the negative feedback loop of *omrAB* repression of *ompR*, and hence *omrAB* self-limitation, to have

been initiated in Ecl8 under iron limited media (ID-CAMHB) (3.4.1.; Figure 43). This further validates the upregulated *cirA, fiu, fepA* and *fecA* expression observed under Ecl8 (3.2.1.; Figure 11). With *ompR* expression remaining upregulated, this data was also deemed sufficient to validate that *feoB* expression, positively regulated by EnvZ-OmpR, remained upregulated. This therefore leads to FeoB further contributing to the repression of the IROMPs through its feedback association with FUR (1.5., Figure 2; 1.6.1., Figure 4).

This data aligns with prior study evidencing both sRNAs OmrA and OmrB to be required simultaneously to induce the negative feedback loop of *ompR* repression, and subsequent IROMP derepression, under iron limitation (Guillier and Gottesman, 2006; Guillier and Gottesman, 2008; Brosse, Korobeinikova, Gottesman and Guillier, 2016). Hence, this data explains the 4-fold increased CFDC MIC conferred by Ecl8*omrA*<km> under ID-CAMHB.

From this data, it can be concluded that an isogenic strain of Ecl8 deleted of both *omrA* and *omrB* should have instead been employed as the additional negative control for Ecl8*envZompR*<km> in CFDC susceptibility testing.

References

Alteri, C.J. and Mobley, H.L. (2007) 'Quantitative profile of the uropathogenic *Escherichia coli* outer membrane proteome during growth in human urine', *Infection and Immunity*, 75(6), pp. 2679-88. Available at: 10.1128/iai.00076-07

Anes, J., McCusker, M.P., Fanning, S. and Martins, M. (2015) 'The ins and outs of RND efflux pumps in *Escherichia coli*', *Frontiers in Microbiology*, 6, p. 587. Available at: 10.3389/fmicb.2015.00587

Arcari, G., Cecilia, F., Oliva, A., Polani, R., Raponi, G., Sacco, F., De Francesco, A., Pugliese, F. and Carattoli, A. (2023) 'Genotypic Evolution of *Klebsiella pneumoniae* Sequence Type 512 during Ceftazidime/Avibactam, Meropenem/Vaborbactam, and Cefiderocol Treatment, Italy', *Emerging Infectious Diseases*, 29(11), pp. 2266-2274. Available at: 10.3201/eid2911.230921

Asempa, T.E., Abdelraouf, K. and Nicolau, D.P. (2020) 'Metallo-β-lactamase resistance in Enterobacteriaceae is an artefact of currently utilized antimicrobial susceptibility testing methods', *Journal of Antimicrobial Chemotherapy*, 75(4), pp. 997-1005. Available at: 10.1093/jac/dkz532

Avican, K., Aldahdooh, J., Togninalli, M., Mahmud, A.K.M.F., Tang, J., Borgwardt, K.M., Rhen, M. and Fällman, M. (2021) 'RNA atlas of human bacterial pathogens uncovers stress dynamics linked to infection', *Nature Communications*, 12(1), p. 3282. Available at: 10.1038/s41467-021-23588-w

Babu, M., Kagan, O., Guo, H., Greenblatt, J. and Emili, A. (2012) 'Identification of protein complexes in *Escherichia coli* using sequential peptide affinity purification in combination with tandem mass spectrometry', *Journal of Visualised Experiments*, (69) Available at: 10.3791/4057

Bailey, A.M., Ivens, A., Kingsley, R., Cottell, J.L., Wain, J. and Piddock, L.J. (2010) 'RamA, a member of the AraC/XylS family, influences both virulence and efflux in *Salmonella enterica* serovar Typhimurium', *Journal of Bacteriology*, 192(6), pp. 1607-16. Available at: 10.1128/jb.01517-09

Baranova, N. and Nikaido, H. (2002) 'The baeSR two-component regulatory system activates transcription of the yegMNOB (mdtABCD) transporter gene cluster in *Escherichia coli* and increases its resistance to novobiocin and deoxycholate', *Journal of Bacteriology*, 184(15), pp. 4168-76. Available at: 10.1128/jb.184.15.4168-4176.2002

Bianco, G., Boattini, M., Comini, S., Banche, G., Cavallo, R. and Costa, C. (2023) 'Disc Diffusion and ComASP(®) Cefiderocol Microdilution Panel to Overcome the Challenge of Cefiderocol Susceptibility Testing in Clinical Laboratory Routine', *Antibiotics (Basel)*, 12(3) Available at: 10.3390/antibiotics12030604

Bleuel, C., Grosse, C., Taudte, N., Scherer, J., Wesenberg, D., Krauss, G.J., Nies, D.H. and Grass, G. (2005) 'TolC is involved in enterobactin efflux across the outer membrane of *Escherichia coli*', *Journal of Bacteriology*, 187(19), pp. 6701-7. Available at: 10.1128/jb.187.19.6701-6707.2005

Bonnin, R.A., Emeraud, C., Jousset, A.B., Naas, T. and Dortet, L. (2022) 'Comparison of disk diffusion, MIC test strip and broth microdilution methods for cefiderocol susceptibility testing on carbapenemresistant enterobacterales', *Clinical Microbiology and Infection*, 28(8), pp. 1156.e1-1156.e5. Available at: 10.1016/j.cmi.2022.04.013

Borde, K., Kareem, M.A., Sharma, R.M., Dass, S.M., Ravi, V. and Mathai, D. (2023) *'In vitro* activity of cefiderocol against comparators (ceftazidime-avibactam, ceftazidime-avibactam/ aztreonam combination, and colistin) against clinical isolates of meropenem-resistant *Klebsiella pneumoniae* from India', *Microbiology Spectrum*, 11(5), p. e0084723. Available at: 10.1128/spectrum.00847-23
Braun, V. (1995) 'Energy-coupled transport and signal transduction through the Gram-negative outer membrane via TonB-ExbB-ExbD-dependent receptor proteins', *FEMS Microbiology Reviews*, 16(4), pp. 295-307. Available at: 10.1111/j.1574-6976.1995.tb00177.x

Braun, V., Ratliff, A.C., Celia, H. and Buchanan, S.K. (2023) 'Energization of Outer Membrane Transport by the ExbB ExbD Molecular Motor', *Journal of Bacteriology*, 205(6), p. e0003523. Available at: 10.1128/jb.00035-23

Brosse, A., Korobeinikova, A., Gottesman, S. and Guillier, M. (2016) 'Unexpected properties of sRNA promoters allow feedback control via regulation of a two-component system', *Nucleic Acids Research*, 44(20), pp. 9650-9666. Available at: 10.1093/nar/gkw642

Brown, N.P., Leroy, C. and Sander, C. (1998) 'MView: a web-compatible database search or multiple alignment viewer', *Bioinformatics*, 14(4), pp. 380-1. Available at: 10.1093/bioinformatics/14.4.380

Buchanan, S.K., Smith, B.S., Venkatramani, L., Xia, D., Esser, L., Palnitkar, M., Chakraborty, R., van der Helm, D. and Deisenhofer, J. (1999) 'Crystal structure of the outer membrane active transporter FepA from *Escherichia coli*', *Nature Structural & Molecular Biology*, 6(1), pp. 56-63. Available at: 10.1038/4931

Buffet, A., Rocha, E.P.C. and Rendueles, O. (2021) 'Nutrient conditions are primary drivers of bacterial capsule maintenance in *Klebsiella*', *Proceedings of the Royal Society B: Biological Sciences*, 288(1946), p. 20202876. Available at: 10.1098/rspb.2020.2876

Burmeister, A.R. (2015) 'Horizontal Gene Transfer', *Evolution, Medicine & Public Health*, 2015(1), pp. 193-4. Available at: 10.1093/emph/eov018

Butland, G., Peregrín-Alvarez, J.M., Li, J., Yang, W., Yang, X., Canadien, V., Starostine, A., Richards, D., Beattie, B., Krogan, N., Davey, M., Parkinson, J., Greenblatt, J. and Emili, A. (2005) 'Interaction network containing conserved and essential protein complexes in *Escherichia coli*', *Nature*, 433(7025), pp. 531-537. Available at: 10.1038/nature03239

Cahill, B.K., Seeley, K.W., Gutel, D. and Ellis, T.N. (2015) '*Klebsiella pneumoniae* O antigen loss alters the outer membrane protein composition and the selective packaging of proteins into secreted outer membrane vesicles', *Microbiological Research*, 180, pp. 1-10. Available at: https://doi.org/10.1016/j.micres.2015.06.012

Caza, M. and Kronstad, J.W. (2013) 'Shared and distinct mechanisms of iron acquisition by bacterial and fungal pathogens of humans', *Frontiers in Cellular and Infection Microbiology*, 3, p. 80. Available at: 10.3389/fcimb.2013.00080

Chang, D., Sharma, L., Dela Cruz, C.S. and Zhang, D. (2021) 'Clinical Epidemiology, Risk Factors, and Control Strategies of *Klebsiella pneumoniae* Infection', *Frontiers in Microbiology*, 12 Available at: 10.3389/fmicb.2021.750662

Chen, J., Yang, Y., Yao, H., Bu, S., Li, L., Wang, F., Chen, F. and Yao, H. (2022) 'Prediction of Prognosis in Adult Patients With Carbapenem-Resistant *Klebsiella pneumoniae* Infection', Frontiers in Cellular and Infection Microbiology, 11, pp. 818308-818308. Available at: 10.3389/fcimb.2021.818308

Cheng, C., Ying, Y., Zhou, D., Zhu, L., Lu, J., Li, A., Bao, Q. and Zhu, M. (2020) 'RamA, a transcriptional regulator conferring florfenicol resistance in Leclercia adecarboxylata R25', *Folia Microbiologica (Praha)*, 65(6), pp. 1051-1060. Available at: 10.1007/s12223-020-00816-2

Choby, J.E., Howard-Anderson, J. and Weiss, D.S. (2020) 'Hypervirulent *Klebsiella pneumoniae* - clinical and molecular perspectives', *Journal of Internal Medicine*, 287(3), pp. 283-300. Available at: 10.1111/joim.13007

Choi, J. and Ryu, S. (2019) 'Regulation of Iron Uptake by Fine-Tuning the Iron Responsiveness of the Iron Sensor FUR', *Applied Environmental Microbiology*, 85(9) Available at: 10.1128/aem.03026-18

Cissé, C., Mathieu, S.V., Abeih, M.B., Flanagan, L., Vitale, S., Catty, P., Boturyn, D., Michaud-Soret, I. and Crouzy, S. (2014) 'Inhibition of the ferric uptake regulator by peptides derived from anti-FUR peptide aptamers: coupled theoretical and experimental approaches', *ACS Chemical Biology*, 9(12), pp. 2779-86. Available at: 10.1021/cb5005977

Clements, A., Gaboriaud, F., Duval, J.F., Farn, J.L., Jenney, A.W., Lithgow, T., Wijburg, O.L., Hartland, E.L. and Strugnell, R.A. (2008) 'The major surface-associated saccharides of *Klebsiella pneumoniae* contribute to host cell association', *PLoS One*, 3(11), p. e3817. Available at: 10.1371/journal.pone.0003817

Coppi, M., Antonelli, A., Niccolai, C., Bartolini, A., Bartolini, L., Grazzini, M., Mantengoli, E., Farese, A., Pieralli, F., Mechi, M.T., Di Pilato, V., Giani, T. and Rossolini, G.M. (2022) 'Nosocomial outbreak by NDM-1-producing *Klebsiella pneumoniae* highly resistant to cefiderocol, Florence, Italy, August 2021 to June 2022', *Euro Surveillance*, 27(43) Available at: 10.2807/1560-7917.Es.2022.27.43.2200795

Cramer, A. and Eikmanns, B.J. (2007) 'RamA, the transcriptional regulator of acetate metabolism in Corynebacterium glutamicum, is subject to negative autoregulation', *Journal of Molecular Microbiology and Biotechnology*, 12(1-2), pp. 51-9. Available at: 10.1159/000096459

Cruz-López, F., Martínez-Meléndez, A., Morfin-Otero, R., Rodriguez-Noriega, E., Maldonado-Garza, H.J. and Garza-González, E. (2022) 'Efficacy and In Vitro Activity of Novel Antibiotics for Infections With Carbapenem-Resistant Gram-Negative Pathogens', *Frontiers in Cellular and Infection Microbiology*, 12, p. 884365. Available at: 10.3389/fcimb.2022.884365

Cunrath, O. and Palmer, J. (2021) 'An overview of *Salmonella enterica* metal homeostasis pathways during infection', *microLife*, 2. Available at: 10.1093/femsml/uqab001

Daoud, L., Al-Marzooq, F., Moubareck, C.A., Ghazawi, A. and Collyns, T. (2022) 'Elucidating the effect of iron acquisition systems in *Klebsiella pneumoniae* on susceptibility to the novel siderophorecephalosporin cefiderocol', *PLoS One*, 17(12), p. e0277946. Available at: 10.1371/journal.pone.0277946

De Gaetano, G.V., Lentini, G., Famà, A., Coppolino, F. and Beninati, C. (2023) 'Antimicrobial Resistance: Two-Component Regulatory Systems and Multidrug Efflux Pumps', *Antibiotics*, 12(6), p. 965. Available at: https://www.mdpi.com/2079-6382/12/6/965.

De Majumdar, S., Yu, J., Fookes, M., McAteer, S.P., Llobet, E., Finn, S., Spence, S., Monaghan, A., Kissenpfennig, A., Ingram, R.J., Bengoechea, J., Gally, D.L., Fanning, S., Elborn, J.S. and Schneiders, T.

(2015) 'Elucidation of the RamA Regulon *in Klebsiella pneumoniae* Reveals a Role in LPS Regulation', *PLoS Pathogens*, 11(1), pp. 1–22. Available at: https://doi.org/10.1371/journal.ppat.1004627

Deroche, L., Arrivé, F., Martellosio, J.-P., Marchand, S. and Buyck, J., M (2023) 'Development of cefiderocol resistance during treatment in *Klebsiella pneumoniae*', *33rd ECCMID*. Copenhagen, Denmark, 2023-04-15. Available at: https://hal.science/hal-04142293.

Domingues, S., Lima, T., Saavedra, M.J. and Da Silva, G.J. (2023) 'An Overview of Cefiderocol's Therapeutic Potential and Underlying Resistance Mechanisms', *Life (Basel)*, 13(7) Available at: 10.3390/life13071427

Elias, R., Melo-Cristino, J., Lito, L., Pinto, M., Gonçalves, L., Campino, S., Clark, T.G., Duarte, A. and Perdigão, J. (2021) *'Klebsiella pneumoniae* and Colistin Susceptibility Testing: Performance Evaluation for Broth Microdilution, Agar Dilution and Minimum Inhibitory Concentration Test Strips and Impact of the "Skipped Well" Phenomenon', *Diagnostics (Basel)*, 11(12) Available at: 10.3390/diagnostics11122352

El-Lababidi, R.M. and Rizk, J.G. (2020) 'Cefiderocol: A Siderophore Cephalosporin', *Annals of Pharmacotherapy*, 54(12), pp. 1215-1231. Available at: 10.1177/1060028020929988

Escolar, L., Pérez-Martín, J. and de Lorenzo, V. (1999) 'Opening the iron box: transcriptional metalloregulation by the FUR protein', *Journal of Bacteriology*, 181(20), pp. 6223-9. Available at: 10.1128/jb.181.20.6223-6229.1999

Favre-Bonte, S., Joly, B. and Forestier, C. (1999) 'Consequences of reduction of *Klebsiella pneumoniae* capsule expression on interactions of this bacterium with epithelial cells', *Infection and Immunity*, 67(2), pp. 554-61. Available at: 10.1128/iai.67.2.554-561.1999

Flanagan, S.E., Patch, A.M. and Ellard, S. (2010) 'Using SIFT and PolyPhen to predict loss-of-function and gain-of-function mutations', *Genetic Testing and Molecular Biomarkers*, 14(4), pp. 533-7. Available at: 10.1089/gtmb.2010.0036

Fookes, M., Yu, J., De Majumdar, S., Thomson, N. and Schneiders, T. (2013) 'Genome Sequence of *Klebsiella pneumoniae* Ecl8, a Reference Strain for Targeted Genetic Manipulation', *Genome Announcements*, 1(1) Available at: 10.1128/genomeA.00027-12

Freiberg, J.A., Tao, L., Manuel, C., Mike, L.A., Nelson, G.E., Harris, B.D., Mathers, A.J., Talbot, T.R., Skaar, E.P. and Humphries, R.M. (2024) 'A multi-species outbreak of VIM-producing carbapenemresistant bacteria in a burn unit and subsequent investigation of rapid development of cefiderocol resistance', *Antimicrobial Agents in Chemotherapy*, 68(4), p. e0150723. Available at: 10.1128/aac.01507-23

Garofalo, R., Wohlgemuth, I., Pearson, M., Lenz, C., Urlaub, H. and Rodnina, M.V. (2019) 'Broad range of missense error frequencies in cellular proteins', *Nucleic Acids Research*, 47(6), pp. 2932-2945. Available at: 10.1093/nar/gky1319

Gasteiger, E., Gattiker, A., Hoogland, C., Ivanyi, I., Appel, R.D. and Bairoch, A. (2003) 'ExPASy: the proteomics server for in-depth protein knowledge and analysis', *Nucleic Acids Research,* 31:37843788.

Gerken, H., Vuong, P., Soparkar, K. and Misra, R. (2020) 'Roles of the EnvZ/OmpR Two-Component System and Porins in Iron Acquisition in *Escherichia coli*', *mBio*, 11(3) Available at: 10.1128/mBio.01192-20

Grinter, R. and Lithgow, T. (2019) 'The structure of the bacterial iron-catecholate transporter Fiu suggests that it imports substrates via a two-step mechanism', *Journal of Biological Chemistry*, 294(51), pp. 19523-19534. Available at: 10.1074/jbc.RA119.011018

Groban, E.S., Clarke, E.J., Salis, H.M., Miller, S.M. and Voigt, C.A. (2009) 'Kinetic Buffering of Cross Talk between Bacterial Two-Component Sensors', *Journal of Molecular Biology*, 390(3), pp. 380-393. Available at: https://doi.org/10.1016/j.jmb.2009.05.007

Guillier, M. and Gottesman, S. (2006) 'Remodelling of the Escherichia coli outer membrane by two small regulatory RNAs', *Molecular Microbiology*, 59(1), pp. 231-247. Available at: https://doi.org/10.1111/j.1365-2958.2005.04929.x

Guillier, M. and Gottesman, S. (2008) 'The 5' end of two redundant sRNAs is involved in the regulation of multiple targets, including their own regulator', *Nucleic Acids Research*, 36(21), pp. 6781-6794. Available at: 10.1093/nar/gkn742

Hackel, M.A., Tsuji, M., Yamano, Y., Echols, R., Karlowsky, J.A. and Sahm, D.F. (2019) 'Reproducibility of broth microdilution MICs for the novel siderophore cephalosporin, cefiderocol, determined using iron-depleted cation-adjusted Mueller-Hinton broth', *Diagnostic Microbiology and Infectious Disease*, 94(4), pp. 321-325. Available at: https://doi.org/10.1016/j.diagmicrobio.2019.03.003

Himpsl, S.D. and Mobley, H.L.T. (2019) 'Siderophore Detection Using Chrome Azurol S and Cross-Feeding Assays', *Methods in Molecular Biology*, 2021, pp. 97-108. Available at: 10.1007/978-1-49399601-8_10

Hirakawa, H., Kurushima, J., Hashimoto, Y. and Tomita, H. (2020) 'Progress Overview of Bacterial Two-Component Regulatory Systems as Potential Targets for Antimicrobial Chemotherapy', *Antibiotics (Basel)*, 9(10) Available at: 10.3390/antibiotics9100635

Hirakawa, H., Nishino, K., Yamada, J., Hirata, T. and Yamaguchi, A. (2003) 'Beta-lactam resistance modulated by the overexpression of response regulators of two-component signal transduction systems in *Escherichia coli*', *Journal of Antimicrobial Chemotherapy*, 52(4), pp. 576-82. Available at: 10.1093/jac/dkg406

Ho, T.D. and Ellermeier, C.D. (2015) 'Ferric Uptake Regulator FUR Control of Putative Iron Acquisition Systems in *Clostridium difficile*', *Journal of Bacteriology*, 197(18), pp. 2930-40. Available at: 10.1128/jb.00098-15

Horiyama, T. and Nishino, K. (2014) 'AcrB, AcrD, and MdtABC multidrug efflux systems are involved in enterobactin export in *Escherichia coli*', *PLoS One*, 9(9), p. e108642. Available at: 10.1371/journal.pone.0108642

Hou, C., Liu, L., Ju, X., Xiao, Y., Li, B. and You, C. (2023) 'Revisiting FUR Regulon Leads to a Comprehensive Understanding of Iron and FUR Regulation', *International Journal of Molecular Sciences*, 24(10) Available at: 10.3390/ijms24109078

Hsu, C.-R., Liao, C.-H., Lin, T.-L., Yang, H.-R., Yang, F.-L., Hsieh, P.-F., Wu, S.-H. and Wang, J.-T. (2016) 'Identification of a capsular variant and characterization of capsular acetylation in *Klebsiella pneumoniae* PLA-associated type K57', *Scientific Reports*, 6(1), p. 31946. Available at: 10.1038/srep31946

Hutchings, M.I., Truman, A.W. and Wilkinson, B. (2019) 'Antibiotics: past, present and future', *Current Opinion in Microbiology*, 51, pp. 72-80. Available at: https://doi.org/10.1016/j.mib.2019.10.008

Ikawa, S., Yamasaki, S., Morita, Y. and Nishino, K. (2022) 'Role of the drug efflux pump in the intrinsic cefiderocol resistance of *Pseudomonas aeruginosa*', *bioRxiv*, p. 2022.05.31.494263. Available at: 10.1101/2022.05.31.494263

Isler, B., Vatansever, C., Özer, B., Çınar, G., Aslan, A.T., Falconer, C., Bauer, M.J., Forde, B., Şimşek, F., Tülek, N., Demirkaya, H., Menekşe, Ş., Akalin, H., Balkan, İ.İ., Aydın, M., Tigen, E.T., Demir, S.K., Kapmaz, M., Keske, Ş., Doğan, Ö., Arabacı, Ç., Yağcı, S., Hazırolan, G., Bakır, V.O., Gönen, M., Saltoğlu, N., Azap, A., Azap, Ö., Akova, M., Ergönül, Ö., Can, F., Paterson, D.L. and Harris, P.N.A. (2023) 'Higher rates of cefiderocol resistance among NDM producing *Klebsiella* bloodstream isolates applying EUCAST over CLSI breakpoints', *Infectious Diseases*, 55(9), pp. 607-613. Available at: 10.1080/23744235.2023.2226709

Ito, A., Nishikawa, T., Matsumoto, S., Yoshizawa, H., Sato, T., Nakamura, R., Tsuji, M. and Yamano, Y. (2016) 'Siderophore Cephalosporin Cefiderocol Utilizes Ferric Iron Transporter Systems for Antibacterial Activity against *Pseudomonas aeruginosa*', *Antimicrobial Agents in Chemotherapy*, 60(12), pp. 7396-7401. Available at: 10.1128/aac.01405-16

Ito, A., Sato, T., Ota, M., Takemura, M., Nishikawa, T., Toba, S., Kohira, N., Miyagawa, S., Ishibashi, N., Matsumoto, S., Nakamura, R., Tsuji, M. and Yamano, Y. (2018) *'In Vitro* Antibacterial Properties of Cefiderocol, a Novel Siderophore Cephalosporin, against Gram-Negative Bacteria', *Antimicrobial Agents in Chemotherapy*, 62(1) Available at: 10.1128/aac.01454-17

Jiménez-Castellanos, J.-C., Ismah, W.A.K.W.N., Takebayashi, Y., Findlay, J., Schneiders, T., Heesom, K.J. and Avison, M.B. (2018) 'Envelope proteome changes driven by RamA overproduction *in Klebsiella pneumoniae* that enhance acquired β-lactam resistance', *Journal of Antimicrobial Chemotherapy*, 73(1), pp. 88-94. Available at: 10.1093/jac/dkx345

Jiménez-Castellanos, J.-C., Kamil, W.N.I.W.A., Cheung, C.H.P., Tobin, M.S., Brown, J., Isaac, S.G., Heesom, K.J., Schneiders, T. and Avison, M.B. (2016) 'Comparative effects of overproducing the AraCtype transcriptional regulators MarA, SoxS, RarA and RamA on antimicrobial drug susceptibility in
Klebsiella pneumoniae', *Journal of Antimicrobial Chemotherapy*, 71(7), pp. 1820-1825. Available at: 10.1093/jac/dkw088

Karakonstantis, S., Rousaki, M. and Kritsotakis, E.I. (2022) 'Cefiderocol: Systematic Review of Mechanisms of Resistance, Heteroresistance and *In Vivo* Emergence of Resistance', *Antibiotics (Basel)*, 11(6) Available at: 10.3390/antibiotics11060723

Katoh, K. and Standley, D.M. (2013) 'MAFFT multiple sequence alignment software version 7: improvements in performance and usability', *Molecular Biology and Evolution*, 30(4), pp. 772-80. Available at: 10.1093/molbev/mst010

Kaye, K.S., Naas, T., Pogue, J.M. and Rossolini, G.M. (2023) 'Cefiderocol, a Siderophore Cephalosporin, as a Treatment Option for Infections Caused by Carbapenem-Resistant Enterobacterales', *Infectious Diseases and Therapy*, 12(3), pp. 777-806. Available at: 10.1007/s40121-023-00773-6

Klein, S., Boutin, S., Kocer, K., Fiedler, M.O., Störzinger, D., Weigand, M.A., Tan, B., Richter, D., Rupp, C., Mieth, M., Mehrabi, A., Hackert, T., Zimmermann, S., Heeg, K. and Nurjadi, D. (2022) 'Rapid Development of Cefiderocol Resistance in Carbapenem-resistant *Enterobacter cloacae* During

Therapy Is Associated With Heterogeneous Mutations in the Catecholate Siderophore Receptor *cirA*', *Clinical Infectious Diseases*, 74(5), pp. 905-908. Available at: 10.1093/cid/ciab511

Ko, D. and Choi, S.H. (2022) 'Mechanistic understanding of antibiotic resistance mediated by EnvZ/OmpR two-component system in Salmonella enterica serovar Enteritidis', *Journal of Antimicrobial Chemotherapy*, 77(9), pp. 2419-2428. Available at: 10.1093/jac/dkac223

Kocer, K., Boudour-Halil, D., Chanthalangsy, Q., Sähr, A., Heeg, K., Boutin, S. and Nurjadi, D. (2023) 'Genomic Modification of TonB and Emergence of Small-Colony Phenotype in VIM- and NDMProducing *Escherichia coli* following Cefiderocol Exposure *In Vitro*', *Antimicrobial Agents and Chemotherapy*, 67(5), pp. e00118-23. Available at: 10.1128/aac.00118-23

Kolesnik-Goldmann, N., Seth-Smith, H.M.B., Haldimann, K., Imkamp, F., Roloff, T., Zbinden, R., Hobbie, S.N., Egli, A. and Mancini, S. (2023) 'Comparison of Disk Diffusion, E-Test, and Broth Microdilution Methods for Testing *In Vitro* Activity of Cefiderocol in *Acinetobacter baumannii*', *Antibiotics (Basel)*, 12(7) Available at: 10.3390/antibiotics12071212

Krewulak, K.D. and Vogel, H.J. (2008) 'Structural biology of bacterial iron uptake', *Biochimica et Biophysica Acta (BBA) - Biomembranes*, 1778(9), pp. 1781-1804. Available at: https://doi.org/10.1016/j.bbamem.2007.07.026

Kriz, R., Spettel, K., Pichler, A., Schefberger, K., Sanz-Codina, M., Lötsch, F., Harrison, N., Willinger, B., Zeitlinger, M., Burgmann, H. and Lagler, H. (2024) 'In vitro resistance development gives insights into molecular resistance mechanisms against cefiderocol', *The Journal of Antibiotics*, Available at: 10.1038/s41429-024-00762-y

Kumar, A., Chakravorty, S., Yang, T., Russo, T.A., Newton, S.M. and Klebba, P.E. (2024) 'Siderophoremediated iron acquisition by *Klebsiella pneumoniae*', *Journal of Bacteriology*, 206(5), pp. e00024-24. Available at: doi:10.1128/jb.00024-24

Lan, P., Lu, Y., Jiang, Y., Wu, X., Yu, Y. and Zhou, J. (2022) 'Catecholate siderophore receptor CirA impacts cefiderocol susceptibility in *Klebsiella pneumoniae*', *International Journal of Antimicrobial Agents*, 60(4), p. 106646. Available at: 10.1016/j.ijantimicag.2022.106646

Landman, D., Singh, M., El-Imad, B., Miller, E., Win, T. and Quale, J. (2014) *'In vitro* activity of the siderophore monosulfactam BAL30072 against contemporary Gram-negative pathogens from New York City, including multidrug-resistant isolates', *International Journal of Antimicrobial Agents*, 43(6), pp. 527-532. Available at: https://doi.org/10.1016/j.ijantimicag.2014.02.017

Leaden, L., Silva, L.G., Ribeiro, R.A., Dos Santos, N.M., Lorenzetti, A.P.R., Alegria, T.G.P., Schulz, M.L., Medeiros, M.H.G., Koide, T. and Marques, M.V. (2018) 'Iron Deficiency Generates Oxidative Stress and Activation of the SOS Response in *Caulobacter crescentus*', *Frontiers in Microbiology*, 9, p. 2014. Available at: 10.3389/fmicb.2018.02014

Leblanc, S.K., Oates, C.W. and Raivio, T.L. (2011) 'Characterization of the induction and cellular role of the BaeSR two-component envelope stress response of *Escherichia coli*', *Journal of Bacteriology*, 193(13), pp. 3367-75. Available at: 10.1128/jb.01534-10

Lery, L.M., Frangeul, L., Tomas, A., Passet, V., Almeida, A.S., Bialek-Davenet, S., Barbe, V., Bengoechea, J.A., Sansonetti, P., Brisse, S. and Tournebize, R. (2014) 'Comparative analysis of *Klebsiella pneumoniae* genomes identifies a phospholipase D family protein as a novel virulence factor', *BMC Biology*, 12, p. 41. Available at: 10.1186/1741-7007-12-41

Letunic, I. and Bork, P. (2021) 'Interactive Tree Of Life (iTOL) v5: an online tool for phylogenetic tree display and annotation', *Nucleic Acids Research*, 49(W1), pp. W293-W296. Available at: 10.1093/nar/gkab301

Li, L., Ma, J., Cheng, P., Li, M., Yu, Z., Song, X., Yu, Z., Sun, H., Zhang, W. and Wang, Z. (2023) 'Roles of two-component regulatory systems in *Klebsiella pneumoniae*: Regulation of virulence, antibiotic resistance, and stress responses', *Microbiological Research*, 272, pp. 127374-127374. Available at: 10.1016/j.micres.2023.127374

Li, X.Z., Plésiat, P. and Nikaido, H. (2015) 'The challenge of efflux-mediated antibiotic resistance in Gram-negative bacteria', *Clinical Microbiology Reviews*, 28(2), pp. 337-418. Available at: 10.1128/cmr.00117-14

Litwin, C.M. and Calderwood, S.B. (1993) 'Role of iron in regulation of virulence genes', *Clinical Microbiology Reviews*, 6(2), pp. 137-49. Available at: 10.1128/cmr.6.2.137

Lin, C.T., Wu, C.C., Chen, Y. S., Lai, Y. C., Chi, C. and Lin, J.C. (2011) 'FUR regulation of the capsular polysaccharide biosynthesis and iron acquisition systems in *Klebsiella pneumoniae* CG43', *Microbiology*, 157(2), pp. 419–429. Available at: https://doi.org/10.1099/mic.0.044065-0.

Lin, J.-C., Koh, T.H., Lee, N., Fung, C.-P., Chang, F.-Y., Tsai, Y.-K., Ip, M. and Siu, L.K. (2014) 'Genotypes and virulence in serotype K2 *Klebsiella pneumoniae* from liver abscess and non-infectious carriers in Hong Kong, Singapore and Taiwan', *Gut Pathogens*, 6(1), p. 21. Available at: 10.1186/1757-4749-6-21

Liu, X., Chang, Y., Xu, Q., Zhang, W., Huang, Z., Zhang, L., Weng, S., Leptihn, S., Jiang, Y., Yu, Y. and Hua, X. (2023) 'Mutation in the two-component regulator BaeSR mediates cefiderocol resistance and enhances virulence in *Acinetobacter baumannii*', *mSystems,* 8(4), pp. e01291-22. Available at: doi:10.1128/msystems.01291-22

Livak, K.J. and Schmittgen, T.D. (2001) 'Analysis of relative gene expression data using real-time quantitative PCR and the 2(-Delta Delta C(T)) Method', *Methods*, 25(4), pp. 402-8. Available at: 10.1006/meth.2001.1262

Lodge, J.M., Williams, P. and Brown, M.R. (1986) 'Influence of growth rate and iron limitation on the expression of outer membrane proteins and enterobactin by *Klebsiella pneumoniae* grown in continuous culture', *Journal of Bacteriology*, 165(2), pp. 353-6. Available at: 10.1128/jb.165.2.353356.1986

Lundrigan, M. and Earhart, C.F. (1981) 'Reduction in three iron-regulated outer membrane proteins and protein a by the *Escherichia coli* K-12 perA mutation', *Journal of Bacteriology*, 146(2), pp. 804-7. Available at: 10.1128/jb.146.2.804-807.1981

Martin, R.M. and Bachman, M.A. (2018) 'Colonization, Infection, and the Accessory Genome of *Klebsiella pneumoniae*', *Frontiers in Cellular and Infection Microbiology*, 8, p. 4. Available at: 10.3389/fcimb.2018.00004

McCreary, E.K., Heil, E.L. and Tamma, P.D. (2021) 'New Perspectives on Antimicrobial Agents: Cefiderocol', *Antimicrobial Agents in Chemotherapy*, 65(8), p. e0217120. Available at: 10.1128/aac.02171-20

McElheny, C.L., Fowler, E.L., Iovleva, A., Shields, R.K. and Doi, Y. (2021) *'In Vitro* Evolution of Cefiderocol Resistance in an NDM-Producing *Klebsiella pneumoniae* Due to Functional Loss of CirA', *Microbiology Spectrum,* 9(3), p. e0177921. Available at: 10.1128/Spectrum.01779-21

Merlin, C., McAteer, S. and Masters, M. (2002) 'Tools for characterization of *Escherichia coli* genes of unknown function', *Journal of Bacteriology*, 184(16), pp. 4573-81. Available at: 10.1128/jb.184.16.4573-4581.2002

Mizuno, T. and Mizushima, S. (1987) 'Isolation and characterization of deletion mutants of *ompR* and *envZ*, regulatory genes for expression of the outer membrane proteins OmpC and OmpF in *Escherichia coli'*, *Journal of Biochemistry*, 101(2), pp. 387-96. Available at: 10.1093/oxfordjournals.jbchem.a121923

Molitor, A., James, C.E., Fanning, S., Pagès, J.M. and Davin-Regli, A. (2018) 'Ram locus is a key regulator to trigger multidrug resistance in *Enterobacter aerogenes*', *Journal of Medical Microbiology*, 67(2), pp. 148-159. Available at: 10.1099/jmm.0.000667

Møller, T., Franch, T., Højrup, P., Keene, D.R., Bächinger, H.P., Brennan, R.G. and Valentin-Hansen, P. (2002) 'Hfq: A Bacterial Sm-like Protein that Mediates RNA-RNA Interaction', *Molecular Cell*, 9(1), pp. 23-30. Available at: https://doi.org/10.1016/S1097-2765(01)00436-1

Moynié, L., Milenkovic, S., Mislin, G.L.A., Gasser, V., Malloci, G., Baco, E., McCaughan, R.P., Page, M.G.P., Schalk, I.J., Ceccarelli, M. and Naismith, J.H. (2019) 'The complex of ferric-enterobactin with its transporter from *Pseudomonas aeruginosa* suggests a two-site model', *Nature Communications,* 10(1), p. 3673. Available at: 10.1038/s41467-019-11508-y

Nagakubo, S., Nishino, K., Hirata, T. and Yamaguchi, A. (2002) 'The putative response regulator BaeR stimulates multidrug resistance of *Escherichia coli* via a novel multidrug exporter system, MdtABC', *Journal of Bacteriology*, 184(15), pp. 4161-7. Available at: 10.1128/jb.184.15.4161-4167.2002

Nairz, M., Schroll, A., Sonnweber, T. and Weiss, G. (2010) 'The struggle for iron – a metal at the host–pathogen interface', *Cellular Microbiology*, 12(12), pp. 1691-1702. Available at: https://doi.org/10.1111/j.1462-5822.2010.01529.x

Nemati Zargaran, F., Akya, A., Ghadiri, K., Ranjbarian, P. and Rostamian, M. (2021) 'Detecting the Dominant T and B Epitopes of *Klebsiella pneumoniae* Ferric Enterobactin Protein (FepA) and Introducing a Single Epitopic Peptide as Vaccine Candidate', *International Journal of Peptide Research and Therapeutics*, 27(4), pp. 2209-2221. Available at: 10.1007/s10989-021-10247-3

Nishino, K., Honda, T. and Yamaguchi, A. (2005) 'Genome-Wide Analyses of *Escherichia coli* Gene Expression Responsive to the BaeSR Two-Component Regulatory System', *Journal of Bacteriology*, 187(5), pp. 1763-1772. Available at: 10.1128/JB.187.5.1763-1772.2005

Nishino, K., Yamada, J., Hirakawa, H., Hirata, T. and Yamaguchi, A. (2003) 'Roles of TolC-dependent multidrug transporters of *Escherichia coli* in resistance to beta-lactams', *Antimicrobial Agents in Chemotherapy*, 47(9), pp. 3030-3. Available at: 10.1128/aac.47.9.3030-3033.2003

Noinaj, N., Guillier, M., Barnard, T.J. and Buchanan, S.K. (2010) 'TonB-dependent transporters: regulation, structure, and function', *Annual Review of Microbiology*, 64, pp. 43-60. Available at: 10.1146/annurev.micro.112408.134247

Nordmann, P., Shields, R., Doi, Y., Takemura, M., Echols, R., Matsunaga, Y. and Yamano, Y. (2022) 'Mechanisms of Reduced Susceptibility to Cefiderocol Among Isolates from the CREDIBLE-CR and APEKS-NP Clinical Trials', *Microbial Drug Resistance*, 28(4), pp. 398-407. Available at: 10.1089/mdr.2021.0180

Nucci, A., Rocha, E.P.C. and Rendueles, O. (2022) 'Adaptation to novel spatially-structured environments is driven by the capsule and alters virulence-associated traits', *Nature Communications*, 13(1), p. 4751. Available at: 10.1038/s41467-022-32504-9

OECD (2018) 'Stemming the Superbug Tide.' OECD (OECD Health Policy Studies). Available at: https://doi.org/10.1787/9789264307599-en.

O'Neill, J. (2016) 'Tackling Drug-Resistant Infections Globally: Final Report and Recommendations. Review on Antimicrobial Resistance.' Wellcome Trust and HM Government. Available at: https://amr-review.org/sites/default/files/160525_Final%20paper_with%20cover.pdf

Opoku-Temeng, C., Kobayashi, S.D. and DeLeo, F.R. (2019) *'Klebsiella pneumoniae* capsule polysaccharide as a target for therapeutics and vaccines', *Computational and Structural Biotechnology Journal*, 17, pp. 1360-1366. Available at: https://doi.org/10.1016/j.csbj.2019.09.011

Padovani, M., Bertelli, A., Corbellini, S., Piccinelli, G., Gurrieri, F. and De Francesco, M.A. (2023) *'In Vitro* Activity of Cefiderocol on Multiresistant Bacterial Strains and Genomic Analysis of Two Cefiderocol Resistant Strains', *Antibiotics (Basel)*, 12(4), p. 785. Available at: 10.3390/antibiotics12040785

Page, M.G.P. (2019) 'The Role of Iron and Siderophores in Infection, and the Development of Siderophore Antibiotics', *Clinical Infectious Diseases*, 69(Supplement_7), pp. S529-S537. Available at: 10.1093/cid/ciz825

Poirel, L., Sadek, M., Kusaksizoglu, A. and Nordmann, P. (2022) 'Co-resistance to ceftazidimeavibactam and cefiderocol in clinical isolates producing KPC variants', *European Journal of Clinical Microbiology and Infectious Diseases*, 41(4), pp. 677-680. Available at: 10.1007/s10096-021-04397-x

Rajput, A., Seif, Y., Choudhary, K.S., Dalldorf, C., Poudel, S., Monk, J.M. and Palsson, B.O. (2021) 'Pangenome Analytics Reveal Two-Component Systems as Conserved Targets in ESKAPEE Pathogens', *mSystems*, 6(1) Available at: 10.1128/mSystems.00981-20

Ramos, P.I., Custódio, M.G., Quispe Saji, G.D., Cardoso, T., da Silva, G.L., Braun, G., Martins, W.M., Girardello, R., de Vasconcelos, A.T., Fernández, E., Gales, A.C. and Nicolás, M.F. (2016) 'The polymyxin B-induced transcriptomic response of a clinical, multidrug-resistant *Klebsiella pneumoniae* involves multiple regulatory elements and intracellular targets', *BMC Genomics*, 17(8), p. 737. Available at: 10.1186/s12864-016-3070-y

Raymond, K.N., Dertz, E.A. and Kim, S.S. (2003) 'Enterobactin: An archetype for microbial iron transport', *Proceedings of the National Academy of Sciences,* 100(7), pp. 3584-3588. Available at: doi:10.1073/pnas.0630018100

Rebizant, J. (2022) 'The design, synthesis and microbiological investigation of tobramycin catecholate conjugates'. The University of Manitoba. Available at: https://mspace.lib.umanitoba.ca/items/517ca820-aab9-41fb-bdca-82ac052b9c2f

Rendueles, O. (2020) 'Deciphering the role of the capsule of *Klebsiella pneumoniae* during pathogenesis: A cautionary tale', *Molecular Microbiology,* 113(5), pp. 883-888. Available at: 10.1111/mmi.14474

Reygaert, W.C. (2018) 'An overview of the antimicrobial resistance mechanisms of bacteria', *AIMS Microbiology*, 4(3), pp. 482-501. Available at: 10.3934/microbiol.2018.3.482

Rice, L.B. (2012) 'Mechanisms of resistance and clinical relevance of resistance to β-lactams, glycopeptides, and fluoroquinolones', *Mayo Clinic Proceedings*, 87(2), pp. 198-208. Available at: 10.1016/j.mayocp.2011.12.003

Rocha, D., Castro, T.L.P., Aguiar, E. and Pacheco, L.G.C. (2020) 'Gene Expression Analysis in Bacteria by RT-qPCR', *Methods in Molecular Biology*, 2065, pp. 119-137. Available at: 10.1007/978-1-4939-98333_10

Rodríguez, D. and González-Bello, C. (2023) 'Siderophores: Chemical tools for precise antibiotic delivery', *Bioorganic & Medicinal Chemistry Letters*, 87, p. 129282. Available at: https://doi.org/10.1016/j.bmcl.2023.129282

Saisho, Y., Katsube, T., White, S., Fukase, H. and Shimada, J. (2018) 'Pharmacokinetics, Safety, and Tolerability of Cefiderocol, a Novel Siderophore Cephalosporin for Gram-Negative Bacteria, in Healthy Subjects', *Antimicrobial Agents in Chemotherapy*, 62(3) Available at: 10.1128/aac.02163-17

Salam, M.A., Al-Amin, M.Y., Salam, M.T., Pawar, J.S., Akhter, N., Rabaan, A.A. and Alqumber, M.A.A. (2023) 'Antimicrobial Resistance: A Growing Serious Threat for Global Public Health', *Healthcare (Basel)*, 11(13) Available at: 10.3390/healthcare11131946

Salgado, H., Gama-Castro, S., Lara, P., Mejia-Almonte, C., Alarcón-Carranza, G., López-Almazo, A.G., Betancourt-Figueroa, F., Peña-Loredo, P., Alquicira-Hernández, S., Ledezma-Tejeida, D., ArizmendiZagal, L., Mendez-Hernandez, F., Diaz-Gomez, A.K., Ochoa-Praxedis, E., Muñiz-Rascado, L.J., GarcíaSotelo, J.S., Flores-Gallegos, F.A., Gómez, L., Bonavides-Martínez, C., del Moral-Chávez, V.M., Hernández-Alvarez, A.J., Santos-Zavaleta, A., Capella-Gutierrez, S., Gelpi, J.L. and Collado-Vides, J.
(2023) 'RegulonDB v12.0: a comprehensive resource of transcriptional regulation in *E. coli* K-12', *Nucleic Acids Research*, 52(D1), pp. D255-D264. Available at: 10.1093/nar/gkad1072

Salvail, H., Caron, M.P., Bélanger, J. and Massé, E. (2013) 'Antagonistic functions between the RNA chaperone Hfq and an sRNA regulate sensitivity to the antibiotic colicin', *Embo Journal,* 32(20), pp. 2764-78. Available at: 10.1038/emboj.2013.205

Santos, R., Batista, B.B. and da Silva Neto, J.F. (2020) 'Ferric Uptake Regulator Fur Coordinates Siderophore Production and Defense against Iron Toxicity and Oxidative Stress and Contributes to Virulence in *Chromobacterium violaceum*', *Applied Environmental Microbiology*, 86(21) Available at: 10.1128/aem.01620-20

Sato, T. and Yamawaki, K. (2019) 'Cefiderocol: Discovery, Chemistry, and In Vivo Profiles of a Novel Siderophore Cephalosporin', *Clinical Infectious Diseases*, 69(Suppl 7), pp. S538-s543. Available at: 10.1093/cid/ciz826

Schaufler, K., Echelmeyer, T., Schwabe, M., Guenther, S., Bohnert, J.A., Becker, K., Fickenscher, H., Bueter, A., Maschkowitz, G., Krumbholz, A., Nurjadi, D., Heiden, S.E. and Eger, E. (2023) 'Convergent *Klebsiella pneumoniae* strains belonging to a sequence type 307 outbreak clone combine cefiderocol

and carbapenem resistance with hypervirulence', *Emerging Microbes & Infections*, p. 2271096. Available at: 10.1080/22221751.2023.2271096

Schneider, C.A., Rasband, W.S. and Eliceiri, K.W. (2012) 'NIH Image to ImageJ: 25 years of image analysis', *Nature Methods*, 9(7), pp. 671-675. Available at: 10.1038/nmeth.2089

Schwyn, B. and Neilands, J.B. (1987) 'Universal chemical assay for the detection and determination of siderophores', *Analytical Biochemistry*, 160(1), pp. 47-56. Available at: https://doi.org/10.1016/00032697(87)90612-9

Seo, S.W., Kim, D., Latif, H., O'Brien, E.J., Szubin, R. and Palsson, B.O. (2014) 'Deciphering FUR transcriptional regulatory network highlights its complex role beyond iron metabolism in *Escherichia coli*', *Nature Communications*, 5(1), p. 4910. Available at: 10.1038/ncomms5910

Shen, Z., Ding, B., Ye, M., Wang, P., Bi, Y., Wu, S., Xu, X., Guo, Q. and Wang, M. (2017) 'High ceftazidime hydrolysis activity and porin OmpK35 deficiency contribute to the decreased susceptibility to ceftazidime/avibactam in KPC-producing *Klebsiella pneumoniae*', *Journal of Antimicrobial Chemotherapy*, 72(7), pp. 1930-1936. Available at: 10.1093/jac/dkx066

Simner, P.J., Beisken, S., Bergman, Y., Ante, M., Posch, A.E. and Tamma, P.D. (2021) 'Defining Baseline Mechanisms of Cefiderocol Resistance in the Enterobacterales', *Microbial Drug Resistance*, 28(2), pp. 161-170. Available at: 10.1089/mdr.2021.0095

Simner, P.J., Bergman, Y., Conzemius, R., Jacobs, E., Tekle, T., Beisken, S. and Tamma, P.D. (2023) 'An NDM-Producing Escherichia coli Clinical Isolate Exhibiting Resistance to Cefiderocol and the Combination of Ceftazidime-Avibactam and Aztreonam: Another Step Toward Pan-β-Lactam Resistance', *Open Forum Infectious Diseases*, 10(7), p. ofad276. Available at: 10.1093/ofid/ofad27

Simner, P.J., Mostafa, H.H., Bergman, Y., Ante, M., Tekle, T., Adebayo, A., Beisken, S., Dzintars, K. and Tamma, P.D. (2022) 'Progressive Development of Cefiderocol Resistance in *Escherichia coli* During Therapy is Associated With an Increase in blaNDM-5 Copy Number and Gene Expression', *Clinical Infectious Diseases*, 75(1), pp. 47-54. Available at: 10.1093/cid/ciab888

Stanton, T.D. (2022) 'Establishing the mechanistic basis of action for novel siderophore-based antibiotics in Gram-negative bacteria'. The University of Edinburgh. Available at: https://era.ed.ac.uk/handle/1842/41769

Sugawara, E., Kojima, S. and Nikaido, H. (2016) *'Klebsiella pneumoniae* Major Porins OmpK35 and OmpK36 Allow More Efficient Diffusion of β-Lactams than Their *Escherichia coli* Homologs OmpF and OmpC', *Journal of Bacteriology*, 198(23), pp. 3200-3208. Available at: 10.1128/jb.00590-16

Syed, Y.Y. (2021) 'Cefiderocol: A Review in Serious Gram-Negative Bacterial Infections', *Drugs*, 81(13), pp. 1559-1571. Available at: 10.1007/s40265-021-01580-4

Tierney, A.R. and Rather, P.N. (2019) 'Roles of two-component regulatory systems in antibiotic resistance', *Future Microbiology*, 14(6), pp. 533-552. Available at: 10.2217/fmb-2019-0002

Tillotson, G.S. (2016) 'Trojan Horse Antibiotics-A Novel Way to Circumvent Gram-Negative Bacterial Resistance?', *Infectious Diseases (Auckland)*, 9, pp. 45-52. Available at: 10.4137/idrt.S31567

Tooke, C., Hinchliffe, P., Bragginton, E., Colenso, C., Hirvonen, V., Takebayashi, Y. and Spencer, J., 2019. β-Lactamases and β-Lactamase Inhibitors in the 21st Century. *Journal of Molecular Biology*, 431(18), pp.3472-3500.

UK Health Security Agency (2023) 'English surveillance programme for antimicrobial utilisation and resistance (ESPAUR) report 2022 to 2023'. Available at:

https://assets.publishing.service.gov.uk/media/65cf498ee1bdec001132225c/ESPAUR-report-2022to-2023.pdf

Vajrala, N., Sayavedra-Soto, L.A., Bottomley, P.J. and Arp, D.J. (2011) 'Role of a FUR homolog in iron metabolism *in Nitrosomonas europaea*', *BMC Microbiology*, 11, p. 37. Available at: 10.1186/14712180-11-37

Wang, C.H., Lu, P.L., Liu, E.Y., Chen, Y.Y., Lin, F.M., Lin, Y.T., Chang, F.Y. and Lin, J.C. (2019) 'Rapid identification of capsular serotype K1/K2 *Klebsiella pneumoniae* in pus samples from liver abscess patients and positive blood culture samples from bacteremia cases via an immunochromatographic strip assay', *Gut Pathogens*, 11, p. 11. Available at: 10.1186/s13099-019-0285-x

Wang, Q., Jin, L., Sun, S., Yin, Y., Wang, R., Chen, F., Wang, X., Zhang, Y., Hou, J., Zhang, Y., Zhang, Z., Luo, L., Guo, Z., Li, Z., Lin, X., Bi, L. and Wang, H. (2022) 'Occurrence of High Levels of Cefiderocol Resistance in Carbapenem-Resistant Escherichia coli before Its Approval in China: a Report from China CRE-Network', *Microbiology Spectrum*, 10(3), p. e0267021. Available at: 10.1128/spectrum.02670-21

WHO Bacterial Priority Pathogens List (2024) 'Bacterial pathogens of public health importance to guide research, development and strategies to prevent and control antimicrobial resistance', Geneva: World Health Organization; 2024. Licence: CC BY-NC-SA 3.0 IGO. Available at: https://iris.who.int/bitstream/handle/10665/376776/9789240093461-eng.pdf?sequence=1

Wu, J.Y., Srinivas, P. and Pogue, J.M. (2020) 'Cefiderocol: A Novel Agent for the Management of Multidrug-Resistant Gram-Negative Organisms', *Infectious Diseases & Therapy*, 9(1), pp. 17-40. Available at: 10.1007/s40121-020-00286-6

Wuchty, S. and Uetz, P. (2014) 'Protein-protein Interaction Networks of *E. coli* and *S. cerevisiae* are similar', *Scientific Reports*, 4(1), p. 7187. Available at: 10.1038/srep07187

Xie, M., Yang, X., Xu, Q., Ye, L., Chen, K., Zheng, Z., Dong, N., Sun, Q., Shu, L., Gu, D., Chan, E.W.-C., Zhang, R. and Chen, S. (2021) 'Clinical evolution of ST11 carbapenem resistant and hypervirulent *Klebsiella pneumoniae*', *Communications Biology*, 4(1), p. 650. Available at: 10.1038/s42003-02102148-4

Yamano, Y., Nakamura, R., Takemura, M. and Echols, R. (2020) '1455. Potential Mechanisms of Cefiderocol MIC Increase in Enterobacterales in *In Vitro* Resistance Acquisition Studies', *Open forum infectious diseases*, 7(Supplement_1), pp. S730-S730. Available at: 10.1093/ofid/ofaa439.1636

Yang, X., Wang, D., Zhou, Q., Nie, F., Du, H., Pang, X., Fan, Y., Bai, T. and Xu, Y. (2019) 'Antimicrobial susceptibility testing of Enterobacteriaceae: determination of disk content and Kirby-Bauer breakpoint for ceftazidime/avibactam', *BMC Microbiology*, 19(1), p. 240. Available at: 10.1186/s12866-019-1613-5

Yao, J., Wang, J., Chen, M. and Cai, Y. (2021) 'Cefiderocol: An Overview of Its *in-vitro* and *in-vivo* Activity and Underlying Resistant Mechanisms', *Frontiers in Medicine (Lausanne)*, 8, p. 741940. Available at: 10.3389/fmed.2021.741940

Yuan, L., Li, X., Du, L., Su, K., Zhang, J., Liu, P., He, Q., Zhang, Z., Peng, D., Shen, L., Qiu, J. and Li, Y. (2020) 'RcsAB and Fur Coregulate the Iron-Acquisition System via entC in *Klebsiella pneumoniae* NTUH-K2044 in Response to Iron Availability', *Frontiers in Cellular and Infection Microbiology*, 10, p. 282. Available at: 10.3389/fcimb.2020.00282

Zapun, A., Contreras-Martel, C. and Vernet, T. (2008) 'Penicillin-binding proteins and β-lactam resistance', *FEMS Microbiology Reviews*, 32(2), pp. 361-385. Available at: 10.1111/j.15746976.2007.00095.

Zgurskaya, H.I., Krishnamoorthy, G., Ntreh, A. and Lu, S. (2011) 'Mechanism and Function of the Outer Membrane Channel TolC in Multidrug Resistance and Physiology of Enterobacteria', *Frontiers in Microbiology,* 2, p. 189. Available at: 10.3389/fmicb.2011.00189

Zhanel, G.G., Golden, A.R., Zelenitsky, S., Wiebe, K., Lawrence, C.K., Adam, H.J., Idowu, T., Domalaon, R., Schweizer, F., Zhanel, M.A., Lagacé-Wiens, P.R.S., Walkty, A.J., Noreddin, A., Lynch Iii, J.P. and Karlowsky, J.A. (2019) 'Cefiderocol: A Siderophore Cephalosporin with Activity Against CarbapenemResistant and Multidrug-Resistant Gram-Negative Bacilli', *Drugs*, 79(3), pp. 271-289. Available at: 10.1007/s40265-019-1055-2

Zhang, K., Liu, L., Yang, M., Chen, C., Li, X., Tian, J., Luo, C., Wang, X. and Wang, M. (2022) 'Reduced porin expression with EnvZ-OmpR, PhoPQ, BaeSR two-component system down-regulation in carbapenem resistance of *Klebsiella pneumoniae* based on proteomic analysis', *Microbial Pathogenesis*, 170, p. 105686. Available at: https://doi.org/10.1016/j.micpath.2022.105686

Zhang, Q., Neidig, N., Chu, T.-Y., Divoky, C., Carpenter, J., Lee-Hsiao, C., Threatt, H., Sultana, R. and Bush, K. (2022) 'In vitro antibacterial activity of cefiderocol against recent multidrug-resistant carbapenem-nonsusceptible Enterobacterales isolates', *Diagnostic Microbiology and Infectious Disease*, 103(1), p. 115651. Available at: https://doi.org/10.1016/j.diagmicrobio.2022.115651

Zhou, G., Wang, Q., Wang, Y., Wen, X., Peng, H., Peng, R., Shi, Q., Xie, X. and Li, L. (2023) 'Outer Membrane Porins Contribute to Antimicrobial Resistance in Gram-Negative Bacteria', *Microorganisms*, 11(7), p. 1690. Available at: https://www.mdpi.com/2076-2607/11/7/1690.

Zhou, X.H., van der Helm, D. and Venkatramani, L. (1995) 'Binding characterization of the iron transport receptor from the outer membrane of *Escherichia coli* (FepA): differentiation between FepA and FecA', *Biometals*, 8(2), pp. 129-136. Available at: 10.1007/BF00142012